

**UNIVERSIDADE FEDERAL DO RIO GRANDE DO SUL
INSTITUTO DE GEOCIÊNCIAS
PROGRAMA DE PÓS-GRADUAÇÃO EM GEOCIÊNCIAS**

**SISTEMAS FLUVIAIS DOMINADOS POR ESTRUTURAS
SUPERCRÍTICAS EM CLIMA SEMIÁRIDO NO
EOTRIÁSSICO: REINTERPRETAÇÃO SEDIMENTAR DA
FORMAÇÃO SANGA DO CABRAL**

PEDRO LUIS AMMON XAVIER

ORIENTADOR — Prof. Dr. Claiton Marlon dos Santos Scherer
COORIENTADORA — Prof.^a Dr.^a Graciela Piñeiro

Porto Alegre, 2023

**UNIVERSIDADE FEDERAL DO RIO GRANDE DO SUL
INSTITUTO DE GEOCIÊNCIAS
PROGRAMA DE PÓS-GRADUAÇÃO EM GEOCIÊNCIAS**

**SISTEMAS FLUVIAIS DOMINADOS POR ESTRUTURAS
SUPERCRÍTICAS EM CLIMA SEMIÁRIDO NO
EOTRIÁSSICO: REINTERPRETAÇÃO SEDIMENTAR DA
FORMAÇÃO SANGA DO CABRAL**

PEDRO LUIS AMMON XAVIER

ORIENTADOR — Prof. Dr. Claiton Marlon dos Santos Scherer

COORIENTADORA — Prof.^a Dr.^a Graciela Piñeiro

BANCA EXAMINADORA

Dr. Bruno Ludovico Dihl Horn — Serviço Geológico do Brasil (CPRM)

Prof. Dr. Ernesto Luiz Correa Lavina — Universidade do Vale do Rio dos Sinos
(UNISINOS)

Dr. Henrique Zerfass — Centro de Pesquisas, Desenvolvimento e Inovação Leopoldo
Américo Miguez de Mello (Cenpes), Petrobras

Tese de doutorado apresentada como
requisito parcial para a obtenção do Título de
Doutor em Ciências.

Porto Alegre, 2023

CIP - Catalogação na Publicação

Xavier, Pedro Luis Ammon
Sistemas fluviais dominados por estruturas supercríticas em clima semiárido no Eotriássico: reinterpretação sedimentar da Formação Sanga do Cabral / Pedro Luis Ammon Xavier. -- 2023.
182 f.
Orientador: Claiton Marlon dos Santos Scherer.

Coorientadora: Graciela Piñeiro.

Tese (Doutorado) -- Universidade Federal do Rio Grande do Sul, Instituto de Geociências, Programa de Pós-Graduação em Geociências, Porto Alegre, BR-RS, 2023.

1. Sanga do Cabral. 2. estruturas supercríticas. 3. rio de alta variabilidade. 4. paleossolo. 5. poeira eólica. I. Scherer, Claiton Marlon dos Santos, orient. II. Piñeiro, Graciela, coorient. III. Título.

DEDICATÓRIA

À minha mãe, Giselle, e a meu avô, Günther.

Ambos construíram, moldaram e incentivaram meu amor pela ciência, e o caminho que percorri. Foram suporte constante e incondicional a minhas escolhas, e referência nelas.

A vocês, dedico esta tese.

AGRADECIMENTOS

Inicio meus agradecimentos por meu orientador, Claiton Scherer e minha coorientadora, Graciela Piñeiro. Ao Claiton por ter aceitado, com entusiasmo, receber como orientando alguém que já está na metade do curso, e ter se dedicado e dado os plenos recursos para que a pesquisa acontecesse. A Graciela, por seguir apoiando um proyecto que mucho cambi6, para muy lejos de su 6rea de especialidad — y seguir apoyando mi aprendizaje de espa6ol.

A meu ex-orientador, Cesar Schultz, e a Bruno Horn pela ajuda nos trabalhos de campo no Uruguai, mesmo que o tema da tese tenha mudado completamente desde aquele momento e n6o tenham mais envolvimento. O aprendizado certamente ficou, mas mais importante, o legado de parceria internacional.

A Sebasti6n, Antonela, y Mart6n, muchas gracias por el campo buen6simo en Uruguay. Algunas aventuras, algunos chistes, mucho aprendizaje y mucho trabajo. Espero much6simo que sigamos con nuestros intercambios de conocimientos, ¡y que nos volvamos a ver pronto!

Aos colegas da estratigrafia, Adriano (agora professor da UnB! Parab6ns!), Francyne, Rossano e Bruno, e ao Prof. Ezequiel pela ajuda no trabalho de campo. O tempo jamais teria sido suficiente n6o fosse a ajuda de voc6s. E obrigado ao Prof. Guadagnim pela opera66o do drone; as imagens ficaram fant6sticas. Mando um agradecimento extra 6 Prof.^a Amanda, que foi praticamente uma mini-coorientadora (trocadilho n6o intencional) nos 6ltimos meses de prepara66o do segundo artigo.

Agrade6o ao CNPq, 6 UFRGS, e em especial ao povo brasileiro pelo financiamento fornecimento de estrutura para esta pesquisa, atrav6s tamb6m, mas n6o somente, da bolsa 141101/2018-0.

Quero agradecer a meus pais, Giselle e Pedro, e a meus av6s, Iara e G6nther, Lorena e Leo (*in memoriam*), por terem me apoiado e incentivado minha vida toda. Nem todas as pessoas t6m a sorte de ter uma fam6lia a lhe conceder apoio e amor incondicionais, e sou muito feliz por ter tido essa sorte. A meus irm6os, Ana e Jo6o, pelas risadas e companheirismo, e por serem sempre um incentivo para eu tirar um tempo e voltar para desfrutar da companhia deles.

A meus caros amigos de Florianópolis, Rodrigo, Eduardo e Matheus. É muito bom saber que mesmo depois de tanto tempo, e com a distância, ainda tem alguém lá que quer a sua presença por nenhum motivo em especial.

A meus amigos de Porto Alegre, por estarem comigo e terem a exímia paciência com minha falta de tempo nos últimos meses (ou anos talvez), Garcia, Guedes, Jéssica, Paola, Rafael e Júlia. Minhas ex-colegas de apartamento, das quais jamais esquecerei, Monique e Laryssa, e seus agregados que realmente agregam, João e Onzi. Também o “pessoal da faculdade”: os colegas da Paleontologia, Rafael e Francesco, e os colegas das Geociências, Talita, Igor, Diego, Franciele, Edvaldo, e Edgar e seu grande companheiro Jeferson.

A meus colegas de apartamento (ex- e presentes durante este trajeto) e amigos Matheus Battisti, Cícero, Alejandro, Murilo e Douglas. Passei com alguns de vocês a maior crise sanitária da humanidade nos últimos 100 anos, não há como esquecer isso, e foi um pouco mais fácil graças a vocês. E com todos, dividi e divido um pouco do meu eu mais autêntico.

Meus amigos à distância Val, Matheus Alves, Gabriel, Giovani e Nelson, fontes inesgotáveis de memes, e ocasionais comentários lúcidos. Também à distância, meus amigos do saudoso grupo do Age da Paleonto, onde as conversas oscilam sem cerimônia alguma entre discussões científicas de ponta e bobagens tão grandes que temos vergonha que outras pessoas vejam. Queria também deixar aqui um salve para o grupo dos Pedros da UFRGS, fonte de leveza e boas risadas nesse meu último ano como estudante.

Fica aqui um agradecimento também aos colegas do Movimento Correnteza e da APG, que lutam a batalha por uma universidade, e um mundo melhor. Infelizmente são pessoas demais para nomear, e terei que me ater aos com que mais convivo: Cauã, Kenji, Beraldo, Henrique, Diogo, Bruno, Samuel, Maurício, Bruna (à distância, mas presente), Samara, Júlia, Amanda, Paulo. Aprendi com vocês mais coisas do que eu poderia imaginar, e coisas que livro nenhum jamais poderia ensinar. Até a vitória!

Por fim, deixo um grande e especial agradecimento à querida Larissa, minha companheira nessa jornada de mais de cinco anos, atravessando todo tipo de dificuldade, mudanças forçadas, dramas, tristezas, e a maior crise sanitária da história da humanidade nos últimos 100 anos. Ela trouxe e traz alegria, risadas, e amor, me ajudando em absolutamente tudo o que pode. Obrigado.

“E o que é impossível para a ciência?”

— Friedrich Engels

RESUMO

Formas de leito supercríticas e suas estruturas sedimentares associadas têm sido objeto de crescente interesse na última década. Antes pensadas como raramente preservadas, essas estruturas têm sido cada vez mais identificadas em ambientes modernos e no registro geológico. Em sistemas fluviais sua prevalência indica rios de alta variabilidade de descarga. Apesar desse reconhecimento crescente, modelos de fácies para tais rios continuam tentativos, restritos a poucos estudos de caso. A Formação Sanga do Cabral do Triássico Inferior no sul do Brasil representa um sistema fluvial de alta variabilidade de descarga desenvolvido em um contexto árido a semiárido, com abundantes nódulos de carbonato, intraclastos cimentados por carbonato, além de paleossolos incipientes. A presente tese utiliza uma análise integrada de fácies e petrografia para reconstrução do sistema fluvial da Formação Sanga do Cabral. Três Estilos Fluviais (EF) são descritos: EF1 compreende principalmente camadas finas de arenitos maciços ou fracamente laminados, com níveis de intraclastos de lama, ocasionalmente interrompidos por conglomerados intraclásticos. É interpretado como resultado de fluxos hiperconcentrados não confinados. EF2 mostra uma sucessão granodecrescente, iniciando com intervalos basais de depósitos de *cyclic steps* que transicionam para estratificação ondulada, seguidos por intervalos intermediários de arenitos com estratificação ondulada truncada e depósitos de *chutes-and-pools* sobrepostos por escavações preenchidas com estratificação cruzada tangencial e sigmoidal, e um intervalo de topo com estratificação cruzada sigmoidal e *ripples* com laminação difusa, e estrutura maciça ou blocosa no topo. É interpretado como resultado de enchentes relâmpago ocorrendo em curtos períodos durante as estações úmidas. EF3 é caracterizado arenitos com estratificação ondulada contínua e truncada de grande escala e depósitos de *cyclic steps*, com intraclastos de lama. É associado a enchentes relâmpago catastróficas de alta descarga e velocidade, ocorrendo em eventos isolados. As rochas estudadas foram interpretadas como tendo passado por pedogênese incipiente e eodiagênese sob clima árido, os carbonatos foram interpretados como calcretes freáticos, e a sedimentação é considerada como tendo uma importante contribuição de poeira eólica. A faixa de precipitação estimada é interpretada como sendo de 100 a 400–600 mm/ano.

Palavras-chave: Sanga do Cabral; estruturas supercríticas; rio de alta variabilidade de descarga; árido; semiárido; calcrete; paleossolo; poeira eólica

ABSTRACT

Froude-supercritical bedforms and associated sedimentary structures have seen a surge in interest in the last decade. Initially perceived as rarely preserved, these structures are now increasingly identified in modern settings and the geological record. Particularly in fluvial systems, their prevalence is being recognized as signifying rivers of high discharge variability. However, despite this increasing recognition, developing facies models for such rivers, especially in the rock record, remains a tentative task, restricted to few case studies. The Early Triassic Sanga do Cabral Formation in southern Brazil represents a high-variability fluvial system developed in an arid to semiarid context, containing abundant carbonate nodules and carbonate-cemented intraclasts, as well as incipient paleosols. The present thesis uses an integrated facies-petrographic analysis in order to reconstruct the fluvial system of the Sanga do Cabral Formation. Three Fluvial Styles (FS) are described: FS1 predominantly comprises thin beds of fine-grained massive or faint-laminated sandstones with some mud-intraclast levels, occasionally interrupted by intraclastic conglomerates. It is interpreted as a product of unconfined hyperconcentrated flows. FS2 shows a fining-upwards succession, initiating with basal intervals of cyclic steps deposits which transition to undulating stratification, followed by intermediate intervals of sandstones with truncated undulatory stratification and chute-and-pool deposits overlain by scours filled by tangential and sigmoidal cross-stratification, and an upper interval with sigmoidal cross-stratification and ripples with diffuse lamination, and massive or blocky structure at the top. It is interpreted as the result of flash floods occurring within short periods during wet seasons. FS3 is characterized by large-scale continuous and truncated undulatory laminae and cyclic steps deposits, with mud intraclasts. It is linked to catastrophic flash floods with high discharge and velocity, occurring in single events. The studied rocks were interpreted to have undergone incipient pedogenesis and early diagenesis under arid climate, the carbonates were interpreted as groundwater calcretes, and sedimentation is considered to have had an important contribution from aeolian dust. Estimated precipitation range is interpreted as 100 to 400–600 mm/year.

Keywords: Sanga do Cabral; supercritical structures; high-variability discharge river; arid; semiarid; calcrete; paleosol; aeolian dust

LISTA DE FIGURAS

- Figura 1. Coluna cronoestratigráfica ilustrando posição, elementos sedimentares característicos, e zonas bioestratigráficas das unidades estratigráficas Neopaleozoicas e Triássicas. Modificado de Horn *et al.* (2014), sobre Zerfass *et al.* (2003). Outras modificações: Formação Buena Vista por Scherer *et al.* (2023); Supersequência Santa Maria por Schultz *et al.* (2020); Amplitude da Formação e Supersequência Sanga do Cabral correlacionada aos pacotes de intervalos estratigráficos “Upper Katberg” 1 & 2 de Viglietti *et al.* (2022), na Bacia do Karoo na África do Sul, onde *Procolophon trigoniceps* é o táxon dominante. 11
- Figura 2. Mapa com localização geográfica da área de estudo. A) Bacia do Paraná e estado do Rio Grande do Sul na América do Sul. B) Mapa geológico simplificado do Rio Grande do Sul. C) Mapa geológico simplificado da região de estudo, indicando afloramento, e principais áreas urbanas e vias de acesso. Modificado de Goldberg (2001) e CPRM (2006). 12
- Figura 3. Ilustração conceitual dos parâmetros envolvidos no Número de Froude. A) Visualização conceitual da relação da profundidade da lâmina d’água e velocidade de escoamento do fluxo. B) Visualização conceitual do acúmulo de velocidade inercial, em contraste com a velocidade de escoamento, a qual depende apenas da profundidade. C) Abstração da resposta do Número de Froude à mudança da proporção entre as velocidades inercial e de escoamento em um fluxo. 15
- Figura 4. Antidunas estáveis, formadas sob fluxo supercrítico ($Fr > 1$). Modificado de Slotman & Cartigny (2020). 17
- Figura 5. Panorama representativo idealizado de quatro estágios em fluxos supercríticos unidirecionais, correspondendo ao desenvolvimento de quatro tipos de configurações de leito. Fluxo da direita para a esquerda. Escala vertical exagerada para melhor clareza. Quadros adicionais para antidunas instáveis e *chutes-and-pools* ilustram a dinâmica associada ao processo. Modificado de Cartigny *et al.* (2014). .. 18
- Figura 6. Comportamento do fluxo formativo da antiduna que migra à jusante. A superfície da água está em fase com a forma de leito, mas a variação de profundidade está fora de fase com o leito. Então, o fluxo acelera da depressão para a crista, causando erosão à montante e deposição à jusante, causando a forma de leito migrar à jusante. 19

Figura 7. Representação idealizada de sucessivos saltos hidráulicos formando <i>cyclic steps</i> . O salto hidráulico opera igualmente no <i>chute-and-pool</i> , mas é isolado e efêmero. Modificado de Cartigny <i>et al.</i> (2011).....	20
Figura 8. <i>Cyclic steps</i> parcialmente deposicionais, gerando laminações contracorrente truncadas. Modificado de <i>Slootman & Cartigny (2020)</i>	23
Figura 9. Carta cronoestratigráfica da Bacia do Paraná de Milani <i>et al.</i> (2007), mostrando a distribuição espacial e temporal das formações litoestratigráficas e das seis supersequências.....	37
Figura 10. Quadro bioestratigráfico da Bacia do Karoo mostrando a proposta “zona de abundância de <i>Procolophon</i> ” na porção superior da Zona de <i>Lystrosaurus</i> . Modificado de Rubidge (2005).	40

SUMÁRIO

DEDICATÓRIA.....	4
AGRADECIMENTOS	5
RESUMO.....	1
ABSTRACT	2
LISTA DE FIGURAS	3
SUMÁRIO.....	5
ESTRUTURA DA TESE	7
TEXTO INTEGRADOR	9
1. Introdução.....	9
2. Objetivo da pesquisa	13
3. Estado da arte	14
3.1. Formas de leito supercríticas e seus produtos sedimentares	14
3.2. Rios de alta variabilidade	23
3.3. Calcretes freáticos	28
3.4. Paleosolos.....	30
3.5. Poeira eólica	32
4. Materiais e métodos	32
4.1. Ortofotos e arquitetura de fácies	32
4.2. Petrografia.....	33
4.3. Difractometria de raios-X	34
4.4. Microscopia Eletrônica de Varredura (MEV) e Espectrometria de Energia Dispersiva (EED)	35
5. Contexto geológico da área	35
5.1. Bacia do Paraná.....	35
5.2. Formação Sanga do Cabral	36
6. Resumo dos resultados	40
6.1. Estilos fluviais supercríticos e a aridez oscilante no Eotriássico: o exemplo da Formação Sanga do Cabral, Bacia do Paraná, Brasil	41

6.2. O papel de calcretes em conglomerados intraformacionais multicíclicos de um sistema fluvial dominado por estruturas supercríticas, com contribuição de poeira eólica (Eotriássico, Bacia do Paraná, Brasil)	42
7. Considerações finais	43
8. Referências bibliográficas.....	44
PRIMEIRO ARTIGO	60
SEGUNDO ARTIGO	119
ANEXOS	169
Anexo I — Material suplementar do segundo artigo.....	170
Anexo II	173
Anexo III	175

ESTRUTURA DA TESE

Esta tese de doutorado está estruturada com base em dois artigos científicos, um aceito e um submetido, em periódicos classificados nos estratos N2 da Classificação PPGGEO de Periódicos. A sua organização compreende as seguintes partes principais:

TEXTO INTEGRADOR

Texto Integrador composto pelos seguintes capítulos: introdução; objetivos da pesquisa; estado da arte do tema da pesquisa; os materiais e métodos utilizados; contexto geológico da área; resumo dos principais resultados obtidos; conclusões; referências bibliográficas.

O tema principal abordado no estado da arte foi o de formas de leito supercríticas e suas estruturas sedimentares associadas, e rios de alta variabilidade de descarga. Outros temas considerado também essenciais, mas não no mesmo nível, foram abordados mais sucintamente, quais sejam: calcretes freáticos, paleossolos e poeira eólica.

ARTIGOS

Corpo Principal da Tese, constituído por dois artigos publicados e/ou submetidos. O texto é idêntico ao enviado para as revistas. Porém, as figuras e suas legendas foram dispostas em meio ao texto, em locais apropriados, para facilitar a leitura.

O primeiro artigo, intitulado “*Supercritical fluvial styles and the shifting aridity in the Early Triassic: the example of the Sanga do Cabral Formation, Paraná Basin, Brazil*” de Xavier, P.L.A.; Scherer, C.M.S.; Reis, A.D.; Souza, E.G.; Guadagnin, F.; Piñeiro, G., foi publicado no periódico *Journal of Sedimentary Research*.

O segundo artigo, intitulado “*The role of calcretes in multi-cycle intraformational conglomerates from a supercritical-dominated fluvial system with eolian dust contribution (Early Triassic, Paraná Basin, Brazil)*” de Xavier, P.L.A.; Scherer, C.M.S.; Rodrigues, A.G.; Reis, A.D.; Souza, E.G.; Guadagnin, F.; Piñeiro, G., foi submetido ao periódico *Sedimentary Geology*.

ANEXOS

Na terceira parte da tese serão apresentados anexos com os dados suplementares do segundo artigo, e resumos de trabalhos publicados em que o presente autor participou durante a produção da tese, mas não integram o corpo principal desta tese. São estes trabalhos:

O artigo intitulado “*Age constraints on the Paleozoic Yaguarí-Buena Vista succession from Uruguay: paleomagnetic and paleontologic information*” de Ernesto, M.; Demarco, P.N.; Xavier, P.L.A.; Sanchez, L.; Schultz, C.; Graciela, P. Publicado no periódico *Journal of South American Earth Sciences* em 2020. DOI: <https://doi.org/10.1016/j.jsames.2019.102489>.

O artigo intitulado “*Enigmatic wood and first evidence of tetrapods in the Yaguarí Formation (Middle-Late Permian), Uruguay*” de Piñeiro, G.H.; Marchetti, L.; Marmol, S.; Celio, A.; Xavier, P.L.A.; Francia, M.; Schultz, C.L. Publicado no periódico *Agrociencia Uruguay* em 2022. DOI: <https://doi.org/10.31285/AGRO.26.504>.

TEXTO INTEGRADOR

1. Introdução

Estruturas sedimentares são produtos das condições físicas nas quais os sedimentos foram transportados e depositados, e portanto podem ser usadas para inferir tais condições no passado. Dessa constatação, que nada mais é que um caso particular do princípio do uniformitarismo (Gould, 1991), tem-se a contrapartida de que uma compreensão correta dos processos sedimentares atuais é necessária para uma correta interpretação de ambientes sedimentares passados.

Uma lacuna na compreensão sobre estruturas sedimentares começou a ser notada entre as décadas de 1990 e 2000: a geração e preservação de estruturas depositadas sob regime de fluxo superior, para além de estratificação plano-paralela, havia sido até então pouco estudada (Fielding, 1993, 2006; Alexander & Fielding, 1997; Yokokawa *et al.*, 2010). Estas são conhecidas como “estruturas supercríticas”, formada em fluxos onde o número de Froude é maior que 1 ($Fr > 1$; Seção 3.1.1; Kennedy, 1963). Em adição, se acentuou a percepção de que rios perenes de altas latitudes estariam talvez sobrerrepresentados em modelos de fácies (Fielding, 1993).

Estruturas supercríticas receberam desde então um crescente número de estudos (e.g., Alexander & Fielding, 1997; Alexander *et al.*, 2001; Yokokawa *et al.*, 2010; Cartigny *et al.*, 2014; Slooman *et al.*, 2021). Destaca-se o trabalho de Parker (1996), onde é pela primeira vez descrita e nomeada uma nova forma de leito: os *cyclic steps* (seção 3.1.5). Muito do crescente interesse deve-se a que esta nova forma de leito foi utilizada para explicar as “ondas de sedimento” (“*sediment waves*”), estruturas de grande escala presentes em sistemas turbidíticos, até então sem explicação satisfatória (Fildani *et al.*, 2006; Lamb *et al.*, 2008; Spinewine *et al.*, 2009; Cartigny *et al.*, 2011; Covault *et al.*, 2017). Isto, é claro, é de grande interesse para a indústria petrolífera. Desse modo, uma série de estudos contemplando formas de leito supercríticas foram realizados nos últimos anos, com o objetivo de compreender as estruturas que elas geram (Parker & Izumi, 2000; Alexander *et al.*, 2001; Yokokawa *et al.*, 2010; Cartigny *et al.*, 2014; Slooman & Cartigny, 2020; Ono *et al.*, 2021).

No âmbito continental, a conexão entre rios de alta variabilidade de descarga e estruturas supercríticas vem se fortalecendo (Tunbridge, 1981; Abdullatif, 1989;

Fielding & Alexander, 1996; Fielding *et al.*, 2009, 2018; Plink-Björklund, 2015; Dario, 2017; Hansford *et al.*, 2020; Zellman *et al.*, 2021; Walker & Holbrook, 2022). Isso implica que estas estruturas apresentam grande potencial para novas interpretações de sistemas fluviais, e de regimes pluviométricos no passado geológico.

No estado do Rio Grande do Sul, no sul do Brasil, a Formação Sanga do Cabral (Andreis *et al.*, 1980) é uma unidade geológica enigmática, e por vezes problemática, do Triássico Inferior (Figura 1; Lavina, 1983; Cisneros, 2008), que aflora na região central do estado (Figura 2). A formação recebeu diversas interpretações ao longo dos anos (Lavina, 1991), sendo a mais aceita nas últimas décadas a hipótese de Zerfass *et al.* (2003): lentes pouco espessas de conglomerados intraformacionais, maciços ou com estratificação cruzada acanalada, e arenitos principalmente com estratificação horizontal. Estes teriam sido depositados por canais pouco confinados em uma planície aluvial de baixo gradiente, e com baixa taxa de acomodação, alimentados por inundações relâmpago sob clima árido ou semiárido. Lentes de pelitos haveriam sido depositadas em pequenas poças e lagos.

Porém, a Formação apresenta algumas estruturas não plenamente explicadas pelas propostas até então existentes, como estratificações convexas para cima, lembrando estratificação cruzada *hummocky*, o que intrigava os pesquisadores em décadas passadas (Claiton Scherer, com. pess., 2023). Com as novas descrições de estruturas supercríticas, e em especial o avanço do reconhecimento destas estruturas em campo (Fielding, 2006; Duller *et al.*, 2008; Lang & Winsemann, 2013; Plink-Björklund, 2015; Froude *et al.*, 2017; Lang *et al.*, 2017, 2021; Slootman & Cartigny, 2020; Slootman *et al.*, 2021; Tan & Plink-Björklund, 2021; Zellman *et al.*, 2021), foram feitos primeiros reconhecimentos na Formação Sanga do Cabral por Dario (2017).

O primeiro artigo deste trabalho, então, propõe uma reinterpretação das estruturas sedimentares da Formação Sanga do Cabral sob a luz destes novos conhecimentos acerca de estruturas formadas por fluxos supercríticos em rios de alta variabilidade de descarga. O trabalho possibilitou também estimativas de parâmetros do paleofluxo, utilizando de equações advindas de estudos em tanques (e.g., Kennedy, 1963; Alexander *et al.*, 2001). Modelos de fácies, arquitetura de fácies e elementos arquiteturais típicos para rios de alta variabilidade de descarga ainda não são bem estabelecidos (Fielding *et al.*, 2018; Walker & Holbrook, 2022), e neste

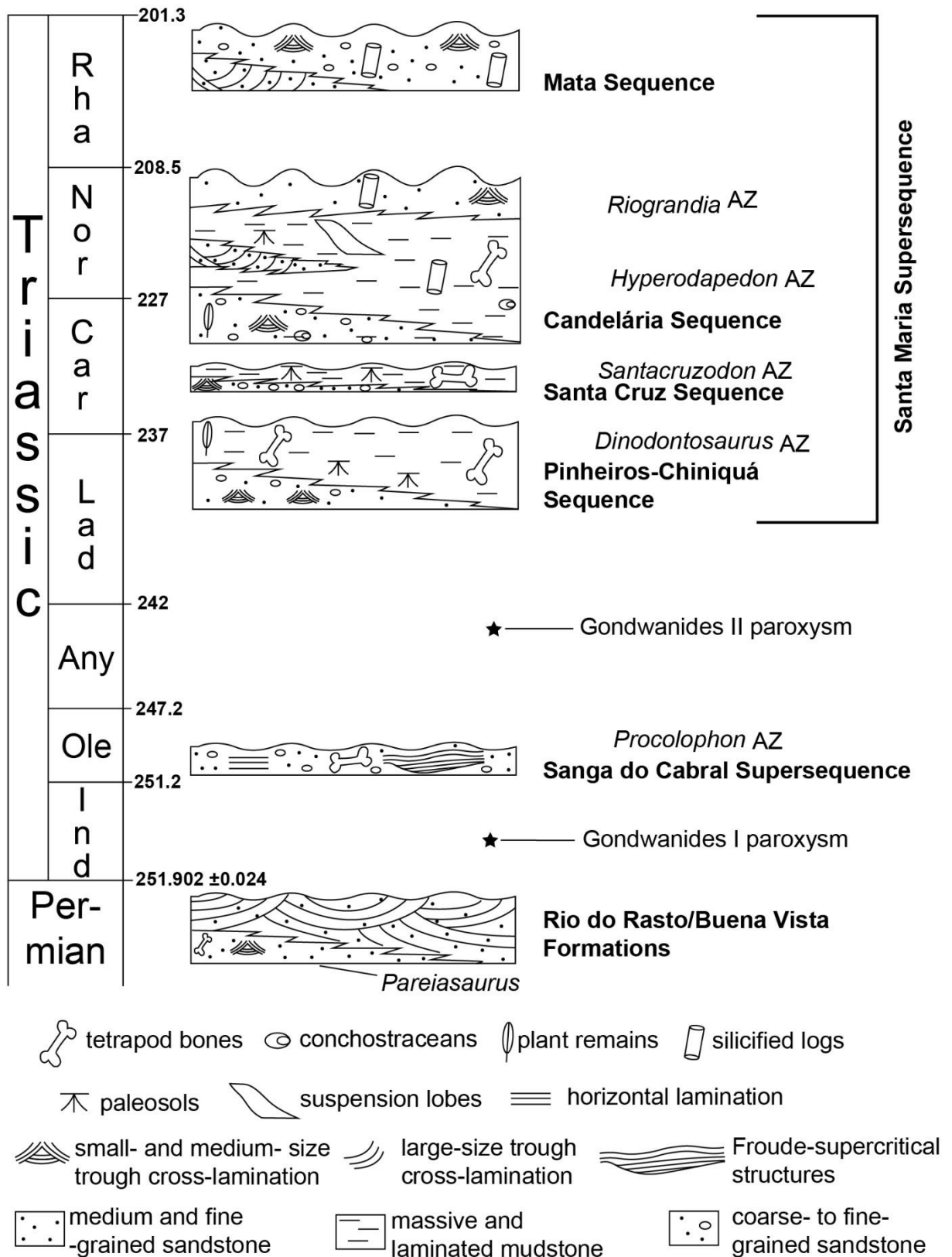


Figura 1. Coluna cronoestratigráfica ilustrando posição, elementos sedimentares característicos, e zonas bioestratigráficas das unidades estratigráficas Neopaleozoicas e Triássicas. Modificado de Horn *et al.* (2014), sobre Zeffass *et al.* (2003). Outras modificações: Formação Buena Vista por Scherer *et al.* (2023); Supersequência Santa Maria por Schultz *et al.* (2020); Amplitude da Formação e Supersequência Sanga do Cabral correlacionada aos pacotes de intervalos estratigráficos “Upper Katberg” 1 & 2 de Viglietti *et al.* (2022), na Bacia do Karoo na África do Sul, onde *Procolophon trigoniceps* é o táxon dominante.

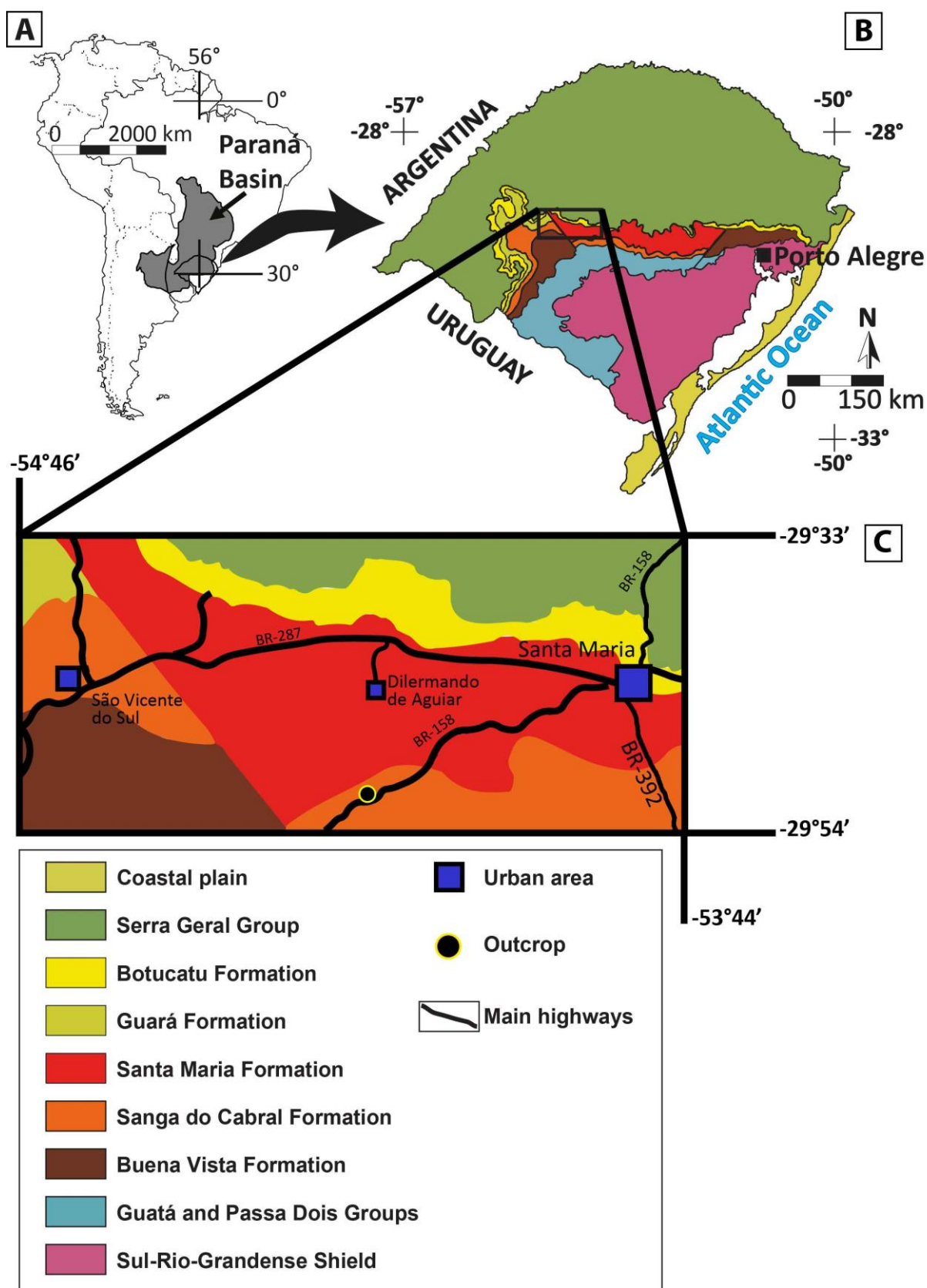


Figura 2. Mapa com localização geográfica da área de estudo. **A)** Bacia do Paraná e estado do Rio Grande do Sul na América do Sul. **B)** Mapa geológico simplificado do Rio Grande do Sul. **C)** Mapa geológico simplificado da região de estudo, indicando afloramento, e principais áreas urbanas e vias de acesso. Modificado de Goldberg (2001) e CPRM (2006).

contexto a Formação Sanga do Cabral se mostra uma excelente contribuição para este conhecimento.

Porém, trabalhos de revisão avaliando rios de alta variabilidade modernos e do registro (Plink-Björklund, 2015; Fielding *et al.*, 2018; Hansford *et al.*, 2020) perceberam que estes ocorrem em uma grande variedade de climas, tendo a variabilidade de descarga uma dominância na modelagem da disposição das fácies dentro dos canais fluviais. Deste modo, para uma averiguação do clima no qual o rio se estabeleceu, faz-se necessário corroborar estas interpretações por outros meios (Zellman *et al.*, 2021). Neste contexto insere-se o segundo artigo desta tese, em que são avaliados os aspectos diagenéticos, e também outros aspectos relacionados ao paleoclima da formação.

Assim sendo, a presente tese constitui uma reavaliação e um aprofundamento do conhecimento do sistema sedimentar da Formação Sanga do Cabral, e as diferentes respostas e produtos deste sistema a mudanças nas condições ambientais.

2. Objetivo da pesquisa

O objetivo da presente pesquisa é reinterpretar a dinâmica e o ambiente sedimentar da Formação Sanga do Cabral sob a luz destes novos conhecimentos de estruturas supercríticas e de rios de alta variabilidade de descarga. Como objetivos específicos pode-se destacar:

- i) Redescrever a faciologia do Afloramento Estrada de Ferro Inacabada, um afloramento representativo da FSC, considerando os novos conhecimentos de estruturas supercríticas.
- ii) Descrever e interpretar estruturas sedimentares supercríticas.
- iii) Analisar a arquitetura das fácies e relações entre as mesmas.
- iv) Propor um modelo deposicional que abarque estas novas interpretações.
- v) Gerar um modelo a partir da caracterização petrográfica da gênese dos depósitos de intraclastos carbonáticos da formação
- vi) Reconstruir o contexto paleoclimático vigente durante a deposição da FSC, a partir da integração sedimentológica e petrográfica.

3. Estado da arte

O estado do conhecimento discutido no presente trabalho tem como principal elemento o presente estado da compreensão sobre a dinâmica de formas de leito geradas por fluxos supercríticos (onde o Número de Froude $Fr > 1$) e seus produtos deposicionais na forma de estruturas sedimentares (aqui referidas por 'estruturas supercríticas'). Compreensão das mesmas passa por interpretar sua hidrodinâmica, e seu processo de erosão do leito, transporte e deposição de sedimentos. Segue abaixo um comentário sobre a atual compreensão destas estruturas no contexto do conhecimento dos rios de alta variabilidade de descarga, e os modelos de fácies para o registro sedimentar.

Outros temas abordados são calcretes, paleosolos, e poeira eólica. Estes temas serão abordados em menor detalhe, havendo um foco em sua aplicação para o reconhecimento de ambientes áridos a semiáridos.

3.1. Formas de leito supercríticas e seus produtos sedimentares

Como comentado acima, formas de leito supercríticas e as estruturas sedimentares por elas geradas estão sendo melhor compreendidas somente nos últimos anos. Consequentemente, são relativamente pouco abordadas nos cursos de geologia. Por causa disso, considera-se próprio apresentar aqui uma os conceitos básicos relacionados a este tema.

3.1.1. Número de Froude e outros parâmetros

O Número de Froude é um parâmetro que em hidrodinâmica indica se um fluxo tem uma velocidade maior por inércia, ou por aceleração da gravidade. Tal relação é dada pela equação (1):

$$Fr = \frac{U}{\sqrt{gh}}$$

(1)

onde U é a velocidade do fluxo, g a aceleração da gravidade, e h a profundidade do fluxo. Para fluxos subaéreos em canais abertos, a profundidade do fluxo é a mesma da lâmina d'água.

Mas o que isso significa em termos práticos? Para melhor compreender a equação, consideraremos como a gravidade acelera um fluxo, o chão estando na horizontal (Figura 3A): quanto maior a coluna d'água (h), maior a pressão que as moléculas de água acima exercem sobre as moléculas de água abaixo. Chamaremos isso de velocidade de *escoamento* (U_{esc}).

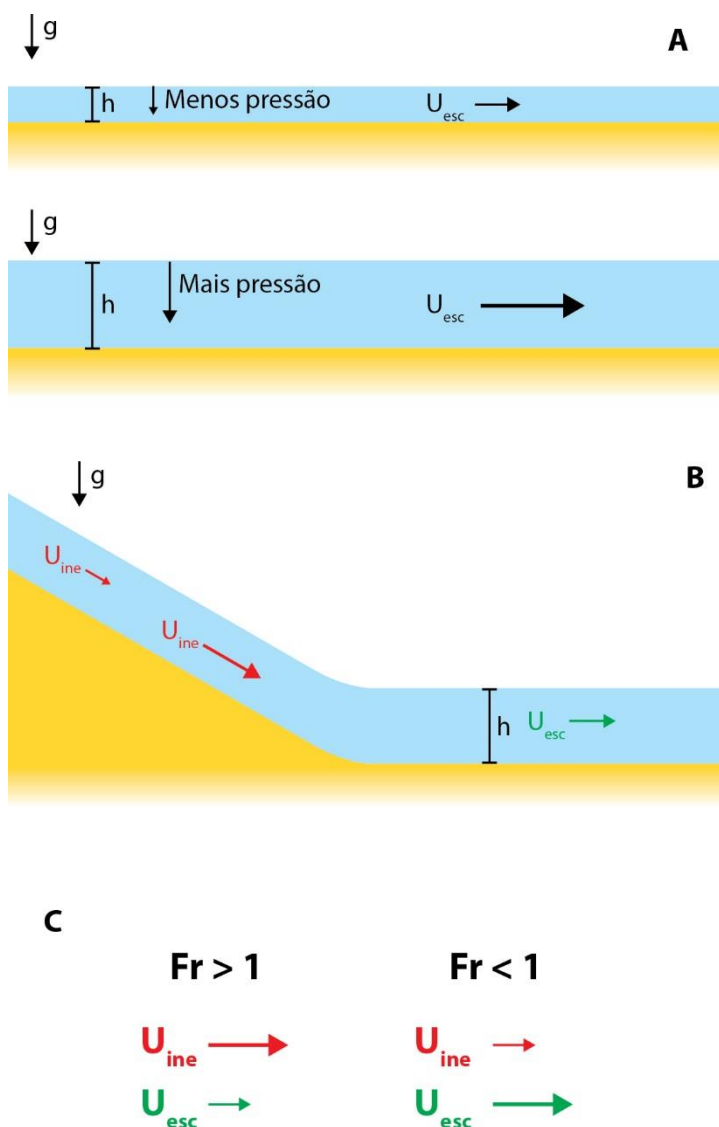


Figura 3. Ilustração conceitual dos parâmetros envolvidos no Número de Froude. **A)** Visualização conceitual da relação da profundidade da lâmina d'água e velocidade de escoamento do fluxo. **B)** Visualização conceitual do acúmulo de velocidade inercial, em contraste com a velocidade de escoamento, a qual depende apenas da profundidade. **C)** Abstração da resposta do Número de Froude à mudança da proporção entre as velocidades inercial e de escoamento em um fluxo.

Porém, um fluxo pode ter velocidade já acumulada por outra fonte. Por exemplo, advindo de uma bomba hidráulica, ou estar descendo um declive. Essa velocidade já acumulada chamaremos de velocidade de *inércia* ou *inercial* (U_{ine}). No exemplo da Figura 3B a velocidade inercial U_{ine} vai aumentando no declive por conta da gravidade.

O Número de Froude, então, nada mais é que uma relação entre a velocidade que o fluxo já tem em um determinado ponto (inercial, que é U na equação (1)), e a velocidade de escoamento. Mais especificamente, o termo \sqrt{gh} da equação (1) é a

velocidade de propagação de uma onda na superfície do fluxo, e é válido quando o comprimento de onda é consideravelmente maior que a profundidade (Lighthill, 1978). Esta propagação da onda na superfície é proporcional, ou seja, se correlaciona positivamente, com a velocidade de escoamento (U_{esc}).

Falando em outros termos e de modo simplificado, o Número de Froude representa “quanto volume de água está chegando neste determinado ponto” (U_{ine}), versus “quanto volume de água o sistema consegue escoar dali” (U_{esc}). Quando a velocidade inercial domina, $Fr > 1$; quando a velocidade de escoamento domina, então $Fr < 1$ (Figura 3C).

Outro parâmetro significativo, mas com uma relevância menor para a presente tese é o Número de Reynolds (2), que distingue entre fluxo laminar e turbulento (Robertson & Rouse, 1941):

$$Re = \frac{Uh}{\nu} \quad (2)$$

onde ν é a viscosidade cinemática do fluido. Quando $Re > 2000$, o fluxo passa de laminar a turbulento.

E, finalmente, o Número de Vedernikov (3), que demonstra a passagem de um fluxo estável para um instável (Chow, 1959):

$$Ve = xFr \quad (3)$$

onde x é um coeficiente que demonstra o quanto a velocidade do fluxo depende da sua profundidade, seu valor podendo ser 1/2 ou 2/3 (Cartigny *et al.*, 2014). O fluxo é estável quando $Ve < 1$ e instável quando $Ve > 1$. Isso implica que há uma transição de fluxo estável para instável quando Fr está entre 1,5 e 2. Em um fluxo estável, ondas na superfície tendem a dissipar-se, enquanto que em um instável, tendem a ampliar-se e quebrar.

3.1.2. Antidunas estáveis

Quando a velocidade do fluxo é aumentada e o Número de Froude se aproxima de 1, a superfície da água começa a formar ondulações, as quais causam a formação também de ondulações no leito, em fase com as da superfície (**Figura 4**; Kennedy,

1963). Estas ondulações no leito foram originalmente observadas tendo sedimentos depositados em sua face à montante, sendo simultaneamente erodidas à jusante, o que causa-as migrar contra o fluxo, e portanto receberam o nome de antidunas (Cornish, 1899; Gilbert & Murphy, 1914).

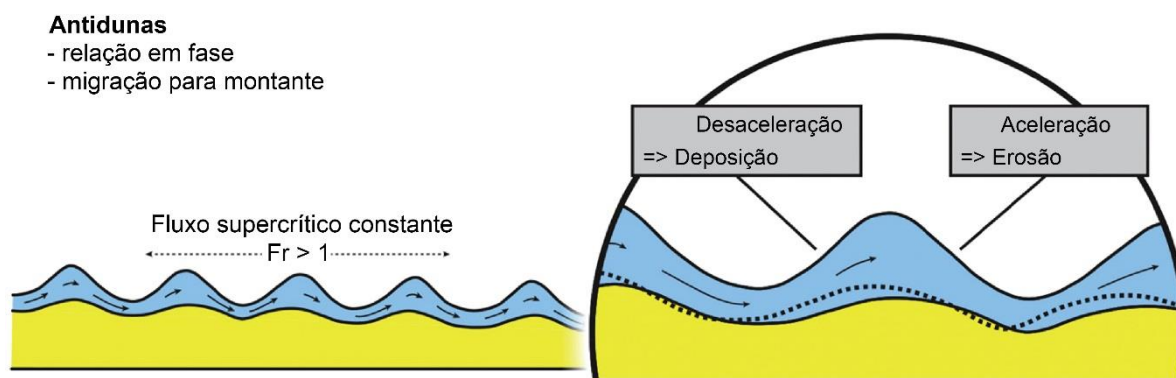


Figura 4. Antidunas estáveis, formadas sob fluxo supercrítico ($Fr > 1$). Modificado de Slooman & Cartigny (2020).

A formação das ondulações se dá, pois, como representado pelo Número de Froude se aproximando e ultrapassando 1, a velocidade inercial passa a dominar sobre a velocidade de escoamento. O volume de água ingressante no espaço então “empurra” o volume de água a sua frente, gerando ondulações.

Antidunas são estáveis em Números de Froude entre 0,84 e 1,77 (Allen, 1982), e podem migrar contra o fluxo, a favor do fluxo, ou manter-se imóveis e agradar (Kennedy, 1963). Quando migrando contra o fluxo, que é a dinâmica mais comum, o mecanismo de deposição ocorre pelo acompanhar do corpo d’água à ondulação do fundo. Quando o corpo d’água sobe a face posterior (à montante) da antiduna, o fluxo desacelera por ação da gravidade, e ocorre deposição (Figura 4). Isso causa também que a altura da lâmina d’água seja maior sobre a crista. Quando o corpo d’água desce pela face frontal, o fluxo volta a acelerar, e ocorre erosão. Assim a forma de leito migra para montante, depositando a típica estratificação cruzada contracorrente (**Figura 5A**).

Quando a razão entre profundidade e comprimento de onda se encontra abaixo de um valor crítico, a reação do corpo d’água em movimento não é mais a de inteiramente acompanhar a ondulação de fundo, mas é em parte acelerar ao se aproximar da crista da antiduna (**Figura 6**), de modo a manter a vazão constante. Esta aceleração em direção à crista da antiduna causa erosão da face posterior da crista, e deposição sobre a face frontal. Desse modo, a antiduna migra para jusante. Por sua vez, a

antiduna se manterá estática quando do equilíbrio entre estas duas condições e, caso o aporte sedimentar seja suficiente, sofrerá agradação.

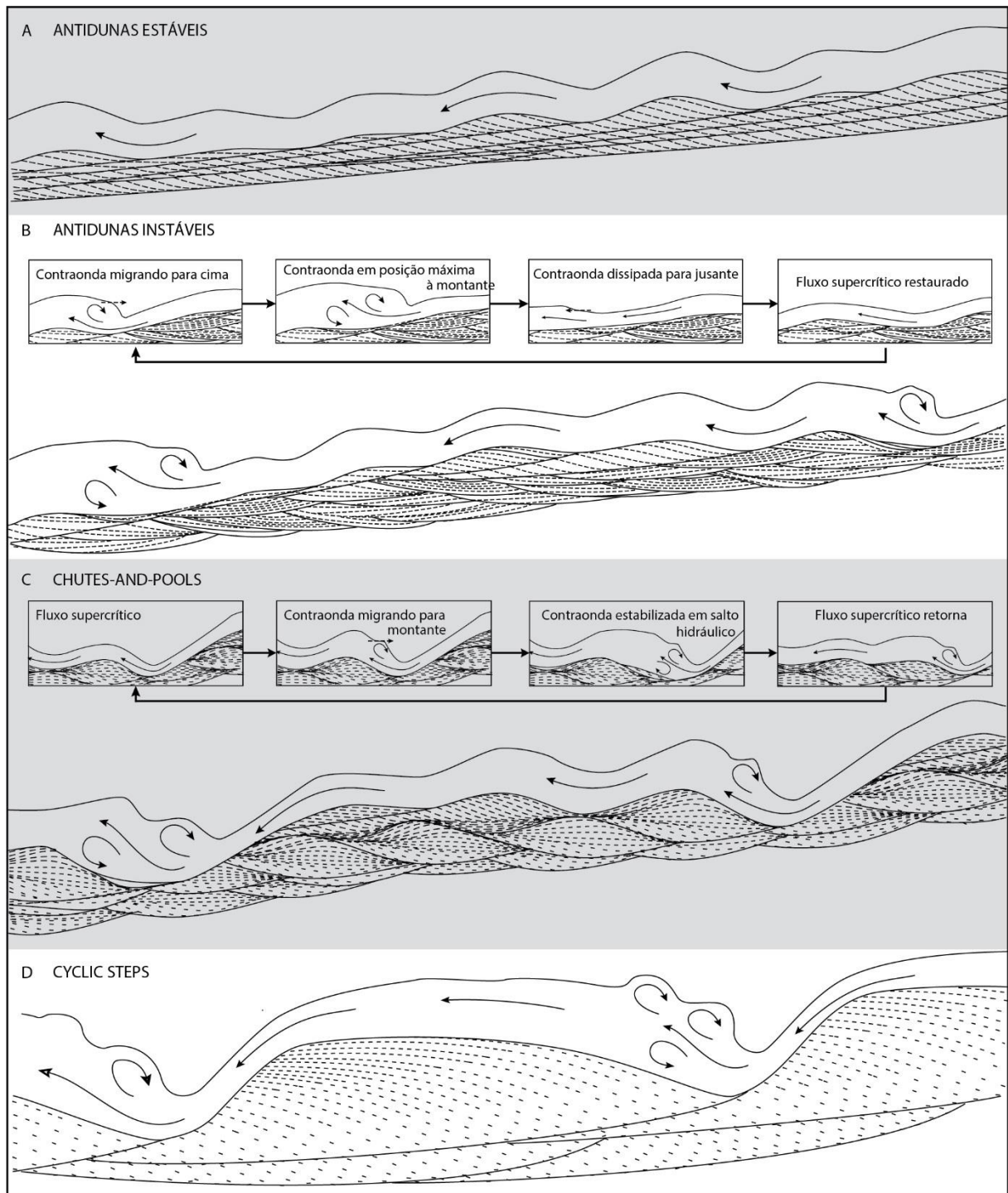


Figura 5. Panorama representativo idealizado de quatro estágios em fluxos supercríticos unidirecionais, correspondendo ao desenvolvimento de quatro tipos de configurações de leito. Fluxo da direita para a esquerda. Escala vertical exagerada para melhor clareza. Quadros adicionais para antidunas instáveis e *chutes-and-pools* ilustram a dinâmica associada ao processo. Modificado de Cartigny *et al.* (2014).

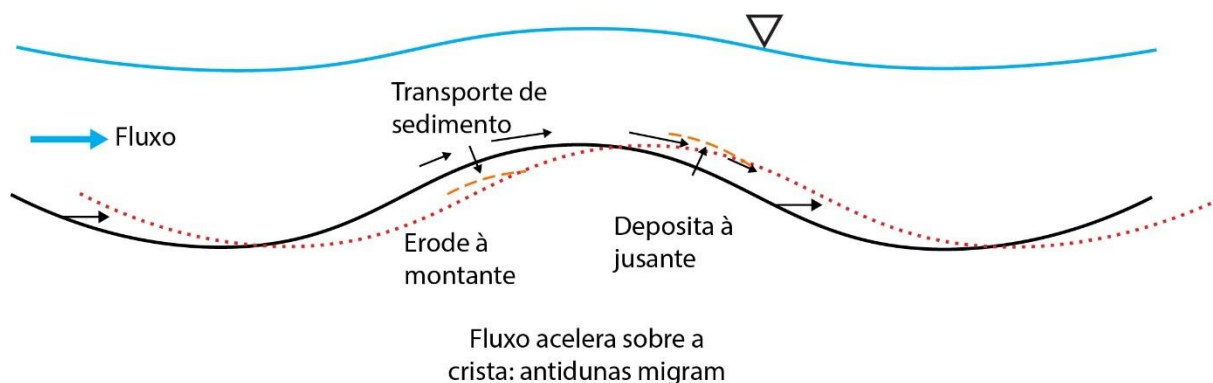


Figura 6. Comportamento do fluxo formativo da antiduna que migra à jusante. A superfície da água está em fase com a forma de leito, mas a variação de profundidade está fora de fase com o leito. Então, o fluxo acelera da depressão para a crista, causando erosão à montante e deposição à jusante, causando a forma de leito migrar à jusante.

3.1.3. Antidunas instáveis

Com o aumento do Número de Froude, as antidunas aumentam sua amplitude, até que as ondas de superfície acima delas atingem um ponto crítico e começam a quebrar (Michell, 1893) periodicamente (Gilbert & Murphy, 1914; Kennedy, 1963). A quebra da onda se dá para trás (à montante), e gera uma contraonda na superfície e aumento da profundidade da lâmina d'água; essa contraonda é pouco depois carregada para jusante (para frente), perdendo amplitude, e o fluxo supercrítico é então reestabelecido (Figura 5B; Gilbert & Murphy, 1914; Cartigny *et al.*, 2014).

Esta quebra da onda destrói a antiduna abaixo (Figura 5B; Kennedy, 1963), e pode gerar um leito plano, uma escavação erosiva, ou deposição no vale em frente à antiduna posterior (Kennedy, 1963; Cartigny *et al.*, 2014). Esta deposição gera, na maior parte das vezes, laminação côncava para cima, truncada (Alexander *et al.*, 2001; Yokokawa *et al.*, 2010), mas também pode gerar laminação cruzada de baixo ângulo, ou pode preservar a laminação contracorrente (Kennedy, 1960, 1963; Simons & Richardson, 1961; Guy *et al.*, 1966; Alexander *et al.*, 2001; Cartigny *et al.*, 2014). A repetição deste processo em condições de agradação gera depósitos lenticulares com repetidos truncamentos internos e entre as lentes (Figura 5; Yokokawa *et al.*, 2010; Cartigny *et al.*, 2014).

3.1.4. Chute-and-pool

Com continuação do aumento do Número de Froude, começam a ocorrer, em meio às ondulações, saltos hidráulicos (Simons & Richardson, 1961; Cartigny *et al.*, 2014). Saltos hidráulicos são locais onde o fluxo transiciona abruptamente de

supercrítico para subcrítico; neste ponto há um súbito aumento de profundidade e redução da velocidade do fluxo (Simons & Richardson, 1961; Cartigny *et al.*, 2014), e turbilhões sentido contracorrente (**Figura 7**).

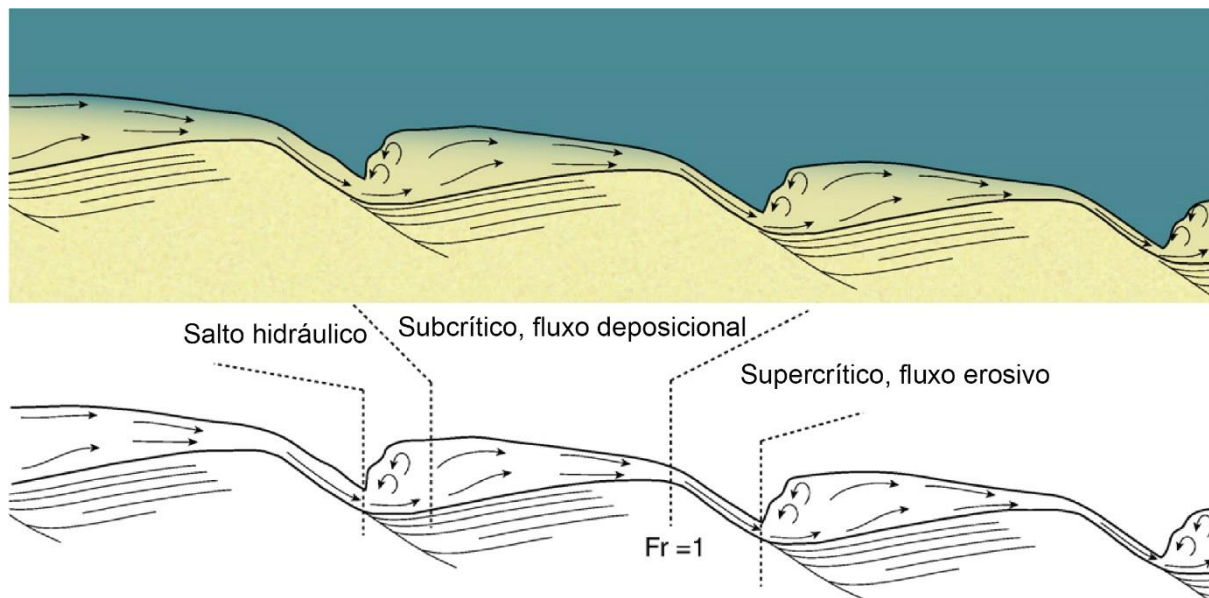


Figura 7. Representação idealizada de sucessivos saltos hidráulicos formando *cyclic steps*. O salto hidráulico opera igualmente no *chute-and-pool*, mas é isolado e efêmero. Modificado de Cartigny *et al.* (2011).

O salto hidráulico ocorre porque a velocidade inercial se torna muito superior à velocidade de escoamento (vide equação (1)). A diferença de velocidade é tão grande que o volume de água ingressante deixa de “conseguir empurrar” o volume de água à frente. Este volume de água à frente atua quase como se fosse um sólido imóvel, e o volume de água ingressante se espalha (parcialmente). Como há água para os lados e o leito abaixo, esta parte da água ingressante se desloca para cima e para trás, gerando o aumento de profundidade e os turbilhões contracorrente (Figura 5C Figura 7).

O salto hidráulico tem alto poder erosivo, gerando à sua montante uma superfície erosiva de alto ângulo, uma escavação abaixo, e põe em suspensão uma grande quantidade de sedimentos (Simons & Richardson, 1961; Alexander *et al.*, 2001; Cartigny *et al.*, 2014). Ele migra lentamente para trás (para montante), erodindo o que está abaixo e truncando as laminações à montante, o que gera uma depressão erosiva à frente (à jusante; Figura 5C, Figura 7; Cartigny *et al.*, 2014; Slooman *et al.*, 2021).

O sedimento em suspensão é rapidamente depositado à frente do salto hidráulico, comumente com laminação ondulada (Slooman *et al.*, 2021), e esta

deposição passa a diminuir a profundidade do fluxo à frente, reestabelecendo as condições supercríticas (pois Fr é aumenta com a diminuição da profundidade h , vide equação (1); Figura 5C), e fazendo o salto hidráulico desaparecer (Alexander *et al.*, 2001; Cartigny *et al.*, 2014). O processo então se repete.

O resultado da formação e desaparecimento do salto hidráulico é uma escavação erosiva assimétrica, com a face à montante mais íngreme, e a face à jusante mais suave. O fluxo passando sobre a face íngreme é supercrítico, enquanto à frente do salto, sobre a escavação, o fluxo é subcrítico, e vai acelerando à medida que sobe a face suave e a profundidade diminui, até tornar-se supercrítico novamente. A laminação do sedimento preenchendo a depressão tipicamente acompanha a face suave, gerando laminação cruzada contracorrente, mas sofrendo uma leve inflexão para cima ao chegar próxima à face íngreme (Figura 7). Estas laminações sofrem estrangulamento e truncamento ao chegar ao topo da face íngreme (Figura 7). À jusante, as laminações transicionam para ondulada (Slootman *et al.*, 2021), pois *chute-and-pools* tipicamente coexistem com antidunas instáveis (Figura 5C; Simons & Richardson, 1961; Alexander *et al.*, 2001; Cartigny *et al.*, 2014). Slootman *et al.* (2021) apresentam uma sequência de figuras, formando um filme, que ilustram em grande detalhe o processo formativo de um *chute-and-pool* com alta taxa de agradação, em seus materiais suplementares.

O preenchimento da depressão erosiva pode também depositar laminação côncava, ou maciça (Figura 5C Alexander *et al.*, 2001; Cartigny *et al.*, 2014). No caso de uma taxa de agradação não tão alta, a repetição do processo gerará uma série de lentes truncadas, preenchidas preferencialmente com laminação côncava ou contracorrente. A diferenciação de depósitos de *chute-and-pool* para antidunas instáveis pode ser difícil (Lang & Winsemann, 2013; Cartigny *et al.*, 2014).

3.1.5. Cyclic steps

Com o Número de Froude atingindo valores $Fr > 1,6$, os saltos hidráulicos param de ser extintos com a sedimentação na escavação, e tornam-se mais estáveis (Parker, 1996; Parker & Izumi, 2000; Cartigny *et al.*, 2014). Vários saltos hidráulicos se formam em sequência, gerando escavações assimétricas sucessivas (Parker, 1996). Eles migram para montante a velocidades relativamente constantes, mas ainda variáveis (Ono *et al.*, 2021). Deste modo, o fluxo que sobe a face suave de uma escavação e

vai se tornando supercrítico, logo inflete para baixo, gerando a face íngreme e erosiva da escavação à jusante, e encontrando o próximo salto hidráulico (Figura 5D, Figura 7). Esta configuração do leito assemelha-se a uma série de degraus, a qual é a origem do termo (Parker, 1996).

As antidunas instáveis e *chute-and-pools* são relativamente efêmeros porque o excedente do volume de água ingressante que não consegue ser escoado vai sendo dinamicamente acumulado no aumento da amplitude da onda, ou no aumento de profundidade gerado pelo salto hidráulico, com uma energia potencial, mas que consegue ser liberada. No caso dos *cyclic steps*, o excedente de energia entra em um ponto que não é possível que ela seja liberada pelo sistema, e portanto os saltos hidráulicos se estabilizam.

O resultado deposicional em cada escavação, em condições de aporte sedimentar moderado, é similar ao dos *chute-and-pools*, sendo preenchidas, por laminação cruzada contracorrente (Figura 5D, Figura 7). A recorrência causa as laminações à montante e à jusante da escavação sofrerem estrangulamento e truncamento (Figura 5D, Figura 7). Porém, a recorrência dos *cyclic steps* também gera a possibilidade de uma ampla miríade de estruturas possíveis, a depender da taxa de deposição (Slootman & Cartigny, 2020), e também dos sedimentos disponíveis (Ono *et al.*, 2021). Uma revisão de toda essa gama de variações está além do objetivo desta breve revisão, mas algumas destas possibilidades são interpretadas no primeiro artigo desta tese. A configuração que talvez seja a mais relevante de ser aqui citada é a de *cyclic steps* sob taxa de agitação moderadamente baixa (*cyclic steps* parcialmente deposicionais; Slootman & Cartigny, 2020), onde o salto hidráulico, ao migrar para trás, causa que a face íngreme de sua escavação eroda parte das laminações depositadas na face suave da escavação atrás (à montante). Deste modo a configuração fica de laminações contracorrente truncadas por faces íngremes (**Figura 8**).

Cyclic steps parcialmente deposicionais (deposição na face à montante > erosão à jusante)

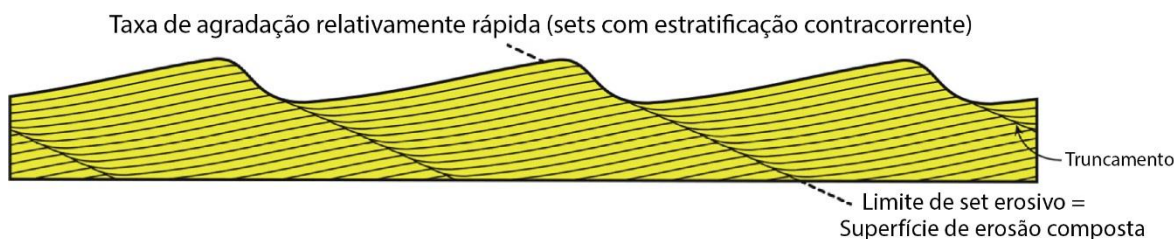


Figura 8. *Cyclic steps* parcialmente deposicionais, gerando laminações contracorrente truncadas. Modificado de Slooman & Cartigny (2020).

3.2. Rios de alta variabilidade

Como comentado no item 1, chegou-se a uma percepção de que rios perenes de altas latitudes estavam sobrerrepresentados na literatura, e que as tão-bem-estabelecidas classificações planiformes de rios (entrelaçado, meandrante e anastomosado) não representam efetivamente tipos diferentes de rios, já que o mesmo rio pode apresentar estas diferentes configurações (Brierley & Hickin, 1991; Fielding, 1993; Ethridge, 2011). Disso, implica-se que os presentes modelos de fácies, baseados em “pontos finais” destas classes planiformes, não têm poder preditivo (Brierley & Hickin, 1991; Ethridge, 2011; Nicholas *et al.*, 2016). Logo, faz-se necessário procurar outros parâmetros que condicionem a arquitetura faciológica de rios.

Com o aumento do estudo de rios de alta variabilidade, os quais ocorrem em regimes pluviais e climas variados (e.g., Tunbridge, 1981; Sneh, 1983; Abdullatif, 1989; Fielding & Alexander, 1996; North & Taylor, 1996; Alexander & Fielding, 1997; Tan & Plink-Björklund, 2021; Zellman *et al.*, 2021; Walker & Holbrook, 2022), notou-se que estes podem apresentar também uma gama de expressões sedimentares diferentes (Fielding *et al.*, 2009, 2018; Plink-Björklund, 2015; Hansford *et al.*, 2020).

As principais características de rios de alta variabilidade são: (1) litossomas de preenchimento de canal com base erosiva e transições laterais de fácies complexas, podendo ser lateralmente muito extensos; (2) litossomas formados por canais amalgamados; (3) arquitetura de fácies interna complexa, com poucas ou nenhuma macroforma; (4) partições lamosas abundantes, modificadas por pedogênese, ou pedogênese no topo de litossomas; (5) abundância a dominância de estruturas sedimentares de regime de fluxo superior, em especial transcíticas e supercíticas; (6) estruturas supercíticas transicionam diretamente para *ripples* cavalgantes ou para *drapes* de lama; (7) fósseis de vegetação dentro do canal, por vezes árvores *in situ*;

(8) bioturbação dentro do canal; (9) depósitos de lama dentro do canal; (10) abundância e/ou camadas espessas de conglomerados intraclásticos lamosos na base de canais e acima de superfícies de erosão internas; (11) abundante deformação sindeposicional (laminação convoluta, escape de água, etc.; Fielding *et al.*, 2009, 2018; Plink-Björklund, 2015)

Algumas destas características, como abundância a dominância de estruturas de regime de fluxo superior, são exclusivas de sistemas fluviais de alta variabilidade e ocorrem em todos. Outras, como a presença de vegetação no canal, em especial *in situ*, são exclusivas, porém não ocorrem em todos os rios ou depósitos. Já elementos como conglomerados intraclásticos lamosos, não ocorrem em todos os sistemas de alta variabilidade, nem são exclusivos destes (Plink-Björklund, 2015).

Plink-Björklund (2015) estudou a arquitetura de fácies de 17 rios de alta variabilidade modernos, e de 35 unidades geológicas com características sedimentares similares, e propôs quatro categorias de depósitos de rios de alta variabilidade. *Litossomas amalgamados com unidades espessas de inundação* são formados tipicamente por 80–100% de estruturas supercríticas com alta taxa de deposição e numerosos cortes erosivos, gerando corpos tabulares de aparência uniforme, amalgamados lateral e verticalmente. Sedimentos finos são raros, ocorrendo quase unicamente como clastos pelíticos em conglomerados intraformacionais, o que indica alta taxa de erosão de planícies de inundação e desmoronamento das margens. Escavações verticais e alteração pedogênica podem ocorrer em superfícies erosivas, o que indica longos períodos sem deposição. Estes litossomas ocorreriam em rios com alta variabilidade interanual, sem corrente perene (efêmeros). A descarga destes rios ocorreria toda em enchentes relâmpago catastróficas, que se iniciariam e acabariam extremamente rápido, mantendo-se pouco tempo em condições de regime de fluxo inferior. Estas enchentes seriam geradas por tempestades erráticas ou monções anormalmente fortes, que se abateriam em poucos ou em um único evento, com recorrência de alguns anos a décadas. Exemplos modernos seriam a Bacia de Kobo, na Etiópia, onde a pluviosidade é de 750 mm/ano, e a Península do Sinai (Egito) ou o Karoo (África do Sul), onde a precipitação é de menos de 100 mm/ano.

Litossomas com unidades de inundação variáveis apresentam unidades de inundação com estruturas supercríticas que podem ser sobrepostas por elementos de regime de fluxo inferior, como *ripples* e *drapes* de lama (Plink-Björklund, 2015).

Estruturas supercríticas ainda dominam, mas sua proporção é menor em relação aos litossomas amalgamados. Escavações em superfícies erosivas e alteração pedogênica nas camadas de pelitos podem também estar presentes, além de fragmentos macroscópicos de plantas. Estes depósitos também teriam sido gerados predominantemente por inundações de alta magnitude, mas a transição de estruturas de regime de fluxo superior para inferior e para camadas de lama indica um declínio menos abrupto da força do fluxo. Bioturbação e pedogênese dentro dos depósitos de canal e por toda a unidade de inundação indicam que o rio seria efêmero, enquanto estes elementos presentes apenas no topo do preenchimento dos canais indicam que haveria fluxo perene, mesmo que fraco. Exemplos modernos seriam rios no domínio de monção, onde precipitação pode exceder 1100–1600 mm/ano, até rios em regiões subtropicais áridas, com precipitações anuais médias de apenas algumas centenas de mm.

Litossomas com unidades de inundação e depósitos de regime de fluxo inferior apresentam alternância lateral e vertical de unidades de inundação e intervalos dominados por estratificação cruzada, onde estes últimos seriam resultado de fluxos perenes (Plink-Björklund, 2015). Estruturas supercríticas perfazem uma proporção consideravelmente menor dos depósitos, sendo ao redor de 50% das estruturas, e macroformas podem ser melhor desenvolvidas. Fragmentos de plantas são mais comuns, e bioturbação é mais variada que somente escavações verticais. Todas estas características indicam variação entre alta e baixa velocidade do fluxo e taxa de deposição, e a presença mais consistente e significativa de fluxos perenes, assim como uma redução mais gradual do fluxo de enchentes, e presença mais marcada de vegetação. Escavações e paleossolos em depósitos de canal, no entanto, significam que grande parte do(s) canal(is) estariam secos por grandes períodos de tempo. Exemplos modernos vão de rios em regiões de monção a rios em regiões subtropicais áridas com precipitação de apenas 100–150 mm. O pico de descarga nestes rios pode durar apenas alguns dias, e no restante do tempo dominariam condições de regime de fluxo inferior.

Litossomas com vegetação no canal apresentam variações laterais de fácies e arquitetura de fácies extremamente complexas, pois as estruturas formadas são afetadas por essa vegetação (Plink-Björklund, 2015). As plantas causam mudanças abruptas e complexas de litologia, estruturas sedimentares, e espessura e orientação de sets de acreção. Um exemplo moderno é o Rio Burdekin (Austrália), que se

encontra em região subtropical subúmida, e sofre inundações de alta magnitude durante o período monsonal com recorrência de 3–20 anos. Durante os longos períodos de seca, árvores, arbustos e outros tipos de vegetação crescem no canal, e passam a influir no fluxo durante as cheias.

Fielding *et al.* (2018) utilizaram como parâmetro para sua classificação o desvio-padrão exclusivamente da variação interanual do pico de descarga em rios modernos. Em outras palavras, o quanto o pico de descarga do rio a cada ano geralmente é maior do que a média das maiores descargas do ano. Ao comparar os depósitos modernos com o registro, dividiu os rios em três categorias: variação interanual baixa, média e alta/muito alta.

Rios de baixa variação interanual são similares aos modelos de fácies clássicos planiformes tão bem conhecidos na literatura (Fielding *et al.*, 2018). São dominados por estratificação cruzada em várias escalas junto a laminação cruzada de *ripples*, e laminação planar e de baixo ângulo subordinadas. Macroformas são comuns e bem desenvolvidas, como barras de acreção frontal e lateral. Esta configuração ocorreria porque os rios seriam um mosaico de vários eventos sucessivos, sem preservação de eventos excepcionais. Compõem esta classe tanto rios com baixa variação sazonal, como o Mississipi, quanto os de alta variação sazonal, porém que esta variação é constante entre anos, como o Rio Jamuna, nos Himalaias (dentro da zona de monções), ou o Rio Ob, na Sibéria (alimentado por água de degelo). Nota-se que esta classificação, e as estruturas indicadas como características para estes rios com alta variabilidade sazonal, estão em desacordo com os achados de Plink-Björklund (2015).

Rios de variabilidade interanual intermediária são formados por uma combinação de estratificação cruzada de regime de fluxo inferior, e também estruturas de regime de fluxo superior e supercríticas (Fielding *et al.*, 2018). Macroformas não se desenvolvem tão bem, e a influência de vegetação fixada em margens ou em barras colonizadas por plantas (mas não no canal) se torna muito mais significativa na interação com o fluxo do canal durante cheias. Nestes rios, depósitos de cheias não se destacam em meio à arquitetura sedimentar, indicando que a estratigrafia é um registro composto de eventos de variadas magnitudes. Seriam exemplos os Rios Calamus e Wabash nos EUA central.

Rios de variabilidade interanual alta e muito alta são formados por um amálgama de elementos de preenchimento de canal, onde estratificação cruzada pode ser um

constituente subordinado ou mesmo ausente, em favor de estruturas de regime de fluxo superior e supercríticas (Fielding *et al.*, 2018). Macroformas são conspicuamente ausentes, podendo ocorrer apenas localmente, e sendo de difícil reconhecimento quando ocorrem. Um elemento considerado significativo são grandes troncos carregados na corrente, ou mesmo *in situ*, e como interferem no fluxo e estruturas deposicionais. Variações laterais e verticais abruptas de fácies são comuns, assim como a preservação de camadas descontínuas de lama, modificadas por pedogênese. Estes seriam resultados de rios com pouca ou nenhuma corrente perene, em que eventos de grande magnitude que se abatem extremamente rápido causam as estruturas estarem fora de equilíbrio com o fluxo. Diminuição igualmente abrupta do fluxo causa as estruturas supercríticas não serem retrabalhadas pela duração do fluxo em regime inferior, e portanto que não se preservem. São exemplos destes os Rios Burdekin (Austrália, clima subtropical subúmido), Platte e Bijou Creek (EUA central, clima semiárido).

Hansford *et al.* (2020) fizeram uma revisão de estudos de classificações de rios modernos com base em variabilidade de descarga, e propõem que apenas um único parâmetro é insuficiente para fazer uma classificação própria. Combinam então vários parâmetros em análises estatísticas, e os comparam à classificação climática Köppen-Geiger com subtipos, chegando em quatro classes de rios. *Rios de hidrologia persistente* apresentam pouca variabilidade de descarga em condições de precipitação perene. A intensidade do fluxo aumenta e diminui lentamente ao longo da temporada chuvosa, sem grande diferença entre anos, e o pico de descarga dificilmente ultrapassa três vezes a descarga média. Estes ocorrem em florestas tropicais, sendo o melhor exemplo considerado pelos autores o Rio Paraná.

Rios com variabilidade controlada por tempestade única são rios de zonas temperadas, e rios frios que têm sua recarga em parte por água de degelo e em parte por precipitação (Hansford *et al.*, 2020). Estes são fortemente influenciados por tempestades singulares, que podem gerar descargas 5–40 vezes mais fortes que a média. Por conta dessa influência, apresentam marcada variabilidade interanual. Exemplos são os Rios Nottoway e Iowa (EUA).

Rios com hidrologia sazonal são rios de regiões de monções, degelo, e subtropicais úmidas (Hansford *et al.*, 2020). Rios nas duas primeiras regiões apresentam baixa variação interanual, enquanto rios de clima subtropical úmido apresentam alta variação interanual, pois apenas monções anormalmente fortes ou

ciclones tropicais causam intensa precipitação. Descarga máxima pode chegar a 50 vezes a vazão média. São exemplos o rio monsonal Chao Phraya (Tailândia), o rio de degelo Little Beaver (EUA), e o rio subtropical Caiapó (Brasil).

Rios com hidrologia extrema e errática são tipicamente de regiões áridas, com muito pouco ou nenhum fluxo fora de períodos de enchente (Hansford *et al.*, 2020). A hidrologia destes rios é errática, sendo controlada por tempestades irregulares de grande intensidade, que duram de algumas horas a alguns dias. Estas tempestades desencadeiam inundações relâmpago de grande magnitude, 100–1500 vezes maiores que a vazão média. Dependência destas tempestades erráticas gera enorme variação interanual, com o leito dos rios podendo permanecer seco por anos ou mesmo décadas. Citam como exemplo o Rio Smoky Hill (EUA).

Nota-se que a classificação de Hansford *et al.* (2020) não cita rios em zona subtropical subúmida, como é o caso do Rio Burdekin (Austrália). Considerando que este é um rio de alta variabilidade amplamente estudado e foi utilizado como base para um dos poucos modelos de fácies de rios de alta variabilidade presentes (Fielding *et al.*, 2009), esta parece uma omissão significativa. Também, um grande estudo de arquitetura de fácies nos rios estudados por Hansford *et al.* (2020) seria necessário para averiguar se há concordância entre esta classificação e os depósitos, para então serem comparadas ao registro.

Refinamentos destas classificações, e estudos que ponham à prova suas capacidades preditivas podem tornar-se um novo paradigma para a compreensão de sistemas fluviais e suas várias possibilidades de arquiteturas de fácies, substituindo a atual e obsoleta classificação planiforme (Ethridge, 2011; Nicholas *et al.*, 2016; Fielding *et al.*, 2018).

3.3. Calcretes freáticos

Calcrete é uma acumulação terrestre predominantemente de carbonato de cálcio, próxima à superfície (Wright & Tucker, 1991). Ocorrem de várias formas, de nodular a pulverulento, ou muito endurecido, sendo resultado da precipitação de carbonato em solo, sedimento ou rocha porosa, por processos de cimentação, substituição e deslocamento (Wright, 2007; Alonso-Zarza & Wright, 2010). Excluem-se dessa denominação carbonatos lagunares, porém carbonatos gerados em solos paludares

(peri-lagunares) são considerados calcretes (Wright & Tucker, 1991; Alonso-Zarza, 2003).

Tipos de ocorrências morfológicas de calcrete são (Wright & Tucker, 1991): (1) Solo calcário, que como o nome diz é um solo fracamente cimentado por carbonato; (2) Solo calcificado, 10–50% carbonato, com poucos nódulos; (3) Calcrete pulverulento, um corpo contínuo de pó de carbonato de cálcio, sem ou com poucos nódulos; (4) Calcrete pedotubular, onde todo ou quase todo o carbonato secundário forma incrustações ao redor de raízes ou outros tipos de túbulos; (5) Calcrete nodular, formado por concreções discretas maleáveis a muito endurecidas de solo/rocha cimentado e/ou substituído por carbonato. (6) Calcrete em favo-de-mel, formado por nódulos coalescidos, com áreas intersticiais de material menos endurecido. (7) Calcrete duro, um horizonte endurecido quase completamente carbonático, tipicamente com fábrica interna complexa, topo abrupto e base gradacional; (8) Calcrete laminar, formado por níveis tabulares endurecidos por carbonato, tipicamente ondulados; (9) Calcrete em blocos, originado da quebra de calcrete duro.

Wright (1990) dividiu a micromorfologia de calcretes em dois membros-finais em um contínuo: alfa e beta. A classificação se baseia resumidamente na presença ou ausência de elementos biogênicos. Fábricas alfa apresentam pouca ou nenhuma evidência de atuação biogênica, sendo caracterizadas por massas contínuas e amorfas de micrita, minerais euédricos grandes, variações locais de tamanho de cristal e hábito deslocante. Fábricas beta são dominadas por elementos biogênicos como rizoconcreções, tubos microbiais, fábrica alveolar septária, entre outras.

Calcretes são tipicamente associados com solos em ambientes quentes, que é sua ocorrência mais comum (Goudie, 1983), e onde se formam em horizontes típicos, muito bem conhecidos na literatura, com um desenvolvimento ascendente no perfil de solo (Wright & Tucker, 1991; Alonso-Zarza & Wright, 2010). Goudie (1973) aponta que, na maioria dos casos, a precipitação máxima na qual carbonatos ocorrem é 400–600 mm/ano, mas que em alguns casos pode ser bem maior, podendo ocorrer em locais com precipitação maior que 1.000 mm/ano. Como limite mínimo, o autor aponta a marca de cerca de 100 mm/ano, ponto no qual os carbonatos dos calcretes começam a ser substituídos por gipso.

Uma revisão ampla acerca de calcretes formados em solos estão além do escopo do presente trabalho, e podem ser encontradas em Wright & Tucker (1991), Alonso-Zarza (2003), Wright (2007), e Alonso-Zarza & Wright (2010).

Além de sua típica formação em solos, calcretes podem se formar também a partir do lençol freático. Na Austrália, por exemplo, calcretes com esta origem podem formar camadas de até 10 km de largura, 100 km de extensão, com uma média de 10 m de espessura (Arakel & McConchie, 1982). Eles são formados por cimentação intersticial, deslocamento e substituição de sedimentos em sistemas de aquíferos rasos (Alonso-Zarza & Wright, 2010). O principal mecanismo de precipitação é a evapotranspiração pelo calor da superfície, e o carbonato pode precipitar-se tanto na zona capilar, acima do lençol freático, como dentro dele (Wright & Tucker, 1991). Por essa necessidade de calor para a evaporação, calcretes freáticos ocorrem geralmente em ambientes áridos ou semiáridos, e a evaporação é insignificante em profundidades abaixo de 5m. Sua estrutura interna macroscópica é ausente de horizontes internos, porém tipicamente acompanham estratificações, camadas, superfícies erosivas, e outros tipos de estruturas sedimentares (Alonso-Zarza & Wright, 2010). Sua microestrutura é caracterizada pela ausência de elementos biogênicos, e portanto classifica-se na fábrica alfa de Wright (1990); a fábrica cristalina é frequentemente em mosaico, macro- ou microcristalino, com cristais variando de microns a milímetros, sendo influenciados pelo tamanho de poros da rocha cimentada (Wright & Tucker, 1991; Alonso-Zarza & Wright, 2010). Frequentemente também apresentam hábito deslocante, nódulos, e uma variedade de elementos de dessecação.

3.4. Paleosolos

Paleosolos, como o nome indica, são solos fósseis (Retallack, 2001). Paleossolos são de interesse estratigráfico pois representam paradas na sedimentação, permitindo a colonização por plantas ou outros tipos de modificações físicas, químicas ou biológicas sofridas por rochas expostas na superfície. Podem também formar-se caso a sedimentação seja lenta o suficiente para permitir estas alterações (Kraus, 1999). Por conta disso, paleosolos são frequentemente utilizados em estratigrafia como marcadores, pois comumente marcam um diastema ou discordância (Kraus, 1999; Retallack, 2001).

Os três principais tipos de elementos que permitem a identificação de um paleosolo são (1) fósseis ou marcas de raízes; (2) horizontes de solo; e (3) estrutura (Retallack, 1988). Fósseis de raízes são identificáveis por sua forma irregular alongada que se espalha e divide para baixo, sejam estes fósseis matéria orgânica, ou preenchimento posterior por sedimentos finos ou minerais precipitados (Retallack, 1988). Estes fósseis, porém, nem sempre estão presentes. Contudo, marcas de raízes podem ser reconhecidas por elementos indiretos. O metabolismo da planta causa alterações químicas no solo, o que pode favorecer alterações redox ao seu redor. Estas alterações podem propiciar precipitação de material ao redor da raiz, formando túbulos (rizotúbulos). Os materiais que mais comumente se precipitam ao redor de raízes são carbonato de cálcio e oxi-hidróxidos de ferro (Retallack, 1988). Em solos vermelhos oxidados, raízes podem gerar halos de cor mais amarelada, por haverem induzido redução bacteriana dos minerais. Esse processo pode também produzir manchas de minerais de ferro ou magnésio ao redor das raízes (Retallack, 1988).

Horizontes de solo são também uma característica marcante. O horizonte do topo deve estar abruptamente truncado por uma superfície erosiva, enquanto os contatos inferiores devem ser gradacionais. Suas características são similares às de horizontes de solos modernos, e cor pode ser um fator importante, de rápida e fácil identificação (Retallack, 1988).

Processos formativos de solo destroem estruturas da rocha original, por bioturbação por plantas e animais, sucessivos umedecimento e secagem, etc. (Retallack, 1988). A estrutura de solo que começa a se desenvolver são planos irregulares envolvendo agregados mais estáveis — cutans e peds, em terminologia de solo (Retallack, 1988). Cutans podem se formar por preenchimentos de rachaduras formadas no solo por argila infiltrada ou areia. Podem ser também planos ferruginizados, superfícies encrustadas com manganês, ou uma variedade de outras origens (Retallack, 1988). Compactação pode causar movimento ao longo de um cutan, gerando *slickensides* (superfícies estriadas por movimento). Concentrações locais endurecidas de minerais (geralmente agregados calcários, ferruginosos, ou sideríticos) são também comuns (Retallack, 1988).

3.5. Poeira eólica

Poeira eólica pode ser definida como partículas que podem ser transportadas em suspensão por um gás, e no caso da atmosfera terrestre, têm dimensões menores do que 100 μm (Pye, 1987). No caso de partículas transportadas a longas distâncias, a maioria tem menos de 10 μm , e grande parte é menor que 2 μm . Depósitos de poeira eólica (loess) são geralmente compostos por partículas de 10–50 μm que não foram transportadas por grandes distâncias (Pye, 1987).

A principal fonte de poeira atmosférica maior que 2 μm é a deflação de sedimentos e solos, geralmente oriundas de regiões áridas ou sazonalmente áridas (Pye, 1987). A produção de partículas se dá por cominuição e abrasão de grãos maiores, principalmente por processos físicos (Pye, 1987; Li *et al.*, 2020), mas agregados de argila tamanho silte podem ser contribuições importantes (Jeong, 2008). Quartzo, feldspato e micas são ubíquos, enquanto a presença de argilominerais e outros tipos de minerais dependerá da área-fonte. Por exemplo, Chester *et al.* (1972) identificou que poeira advinda de regiões tropicais úmidas da África contêm mais caulinita e esmectita, enquanto regiões desérticas do Saara e da Namíbia são mais ricas em illita. A concentração de carbonato é muito variável, e pode ser uma importante fonte deste componente para solos (Alonso-Zarza & Wright, 2010).

Poeira eólica, para ser efetivamente depositada e incorporada ao registro sedimentar, necessita de um mecanismo de captura, seja uma planície úmida, com vegetação, ou adjacente a uma barreira (Pye, 1987; Li *et al.*, 2020). Isso significa que estes sedimentos, em muitas situações, passam por locais de acumulação temporária, e podem ser novamente transportados caso o mecanismo de captura desapareça (e.g., perda da cobertura vegetal; Li *et al.*, 2020). Isso implica que poeira eólica frequentemente apresenta modificações pedogênicas ou eodiagenéticas destes locais de acumulação temporários, como argilas autigênicas em agregados ou como cutículas (Singer, 1988; Jeong, 2008; Jeong *et al.*, 2011).

4. Materiais e métodos

4.1. Ortofotos e arquitetura de fácies

Um veículo aéreo não-tripulado (“drone”) foi manualmente operado de modo a tirar fotos do afloramento, a altura e distância constantes. Estas fotos foram utilizadas

para criar um modelo virtual em três dimensões de alta resolução do afloramento (3,58 mm/pixel) utilizando o método *Structure From Motion Multi View Stereo* (SFM-MVS; James & Robson, 2012) no programa Move®. Deste modelo, duas imagens ortogonais (ortofotos) aos paredões da exposição do afloramento foram geradas.

Estas ortofotos foram impressas e plastificadas. Sobre estas imagens as estruturas sedimentares, sua arquitetura e sua inter-relação foram desenhadas segundo o método de Miall (1985, 2016). Vários perfis colunares em escala 1:50 foram confeccionados ao longo do afloramento, num total de 76,1 m, para uma descrição mais detalhada das fácies, em especial aquelas com estruturas muito pequenas para a serem propriamente representadas nas ortofotos. Descrição das rochas incluiu granulometria, textura, cor, estruturas sedimentares, composição geral, contatos basais e de topo das camadas, forma externa e variações laterais das camadas, e, quando presentes, fósseis e modificações diagenéticas ou pedogenéticas observáveis macroscopicamente. O conjunto destes dados foi então usado para interpretações de processos sedimentares e suas inter-relações, e seu ambiente sedimentar, segundo o método de análise de fácies (Dalrymple, 2010; Miall, 2016).

4.2. Petrografia

Vinte amostras foram recolhidas de posições estratigráficas variadas para a confecção de lâminas delgadas e análise petrográfica. Houve um foco em rochas de siltito a arenito fino maciços ou fracamente laminados, que apresentam nódulos carbonáticos em um mesmo nível, e nos conglomerados intraformacionais e seus intraclastos carbonáticos, para fins de comparação. As amostras foram processadas pela empresa PetrografiaBR®, seguindo procedimento padrão. Elas foram serradas para separar um pequeno bloco, então impregnadas com resina epóxi azul, de modo que ficassem mais resistentes, e que os poros ficassem destacados em lâmina. A seguir as amostras foram coladas também com resina a uma lâmina de vidro de 27 x 46 x 2 mm, e então desgastadas até a espessura de 30 µm.

A descrição microscópica foi feita com um microscópio Zeiss Axio, e fotomicrografias foram feitas com uma câmera AxioCam MRc acoplada ao microscópio. A análise petrográfica se deu de modo qualitativo, por identificação dos minerais presentes nas lâminas por suas propriedades óticas. Incluiu-se descrição da textura, composição detrítica, composição diagenética, e classificação e interpretação

de proveniência. As amostras analisadas foram classificadas em um diagrama ternário de primeira ordem a fim de separar os diferentes grupos composicionais, e então classificadas textural e composicionalmente de acordo com Folk (1981).

4.3. Difractometria de raios-X

Cinco amostras foram estudadas no Laboratório de Difractometria de Raios-X da UFRGS utilizando o método orientado. Estas foram quarteadas e desagregadas primeiramente com almofariz e pistilo de porcelana, formando um pó. Foram então mais finamente desagregadas por agitação durante 14 horas em um agitador orbital, e após por ultrassom de ponteira durante cinco minutos com a amostra em solução. A temperatura foi então estabilizada para controle da viscosidade do fluido. A fração < 4 mm foi separada por decantação normal. O tempo de decantação foi calculado pela Lei de Stokes em 1 h 12 min 51 s. A fração separada foi em seguida orientada em lâmina delgada por pipetagem.

Neste processo privilegiam-se as faces (001) para a identificação de argilominerais, chamando-se esta amostra de *orientada natural*. Para verificação da existência de argilominerais expansivos, parte da amostra orientada natural foi saturada em etileno glicol, sendo então chamada amostra *glicolada*. Parte também da amostra orientada natural foi aquecida a 550° C durante duas horas para avaliar argilominerais que colapsam sua estrutura nestas condições (e. g., argilominerais do grupo das caulinitas), permitindo uma identificação mais precisa. Esta é chamada amostra *calcinação*.

O difratômetro utilizado é um BRUKER AXS modelo D-5000 da marca Siemens, equipado com tubo de ânodo fixo de Cu K α ($\lambda = 1,5406 \text{ \AA}$), operando a 40 kV e 30 mA no feixe primário e monocromador curvado de grafite no feixe secundário. As amostras orientadas naturais e as calcinadas foram analisadas no intervalo angular de 3 a 32° 2 θ em passo de 0,02°/2 s, utilizando-se fendas de divergência e anti-espalhamento de 2 mm e 0,2 mm no detector. Para as amostras glicoladas, foi utilizado um passo de 0,02°/3 s, enquanto demais parâmetros se mantiveram em relação aos outros tipos de amostras.

4.4. Microscopia Eletrônica de Varredura (MEV) e Espectrometria de Energia Dispersiva (EED)

O MEV permite a geração de imagens por elétrons secundários (IES) e por retroespalhamento de elétrons (REE). As imagens geradas por IES permitem observar o formato em três dimensões dos minerais, com um aumento até de mais de 2.000 vezes. Isto é ideal para observar as relações entre os minerais, seu hábito e relevos em sua superfície. Já as imagens geradas por REE permitem a utilização, em lâminas delgadas, do EDS, o qual detecta a composição química qualitativa de pontos específicos.

Para tais fins, cinco fragmentos de amostras, com suas respectivas lâminas delgadas, foram metalizados, sendo pulverizados com carbono metálico. As análises se deram no Laboratório de Geologia Isotópica (LGI) da UFRGS, com um microscópio eletrônico modelo Jeol 6610-LV, e um espectrômetro de energia dispersiva modelo Bruker XFLASH 5030.

5. Contexto geológico da área

5.1. Bacia do Paraná

A Bacia do Paraná é uma extensa depressão na região centro-sudeste da América do Sul, preenchida por rochas sedimentares e vulcânicas de idades Neo-Ordovicianas a Eocretácicas (Figura 2, **Figura 9**). Abrange uma área aproximada de 1.500 km², distribuídos por Brasil (1.000.000 km²), Paraguai (100.000 km²), Uruguai, onde é conhecida por Bacia Norte (100.000 km²), e Argentina, onde é comumente tratada como uma bacia diferenciada e denominada Bacia do Chaco-Paraná (400.000 km²) (Schneider *et al.*, 1974; Milani & Thomaz Filho, 2000; Milani *et al.*, 2007). É classificada como intracratônica (Milani, 2004), e Milani (1997) relacionou seu preenchimento a seis ciclos de subsidência gerados em resposta a esforços orogênicos compressivos na borda sul-ocidental do Gondwana. Este autor dividiu então o pacote de rochas em seis supersequências (sequências deposicionais de segunda ordem *sensu* Vail *et al.*, 1977) limitadas por discordâncias regionais, nomeadas Rio Ivaí, Paraná, Gondwana I, II e III, e Bauru (Figura 9).

Mais recentemente, mais unidades foram reconhecidas (e.g., Reis *et al.*, 2019, 2022), e Scherer *et al.* (2023) identificaram que diferentes sequências Permo-

Mesozóicas foram depositadas em distintos depocentros, com diferentes mecanismos de subsidência, e diferente morfologia de bacia. Deste modo, consideraram que a “Bacia do Paraná” na verdade corresponde a uma sucessão de bacias ou bacia sucessora, significando que a deposição dos sedimentos se deu em diferentes bacias sedimentares que ocupavam a mesma área geográfica.

Zerfass *et al.* (2003, 2004) identificou discordâncias regionais, e separou a Formação Sanga do Cabral da Supersequência Gondwana I. Considerou, então, esta unidade como uma supersequência separada (Figura 1), que será melhor comentada abaixo.

5.2. Formação Sanga do Cabral

A Formação Sanga do Cabral foi definida por Andreis *et al.* (1980) para denominar os conglomerados intraformacionais e arenitos finos a grossos, vermelhos, com

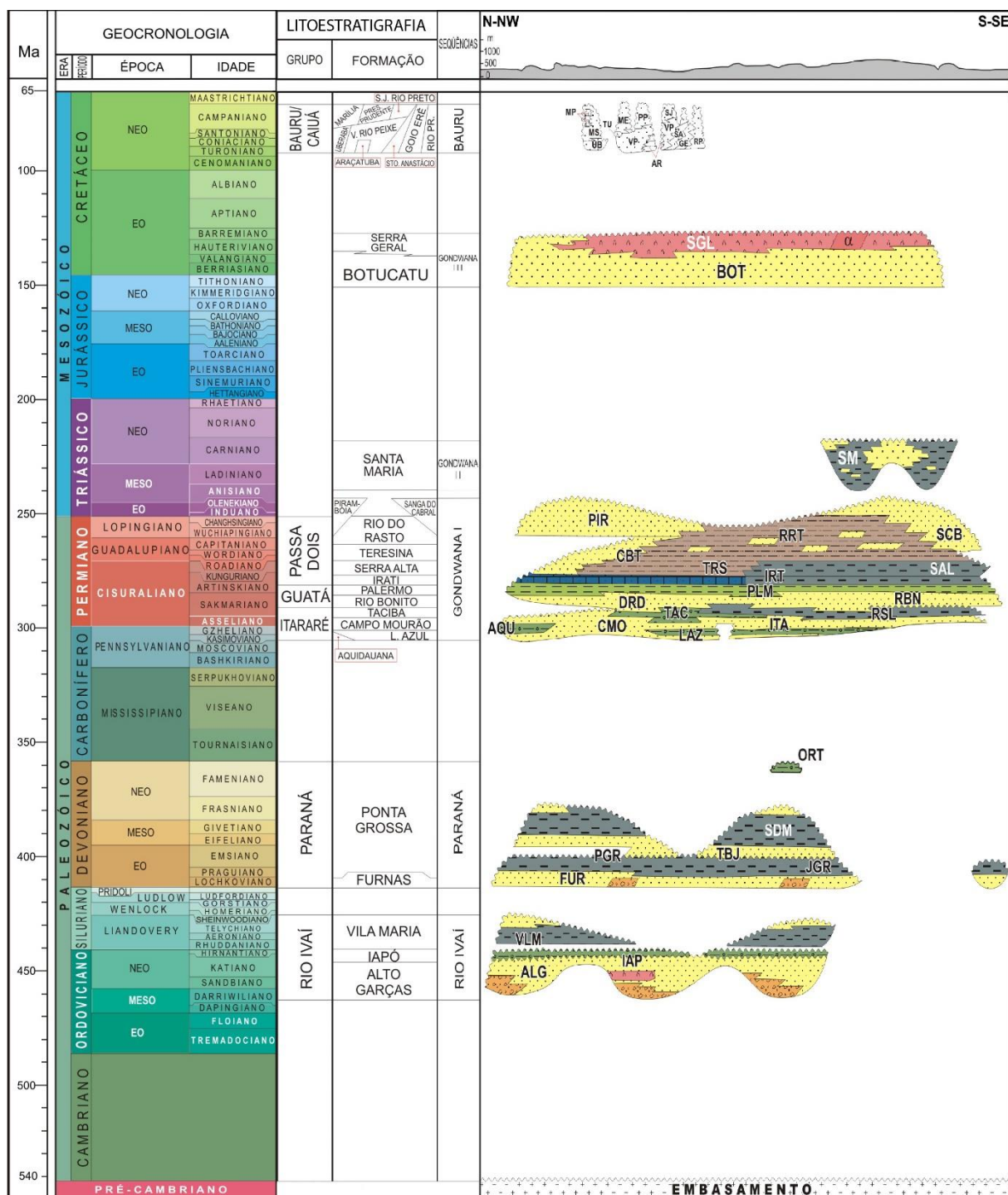


Figura 9. Carta cronoestratigráfica da Bacia do Paraná de Milani *et al.* (2007), mostrando a distribuição espacial e temporal das formações litoestratigráficas e das seis supersequências.

abundantes estratificações cruzadas acanaladas e tangenciais, ocorrendo estratigraficamente acima das unidades permianas da Bacia do Paraná e abaixo da Formação Santa Maria, dotada esta última de fósseis do Meso- a Neotriássico no Rio Grande do Sul. Foi por estes autores interpretada como depositada em ambiente fluvial meandrante com alta taxa de avulsão. Faccini (1989, 2000) interpretou a formação como rios entrelaçados efêmeros, ou uma "planície de entrelaçamento",

comparável a um sistema do tipo "Bijou Creek", e relacionou esse sistema a dunas eólicas subjacentes, considerando estas últimas como a base da formação. O autor também interpreta depósitos finos maciços ou com ondulações ascendentes como originados por "lobos de suspensão" de alta carga suspensa em lagoas efêmeras.

Lavina (1991) relacionou o sistema eólico na base da FSC à Formação Pirambóia, presente no norte da Bacia do Paraná, mas identificou um possível hiato de cerca de 4 milhões de anos entre as dunas eólicas e o sistema fluvial. No entanto, ainda manteve ambos na mesma formação litoestratigráfica. Estes arenitos eólicos passaram a ser tratados separadamente da FSC em trabalhos subsequentes, sendo designados por Formação Pirambóia. Scherer *et al.* (2021, 2023) identificam que o intervalo eólico deve constituir uma unidade estratigráfica independente, denominada Formação Buena Vista, como uma continuação do membro superior da unidade homônima uruguaia, formado por arenitos eólicos, denominado Membro Cerro Conventos (*sensu* de Santa Ana *et al.*, 2006).

A FSC passa então a ser considerada como composta apenas pelos níveis associados aos conglomerados intraformacionais. Zeffass *et al.* (2003, 2004), considerando o hiato de 4 M.a. entre o pacote eólico e o fluvial, identificou discordâncias regionais limitando a FSC, e do propôs a Supersequência Sanga do Cabral, separando-a geneticamente das outras sucessões da bacia.

Análises petrográficas realizadas por Zeffass (1998) e Zeffass *et al.* (2000) dos intraconglomerados e arenitos com estratificação cruzada tangencial associados revelaram uma média de tamanho de grão grosso a muito grosso com empacotamento sempre normal, e predomínio de contatos flutuantes. Clastos pelíticos chegam a perfazer 15% da rocha, sendo normalmente 10%. O cimento é principalmente carbonático eodiagenético e a porosidade é majoritariamente secundária, gerada durante a telodiagênese. Análise de proveniência revelou que materiais de reciclagem têm mais importante participação que materiais de primeiro ciclo, tendo sido fornecidos principalmente por um interior cratônico estável, sem significativas reativações. O ambiente deposicional foi interpretado como uma ampla planície aluvial por onde corriam fluxos efêmeros desconfiados ou fracamente confinados, ocorrendo provavelmente sob um regime de eventos de "inundações relâmpago" (*flash floods*) em clima árido a semiárido, o que geraria preferencialmente os elementos arquiteturais extensos e pouco espessos. Estas enchentes criariam corpos d'água temporários onde se depositaria lama. A baixa ocorrência de depósitos

finos e a abundância de intraclastos pelíticos, somados à predominância de clastos de reciclagem e a ocorrência de fósseis apresentando evidências de retrabalhamento (desarticulação e fragmentação), foram interpretados como o resultado de baixas taxas de criação de espaço de acomodação (Lavina, 1991; Faccini, 2000; Zeffass *et al.*, 2003).

Os fósseis da FSC são, em sua maioria, encontrados em meio aos conglomerados intraformacionais, desarticulados e fragmentados. Porém, recentemente, fósseis em melhores condições têm sido encontrados em meio aos arenitos finos com estratificação plano-paralela (Dias-da-Silva *et al.*, 2017). Procolofonidae é o grupo mais comum na Formação, ocorrendo principalmente de modo fragmentário. Os espécimes previamente descritos *Procolophon pricei* (Lavina, 1983) e *Procolophon brasiliensis* (Cisneros & Schultz, 2002) foram sinonimizados a *Procolophon trigoniceps* (Cisneros, 2008). Na Bacia do Karoo, Botha & Smith (2006) em trabalho minucioso de coleta, constataram a primeira ocorrência de *Procolophon* somente 116 m acima do Limite Permo-Triássico, sendo que o mesmo táxon só se torna comum a partir dos 160 m, ponto a partir do qual passa a ser abundante, até o início da próxima biozona. Nesta porção superior, dominada por *Procolophon*, *Lystrosaurus* se torna muito raro ou mesmo ausente (Figura 10; Neveling *et al.*, 1999; Botha & Smith, 2006). Esta variação foi chamada de “zona de abundância de *Procolophon*” por Botha & Smith (2006), sendo por estes autores considerada de idade Olenekiana. Mesmo que de um modo menos preciso, esta distribuição desigual dos procolofonídeos já era percebida desde o início do século XX (Neveling *et al.*, 1999) e, portanto, a ocorrência (abundante) desse táxon na FSC, desde o início, já sugeria a ausência da porção mais basal do Triássico no RS.

Outros grupos fósseis ocorrem na FSC, embora menos representados. Registros de elementos pós-cranianos de Cynodontia, duas *stapes* isoladas atribuídas a *Lystrosaurus* e um fragmento craniano de *Pareiasaurus* são fragmentários e dúbios, sendo todos mais recentemente reinterpretados como restos de procolofonídeos por Dias-da-Silva *et al.* (2017). Registros de arcossauromorfos são também limitados, apesar de um crânio em bom estado de preservação ter permitido a proposição da espécie *Teyujagua paradoxa* (Pinheiro *et al.*, 2016).

Restos de Temnospôndilos são comuns como fragmentos, com vários espécimes tendo sido atribuídos a Stereospondyli, Rhytidosteidae, Mastodonsauroidea e Plagiosterneninae (Dias-da-Silva *et al.*, 2017). Espécies

formalmente descritas são o rhytidosteídeo *Sangaia lavinae* (originalmente *Cabralia lavinae*; Dias-Da-Silva *et al.*, 2006, modificado por Dias-Da-Silva & Marsicano, 2011) e o capitossauróide *Tomeia witecki* (Eltink *et al.*, 2017). Estes dois táxons, mais o material atribuído a um Plagiosterneninae indeterminado, foram considerados por Dias-da-Silva *et al.* (2017) como indicando idade Eotriássica.

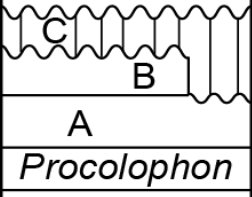
LITOESTRATIGRAFIA		Zonas de Assembleia Reconhecidas	Subdivisões Estratigráficas Propostas
TRIÁSSICO	"STORMBERG"		
	SUBGRUPO TARKASTAD	FM. BURGERSDORP	<i>Cynognathus</i>
		FM. KATBERG	<i>Lystrosaurus</i>
PERMIANO	SUBGRUPO ADELAIDE	FM. BALFOUR Mb. Palingkloof Mb. Elandsberg Mb. Barberskrans Mb. Daggaboersnek	<i>Dicynodon</i>
			

Figura 10. Quadro bioestratigráfico da Bacia do Karoo mostrando a proposta "zona de abundância de *Procolophon*" na porção superior da Zona de *Lystrosaurus*. Modificado de Rubidge (2005).

Piñeiro *et al.* (2015) descreveram vértebras dorsais com arcos neurais inchados e pós-zigapófises expandidas lateralmente como possivelmente atribuíveis a seymouriamorfos ou diadectomorfos. Isto indicaria uma idade permiana ou permotriássica para a FSC, unindo esta unidade à sequência neopermiana subjacente, uma proposição que foi criticada por Dias-da-Silva *et al.* (2017).

6. Resumo dos resultados

Esta tese apresenta uma redescrição da sedimentologia da Formação Sanga do Cabral, sob à luz de novos conhecimentos de processos sedimentares e sistemas fluviais. No primeiro artigo, estes novos conhecimentos acerca de estruturas supercríticas permitiram uma interpretação mais refinada do regime hídrico, e

processos sedimentares atuantes. No segundo artigo, fez-se a corroboração das interpretações de clima, porque, como visto na seção 3.2, as estruturas apontam regime hídrico, mas não clima. Em adição, este segundo artigo revelou aspectos não abordados por trabalhos anteriores: a dinâmica de retrabalhamento do sistema sedimentar e seus calcretes, e a presença de paleosolos e poeira eólica, todas características relacionadas a um clima árido.

Como uma contrapartida aos novos conhecimentos que contribuíram para este trabalho, a arquitetura de fácies interpretada e as características associadas ao sistema contribuem para nosso conhecimento sobre sistemas fluviais de alta variabilidade de descarga. Estes dados adicionam-se à construção desse possível novo paradigma de classificação e interpretação de sistemas fluviais. Particularmente, algumas das descrições de processos formadores de estruturas não existiam na literatura.

6.1. Estilos fluviais supercríticos e a aridez oscilante no Eotriássico: o exemplo da Formação Sanga do Cabral, Bacia do Paraná, Brasil

Este estudo reinterpreta as estruturas sedimentares da Formação Sanga do Cabral como sendo em sua maioria supercríticas, e identifica três Estilos Fluviais (EF). O EF1 consiste predominantemente em arenito fino maciço, com interrupções de conglomerados intraclásticos e, ocasionalmente, laminação tênue e níveis de intraclastos de lama. É interpretado como depositado por fluxos não confinados na parte distal de um sistema fluvial, gerando fluxos hiperconcentrados que resultaram em camadas finas de arenito fino com estrutura maciça ou laminação planar e antidunas incipientes. Este seria o estilo fluvial em condições mais secas, com precipitação ao redor de 300–355 mm/ano.

O EF2 foi depositado por enchentes relâmpago que ocorreram repetidamente em um curto período durante uma estação úmida. Isso resultou em uma sucessão de conglomerados intraclásticos com estruturas supercríticas, passando por arenitos com estruturas supercríticas, e terminando com estratificação cruzada sigmoidal e marcas de *ripples* com laminação difusa. Este seria o estilo fluvial com maior precipitação, cerca de 1100–1600 mm/ano.

O EF3 foi depositado por enchentes relâmpago catastróficas caracterizadas por alta descarga e velocidade de fluxo, possivelmente geradas por tempestades

erráticas, que se abateram em eventos únicos. Esses fluxos catastróficos geraram antidunas arenosas em grande escala e outras formas de leito supercríticas com intraclastos de lama, depositando arenito em laminações onduladas e outras estruturas de fluxo supercrítico. Essas enchentes diminuíram rapidamente, sobrepassando o campo de estabilidade das formas de leito de regime de fluxo inferior. Uma possível estimativa de precipitação anual é de aprox. 750 mm/ano.

Medidas tiradas das estratificações onduladas, interpretadas como depósitos de antidunas, permitiram a estimativa da velocidade e profundidade do paleofluxo. As maiores antidunas tem um comprimento de onda máximo estimado de 28,92 m (média de 15,4 m) e altura máxima estimada de 1,42 m (média de 0,85 m), resultando em uma velocidade do paleofluxo estimada de até 6,72 m/s (média de 4,9 m/s) e uma profundidade do fluxo máxima de 1,59 m (média de 0,9 m). Esses parâmetros são comparáveis aos observados em enchentes fluviais modernas.

6.2. O papel de calcretes em conglomerados intraformacionais multi-cíclicos de um sistema fluvial dominado por estruturas supercríticas, com contribuição de poeira eólica (Eotriássico, Bacia do Paraná, Brasil)

Este trabalho utiliza de petrografia, microscopia eletrônica de varredura, espectroscopia por dispersão de elétrons, e difratometria de raios-X para realizar uma análise integrada dos sedimentos da Formação Sanga do Cabral. Foram reconhecidas evidências petrográficas de incipiente pedogênese (marcas de raízes, óxidos de Mn-Ba, camadas mistas de E/I — aridisol), enfatizando a ocorrência de períodos relativamente longos de não-deposição.

Identificação da precipitação de oxi-hidróxidos de ferro permitiu a interpretação dos calcretes como originados de água subterrânea, indicando alternância de períodos úmidos e secos e baixo relevo. Permitiu também estimativas de precipitação em torno de um mínimo de 100 mm/ano (pela ausência de evaporitos como gesso), e um máximo de cerca de 400–600 mm/ano (máximo geral de chuvas para calcretes).

Descrição dos intraclastos cimentados por carbonato gerou uma interpretação da natureza multicíclica e autofágica dos depósitos, indicando que apesar de sua alta energia, o sistema era distal, e assim esses depósitos de alta energia podem ser atribuídos a descargas altamente concentradas.

Finalmente, o reconhecimento da contribuição significativa de poeira eólica para o depósito corrobora a interpretação paleoclimática da região como estando na margem de um cinturão árido.

7. Considerações finais

A presente tese é um significativo aprofundamento do conhecimento da Formação Sanga do Cabral. Esta formação era há muito “considerada sedimentologicamente estranha”, e modelos propostos até então, apesar de coerentes, não explicavam todas as configurações de fácies presentes — em especial as laminações convexas para cima (Claiton Scherer, com. pess., 2023). Apesar destas dificuldades, trabalhos anteriores (Andreis *et al.*, 1980; Faccini, 1989, 2000; Lavina, 1991; Zeffass *et al.*, 2003, 2004) tiveram sucesso em inferir o caráter não-perene do regime hídrico deste sistema fluvial, em um clima semiárido a árido. Os avanços do conhecimento na comunidade internacional permitiram então, finalmente, o desvendar do mistério destas estruturas. Estes conhecimentos foram primeiramente aplicados no trabalho de Dario (2017), do qual a presente tese é uma continuação direta.

Foram relevantes para esta tese principalmente os estudos experimentais de Cartigny *et al.* (2014) e Ono *et al.* (2021), os quais demonstraram em laboratório uma gama de configurações possíveis para as estruturas geradas por formas de leito supercríticas. Para interpretações mais abrangentes dos estilos fluviais, foram importantes principalmente os modelos de Plink-Björklund (2015). Porém, todos os modelos relacionados a estruturas supercríticas e rios de alta variabilidade de descarga são ainda preliminares e pouco estabelecidos. Uma vez que a classificação planiforme, e por consequência os atuais modelos de fácies cada vez mais se mostram obsoletos (Fielding, 1993; Ethridge, 2011; Fielding *et al.*, 2018), o surgimento de novos modelos depende de estudos de caso que ilustrem as várias possibilidades de configurações de fácies, arquiteturas de fácies, e possíveis elementos associados presentes em rios de alta variabilidade, neste caso específico, em clima árido.

Não se deve perder de vista a importância da FSC no contexto bioestratigráfico mundial. A presença do fóssil *Procolophon trigoniceps* (Lavina, 1983; Cisneros, 2008) permite correlação da FSC com a Formação Katberg, na Bacia do Karoo, na África do Sul (Barberena *et al.*, 1985; Neveling *et al.*, 1999), e posiciona a FSC Triássico Inferior (Viglietti *et al.*, 2022), não muito após a maior extinção da história da vida na Terra, a

Extinção Permo-Triássica ou Finipermissiana (Phillips, 1860; Raup, 1979; Sepkoski, 1984; Erwin, 1994, 2006; Benton, 2008). A chamada Grande Extinção é hoje considerada como causada por um evento hipertermal, com grandes perturbações no clima (Smith & Botha-Brink, 2014; Benton, 2018; Penn *et al.*, 2018; Dal Corso *et al.*, 2022). Uma melhor compreensão da FSC significa uma melhor compreensão do clima e das dificuldades enfrentadas pelos seres vivos durante a Recuperação Biótica após tão grande catástrofe (Erwin, 2001; Sahney & Benton, 2008; Chen & Benton, 2012; Du *et al.*, 2023), a qual mudou o curso da história da vida na Terra (Phillips, 1860; Raup, 1979; Sepkoski, 1984). É neste contexto sedimentar e paleoclimático que se insere a presente tese.

8. Referências bibliográficas

- Abdullatif, O.M.** (1989) Channel-fill and sheet-flood facies sequences in the ephemeral terminal River Gash, Kassala, Sudan. *Sediment. Geol.*, **63**, 171–184.
- Alexander, J., Bridge, J.S., Cheel, R.J. and Leclair, S.F.** (2001) Bedforms and associated sedimentary structures formed under supercritical water flows over aggrading sand beds. *Sedimentology*, **48**, 133–152.
- Alexander, J. and Fielding, C.R.** (1997) Gravel antidunes in the tropical Burdekin River, Queensland, Australia. *Sedimentology*, **44**, 327–337.
- Alexander, J., Fielding, C.R. and Pocock, G.D.** (1999) Flood behaviour of the Burdekin River, tropical north Queensland, Australia. *Floodplains Interdiscip. Approaches*, 27–40.
- Alexander, J., Herbert, C.M., Fielding, C.R. and Amos, K.J.** (2020) Controls on channel deposits of highly variable rivers: Comparing hydrology and event deposits in the Burdekin River, Australia. *Sedimentology*, **67**, 2721–2746.
- Allen, J.P., Fielding, C.R., Gibling, M.R. and Rygel, M.C.** (2014) Recognizing products of palaeoclimate fluctuation in the fluvial stratigraphic record: An example from the Pennsylvanian to Lower Permian of Cape Breton Island, Nova Scotia. *Sedimentology*, **61**, 1332–1381.
- Allen, J.R.L.** (1982) Bedforms in Supercritical and Related Flows: Transverse Ribs, Rhomboid Features, and Antidunes. In: *Sedimentary Structures Their Character and Physical Basis* (Ed. J.R.L. Allen), *Elsevier*, Amsterdam, 383–417.
- Allen, J.R.L.** (1969) Erosional Current Marks of Weakly Cohesive Mud Beds. *SEPM J. Sediment. Res.*, **Vol. 39**, 607–623.
- Allen, J.R.L.** (1968) Current Ripples, Their Relation to Patterns of Water and Sediment Motion. *North-Holland Publishing Company*, Amsterdam, 433 pp.

- Alonso-Zarza, A.M.** (2003) Palaeoenvironmental significance of palustrine carbonates and calcretes in the geological record. *Earth-Science Rev.*, **60**, 261–298.
- Alonso-Zarza, A.M.** and **Wright, V.P.** (2010) Calcretes. In: *Carbonates in Continental Settings: Facies, Environments, and Processes* (Ed. A.M. Alonso-Zarza and L.H. Tanner), *Elsevier*, Oxford, 61, 225–267.
- Andreis, R.R., Bossi, G.E.** and **Montardo, D.K.** (1980) O Grupo Rosário do Sul (Triássico) no Rio Grande do Sul - Brasil. In: *XXXI Congresso Brasileiro de Geologia, Sociedade Brasileira de Geologia*, Balneário Camboriú, SC, 2, 659–673.
- Arakel, A. V.** and **McConchie, D.** (1982) Classification and Genesis of Calcrete and Gypsite Lithofacies in Paleodrainage Systems of Inland Australia and their Relationship to Carnotite Mineralization. *SEPM J. Sediment. Res.*, **52**, 1149–1170.
- Arnott, R.W.C.** and **Hand, B.M.** (1989) Bedforms, Primary Structures and Grain Fabric in the Presence of Suspended Sediment Rain. *J. Sediment. Res.*, **59**, 1062–1069.
- Azevedo, S.A., Lavina, E.L., Barberena, M.C., Ferrando, L.** and **Andreis, R.R.** (1985) Evidências de correlação entre a Formação Yaguari (Uruguai) e as Formações Rio do Rasto e Sanga do Cabral (Rio Grande do Sul - Brasil). *Pesqui. em Geociências*, **17**, 112–121.
- Baas, J.H., Best, J.L.** and **Peakall, J.** (2011) Depositional processes, bedform development and hybrid bed formation in rapidly decelerated cohesive (mud-sand) sediment flows. *Sedimentology*, **58**, 1953–1987.
- Barberena, M.C., Araújo, D.C.F., Lavina, E.L.** and **Azevedo, S.A.K.** (1985) O estado atual do conhecimento sobre os tetrapodes permianos e triássicos do Brasil meridional. In: *Coletânea de trabalhos paleontológicos, Trabalhos apresentados no VIII Congresso Brasileiro de Paleontologia* (Ed. D. de A. Campos and R.C.G. Armesto), *Departamento Nacional de Produção Mineral - DNPM*, Brasília, 21–28.
- Baud, A., Magaritz, M.** and **Holser, W.T.** (1989) Permian-Triassic of the Tethys: Carbon isotope studies. *Geol. Rundschau*, **78**, 649–677.
- Benton, M.J.** (2008) *When Life Nearly Died - The greatest mass extinction of all time*, 2nd edn. *Thames & Hudson*, London, 336 pp.
- Benton, M.J.** (2018) Hyperthermal-driven mass extinctions: Killing models during the Permian-Triassic mass extinction. *Philos Trans R Soc A Math Phys Eng Sci.* doi: 10.1098/rsta.2017.0076
- Benton, M.J.** and **Newell, A.J.** (2014) Impacts of global warming on Permo-Triassic terrestrial ecosystems. *Gondwana Res.*, **25**, 1308–1337.
- Blakey, R.C., Peterson, F.** and **Kocurek, G.** (1988) Synthesis of late Paleozoic and Mesozoic eolian deposits of the Western Interior of the United States. *Sediment. Geol.*, **56**, 3–125.
- Botha, J.** and **Smith, R.M.H.** (2006) Rapid vertebrate recuperation in the Karoo Basin of South Africa following the End-Permian extinction. *J. African Earth Sci.*, **45**, 502–514.

- Botha, J. and Smith, R.M.H.** (2020) Biostratigraphy of the *Lystrosaurus declivis* Assemblage Zone (Beaufort Group, Karoo Supergroup), South Africa. *South African J. Geol.*, **123**, 207–216.
- Boucot, A.J., Xu, C., Scotese, C.R. and Morley, R.J.** (2013) Phanerozoic Paleoclimate. *Society for Sedimentary Geology (SEPM)*, Tulsa, Oklahoma, U.S.A., 360 pp.
- Brierley, G.J. and Hickin, E.J.** (1991) Channel planform as a non-controlling factor in fluvial sedimentology: the case of the squamish river floodplain, British Columbia. *Sediment. Geol.*, **75**, 67–83.
- Bryant, M., Falk, P. and Paola, C.** (1995) Experimental study of avulsion frequency and rate of deposition. *Geology*, **23**, 365–368.
- Bullock, P. and Murphy, C.P.** (1979) Evolution of a paleo-argillic brown earth (paleudalf) from oxfordshire, England. *Geoderma*, **22**, 225–252.
- Burroughs, W.A.** (1985) The hydraulic equivalence of mica; discussion. *J. Sediment. Res.*, **55**, 291–292.
- Cao, C., Love, G.D., Hays, L.E., Wang, W., Shen, S. and Summons, R.E.** (2009) Biogeochemical evidence for euxinic oceans and ecological disturbance presaging the end-Permian mass extinction event. *Earth Planet. Sci. Lett.*, **281**, 188–201.
- Cartigny, M.J.B., Postma, G., van den Berg, J.H. and Mastbergen, D.R.** (2011) A comparative study of sediment waves and cyclic steps based on geometries, internal structures and numerical modeling. *Mar. Geol.*, **280**, 40–56.
- Cartigny, M.J.B., Ventra, D., Postma, G. and van Den Berg, J.H.** (2014) Morphodynamics and sedimentary structures of bedforms under supercritical-flow conditions: New insights from flume experiments. *Sedimentology*, **61**, 712–748.
- Chan, M.A.** (1999) Triassic loessite of north-central Utah; stratigraphy, petrophysical character, and paleoclimate implications. *J. Sediment. Res.*, **69**, 477–485.
- Chen, Z.Q. and Benton, M.J.** (2012) The timing and pattern of biotic recovery following the end-Permian mass extinction. *Nat. Geosci.*, **5**, 375–383.
- Chester, R., Elderfield, H., Griffin, J.J., Johnson, L.R. and Padgham, R.C.** (1972) Eolian dust along the eastern margins of the Atlantic Ocean. *Mar. Geol.*, **13**, 91–105.
- Choquette, P.W. and Pray, L.C.** (1970) Geologic Nomenclature and Classification of Porosity in Sedimentary Carbonates. *Am. Assoc. Pet. Geol. Bull.*, **54**, 207–250.
- Chow, V. Te** (1959) Open-channel Hydraulics, 1st edn. *McGraw-Hill Books*, New York, 697 pp.
- Cisneros, J.C.** (2008) Taxonomic status of the reptile genus *Procolophon* from the Gondwanan Triassic. *Palaeontol. Africana*, **43**, 7–18.
- Cisneros, J.C. and Schultz, C.L.** (2002) *Procolophon brasiliensis* n. sp., a new procolophonid reptile from the Lower Triassic of southern Brazil. *Neues Jahrb. fur Geol. und Palaontologie - Monatshefte*, **2002**, 641–648.

- Cohen, K.M., Finney, S.C., Gibbard, P.L. and Fan, J.-X.** (2013) The ICS International Chronostratigraphic Chart. *Episodes*, **36**, 199–204.
- Cornish, V.** (1899) On Kumatology. (The Study of the Waves and Wave-Structures of the Atmosphere, Hydrosphere, and Lithosphere). *Geogr. J.*, **13**, 624.
- Covault, J.A., Kostic, S., Paull, C.K., Sylvester, Z. and Fildani, A.** (2017) Cyclic steps and related supercritical bedforms: Building blocks of deep-water depositional systems, western North America. *Mar. Geol.*, **393**, 4–20.
- CPRM** (2006) Mapa Geológico do Rio Grande do Sul.
- Dal Corso, J., Song, H., Callegaro, S., Chu, D., Sun, Y., Hilton, J., Grasby, S.E., Joachimski, M.M. and Wignall, P.B.** (2022) Environmental crises at the Permian–Triassic mass extinction. *Nat. Rev. Earth Environ.*, **3**, 197–214.
- Dalrymple, R.W.** (2010) Interpreting Sedimentary Successions: Facies, Facies Analysis and Facies Models. In: *Facies Models 4*, 4th edn. (Ed. N.P. James and R.W. Dalrymple), *Geological Association of Canada*, St. John's, 3–18.
- Dario, E.M.** (2017) Arquitetura de fácies e modelo deposicional dos depósitos fluviais efêmeros da Formação Sanga do Cabral, Triássico Inferior da Bacia Do Paraná, na região central do Rio Grande Do Sul. Universidade Federal do Rio Grande do Sul - UFRGS, Porto Alegre
- de Santa Ana, H., Goso, C. and Daners, G.** (2006) Cuenca Norte: estratigrafía del Carbonífero–Pérmico. In: *Cuencas Sedimentarias de Uruguay – Paleozoico* (Ed. G. Verolavsky, M. Ubilla, and S. Martínez), *DIRAC*, Montevideo, 147–208.
- Dias-Da-Silva, S. and Marsicano, C.** (2011) Phylogenetic reappraisal of Rhytidosteiidae (Stereospondyli: Trematosauria), temnospondyl amphibians from the Permian and Triassic. *J. Syst. Palaeontol.*, **9**, 305–325.
- Dias-Da-Silva, S., Marsicano, C. and Schultz, C.L.** (2006) Rhytidosteid temnospondyls in Gondwana: A new taxon from the Lower Triassic of Brazil. *Palaeontology*, **49**, 381–390.
- Dias-da-Silva, S., Pinheiro, F.L., Stock Da-Rosa, Á.A., Martinelli, A.G., Schultz, C.L., Silva-Neves, E. and Modesto, S.P.** (2017) Biostratigraphic reappraisal of the Lower Triassic Sanga do Cabral Supersequence from South America, with a description of new material attributable to the parareptile genus Procolophon. *J. South Am. Earth Sci.*, **79**, 281–296.
- Dickinson, W.R.** (1985) Interpreting Provenance Relations from Detrital Modes of Sandstones. In: *Provenance of Arenites*, *Springer Netherlands*, Dordrecht, 333–361.
- Donselaar, M.E., Cuevas Gozalo, M.C. and Moyano, S.** (2013) Avulsion processes at the terminus of low-gradient semi-arid fluvial systems: Lessons from the Río Colorado, Altiplano endorheic basin, Bolivia. *Sediment. Geol.*, **283**, 1–14.
- Doyle, L.J., Carder, K.L. and Steward, R.** (1985) The hydraulic equivalence of mica; reply. *J. Sediment. Res.*, **55**, 293–294.

- Doyle, L.J., Carder, K.L. and Steward, R.G.** (1983) The hydraulic equivalence of mica. *J. Sediment. Petrol.*, **53**, 643–648.
- Du, Y., Song, H., Grasby, S.E., Xing, T., Song, H., Tian, L., Chu, D., Wu, Y., Dal Corso, J., Algeo, T.J. and Tong, J.** (2023) Recovery from persistent nutrient-N limitation following the Permian–Triassic mass extinction. *Earth Planet. Sci. Lett.*, **602**, 117944.
- Duller, R.A., Mountney, N.P., Russel, A.J. and Cassidy, N.C.** (2008) Architectural analysis of a volcanoclastic jökulhlaup deposit, southern Iceland: sedimentary evidence for supercritical flow. *Sedimentology*, **55**, 939–964.
- Dunne, E.M., Farnsworth, A., Greene, S.E., Lunt, D.J. and Butler, R.J.** (2021) Climatic drivers of latitudinal variation in Late Triassic tetrapod diversity. *Palaeontology*, **64**, 101–117.
- Eltink, E., Da-Rosa, Á.A.S. and Dias-da-Silva, S.** (2017) A capitosauroid from the Lower Triassic of South America (Sanga do Cabral Supersequence: Paraná Basin), its phylogenetic relationships and biostratigraphic implications. *Hist. Biol.*, **29**, 863–874.
- Ernesto, M., Demarco, P.N., Xavier, P., Sanchez, L., Schultz, C. and Piñeiro, G.** (2020) Age constraints on the Paleozoic Yaguari-Buena Vista succession from Uruguay: paleomagnetic and paleontologic information. *J. South Am. Earth Sci.*, **98**, 102489.
- Erwin, D.H.** (2006) Extinction: How Life on Earth Nearly Ended 250 Million Years Ago. *Princeton University Press*, Princeton, 296 pp.
- Erwin, D.H.** (1994) The Permo–Triassic extinction. *Nature*, **367**, 231–236.
- Erwin, D.H.** (2001) Lessons from the past: Biotic recoveries from mass extinctions. *Proc. Natl. Acad. Sci. U. S. A.*, **98**, 5399–5403.
- Ethridge, F.G.** (2011) Interpretation of Ancient Fluvial Channel Deposits: Review and Recommendations. In: *From River to Rock Record: The preservation of fluvial sediments and their subsequent interpretation — SEPM Special Publication 97* (Ed. S.K. Davidson, S. Leleu, and C.P. North), *SEPM Society for Sedimentary Geology*, Tulsa, Oklahoma, U.S.A., 9–36.
- Faccini, U.F.** (2000) Estratigrafia do Permo-Triássico do Rio Grande do Sul: estilos deposicionais versus espaço de acomodação. Universidade Federal do Rio Grande do Sul - UFRGS
- Faccini, U.F.** (1989) O Permo-Triássico do Rio Grande do Sul: uma análise sob o ponto de vista das seqüências deposicionais. Universidade Federal do Rio Grande do Sul - UFRGS
- Fielding, C.R.** (2006) Upper flow regime sheets, lenses and scour fills: Extending the range of architectural elements for fluvial sediment bodies. *Sediment. Geol.*, **190**, 227–240.
- Fielding, C.R.** (1993) A review of recent research in fluvial sedimentology. *Sediment. Geol.*, **85**, 3–14.
- Fielding, C.R. and Alexander, J.** (1996) Sedimentology of the Upper Burdekin River of North Queensland, Australia—an example of a tropical, variable discharge river. *Terra Nov.*, **8**, 447–457.
- Fielding, C.R., Alexander, J. and Allen, J.P.** (2018) The role of discharge variability in the formation and preservation of alluvial sediment bodies. *Sediment. Geol.*, **365**, 1–20.

- Fielding, C.R., Allen, J.P., Alexander, J. and Gibling, M.R.** (2009) Facies model for fluvial systems in the seasonal tropics and subtropics. *Geology*, **37**, 623–626.
- Fielding, C.R., Frank, T.D., McLoughlin, S., Vajda, V., Mays, C., Tevyaw, A.P., Winguth, A., Winguth, C., Nicoll, R.S., Bocking, M. and Crowley, J.L.** (2019) Age and pattern of the southern high-latitude continental end-Permian extinction constrained by multiproxy analysis. *Nat Commun.* doi: 10.1038/s41467-018-07934-z
- Fielding, C.R., Frank, T.D., Tevyaw, A.P., Savatic, K., Vajda, V., McLoughlin, S., Mays, C., Nicoll, R.S., Bocking, M. and Crowley, J.L.** (2021) Sedimentology of the continental end-Permian extinction event in the Sydney Basin, eastern Australia. *Sedimentology*, **68**, 30–62.
- Fildani, A., Normark, W.R., Kostic, S. and Parker, G.** (2006) Channel formation by flow stripping: Large-scale scour features along the Monterey East Channel and their relation to sediment waves. *Sedimentology*, **53**, 1265–1287.
- Fisher, J.A., Krapf, C.B.E., Langs, S.C., Nichols, G.J. and Payenberg, T.H.D.** (2008) Sedimentology and architecture of the Douglas Creek terminal splay, Lake Eyre, central Australia. *Sedimentology*, **55**, 1915–1930.
- Folk, R.L.** (1981) Petrology of Sedimentary Rocks, 2nd edn. *Hemphill*, Austin, Texas, 184 pp.
- Francischini, H., Dentzien-Dias, P., Guerra-Sommer, M., Menegat, R., Santos, J.O.S., Manfroi, J. and Schultz, C.L.** (2018) A middle Permian (Roadian) lungfish aestivation burrow from the Rio do Rasto Formation (Paraná Basin, Brazil) and associated U-Pb dating. *Palaios*, **33**, 69–84.
- Froude, M.J., Alexander, J., Barclay, J. and Cole, P.** (2017) Interpreting flash flood palaeoflow parameters from antidunes and gravel lenses: An example from Montserrat, West Indies. *Sedimentology*, **64**, 1817–1845.
- Gallego, O.F.** (2010) A new crustacean clam shrimp (Spinicaudata: Eosestheriidae) from the Upper Triassic of Argentina and its importance for ‘conchostracan’ taxonomy. *Alcheringa An Australas. J. Palaeontol.*, **34**, 179–195.
- Gastaldo, R.A. and Neveling, J.** (2016) Comment on: “Anatomy of a mass extinction: Sedimentological and taphonomic evidence for drought-induced die-offs at the Permo-Triassic boundary in the main Karoo Basin, South Africa” by R.M.H. Smith and J. Botha-Brink, *Palaeogeography, Palaeoclimatology, Palaeogeogr. Palaeoclimatol. Palaeoecol.*, **447**, 88–91.
- Ghienne, J.F., Normandeau, A., Dietrich, P., Bouysson, M., Lajeunesse, P. and Schuster, M.** (2021) The depositional signature of cyclic steps: A late Quaternary analogue compared to modern active delta slopes. *Sedimentology*, **68**, 1502–1538.
- Gilbert, G.K. and Murphy, E.C.** (1914) The transportaton of debris by running water. Sacramento, 265 pp.
- Goldberg, K.** (2001) The Paleoclimatic evolution of the Permian in the Paraná Basin in southern Brazil. University of Chicago
- Golden, D.C., Dixon, J.B. and Chen, C.C.** (1986) Ion Exchange, Thermal Transformations, and

Oxidizing Properties of Birnessite. *Clays Clay Miner.*, **34**, 511–520.

- Goso, C., Piñeiro, G., de Santa Ana, H., Rojas, A., Verde, M. and Alves, C.** (2001) Caracterización estratigráfica de los depósitos continentales cuspidales neopérmicos (Formaciones Yaguarí y Buena Vista) en el borde oriental de la Cuenca Norte Uruguaya. In: *Actas del XI Congreso Latinoamericano de Geología*, Montevideo, 18 (CD-ROM).
- Goudie, A.** (1973) Duricrusts in tropical and subtropical landscapes. *Clarendon Press*, Oxford, Uited Kingdom, 174 pp.
- Goudie, A.S.** (1983) Calcrete. In: *Chemical Sediments and Geomorphology* (Ed. A.S. Goudie and K. Pye), *Academic Press*, London, UK, 93–131.
- Gould, S.J.** (1991) Seta do Tempo, Ciclo do Tempo. *Cia. das Letras*, São Paulo, 221 pp.
- Gulbranson, E.L., Ciccioli, P.L., Montañez, I.P., Marensi, S.A., Limarino, C.O., Schmitz, M.D. and Davydov, V.** (2015) Paleoenvironments and age of the Talampaya Formation: The Permo-Triassic boundary in northwestern Argentina. *J. South Am. Earth Sci.*, **63**, 310–322.
- Guy, H.P., Simons, D.B. and Richardson, E.V.** (1966) Summary of Alluvial Channel Data From Flume Experiments , 1956-61. *U. S. Geol. Surv. Prof. Pap.*, **462-I**, 1–104.
- Hallam, A. and Wignall, P.B.** (1997) Mass Extinctions and their Aftermath. *Oxford University Press*, Oxford, Uited Kingdom, 328 pp.
- Hansford, M.R., Plink-Björklund, P. and Jones, E.R.** (2020) Global quantitative analyses of river discharge variability and hydrograph shape with respect to climate types. *Earth-Science Rev.* doi: 10.1016/j.earscirev.2019.102977
- Harris, R., McCall, R., Randall, O., Bin Tawang, M.H., Williams, R., Fairman, J.G. and Schultz, D.M.** (2017) Climate change during the Triassic and Jurassic. *Geol. Today*, **33**, 210–215.
- Holz, M.** (2015) Mesozoic paleogeography and paleoclimates – A discussion of the diverse greenhouse and hothouse conditions of an alien world. *J. South Am. Earth Sci.*, **61**, 91–107.
- Horn, B.L.D., Goldberg, K. and Schultz, C.L.** (2018a) Interpretation of massive sandstones in ephemeral fluvial settings: A case study from the Upper Candelária Sequence (Upper Triassic, Paraná Basin, Brazil). *J. South Am. Earth Sci.*, **81**, 108–121.
- Horn, B.L.D., Goldberg, K. and Schultz, C.L.** (2018b) A loess deposit in the Late Triassic of southern Gondwana, and its significance to global paleoclimate. *J. South Am. Earth Sci.*, **81**, 189–203.
- Horn, B.L.D., Melo, T.P., Schultz, C.L., Philipp, R.P., Kloss, H.P. and Goldberg, K.** (2014) A new third-order sequence stratigraphic framework applied to the Triassic of the Paraná Basin, Rio Grande do Sul, Brazil, based on structural, stratigraphic and paleontological data. *J. South Am. Earth Sci.*, **55**, 123–132.
- Horn, B.L.D., Pereira, V.P. and Schultz, C.L.** (2013) Calcretes of the Santa Maria Supersequence, Middle Triassic, Rio Grande do Sul, Brazil: Classification, genesis and paleoclimatic implications. *Palaeogeogr. Palaeoclimatol. Palaeoecol.*, **376**, 39–47.

- Irmis, R.B. and Whiteside, J.H.** (2012) Delayed recovery of non-marine tetrapods after the end-permian mass extinction tracks global carbon cycle. *Proc. R. Soc. B Biol. Sci.*, **279**, 1310–1318.
- James, M.R. and Robson, S.** (2012) Straightforward reconstruction of 3D surfaces and topography with a camera: Accuracy and geoscience application. *J. Geophys. Res. Earth Surf.*, **117**, 1–17.
- Jefferson, I., Rosenbaum, M. and Smalley, I.** (2002) Mercia Mudstone as a Triassic aeolian desert sediment. *Mercian Geol.*, **15**, 157–162.
- Jeong, G.Y.** (2008) Bulk and single-particle mineralogy of Asian dust and a comparison with its source soils. *J Geophys Res Atmos.* doi: 10.1029/2007JD008606
- Jeong, G.Y., Hillier, S. and Kemp, R.A.** (2011) Changes in mineralogy of loess-paleosol sections across the Chinese Loess Plateau. *Quat. Res.*, **75**, 245–255.
- Johnson, S.Y.** (1989) Significance of Loessite in the Maroon Formation (Middle Pennsylvanian to Lower Permian), Eagle Basin, Northwest Colorado. *J. Sediment. Res.*, **Vol. 59**, 782–791.
- Kabata-Pendias, A.** (2010) Trace Elements in Soils and Plants, 4th edn. *CRC Press*, Boca Raton, USA, 548 pp.
- Kemp, R.A.** (1987) Genesis and environmental significance of a buried middle pleistocene soil in Eastern England. *Geoderma*, **41**, 49–77.
- Kennedy, J.F.** (1963) The mechanics of dunes and antidunes in erodible-bed channels. *J. Fluid Mech.*, **16**, 521–544.
- Kennedy, J.F.** (1960) Stationary waves and antidunes in alluvial channels. California Institute of Technology
- Kessler, J.L.P., Soreghan, G.S. and Wacker, H.J.** (2001) Equatorial Aridity in Western Pangea: Lower Permian Loessite and Dolomitic Paleosols in Northeastern New Mexico, U.S.A. *J. Sediment. Res.*, **71**, 817–832.
- Kiessling, W., Flügel, E. and Golonka, J.** (eds) (2002) Phanerozoic Reef Patterns. *SEPM (Society for Sedimentary Geology)*, 775 pp.
- Kirchner, J.W. and Weil, A.** (2000) Delayed biological recovery from extinctions throughout the fossil record. *Nature*, **404**, 177–180.
- Knapp, J.** (2020) Alluvial Fans, Loess Plains, Lakes, and Distributive Fluvial Systems: Depositional Systems of the Permian-Triassic Red Beds and Evaporites of Wyoming (USA). West Virginia University
- Krapovickas, V., Mancuso, A.C., Marsicano, C.A., Domnanovic, N.S. and Schultz, C.L.** (2013) Large tetrapod burrows from the Middle Triassic of Argentina: a behavioural adaptation to seasonal semi-arid climate? *Lethaia*, **46**, 154–169.
- Kraus, M.J.** (1999) Paleosols in clastic sedimentary rocks: their geologic applications. *Earth-Science Rev.*, **47**, 41–70.
- Kutzbach, J.E. and Gallimore, R.G.** (1989) Pangaeen climates: Megamonsoons of the megacontinent.

J. Geophys. Res., **94**, 3341–3357.

- Labandeira, C. and Sepkoski, J.** (1993) Insect diversity in the fossil record. *Science* (80-.), **261**, 310–315.
- Lamb, M.P., Parsons, J.D., Mullenbach, B.L., Finlayson, D.P., Orange, D.L. and Nittrouer, C.A.** (2008) Evidence for superelevation, channel incision, and formation of cyclic steps by turbidity currents in Eel Canyon, California. *Bull. Geol. Soc. Am.*, **120**, 463–475.
- Lang, J., Le Heron, D.P., Van den Berg, J.H. and Winsemann, J.** (2021) Bedforms and sedimentary structures related to supercritical flows in glacial settings. *Sedimentology*, **68**, 1539–1579.
- Lang, J., Sievers, J., Loewer, M., Igel, J. and Winsemann, J.** (2017) 3D architecture of cyclic-step and antidune deposits in glacial subaqueous fan and delta settings: Integrating outcrop and ground-penetrating radar data. *Sediment. Geol.*, **362**, 83–100.
- Lang, J. and Winsemann, J.** (2013) Lateral and vertical facies relationships of bedforms deposited by aggrading supercritical flows: From cyclic steps to humpback dunes. *Sediment. Geol.*, **296**, 36–54.
- Lavina, E.L.C.** (1983) *Procolophon pricei* sp.n., um novo réptil procolofonídeo do Triássico do Rio Grande do Sul. *Iheringia, Série Geológica*, **9**, 51–78.
- Lavina, E.L.C.** (1991) Geologia sedimentar e paleogeografia do Neopermiano e Eotriássico (intervalo Kazanian-Scythiano) da Bacia do Paraná. Universidade Federal do Rio Grande do Sul - UFRGS
- Li, J., Gastaldo, R.A., Neveling, J. and Geissman, J.W.** (2017) Siltstones across the Daptocephalus (Dicynodon) and Lystrosaurus assemblage zones, Karoo Basin, South Africa, show no evidence for aridification. *J. Sediment. Res.*, **87**, 653–671.
- Li, Y., Shi, W., Aydin, A., Beroya-Eitner, M.A. and Gao, G.** (2020) Loess genesis and worldwide distribution. *Earth-Science Rev.*, **201**, 22.
- Lighthill, J.** (1978) *Waves in Fluids*. Cambridge University Press, Cambridge, 504 pp.
- Looy, C. V., Brugman, W.A., Dilcher, D.L. and Visscher, H.** (1999) The delayed resurgence of equatorial forests after the Permian–Triassic ecologic crisis. *Proc. Natl. Acad. Sci.*, **96**, 13857–13862.
- Lowe, D.R. and LoPiccolo, R.D.** (1974) The Characteristics and Origins of Dish and Pillar Structures. *J. Sediment. Res.*, **44**, 484–501.
- Luppo, T., López de Luchi, M.G., Rapalini, A.E., Martínez Dopico, C.I. and Fanning, C.M.** (2018) Geochronologic evidence of a large magmatic province in northern Patagonia encompassing the Permian-Triassic boundary. *J. South Am. Earth Sci.*, **82**, 346–355.
- MacDougall, M.J., Brocklehurst, N. and Fröbisch, J.** (2019) Species richness and disparity of parareptiles across the end-Permian mass extinction. *Proc. R. Soc. B Biol. Sci.*, **286**, 20182572.
- Mancuso, A.C., Horn, B.L.D., Benavente, C.A., Schultz, C.L. and Irmis, R.B.** (2021) The paleoclimatic context for South American Triassic vertebrate evolution. *J. South Am. Earth Sci.*,

110, 103321.

- Manna, M.O., Scherer, C.M. dos S., Bállico, M.B., Reis, A.D. dos, Moraes, L.V., Ferrari, L.A.B., Roisenberg, H.B. and Oliveira, V.G. de** (2021) Changes in fluvial architecture induced by discharge variability, Jaicós Formation (Silurian-Devonian), Parnaíba Basin, Brazil. *Sediment. Geol.*, **420**, 105924.
- Mao, X., Liu, X. and Zhou, X.** (2021) Permo-Triassic aeolian red clay of southwestern England and its palaeoenvironmental implications. *Aeolian Res.*, **52**, 100726.
- Mays, C., McLoughlin, S., Frank, T.D., Fielding, C.R., Slater, S.M. and Vajda, V.** (2021) Lethal microbial blooms delayed freshwater ecosystem recovery following the end-Permian extinction. *Nat. Commun.*, **12**, 5511.
- Mays, C., Vajda, V., Frank, T.D., Fielding, C.R., Nicoll, R.S., Tevyaw, A.P. and McLoughlin, S.** (2020) Refined Permian–Triassic floristic timeline reveals early collapse and delayed recovery of south polar terrestrial ecosystems. *GSA Bull.*, **132**, 1489–1513.
- McKee, E.D., Crosby, E.J. and Berryhill, H.L.** (1967) Flood deposits, Bijou Creek, Colorado, June 1965. *J. Sediment. Res.*, **37**, 829–851.
- McKenzie, R.M.** (1989) Manganese Oxides and Hydroxides. In: *Minerals in Soil environments*, 2nd edn. (Ed. J.B. Dixon and S.B. Weed), *Soil Science Society of America*, Madison, USA, 439–465.
- Meijer, N., Dupont-Nivet, G., Licht, A., Trabucho-Alexandre, J., Bourquin, S. and Abels, H.A.** (2020) Identifying eolian dust in the geological record. *Earth-Science Rev.* doi: 10.1016/j.earscirev.2020.103410
- Miall, A.D.** (1985) Architectural-element analysis: A new method of facies analysis applied to fluvial deposits. *Earth Sci. Rev.*, **22**, 261–308.
- Miall, A.D.** (2016) *Stratigraphy: A Modern Synthesis*. Springer International Publishing, Cham, Switzerland, 454 pp.
- Miall, A.D.** (1988) Facies architecture in clastic sedimentary basins. In: *New perspectives in basin analysis* (Ed. K. Kleinspehn and C. Paola), Springer-Verlag, New York, 67–81.
- Miall, A.D.** (1977) A review of the braided-river depositional environment. *Earth-Science Rev.*, **13**, 1–62.
- Michell, J.H.** (1893) XLIV. The highest waves in water. *London, Edinburgh, Dublin Philos. Mag. J. Sci.*, **36**, 430–437.
- Milani, E.J.** (2004) Comentários sobre a origem e a evolução tectônica da Bacia do Paraná. In: *Geologia do Continente Sul-Americano: evolução da obra de Fernando Flávio Marques de Almeida* (Ed. V. Mantesso-Neto, A. Bartorelli, C.D.R. Carneiro, and B.B. de Brito-Neves), *Beca*, São Paulo, 265–280.
- Milani, E.J.** (1997) Evolução tectono-estratigráfica da Bacia do Paraná e seu relacionamento com a geodinâmica fanerozóica do Gondwana sul-ocidental. Universidade Federal do Rio Grande do Sul

- Milani, E.J., Melo, J.H.G., Souza, P.A., Fernandes, L.A. and França, A.B.** (2007) Bacia do Paraná. *Bol. Geociências da Petrobras*, **15**, 265–287.
- Milani, E.J. and Thomaz Filho, A.** (2000) Sedimentary Basins of South America. In: *Tectonic Evolution of South America* (Ed. U.G. Cordani, E.J. Milani, A. Thomaz Filho, and D. de A. Campos), 31st International Geological Congress, Rio de Janeiro, 389–449.
- Neveling, J., Rubidge, B.S. and Hancox, P.J.** (1999) A lower Cynognathus Assemblage Zone fossil from the Katberg Formation (Beaufort Group, South Africa). *S. Afr. J. Sci.*, **95**, 555–556.
- Nicholas, A.P., Sambrook Smith, G.H., Amsler, M.L., Ashworth, P.J., Best, J.L., Hardy, R.J., Lane, S.N., Orfeo, O., Parsons, D.R., Reesink, A.J.H., Sandbach, S.D., Simpson, C.J. and Szupiany, R.N.** (2016) The role of discharge variability in determining alluvial stratigraphy. *Geology*, **44**, 3–6.
- Nicolas, M. and Rubidge, B.S.** (2010) Changes in Permo-Triassic terrestrial tetrapod ecological representation in the Beaufort Group (Karoo Supergroup) of South Africa. *Lethaia*, **43**, 45–59.
- North, C.P. and Davidson, S.K.** (2012) Unconfined alluvial flow processes: Recognition and interpretation of their deposits, and the significance for palaeogeographic reconstruction. *Earth-Science Rev.*, **111**, 199–223.
- North, C.P. and Taylor, K.S.** (1996) Ephemeral-fluvial deposits: Integrated outcrop and simulation studies reveal complexity. *Am. Assoc. Pet. Geol. Bull.*, **80**, 811–830.
- Olsen, P.E. and Kent, D. V.** (1996) Milankovitch climate forcing in the tropics of Pangaea during the Late Triassic. *Palaeogeogr. Palaeoclimatol. Palaeoecol.*, **122**, 1–26.
- Ono, K., Plink-Björklund, P., Eggenhuisen, J.T. and Cartigny, M.J.B.** (2021) Froude supercritical flow processes and sedimentary structures: New insights from experiments with a wide range of grain sizes. *Sedimentology*, **68**, 1328–1357.
- Ore, H.T.** (1964) Some criteria for recognition of braided stream deposits. *Rocky Mt. Geol.*, **3**, 1–14.
- Owens, J.S.** (1908) Experiments on the Transporting Power of Sea Currents. *Geogr. J.*, **31**, 415.
- Parker, G.** (1996) Some Speculations on the Relation Between Channel Morphology and Channel-scale Flow Structures. In: *Coherent Flow Structures in Open Channels* (Ed. P.J. Ashworth, S.J. Bennett, J.L. Best, and S.J. McLelland), John Wiley & Sons, Chichester, 423–458.
- Parker, G. and Izumi, N.** (2000) Purely erosional cyclic and solitary steps created by flow over a cohesive bed. *J. Fluid Mech.*, **419**, 203–238.
- Parrish, J.T.** (1993) Climate of the Supercontinent Pangea. *J. Geol.*, **101**, 215–233.
- Payton, R.W.** (1993) Fragipan formation in argillic brown earths (Fragiudalfs) of the Milfield Plain, north-east England. II. Post Devensian developmental processes and the origin of fragipan consistence. *J. Soil Sci.*, **44**, 703–723.
- Penn, J.L., Deutsch, C., Payne, J.L. and Sperling, E.A.** (2018) Temperature-dependent hypoxia explains biogeography and severity of end-Permian marine mass extinction. *Science* (80-). doi: 10.1126/science.aat1327

- Phillips, J.** (1860) Life on the earth : its origin and succession. *Macmillan and co.*, Cambridge, London, 276 pp.
- Piñeiro, G., Ferigolo, J., Ribeiro, A.M. and Velozo, P.** (2015) Reassessing the affinities of vertebral remains from Permo-Triassic beds of Gondwana. *Comptes Rendus - Palevol*, **14**, 387–401.
- Piñeiro, G., Marsicano, C., Goso, C. and Morosi, E.** (2007) Temnospondyl diversity of the Permian-Triassic Colonia Orozco Local Fauna (Buena Vista Formation) of Uruguay. *Rev. Bras. Paleontol.*, **10**, 169–180.
- Piñeiro, G., Ramos, A. and Marsicano, C.** (2012) A rhinesuchid-like temnospondyl from the Permo-Triassic of Uruguay. *Comptes Rendus - Palevol*, **11**, 65–78.
- Piñeiro, G., Rojas, A. and Ubilla, M.** (2004) A new procolophonoid (Reptilia, Parareptilia) from the Upper Permian of Uruguay. *J. Vertebr. Paleontol.*, **24**, 814–821.
- Piñeiro, G., Verde, M., Ubilla, M. and Ferigolo, J.** (2003) First basal synapsids (“pelycosaurs”) from the Upper Permian-?Lower Triassic of Uruguay, South America. *J. Paleontol.*, **77**, 389–392.
- Pinheiro, F.L., França, M.A.G., Lacerda, M.B., Butler, R.J. and Schultz, C.L.** (2016) An exceptional fossil skull from South America and the origins of the archosauriform radiation. *Sci. Rep.*, **6**, 1–7.
- Plink-Björklund, P.** (2015) Morphodynamics of rivers strongly affected by monsoon precipitation: Review of depositional style and forcing factors. *Sediment. Geol.* 323:110–147.
- Potter, R.M. and Rossman, G.R.** (1979) Mineralogy of manganese dendrites and coatings. *Am. Mineral.*, **64**, 1219–1226.
- Preto, N., Kustatscher, E. and Wignall, P.B.** (2010) Triassic climates — State of the art and perspectives. *Palaeogeogr. Palaeoclimatol. Palaeoecol.*, **290**, 1–10.
- Pye, K.** (1987) Aeolian Dust and Dust Deposits. *Academic Press*, London, UK, 334 pp.
- Racki, G.** (1999) Silica-secreting biota and mass extinctions: survival patterns and processes. *Palaeogeogr. Palaeoclimatol. Palaeoecol.*, **154**, 107–132.
- Raup, D.M.** (1979) Size of the Permo-Triassic Bottleneck and Its Evolutionary Implications. *Science* (80-), **206**, 217–218.
- Reis, A.D. dos, Scherer, C.M. dos S., Amarante, F.B. do, Rossetti, M. de M.M., Kifumbi, C., Souza, E.G. de, Ferronato, J.P.F. and Owen, A.** (2019) Sedimentology of the proximal portion of a large-scale, Upper Jurassic fluvial-aeolian system in Paraná Basin, southwestern Gondwana. *J. South Am. Earth Sci.*, **95**, 102248.
- Reis, A.D. Dos, Scherer, C.M.D.S., Owen, A., Amarante, F.B. Do, Ferronato, J.P.F., Pantopoulos, G., de Souza, E.G., Bállico, M.B. and Aguilar, C.A.G.** (2022) a Quantitative Depositional Model of a Large Distributive Fluvial System (Megafan) With Terminal Aeolian Interaction: the Upper Jurassic Guarú Dfs in Southwestern Gondwana. *J. Sediment. Res.*, **92**, 460–485.
- Retallack, G.J.** (1988) Field recognition of paleosols. In: *Paleosols and Weathering Through Geologic Time: Principles and Applications* (Ed. J. Reinhardt and W.R. Sigleo), *Geological Society of*

America, 1–20.

- Retallack, G.J.** (2001) *Soils of the Past: An Introduction to Paleopedology*, 2nd edn. Wiley, 404 pp.
- Retallack, G.J., Veevers, J.J. and Morante, R.** (1996) Global coal gap between Permian–Triassic extinction and Middle Triassic recovery of peat-forming plants. *Geol. Soc. Am. Bull.*, **108**, 195–207.
- Robertson, J.M. and Rouse, H.** (1941) On the Four Regimes of Open Channel Flow. *Civ. Eng. (New York)*, **11**, 169–171.
- Rubidge, B.S.** (2005) Re-uniting lost continents - Fossil reptiles from the ancient Karoo and their wanderlust. *South African J. Geol.*, **108**, 135–172.
- Ruta, M. and Benton, M.J.** (2008) Calibrated diversity, tree topology and the mother of mass extinctions: The lesson of temnospondyls. *Palaeontology*, **51**, 1261–1288.
- Sahney, S. and Benton, M.J.** (2008) Recovery from the most profound mass extinction of all time. *Proc. R. Soc. B Biol. Sci.*, **275**, 759–765.
- Saunderson, H.C. and Lockett, F.P.J.** (1983) Flume Experiments on Bedforms and Structures at the Dune-Bed Transition. In: *Modern and Ancient Fluvial Systems* (Ed. J.D. Collinson and J. Lewin), Blackwell Publishing Ltd., Oxford, UK, 49–58.
- Scherer, C.M. dos S., Lavina, E.L.C., Reis, A.D. dos and Horn, B.L.D.** (2021) Estratigrafia da sucessão sedimentar mesozoica da Bacia do Paraná no Rio Grande do Sul. In: *Contribuições a Geologia do Rio Grande do Sul e de Santa Catarina* (Ed. A.R. Jelinek and C.A. Sommer), Sociedade Brasileira de Geologia Núcleo RS/SC, Compasso Lugar-Cultura, Porto Alegre, 289–304.
- Scherer, C.M.S., Reis, A.D., Horn, B.L.D., Bertolini, G., Lavina, E.L.C., Kifumbi, C. and Goso Aguilar, C.** (2023) The stratigraphic puzzle of the permo-mesozoic southwestern Gondwana: The Paraná Basin record in geotectonic and palaeoclimatic context. *Earth-Science Rev.*, **240**, 104397.
- Schmidt, V. and McDonald, D.A.** (1979) The Role of Secondary Porosity in the Course of Sandstone Diagenesis. In: *Aspects of Diagenesis*, Special Pu (Ed. P.A. Scholle and P.R. Schluger), SEPM (Society for Sedimentary Geology), Tulsa, Oklahoma, U.S.A., 175–207.
- Schneider, R.L., Mühlmann, H., Tommasi, E., Medeiros, R.A., Daemon, R.F. and Nogueira, A.A.** (1974) Revisão estratigráfica da Bacia do Paraná. In: *Anais do Congresso Brasileiro de Geologia*, Sociedade Brasileira de Geologia, Porto Alegre, 1, 41–65.
- Schultz, C.L., Martinelli, A.G., Soares, M.B., Pinheiro, F.L., Kerber, L., Horn, B.L.D., Pretto, F.A., Müller, R.T. and Melo, T.P.** (2020) Triassic faunal successions of the Paraná Basin, southern Brazil. *J. South Am. Earth Sci.*, **104**, 102846.
- Sellwood, B.W. and Valdes, P.J.** (2006) Mesozoic climates: General circulation models and the rock record. *Sediment. Geol.*, **190**, 269–287.
- Sepkoski, J.J.** (1984) A kinetic model of Phanerozoic taxonomic diversity. III. Post-Paleozoic families

and mass extinctions. *Paleobiology*, **10**, 246–267.

Simons, D.B. and Richardson, E.V. (1961) Forms of Bed Roughness in Alluvial Channels. *J. Hydraul. Div.*, **87**, 87–105.

Singer, A. (1988) Illite in aridic soils, desert dusts and desert loess. *Sediment. Geol.*, **59**, 251–259.

Singh, A. and Bhardwaj, B.D. (1991) Fluvial facies model of the Ganga River sediments, India. *Sediment. Geol.*, **72**, 135–146.

Slootman, A. and Cartigny, M.J.B. (2020) Cyclic steps: Review and aggradation-based classification. *Earth-Science Rev.* doi: 10.1016/j.earscirev.2019.102949

Slootman, A., Vellinga, A.J., Moscariello, A. and Cartigny, M.J.B. (2021) The depositional signature of high-aggradation chute-and-pool bedforms: The build-and-fill structure. *Sedimentology*, **68**, 1640–1673.

Smith, R.M.H. and Botha-Brink, J. (2014) Anatomy of a mass extinction: Sedimentological and taphonomic evidence for drought-induced die-offs at the Permo-Triassic boundary in the main Karoo Basin, South Africa. *Palaeogeogr. Palaeoclimatol. Palaeoecol.*, **396**, 99–118.

Sneh, A. (1983) Desert Stream Sequences in the Sinai Peninsula. *J. Sediment. Res.*, **53**, 1271–1279.

Soreghan, G.S.L., Elmore, R.D. and Lewchuck, M.T. (2002) Sedimentologic-magnetic record of western Pangean climate in upper Paleozoic loessite (lower Cutler beds, Utah). *Bull. Geol. Soc. Am.*, **114**, 1019–1035.

Southard, J.B. and Boguchwal, L.A. (1990) Bed configuration in steady unidirectional water flows; Part 2, Synthesis of flume data. *J. Sediment. Res.*, **60**, 658–679.

Spinewine, B., Sequeiros, O.E., Garcia, M.H., Beaubouef, R.T., Sun, T., Savoye, B. and Parker, G. (2009) Experiments on wedge-shaped deep sea sedimentary deposits in minibasins and/or on channel levees emplaced by turbidity currents. Part II. Morphodynamic evolution of the wedge and of the associated bedforms. *J. Sediment. Res.*, **79**, 608–628.

Stanley, S.M. (2016) Estimates of the magnitudes of major marine mass extinctions in earth history. *Proc. Natl. Acad. Sci.*, **113**, E6325–E6334.

Tan, C. and Plink-Björklund, P. (2021) Morphodynamics of supercritical flow in a linked river and delta system, Daihai Lake, Northern China. *Sedimentology*, **68**, 1606–1639.

Trendell, A.M., Nordt, L.C., Atchley, S.C., Leblanc, S.L. and Dworkin, S.I. (2013) Determining floodplain plant distributions and populations using paleopedology and fossil root traces: Upper Triassic Sonsela Member of the Chinle Formation at Petrified Forest National Park, Arizona. *Palaios*, **28**, 471–490.

Tunbridge, I.P. (1981) Sandy high-energy flood sedimentation — Some criteria for recognition, with an example from the Devonian of S.W. England. *Sediment. Geol.*, **28**, 79–95.

Vail, P.R., Mitchum, R.M. and Thompson, S. (1977) Seismic stratigraphy and global changes of sea level, part 3: relative changes of sea level from coastal onlap. In: *Seismic stratigraphy - applications*

to hydrocarbon exploration, Memoir 26 (Ed. C.E. Payton), *American Association of Petroleum Geologists*, Tulsa, 63–81.

- Vaisblat, N., Harris, N.B., Ayranci, K., Power, M., DeBhur, C., Bish, D.L., Chalaturnyk, R., Krause, F., Crombez, V., Euzen, T. and Rohais, S.** (2021) Compositional and diagenetic evolution of a siltstone, with implications for reservoir quality; an example from the Lower Triassic Montney Formation in western Canada. *Mar. Pet. Geol.*, **129**, 29.
- Van Valen, L.M.** (1984) A resetting of Phanerozoic community evolution. *Nature*, **307**, 50–52.
- Viglietti, P.A., Rojas, A., Rosvall, M., Klimes, B. and Angielczyk, K.D.** (2022) Network-based biostratigraphy for the late Permian to mid-Triassic Beaufort Group (Karoo Supergroup) in South Africa enhances biozone applicability and stratigraphic correlation. *Palaeontology*. doi: 10.1111/pala.12622
- Walker, S. and Holbrook, J.** (2022) Structures, architecture, vertical profiles, palaeohydrology and taphonomy of an upper-flow-regime-dominated fluvial system, the Triassic Dockum Group of the Palo Duro Canyon, Texas. *Sedimentology*, **70**, 645–684.
- Walker, T.R., Waugh, B. and Grone, A.J.** (1978) Diagenesis in first-cycle desert alluvium of Cenozoic age, southwestern United States and northwestern Mexico. *Geol. Soc. Am. Bull.*, **89**, 19.
- Wilkins, A.D., Hurst, A., Wilson, M.J. and Archer, S.** (2018) Palaeo-environment in an ancient low-latitude, arid lacustrine basin with loessite: The Smith Bank Formation (Early Triassic) in the Central North Sea, UK Continental Shelf. *Sedimentology*, **65**, 335–359.
- Wilson, K.M., Pollard, D., Hay, W.W., Thompson, S.L. and Wold, C.N.** (1994) General circulation model simulations of Triassic climates: Preliminary results. *Pangea Paleoclimate, Tectonics, Sediment. Dur. Accretion, Zenith, Break. a Supercontinent*, **288**, 91–116.
- Wilson, M.J., Hurst, A., Wilkins, A.D., Wilson, L. and Bowen, L.** (2020) Mineralogical evidence for multiple dust sources in an early Triassic loessite. *Sedimentology*, **67**, 239–260.
- Winguth, A.M.E., Shields, C.A. and Winguth, C.** (2015) Transition into a Hothouse World at the Permian–Triassic boundary—A model study. *Palaeogeogr. Palaeoclimatol. Palaeoecol.*, **440**, 316–327.
- Wright, V.P.** (2007) Calcrete. In: *Geochemical Sediments and Landscapes* (Ed. D.J. Nash and S.J. McLaren), *Blackwell Publishing Ltd.*, 10–45.
- Wright, V.P.** (1990) A micromorphological classification of fossil and recent calcic and petrocalcic microstructures. In: *Soil Micromorphology: A Basic and Applied Science* (Ed. L.A. Douglas), *Elsevier*, Amsterdam, 401–407.
- Wright, V.P., Marriott, S.B. and Vanstone, S.D.** (1991) A “reg” palaeosol from the Lower Triassic of south Devon: stratigraphic and palaeoclimatic implications. *Geol. Mag.*, **128**, 517–523.
- Wright, V.P. and Tucker, M.E.** (1991) Calcretes: an introduction. In: *Calcretes* (Ed. V.P. Wright and M.E. Tucker), *Blackwell Scientific Publications*, Oxford, United Kingdom, 1–22.

- Wu, H., Zhang, S., Feng, Q., Jiang, G., Li, H. and Yang, T.** (2012) Milankovitch and sub-Milankovitch cycles of the early Triassic Daye Formation, South China and their geochronological and paleoclimatic implications. *Gondwana Res.*, **22**, 748–759.
- Xavier, P.L.A., Scherer, C.M. dos S., Reis, A.D. dos, Souza, E.G. de, Guadagnin, F. and Piñeiro, G.** (2023) Supercritical fluvial styles and the shifting aridity in the Early Triassic: the example of the Sanga do Cabral Formation, Paraná Basin, Brazil. *J Sediment Res.* doi: 10.2110/jsr.2022.063
- Yokokawa, M., Hasegawa, K., Kanbayashi, S. and Endo, N.** (2010) Formative conditions and sedimentary structures of sandy 3D antidunes: An application of the gravel step-pool model to fine-grained sand in an experimental flume. *Earth Surf. Process. Landforms*, **35**, 1720–1729.
- Zálan, P.V., Wolff, S., Conceição, J.C.J., Astolfi, M.A.M., Vieira, I.S., Appi, V.T., Zanotto, O.A. and Marques, A.** (1991) Tectonics and sedimentation of the Paraná Basin. In: *Proceedings of the 7th International Gondwana Symposium* (Ed. H.H.G.J. Ulbrich and A.C. Rocha-Campos), *Instituto de Geociências, USP, São Paulo*, 83–117.
- Zellman, K.L., Plink-Björklund, P. and Fricke, H.C.** (2021) Testing hypotheses on signatures of precipitation variability in the river and floodplain deposits of the Paleogene San Juan Basin, New Mexico, U.S.A. *J. Sediment. Res.*, **90**, 1770–1801.
- Zerfass, H.** (1998) Estratigrafia da Sedimentação Meso e Neotriássica no Município de São Pedro do Sul, RS: Faciologia, Análise de Proveniência e História Diagenética. Universidade do Vale do Rio dos Sinos - UNISINOS
- Zerfass, H., Chemale, F., Schultz, C.L. and Lavina, E.** (2004) Tectonics and sedimentation in Southern South America during Triassic. *Sediment. Geol.*, **166**, 265–292.
- Zerfass, H., Garcia, A.J.V., Susczunski, A.M. and Lavina, E.L.C.** (2000) Análise de proveniência dos arenitos Neopermianos e Triássicos da Bacia do Paraná na região de São Pedro do Sul (RS): uma contribuição para o conhecimento da arquitetura estratigráfica e da evolução tectono-sedimentar. *Acta Geol. Leopoldensia*, **XXIII**, 61–84.
- Zerfass, H., Lavina, E.L., Schultz, C.L., Garcia, A.J.V., Faccini, U.F. and Chemale Jr, F.** (2003) Sequence stratigraphy of continental Triassic strata of Southernmost Brazil: a contribution to Southwestern Gondwana palaeogeography and palaeoclimate. *Sediment. Geol.*, **161**, 85–105.
- Zhao, C., Fang, H., Liu, Y., Dey, S. and He, G.** (2020) Impact of Particle Shape on Saltating Mode of Bedload Transport Sheared by Turbulent Flow. *J. Hydraul. Eng.*, **146**, 1–13.
- Zhong, G., Cartigny, M.J.B., Kuang, Z. and Wang, L.** (2015) Cyclic steps along the South Taiwan Shoal and West Penghu submarine canyons on the northeastern continental slope of the South China Sea. *Bull. Geol. Soc. Am.*, **127**, 804–824.

PRIMEIRO ARTIGO**Supercritical fluvial styles and the shifting aridity in the Early Triassic: the example of the Sanga do Cabral Formation, Paraná Basin, Brazil****Xavier, Pedro L.A.^{1*}****Scherer, Claiton M. dos S.^{1, 2}****Reis, Adriano Domingos dos²****Souza, Ezequiel Galvão de³****Guadagnin, Felipe³****Piñeiro, Graciela⁴**

¹ Programa de Pós-Graduação em Geociências, Universidade Federal do Rio Grande do Sul; Av. Bento Gonçalves, 9500, Porto Alegre, Rio Grande do Sul, Brazil.

² Departamento de Paleontologia e Estratigrafia, Universidade Federal do Rio Grande do Sul; Av. Bento Gonçalves, 9500, Porto Alegre, Rio Grande do Sul, Brazil.

³ Universidade Federal do Pampa, Brazil.

⁴ Departamento de Paleontología, Facultad de Ciencias, Universidad de la República; Iguá, 4225, 11400 Montevideo, Uruguay.

* Corresponding author. E-mail: pedro.xavier@ufrgs.br

DOI: <https://doi.org/10.2110/jsr.2022.063>

ABSTRACT

Froude-supercritical bedforms and associated sedimentary structures are formed in turbulent flows when value of the Froude Number is $Fr > 1$. They have been increasingly studied in recent years, and while they were previously considered to be of rare preservation, they have been increasingly identified in modern settings and the rock record. In alluvial systems, these structures are being recognized as characteristic of rivers with high variability of discharge, especially in arid, semiarid, and subhumid tropical and subtropical climates. However, the development of facies models for such rivers remains tentative, particularly for the rock record, and with the exception of Australia, examples in Gondwana are scarce. The Early Triassic Sanga do Cabral Formation represents an arid to semiarid ephemeral fluvial system cropping out in Southern Brazil, Southwestern Gondwana. The present study reinterprets the sedimentary structures in this formation as Froude-supercritical structures, and identifies three Fluvial Styles (FS). FS1 predominantly consists of fine-grained massive sandstone, with interruptions of intraclastic conglomerates, and occasionally visible faint lamination and mud-intraclast levels. It is interpreted as deposited by unconfined flows in the distal part of a fluvial system, generating hyperconcentrated flows which resulted in thin beds of fine-grained sandstone with massive structure or planar lamination and incipient antidunes. FS2 was deposited by flash floods occurring repeatedly within a short period during a wet season. This resulted in a fining-upwards succession of intraclastic conglomerates with supercritical-flow structures, through sandstones with supercritical-flow structures, to sigmoidal cross-stratification and ripple marks with diffuse lamination. FS3 was deposited by catastrophic flash floods characterized by high discharge and flow velocity, possibly generated by erratic storms, which poured in single events. These catastrophic flows generated large-scale sandy antidunes and other Froude-supercritical bedforms with mud intraclasts, which deposited sandstone in undulatory laminae, and other supercritical-flow structures. These floods waned extremely rapidly, bypassing the stability field of lower-flow-regime bedforms. Measurements taken from undulatory stratification, interpreted as antidune deposits, allowed the estimation of paleoflow velocity and depth. The largest antidunes had a maximum estimated wavelength of 28.92 m (with a mean of 15.4 m) and maximum estimated height of 1.42 m (with a mean of 0.85 m), resulting in an estimated paleoflow velocity of up to 6.72 ms^{-1} (with a mean of 4.9 ms^{-1}) and a maximum flow depth of 1.59 m (with a mean of 0.9 m). These parameters are

comparable to those observed in modern fluvial floods. This study reinforces the significance of Froude-supercritical structures in enhancing our understanding of fluvial systems characterized by high variability in discharge, allowing a finer interpretation of their discharge patterns. This approach can be applied to better understand the many arid, semiarid, or strongly seasonal environments of the Early Triassic period in Gondwana, and potentially other regions and geological times.

1. INTRODUCTION

Supercritical bedforms and associated sedimentary structures are formed under unidirectional turbulent flow when the Froude Number ($Fr = \frac{U}{\sqrt{gh}}$) is greater than 1, where U is the flow velocity, h is the flow depth, and g is the acceleration due to gravity. This value above unity means that inertia dominates over gravity (Kennedy, 1960, 1963; Cartigny *et al.*, 2014). The identified bedforms are stable antidunes, unstable (breaking) antidunes, chutes and pools, and the more recently described (Parker, 1996) cyclic steps (Kennedy, 1960; Cartigny *et al.*, 2014). These structures and their significance have been receiving greater attention in the last decades (Slootman & Cartigny, 2020), and while once they were thought to be rarely preserved, they are being increasingly recognized in modern settings and in the rock record (e.g., Fielding, 2006; Fielding *et al.*, 2009; Covault *et al.*, 2017; Lang *et al.*, 2021; Walker and Holbrook, 2022). In alluvial systems, supercritical bedforms are being recognized as characteristic of high-variability discharge rivers (e.g., McKee *et al.*, 1967; Tunbridge, 1981; Sneh, 1983; Fielding and Alexander, 1996; Alexander and Fielding, 1997; Fielding, 2006; Fielding *et al.*, 2009, 2018; Plink-Björklund, 2015; Hansford *et al.*, 2020). These rivers are, in turn, related to environments with high seasonal variation of water supply, such as in glacial or monsoonal settings, or even with high or extreme interannual variation, such as ephemeral rivers in semiarid and arid settings, which may remain dry for several years (Tunbridge, 1981; Sneh, 1983; Fielding & Alexander, 1996; Fielding *et al.*, 2018; Hansford *et al.*, 2020).

However, despite advances in the comprehension of supercritical bedforms brought about by more recent flume studies (e.g., Alexander *et al.*, 2001; Yokokawa *et al.*, 2010), recognition and interpretation of their structures, and differentiation of formative bedforms can still be difficult (Ono *et al.*, 2021), and ambiguous in the field (Lang & Winsemann, 2013; Ghienne *et al.*, 2021). For alluvial systems, the implications

of their recognition are recent, and environmental interpretations are still tentative (Fielding, 2006; Fielding *et al.*, 2009, 2018; Plink-Björklund, 2015; Nicholas *et al.*, 2016). In the architectural classification of Miall (1985), the combinations of these structures would be lumped in the “Laminated Sand Sheets” (SB) element, when several configurations are being identified (Fielding, 2006; Duller *et al.*, 2008; Plink-Björklund, 2015). Although there has been a surge in the descriptions of these structures in the rock record, most are from the northern hemisphere, with few examples from Gondwana (e.g., Manna *et al.*, 2021) — with the exception of Australia (Fielding, 2006; Fielding *et al.*, 2009, 2021; Mays *et al.*, 2020). Additional studies are required in the southern hemisphere to generalize the paleoclimatic significance of supercritical-flow structures.

In the southern part of the Paraná Basin, the Estrada de Ferro Inacabada Outcrop of the Early Triassic Sanga do Cabral Formation (SCF) and Supersequence, in southern Brazil, presents well-exposed supercritical-flow structures of a fluvial system (Fig. 1). The site offers an optimal opportunity to study the significance of these structures and their paleoclimatic significance in Gondwana. Detailed facies analysis was conducted under the light of new knowledge cited above, which resulted in reinterpretation of the sedimentary structures and identification of a dominance of supercritical-flow-generated structures in the exposition. Three different fluvial styles are interpreted, which allowed the inference of changes in water supply discharge and frequency in an arid to semiarid region in interior western Gondwana during the Early Triassic. This knowledge may be likewise applied to other similar ancient river systems.

2. GEOLOGICAL SETTING

The Sanga do Cabral Formation (SCF; Andreis *et al.*, 1980) is an enigmatic and sometimes problematic stratigraphic unit which crops out in the Rio Grande do Sul state, southernmost Brazil (Fig. 1). It is the only Early Triassic unit in the Brazilian area of the Paraná Basin (Milani *et al.*, 2007). The Paraná Basin is a large intracratonic basin occupying an area around 1.5 million km² through Brazil, Uruguay, Paraguay and Argentina (Fig. 1). It comprises a volcano-sedimentary depositional record spanning the Ordovician to the Late Cretaceous (Milani *et al.*, 2007).

The depositional setting of the SCF, and mainly, its correlation to adjacent units, has received many interpretations since its first description by Andreis *et al.* (1980) (Faccini, 1989, 2000; Lavina, 1991; Zeffass *et al.*, 2003, 2004; Ernesto *et al.*, 2020).

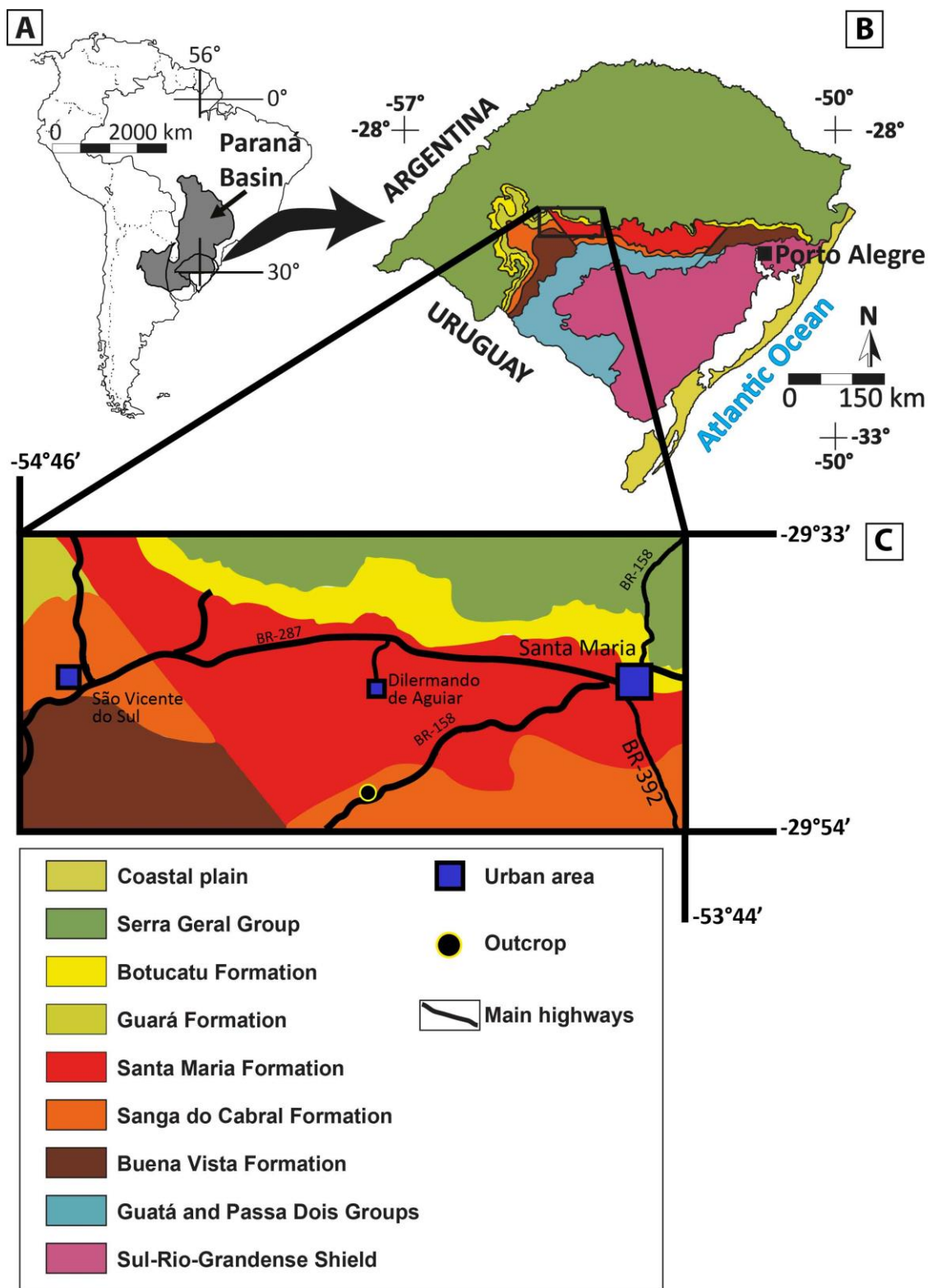


Fig. 1.--- **A**) Location of the Paraná Basin and Rio Grande do Sul state in South America. Modified from Goldberg (2001), after Zálan *et al.* (1991). **B**) Simplified geological map of Rio Grande do Sul, and enclosing of study area. Modified from CPRM (2006). **C**) Location of the Estrada de Ferro Inacabada Outcrop in the state of Rio Grande do Sul.

The formation was first defined as red sandstones, conglomerates, and mudstones with abundant cross-stratification, interpreted as deposited by meandering rivers with a high avulsion rate (Andreis *et al.*, 1980). Faccini (1989, 2000) interpreted the formation as ephemeral braided rivers, or a “braidplain”, comparable to a “Bijou Creek–type system”, and related this system to subjacent eolian dunes, considering the latter as the base of the formation. The author also interprets fine-grained massive or climbing-ripple-bearing deposits as originated by “suspension lobes” of high suspension load into ephemeral ponds. Lavina (1991) considered this eolian system at the base of the SCF as correlated to the Pirambóia Formation, which crops out at the northern region of the Paraná Basin, but identified a possible ca. 4 Myr hiatus between the eolian dunes and the fluvial system. Nevertheless, the author still maintained both in the same lithostratigraphic formation. Zerfass *et al.* (2003, 2004) considered the SCF as a tectonically controlled second-order supersequence in the Paraná Basin, and separated from the subjacent eolian system (Fig. 2). Scherer *et al.* (2021, 2023) also restricted the designation “Sanga do Cabral” to the fluvial sandstones and intraformational conglomerates, as they identified an unconformity which separates those lithologies from the underlying eolian succession. According to these authors, the underlying eolian interval should constitute an independent stratigraphic unit, denominated Buena Vista Formation (after the Uruguayan unit, *sensu de Santa Ana et al.*, 2006; Fig. 2). Zerfass *et al.* (2003, 2004) and Scherer *et al.* (2021, 2023) interpret that the SCF accumulated on a low-gradient alluvial plain and under low accommodation, likely deposited by flash floods under arid or semiarid conditions, alternating with more humid and more arid periods. Mudstone deposition would be linked to small ponds and lakes.

The present work maintains previous interpretations of a fluvial system under a strongly seasonal semiarid climate with ephemeral characteristics, and separated from the underlying eolian system. The sedimentary structures, originally regarded as consisting mainly of trough cross-stratification and planar stratification, are here reinterpreted as generated by a combination of Froude-supercritical bedforms, in accordance to the previous interpretation of Dario (2017).

The fossil content of the SCF is mainly represented by the procolophonid *Procolophon trigoniceps*, a variety of temnospondyls, one archosauromorph species and other less specified specimens (Dias-da-Silva *et al.*, 2017). Records of synapsids

(such as *Lystrosaurus*), pareiasaurs, and seymouriamorphs or diadectomorphs are disputed (Piñeiro *et al.*, 2015; Dias-da-Silva *et al.*, 2017).

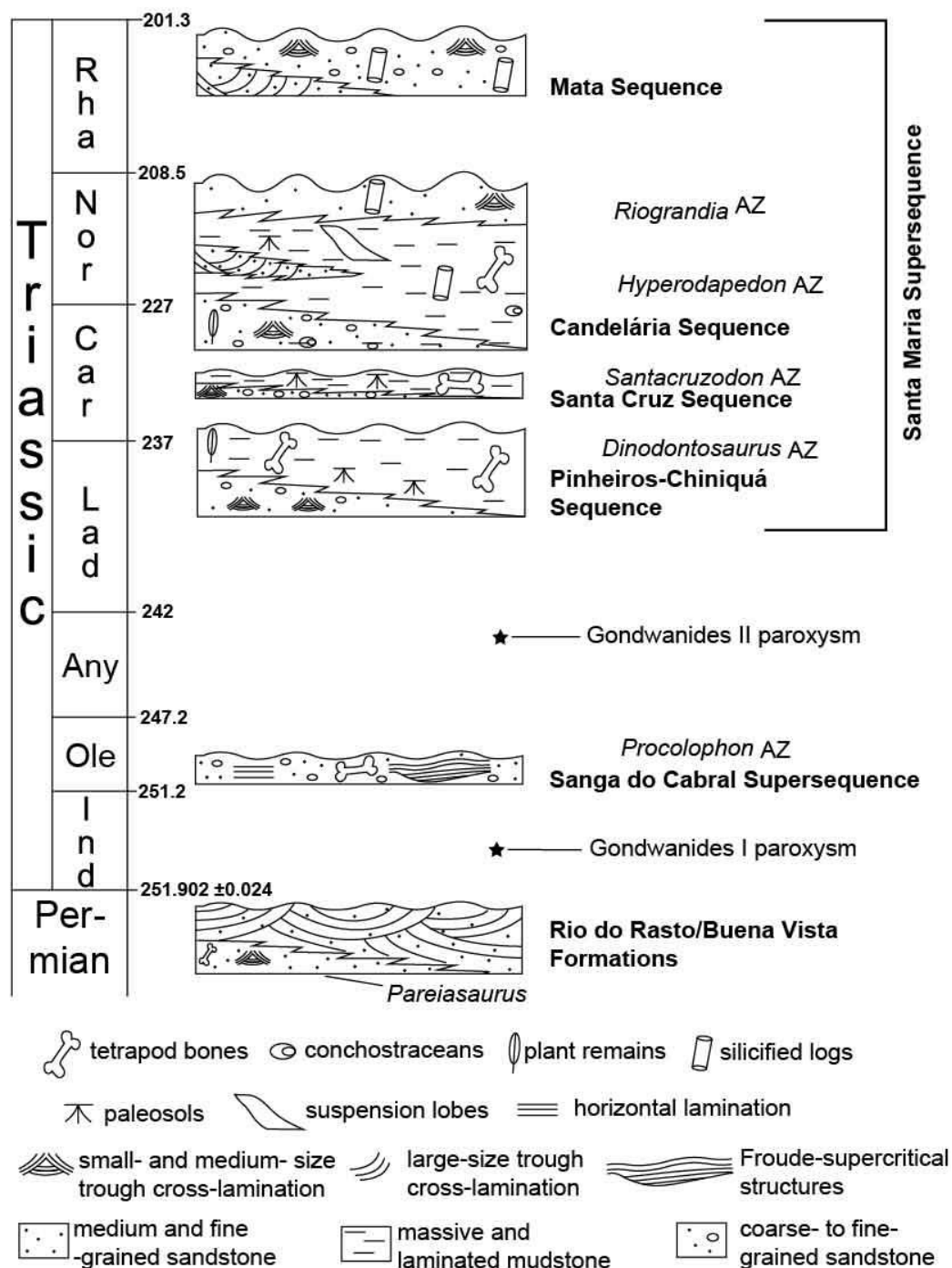


Fig. 2.--- Chronostratigraphic chart of the Triassic second- and third-order sequences of the Paraná Basin, and the Buena Vista and Rio do Rasto Formations. Modified from Zerfass *et al.* (2003) and Horn *et al.* (2014). Santa Maria Supersequence age recalibrations after Schultz *et al.* (2020).

Due to the presence of *Procolophon trigoniceps*, the SCF is correlated to the Katberg Formation of the Karoo Basin in South Africa, tying the geologic unit to an Early Triassic age (Lavina, 1983; Cisneros, 2008). More specifically, as *P. trigoniceps* is the dominant taxon in the SCF (Cisneros & Schultz, 2002; Cisneros, 2008; Dias-da-

Silva *et al.*, 2017), it is commonly correlated to the informal “Procolophon abundant zone” (Neveling *et al.*, 1999; Schultz *et al.*, 2020), which corresponds to the upper third of the Katberg Formation (Botha & Smith, 2006, 2020). Therefore, this correlation positions the SCF in the Early Olenekian (Viglietti *et al.*, 2022). In Argentina, the Vera Formation has been dated as Early Triassic in age (Luppo *et al.*, 2018), making it coeval to the SCF.

In the past, the SCF had historically been considered to have a physical continuation into Uruguayan territory, being correlated to the Uruguayan Buena Vista Formation due to lithological similarity (Azevedo *et al.*, 1985; de Santa Ana *et al.*, 2006). However, the fossiliferous conglomerates in the Uruguayan Buena Vista Formation are stratigraphically below the eolian deposits (Goso *et al.*, 2001; de Santa Ana *et al.*, 2006; Ernesto *et al.*, 2020), which is the opposite of the configuration in Brazilian territory (Fig. 2). In addition, findings of different fossil assemblages (Piñeiro *et al.*, 2003, 2004, 2007, 2012), and magnetic data (Ernesto *et al.*, 2020) have put this correlation into question. Such revaluations are supported in the interpretation of Scherer *et al.* (2021, 2023).

The positioning of the SCF in the Olenekian Stage (Fig. 2) causes it to be approximately 0.702 ± 0.024 Myr younger than the PTB (Cohen *et al.*, 2013 updated 2022-10). This situates the SCF in the context of the biotic recovery after the End-Permian Mass Extinction (Kirchner & Weil, 2000; Chen & Benton, 2012). The End-Permian Mass Extinction was the most severe mass extinction in the geological record (Phillips, 1860; Raup, 1979; Sepkoski, 1984; Hallam & Wignall, 1997; Erwin, 2006; Benton, 2008; Dal Corso *et al.*, 2022), eliminating up to 96% of marine species (Raup, 1979), but probably closer to 81% (Stanley, 2016). On land, estimates go up to 89% of loss of tetrapod genera (Benton & Newell, 2014).

Although post-extinction, the Early Triassic was an abnormal period of instability (Erwin, 2006; Benton, 2008; Fielding *et al.*, 2019; Mays *et al.*, 2020, 2021; Du *et al.*, 2023), as indicated by the absence of coral reefs (Kiessling *et al.*, 2002), chert (Racki, 1999), and coal beds (Retallack *et al.*, 1996; Fielding *et al.*, 2019, 2021; Mays *et al.*, 2020), and the identified extreme fluctuations of atmospheric $\delta^{13}\text{C}$ until the Middle Triassic (Baud *et al.*, 1989; Cao *et al.*, 2009; Chen & Benton, 2012). On land, it is possible that no true forests existed (Looy *et al.*, 1999; Benton & Newell, 2014), and although vertebrate-species diversity rose relatively rapidly, ecosystems and food chains were unstable and unbalanced (Sahney & Benton, 2008). There is also a global

trend of a few taxa dominating horizons (Looy *et al.*, 1999; Benton & Newell, 2014; MacDougall *et al.*, 2019; Botha & Smith, 2020; Viglietti *et al.*, 2022), such as the Dicynodont *Lystrosaurus* in the Karoo Basin, which could reach up to 90% of specimen findings in some levels (Benton, 2008; Nicolas & Rubidge, 2010) and also some groups of temnospondyl amphibians that rapidly diversified (Ruta & Benton, 2008). The SCF, again, does not deviate from these trends, as *P. trigoniceps* dominates the formation's fossil record, and there is a growing number of temnospondyl genera described (Cisneros, 2008; Dias-da-Silva *et al.*, 2017).

The Early Triassic was a unique period in Earth's history, where conditions were especially harsh for marine life as well as on land. The challenges which land life faced were in great part due to climate and the environmental conditions upon which it existed (Irmis & Whiteside, 2012; Benton & Newell, 2014; Mancuso *et al.*, 2021). Thus, understanding climate is crucial to reconstruct the conditions that would later set the stages for the restoration of stable ecosystems that allowed the development of the terrestrial faunas we know (Van Valen, 1984; Labandeira & Sepkoski, 1993; Erwin, 2006; Sahney & Benton, 2008). The SCF occupies a key position in this context, as one of the few Early Triassic units that preserves tetrapod body fossils in Western Gondwana (Mancuso *et al.*, 2021).

3. MATERIALS AND METHODS

An unmanned aerial vehicle was manually operated to collect photographs in two lines parallel to the outcrop exposed walls. These photographs were used to create high-resolution (3.58 mm/pixel) 3D models using the Structure From Motion Multi View Stereo (SFM-MVS) method (James & Robson, 2012) in the software Move®. Two orthophotos were then generated from the models.

The orthophotos were then printed and outcrop-scale sedimentary structures were annotated over it, on site, following the method of Miall (1988, 2016). Vertical profiles along the exposed walls were described, in a total thickness of 76.1 m. To these data the method of Facies Analysis was applied (Dalrymple, 2010; Miall, 2016).

4. SEDIMENTARY FACIES AND FLUVIAL STYLES

Facies analysis resulted in the identification of 15 facies, described in Table 1. Collectively, a dominance of Froude-supercritical structures was identified (Fig. 3), some with varying scale, and most resulting from scour-and-fill processes inherent to the depositional dynamics of their formative bedforms (Cartigny *et al.*, 2014).

Table 1. Recognized lithofacies in the present work.

Code	Designation	Lithology	Geometry	Structure	Relation to other facies	Other features	Interpretation	Figures	Reference
Gcs	Successive asymmetrical scours filled with conglomerate bakcsets	Clast-supported conglomerate. Coarse-grained constituents may be dominated by pebble-sized carbonate-cemented sandstone concretions, by granule-to pebble-sized mud clasts or by a mixture of both. Finer-grained constituents are composed by well-sorted fine-grained sandstone, to poorly-sorted coarse-grained sandstone. Mud clasts and sand grains are red-colored, while the concretions tend to be of dark grey color.	Occurs within wide and thin lenticular layers, laterally persistent for up to more than 70 m, and 5–100 cm thick. Basal contact formed by a series of successive asymmetric erosional scours along a same bounding surface. The asymmetrical scours usually have an upflow steeper and shorter face, and a downflow, longer and gentler face.	Structure consists of low-angle backsets, conformable to the base (gentle face), and onlapping the upslope steep face, sometimes with a slight inflection upwards. The upper laminae may pass above the upflow edge of the scour and dip downwards or continue slightly upwards. At places, a cone-shaped structure, with the wider base pointing downflow, may be observed.	Basal contacts are always erosional. Upper laminae may transition to undulating lamination laterally, or upwards when passing the upflow edge of the scour.	Formation of calcareous nodules around some intraclasts, subparallel to the stratification.	Migration of cyclic steps under highly Froude-supercritical ($Fr > 1.6$) unidirectional flow. The cyclic steps are in turn generated by trains of relatively stable hydraulic jumps which migrate backwards (upflow), generating steep erosional cuts immediately below (steep face). Immediately downflow of the jump, flow velocity (and consequently Froude number) drops, depositing backsets over the gentle face, and then proceeds to reaccelerate until the next jump. Drop in Froude number may cause the flow to enter stability field of antidunes, generating undulating lamination. Cone-shaped structures are interpreted as flute casts	10A, C, D	Allen (1969); Parker (1996); Cartigny <i>et al.</i> (2014); Ono <i>et al.</i> (2021)
Gut	Clast-supported conglomerate with truncated undulating stratification	Clast-supported conglomerate. Coarse-grained constituents may be dominated by pebble-sized carbonate-cemented sandstone concretions, by granule-to pebble-sized mud clasts or by a mixture of both. Finer-grained constituents are composed by well-sorted fine-grained sandstone, to poorly-sorted coarse-grained sandstone. Mud clasts and sand grains are red-colored, while the concretions tend to be of dark grey color.	Occurs within wide and thin lenticular layers, laterally persistent for up to more than 70 m, and 5–100 cm thick. May also occur within amalgamated tabular layers. Basal contact may be erosive or transitional.	Truncated undulating stratification, with mostly low-angle internal truncations, forming lenses with laminasets. There is a preferential preservation of troughs. Some lenses may be partly or completely massive. Clasts may present imbrication.	May transition laterally and vertically from Gcs facies. Contacts with facies other than Gcs are always erosional.	Formation of calcareous nodules around some intraclasts, subparallel to the stratification.	Formation of unstable (breaking) antidunes under Froude-supercritical ($Fr > 1$) unidirectional flow. Antidunes increase in height and start to successively break and form again, causing erosion of previous antidune deposits, and may also aggrade and migrate upflow or downflow. Structureless deposits are interpreted as rapid deposition from sediment clouds, suspended by the high turbulence of the flow.	10B; 11C	Michell, (1893); Cornish, (1899); Kennedy, (1960, 1963); Alexander <i>et al.</i> (2001); Cartigny <i>et al.</i> (2014)

Table 1. (continued)

Code	Designation	Lithology	Geometry	Structure	Relation to other facies	Other features	Interpretation	Figures	Reference
Gs	Clast-supported conglomerate with sigmoidal cross-stratification	Clast-supported conglomerate. Coarse-grained constituents are pebble-sized carbonate-cemented sandstone concretions, and granule- to pebble-sized mudstone clasts. Finer-grained constituent is poorly-sorted and coarse-grained sand. Mud clasts and sand grains are red-colored, while the concretions tend to be of dark grey color.	Occurs within scours of approx. 0.75 m deep and 6 m of lateral extension.	Sigmoidal cross-stratification.	Basal contacts are erosional. Upper contact not observed.	Formation of calcareous nodules around some intraclasts, subparallel to the stratification.	Transversal bedform or filling of erosive cuts downflow from hydraulic jumps, formed on the transition between subcritical and supercritical flow ($Fr \approx 1$; Cartigny, 2014; Miall, 2006).	11C	Saunderson & Lockett (1983)
Gh	Clast-supported conglomerate with plane-parallel stratification	Clast-supported conglomerate. Coarse-grained constituents may be dominated by pebble-sized carbonate-cemented sandstone concretions, by granule- to pebble-sized mud clasts or by a mixture of both. Finer-grained constituents are composed by well-sorted fine-grained sandstone, to poorly-sorted coarse-grained sandstone. Mud clasts and sand grains are red-colored, while the concretions tend to be of dark grey color.	Occurs within wide and thin lenticular layers, laterally persistent for tens of meters, and 5–50 cm thick.	Plane-parallel stratification. Clasts may present imbrication.	Basal contacts are erosional. Upper contacts are abrupt.	Formation of calcareous nodules around some intraclasts, subparallel to the stratification.	Longitudinal bedforms.	6B	Ore (1964)

Table 1. (continued)

Code	Designation	Lithology	Geometry	Structure	Relation to other facies	Other features	Interpretation	Figures	Reference
Scs	Successive asymmetrical scours with sandstone backsets	Red colored, fine- to coarse-grained sandstone. Grains are commonly well-sorted on a same layer, but may be poorly-sorted. Mud intraclasts may be present at the base, decreasing upwards and downflow.	Occurs within lenticular layers, laterally persistent for tens of meters, and 5–100 cm thick. Basal contact is formed by a series of successive asymmetric erosional scours along a same bounding surface. The asymmetric scours usually have an upflow steeper and shorter face, and a downflow, longer and gentler face. In some places, the steep face of the scour truncates the gentle face from the next upflow scour, in lateral amalgamation	Structure consists of low-angle backsets, conformable to the base (gentle face), and onlapping the upslope steep face, sometimes with a slight inflection upwards. The upper laminae may pass above the upflow edge of the scour and dip downwards or continue slightly upwards.	Basal contacts are always erosional. Upper laminae may transition to undulating lamination laterally, or upwards when passing the upflow edge of the scour.	May present carbonatic concretions along scour surfaces.	Migration of cyclic steps under highly Froude-supercritical ($Fr > 1.6$) unidirectional flow. The cyclic steps are in turn generated by trains of relatively stable hydraulic jumps which migrate backwards (upflow), generating steep erosional cuts immediately below (steep face), and the gentle face downflow. Immediately downflow of the jump, flow velocity (and consequently Froude number) drops, depositing backsets over the gentle face, and then proceeds to reaccelerate until the next jump. Drop in Froude number may cause the flow to enter stability field of antidunes, generating undulating lamination. Lateral amalgamation occurs when upflow hydraulic jump migration is faster than deposition rate, and thus the jump erodes the gentle face of the upflow scour.	11A, B; 12	Parker (1996); Cartigny <i>et al.</i> (2014); Slootman & Cartigny (2020); Ono <i>et al.</i> (2021)
Scp	Asymmetric scours filled with sandstone backsets	Red colored, fine- to coarse-grained sandstone. Grains are commonly well-sorted on a same scour, but may be poorly-sorted. Mud intraclasts may be present at the base, decreasing upwards and downflow.	Occurs within amalgamated tabular layers as asymmetric erosional scours. The scours usually have an upflow steeper and shorter face, and a downflow, longer and gentler face.	Backsets subparallel to the longer face, which onlap the steeper face, commonly inflecting upwards.	Basal contacts are always erosional. Upper limits of the scour and lamination are usually truncated by the overlying layer. It is usually accompanied by the S _{ut} , S _h and S _m facies in amalgamated scours and lenses	Abundant carbonatic concretions along scour surfaces.	Formation of chute-and-pool bedforms under Froude-supercritical conditions ($1.58 < Fr < 2.14$). The chute-and-pools are, in turn, generated by an unstable (short-lived) hydraulic jump. The jump erodes the sediment bed below and migrates backwards (upflow), generating the upflow steep face of the scour, and the gentle face downflow. Immediately downflow of the jump, flow velocity (and consequently Froude number) drops, depositing backsets over the gentle face, and then proceeds to reaccelerate until the next jump. Amalgamation with other facies occurs due to the coexistence of chute-and-pool bedforms to breaking antidunes and plane bed, and the highly erosional nature of these bedforms.	14A	Simons & Richardson (1961); Alexander <i>et al.</i> (2001); Cartigny <i>et al.</i> (2014)

Table 1. (continued)

Code	Designation	Lithology	Geometry	Structure	Relation to other facies	Other features	Interpretation	Figures	Reference
Sut	Sandstone with truncated undulated lamination	Red colored, well- to poorly-sorted, fine- to coarse-grained sandstone. Mud intraclasts may be present at the base, decreasing upwards, or dispersed.	Occurs within amalgamated tabular layers. Basal contact may be erosive or transitional.	Truncated undulating lamination to stratification, with mostly low-angle internal truncations, forming lenses with laminasets. There is a preferential preservation of troughs. Some lenses may be partly or completely massive. Lens length may be of small-scale, with 0.5–2.1 m (1–2.32 estimated wavelength), or large-scale, with 4–14.46 m (8–28.92 estimated wavelength).	May transition laterally and vertically from Gcs facies. Contacts with facies other than Gcs are always erosional. It may be accompanied by the Scp, Sh and Sm facies in layers of amalgamated scours and lenses	Large-scale lamination commonly presents carbonate cement along erosional surfaces and laminae.	Formation of unstable (breaking) antidunes under Froude-supercritical ($Fr > 1$) unidirectional flow. Antidunes increase in height and start to successively break and form again, causing erosion of previous antidune deposits, and may also aggrade and migrate upflow or downflow. Structureless deposits are interpreted as rapid deposition from sediment clouds, suspended by the high turbulence of the flow. Amalgamation with other facies occurs due to the coexistence of chute-and-pool bedforms to breaking antidunes and plane bed, and the highly erosional nature of these bedforms.	10C; 13; 17	Michell (1893; Cornish (1899); Kennedy (1960, 1963); Alexander <i>et al.</i> (2001); Cartigny <i>et al.</i> (2014)
Su	Sandstone with continuous undulated lamination	Fine- to medium-grained, red colored, and usually well-sorted sandstone. Mud intraclasts may be present at the base, decreasing upwards, or dispersed.	Occurs as tabular layers with other facies when in smaller-scale, and also as thick lenses when in larger-scale.	Undulating lamination, with lateral continuity of laminae of few to several meters, and few internal truncations. Can be divided in two scales. Small-scale laminae have wavelengths of approx. 40–100 cm, and amplitude of approx. 2–10 cm. Large-scale lamination has wavelengths of approx. 4.5–7.85 m and amplitudes of 3–32 cm.	Basal contacts usually erosional (undulated), but may be abrupt. May transition laterally to Sut and Sh facies.	Large-scale lamination commonly presents carbonate cement along erosional surfaces and laminae.	Aggradation of mostly-stationary (stable) antidunes, under supercritical ($Fr > 1$) unidirectional flow. When the flow reaches $Fr \geq 1$, stationary waves start to form on the water surface and the sediment bed starts in turn to form sediment waves which are in-phase with the surface waves. If deposition rate is enough, the sediment wave aggrades. The system may also migrate downflow or, more commonly, upflow. The different scale of the antidunes is a result of many factors, the major being flow velocity. Lateral transition to Sut facies occurs because stable and unstable antidunes may coexist when Froude number is not high enough to cause constant breaking of waves. Lateral transition to Sh facies occurs because flat bet and antidunes may coexist when $Fr \approx 0.84–1.0$.	12; 13; 15B; 17A	Cornish (1899); Kennedy (1960, 1963); Alexander <i>et al.</i> (2001); Cartigny <i>et al.</i> (2014)

Table 1. (continued)

Code	Designation	Lithology	Geometry	Structure	Relation to other facies	Other features	Interpretation	Figures	Reference
Sh	Sandstone with plane-parallel lamination	Fine- to medium-grained, well- to moderately sorted and red-colored sandstone. Granule- to pebble-sized red-colored mud intraclasts occur in discontinuous trains of clasts, and locally as densely-packed aggregates.	Occurs as tabular layers, or in amalgamated layers with other facies within lenses.	Plane-parallel lamination to stratification.	Basal contacts are erosional. Upper contacts are abrupt. May occur with facies Scp, Sut and Sm in layers of amalgamated scours and lenses. In other instances, may transition laterally to the Su facies.	Occasional carbonate cement along erosional surfaces and laminae.	Particle transport over plane bed under upper-flow regime unidirectional flow. Amalgamation with other facies occurs due to the coexistence of chute-and-pool bedforms to breaking antidunes and plane bed, and the highly erosional nature of these bedforms. Lateral transition to Su facies occurs because flat bet and antidunes may coexist when $Fr \approx 0.84-1.0$.	12	Owens (1908); Kennedy (1960, 1963); McKee <i>et al.</i> (1967); Alexander <i>et al.</i> (2001)
Ss	Sandstone with sigmoidal cross-stratification	(1) Medium-grained and moderately sorted, red-colored sandstone. Granule- to pebble-sized red-colored mud clasts may be present at the base	(1) Occurs within erosional scours of aprox. 30–60 cm deep and 1–3 m long. Upper contact abrupt.	(1) Sigmoidal cross-stratification.	(1) Occurs at the top of successions of supercritical structures.	Commonly presents more developed cementation, highlighting stratification.	(1) Filling of the scours in front of hydraulic jumps. Deceleration and reacceleration of the flow in front of the jump causes the flow to be in the transition from subcritical to supercritical ($Fr \approx 1$) unidirectional flow. The mud clasts are interpreted as lag deposits from erosion of in-channel muds.	14C, D	Abdullatif, (1989); Alexander <i>et al.</i> (1999); Cartigny <i>et al.</i> (2014)
		(2) fine-grained and well-sorted, red-colored sandstone	(2) Occurs in tabular layers with diffuse limits.	(2) Sigmoidal cross-lamination with diffuse laminae, usually discernible by slight color change from "redder" to "more orange" tones. External for of the bedform commonly preserved, and a climbing angle is present at places.	(2) Occurs above successions of supercritical structures, with lateral and upwards transitions to faintly cross-laminated fine-grained sandstone.	(2) Migration and accretion of humpback dunes with high deposition rate, formed in the transition of subcritical and supercritical ($Fr \approx 1$) unidirectional flow.	15A, B	Saunderson & Lockett (1983); Arnott & Hand (1989); Manna <i>et al.</i> (2021)	
St	Sandstone with trough cross-stratification	Fine- to medium-grained, well- to moderately sorted, and red-colored sandstone. Granule- to pebble-sized red-colored mud clasts may be present at the base.	Occurs within erosional scours of aprox. 30–60 cm deep and 1–3 m long. Upper contact abrupt.	Trough cross-stratification.	Occurs at the top of successions of supercritical structures.	Carbonate cementation is occasionally more developed along stratification.	Filling of erosive cuts downflow from hydraulic jumps. Deceleration of the flow in front of the jump causes the flow to momentarily enter Froude-subcritical conditions ($Fr < 1$). The mud clasts are interpreted as lag deposits from erosion of in-channel muds.	14B	Abdullatif, (1989); Alexander <i>et al.</i> (1999); Cartigny <i>et al.</i> (2014)

Table 1. (continued)

Code	Designation	Lithology	Geometry	Structure	Relation to other facies	Other features	Interpretation	Figures	Reference
Sr	Sandstone with ripple cross-lamination	Red-colored, fine-grained and well-sorted sandstone.	Occurs in tabular layers with diffuse limits.	Faint ripple cross-lamination with diffuse laminae. External form of the bedform may be preserved, and climbing angle is preserved at places.	Faint lamination may be difficult to observe, so that the facies "transitions" laterally to and from massive. Usually occurs with Sm, Ss (small), and B facies.		Migration of current ripples under Froude-subcritical ($Fr < 1$) unidirectional flow, with high deposition rate.	15C, D	Allen (1968); Arnott & Hand (1989)
Sr(c)	Sandstone with convolute cross-lamination	Red-colored, fine-grained and well-sorted sandstone.	Occurs in lenticular layers with diffuse limits.	Convolute, distorted and disconnected ripple cross-lamination.	this facies occurs exclusively above faint ripple cross-lamination (Sr facies).		Rapid deposition causing a rapid expulsion of water from intergranular space and movement of the grains, distorting the lamination	15C	Lowe & LoPiccolo (1974)
Sm	Massive or incipiently-laminated sandstone	Very fine- to medium-grained, red-colored sandstone. Grains are usually well- to moderately sorted. Occasional trains and densely-packed aggregates of granule-sized red mudstone clasts occur.	Occurs as tabular layers with diffuse limits, and within lenses and scour-fills in amalgamated tabular layers.	Structureless, or faint and incipient lamination (trough, plane-parallel, undulated) . Faint thin-bedding may be observable.	This facies is more common at the top of successions. Relation to Sr and Ss (small) facies is usually laterally and vertically transitional with diffuse limits. Occurs as amalgamated lenses and scour fills alongside Scp and Sut facies, with erosional contacts. When in wide lenses, it may occur without any other facies, or intercalated with Gh facies.	Abundant concretions, which may be dispersed but are more commonly concentrated on a same level.	Combination of processes: (1) rapid deposition of high sediment load; (2) cohesive transitional flows; (3) incipient pedogenesis.	6A–C, E; 15B, C, E	Lowe & LoPiccolo, (1974); Retallack, (1988); Alexander <i>et al.</i> (2001); Baas <i>et al.</i> (2011)

Table 1. (continued)

Code	Designation	Lithology	Geometry	Structure	Relation to other facies	Other features	Interpretation	Figures	Reference
Fm	Massive mudstone	Red-colored, massive or weakly-laminated mudstone	This facies occurs in rare, relatively small lenses, up to 0.75 m thick and 3 m long, with basal contact concordant to the underlying facies. Top of the lenses usually have erosional contacts.	Structureless, or faint and incipient plane-parallel lamination	Rare occurrence, amidst scour-and-fill structures (Sut, St, Sh facies)		Gravitational settling of fines from suspension after waning flow in pools.		Abdullatif, (1989); Alexander <i>et al.</i> (1999)
Sb	Sandstone with blocky structure	Very fine- to medium-grained, red-colored sandstone. Grains are usually well- to moderately sorted.	Is present mainly at the top of successions, but may occur laterally to other facies, in a same layer.	Horizontal, vertical and oblique disjunctions, resulting in a hexagonal or horizontally-elongated rectangular blocky texture; number and interconnection of the disjunctions increases upwards.	May occur superimposed over massive or incipiently-laminated sandstones.		Formation of cutans and peds by pedogenesis.	6D; 15B	Retallack (1988)

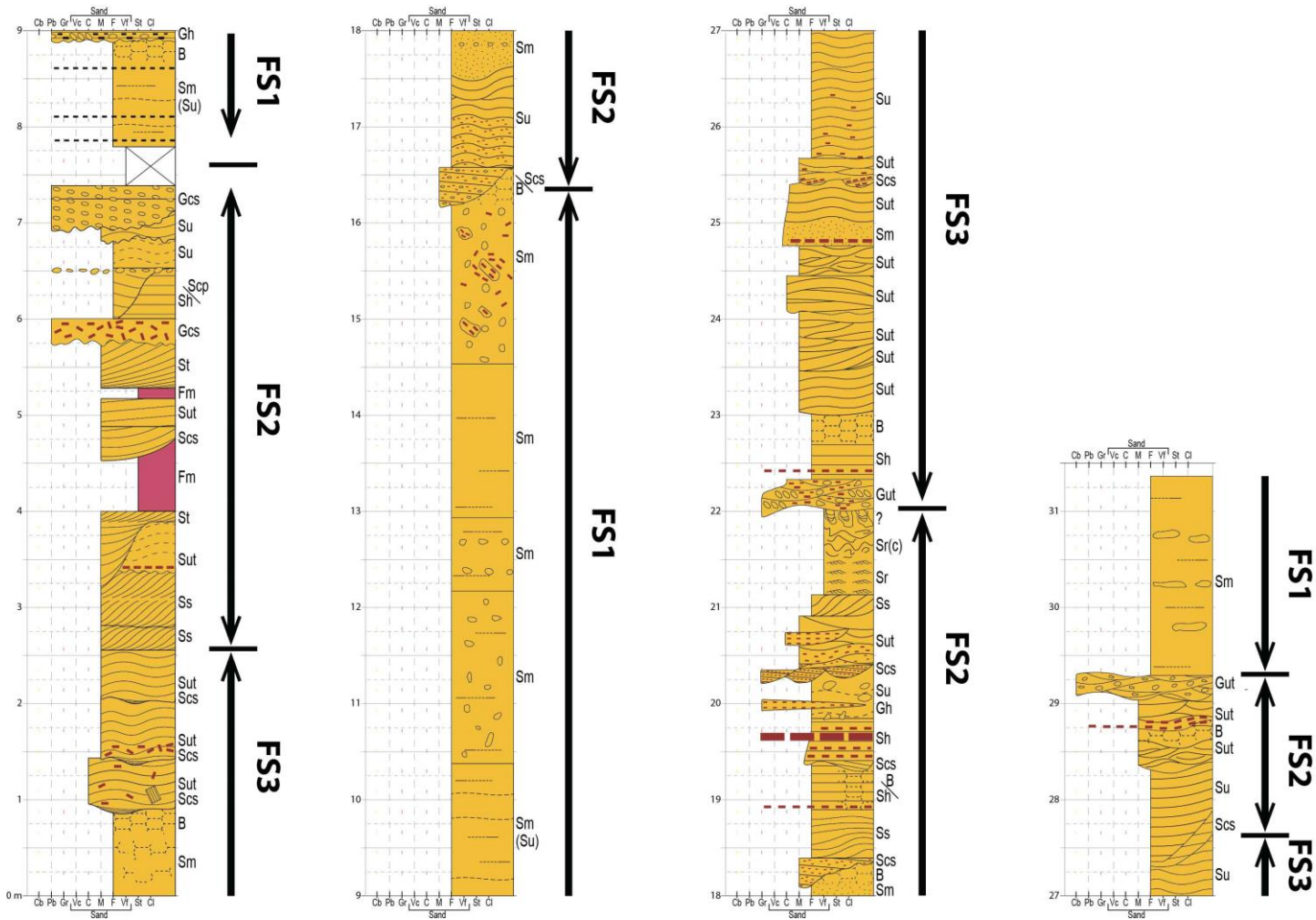


Fig. 3.--- Composite profile of the studied section with denotation of the interpreted Fluvial Styles. A cyclicity of the Fluvial Styles is interpreted. Facies are described in Table 1.

Lateral and vertical relations of the facies allowed their grouping in three different recurring Fluvial Styles (Fig. 3). Most facies are present in all Styles; however, their relative abundance, scale, external layer form, and relation to the other facies varied. Fluvial Style 1 (FS1) is characterized by the predominance of the Sm facies, with some interruptions of other facies. Fluvial Style 2 (FS2) is marked by a fining-upwards sequence ranging from Froude-supercritical, erosionally based and amalgamated structures, into lower-flow-regime structures with high deposition rate. Fluvial Style 3 (FS3), in turn, is also defined by Froude-supercritical structures. However, these structures present much larger scale and lateral continuity, and are more restricted to lower-Froude-number structures (even though they are of greater scale).

4.1 Fluvial Style 1

Description.--- Fluvial Style 1 comprises bodies with tabular external form of overwhelmingly fine-grained sandstone, up to 7 m in thickness (Fig. 4) and laterally extensive up to approx. 90 m in the studied outcrop (Figs. 4, 5). The rock is mostly composed of the Sm facies (Figs. 4–6), with some occurrences of the Gh facies, laterally persistent for up to approx. 26 m (Figs. 4, 6B).

The style is characterized by the seemingly monotonous succession of fine-grained massive sandstone (Figs. 4–6A). At distance, a wide stratification (approx. 0.2–1 m) can be perceived, in great part conditioned by the presence of horizons where abundant carbonate concretions are aligned (Figs. 4, 6B), but limits of the stratification are in most places not readily identifiable on a closer observation (Fig. 6A). However, careful inspection allows identification, in some places, of thin levels of mud clasts, and color differences or subtle changes in grain size from fine- to very fine-grained sandstone, which reveal the presence of thin beds (Fig. 6B, C). These are more recognizable at the base of the lower FS1 occurrence (Fig. 6B, C; 7.75–8.9 m of the composite section, Fig. 3), where incipient undulations can be observed (Fig. 6C), although they occur sparsely in the succession. Blocky structure (Sb facies) is more well-developed just below erosion surfaces (Figs. 6D; at 8.75 m and 16.75 m in the composite section of Fig. 3).

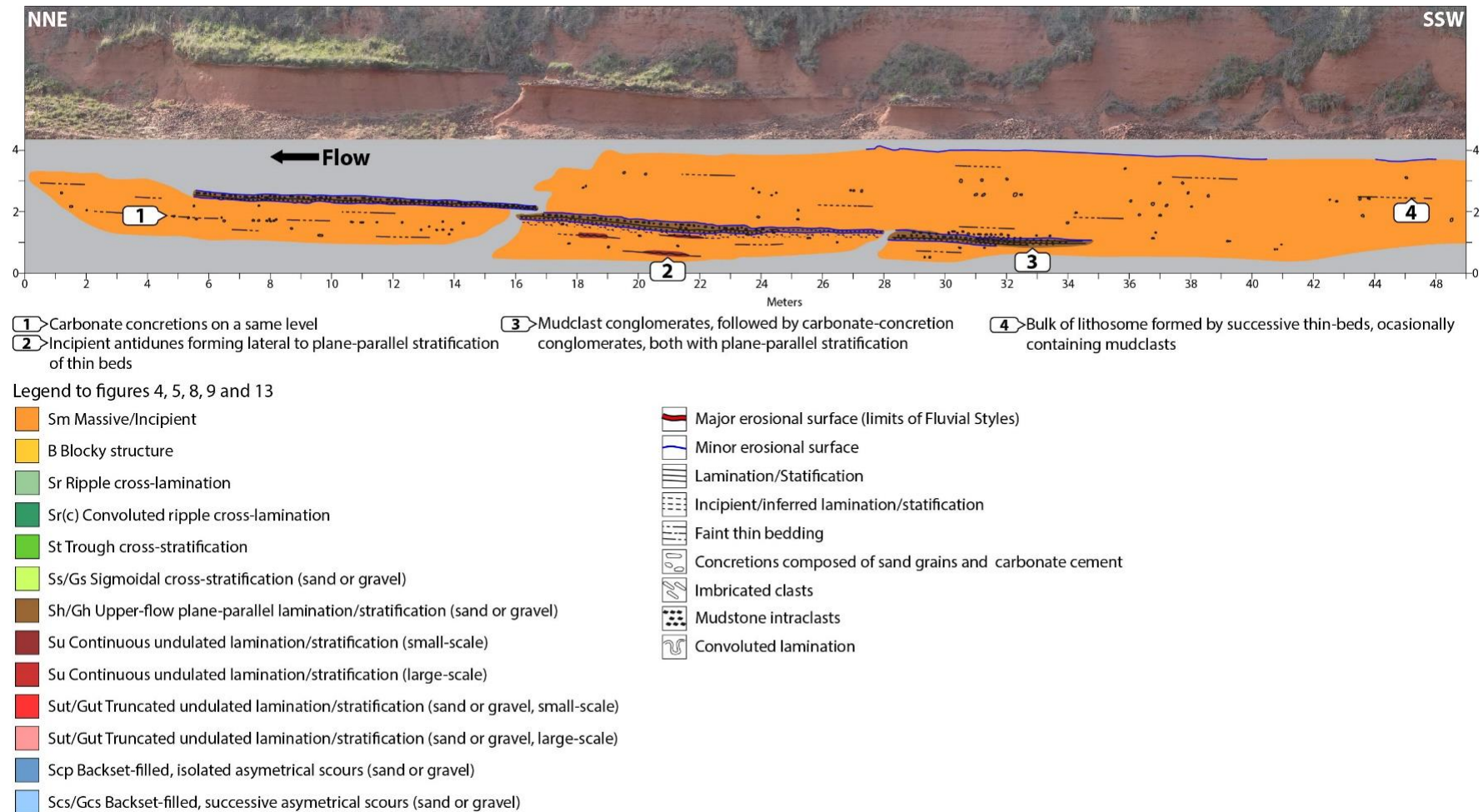


Fig. 4.--- Panel displaying facies distribution of Fluvial Style 1 on the northern east exposure of the studied outcrop, and legend to other panel figures. Numbered balloons indicate features of special interest. See text for further explanation.

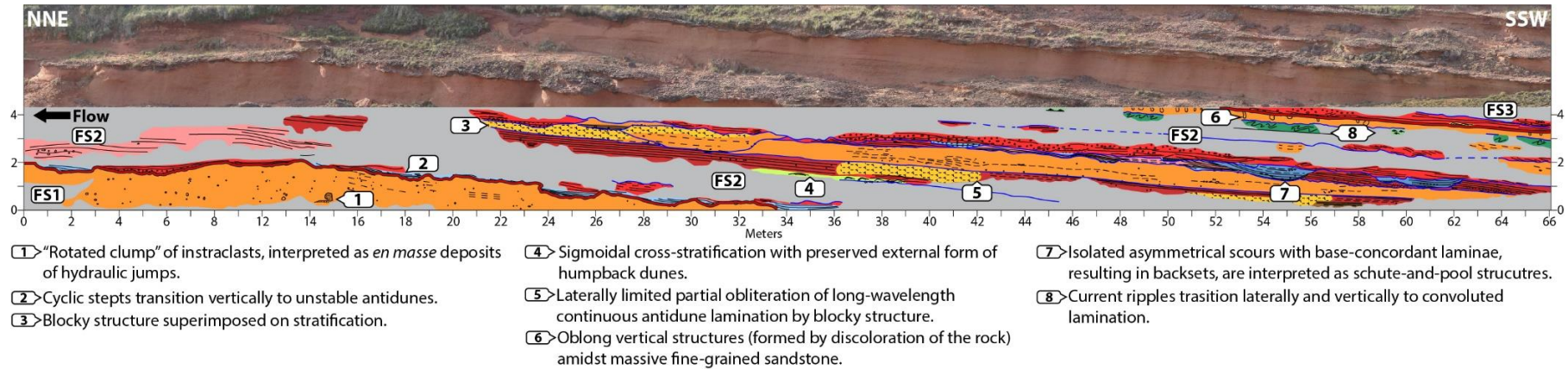


Fig. 5.--- Panel displaying distribution of facies of Fluvial Styles 1 and 2 on the southern east exposition of the studied outcrop. Numbered balloons indicate features of special interest. See text for further explanation.

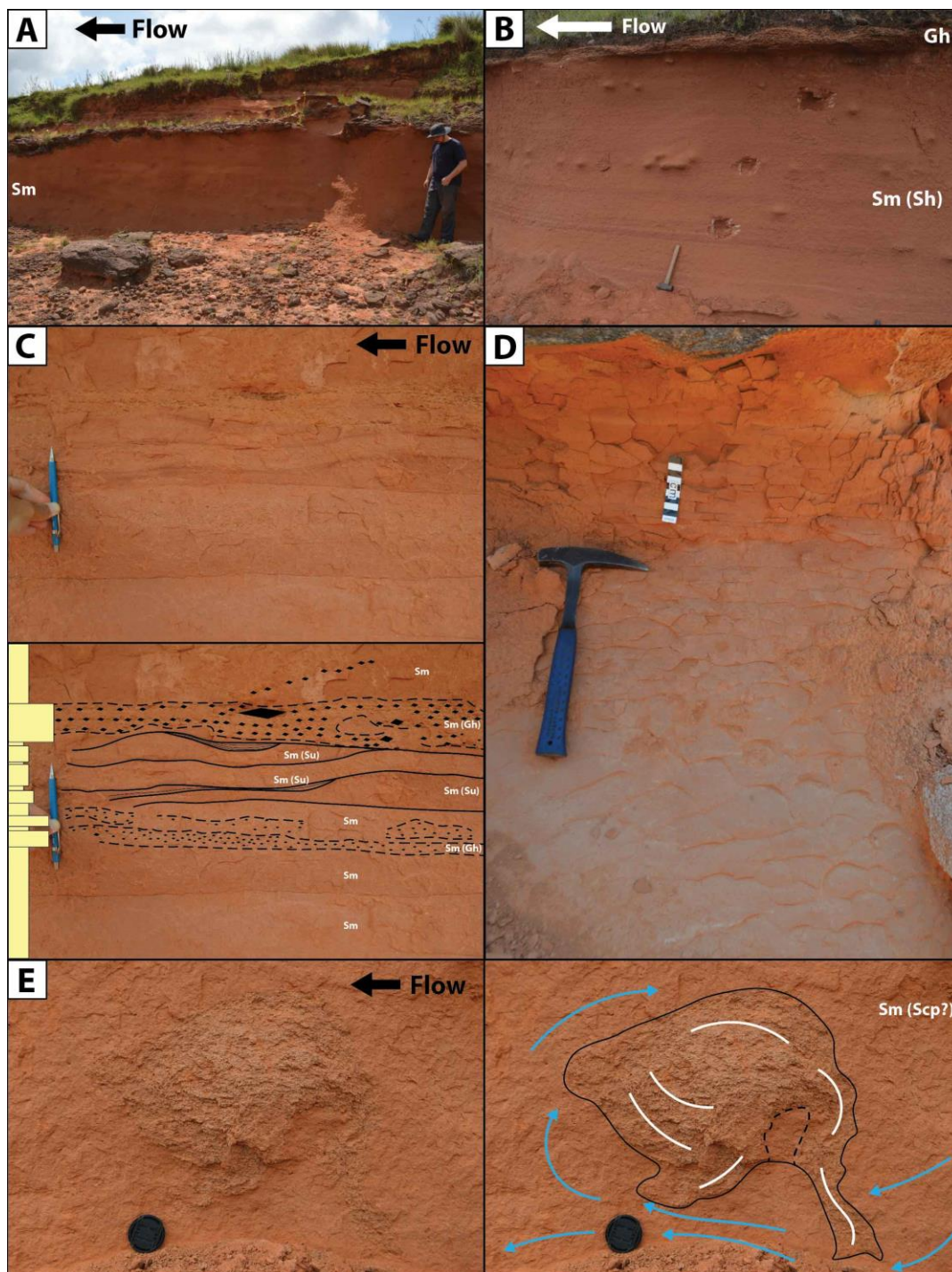


Fig. 6.--- Facies of Fluvial Style 1. **A)** General aspect of the Sm facies, most common throughout the studied area. Person is approx. 1.7 m tall. **B)** Mud-clast conglomerate with planar stratification (Gh) at the top of picture, overlying Sm facies where thin beds with planar lamination are visible. Hammer is 40 cm long. **C)** Faint thin beds presenting undulations, and thin levels of mudstone intraclasts presenting planar alignment amidst massive deposits. In the annotated lower image, to the left, the column indicates grain size, from very fine sand to gravel. Mechanical pencil is 13 cm long. **D)** Vertical succession of blocky structure (Sb facies), interpreted as pedogenic in origin. The top of the succession is an erosional surface overlain by a mudclast conglomerate. **E)** “Rotated mud-intraclast clump”. It is interpreted as the result of partial erosion of a mudstone deposit, followed by *en masse* deposition downflow from a hydraulic jump, due to abrupt loss of capacity from the transition flow from supercritical before the hydraulic jump, to subcritical immediately in front of it (Zellman *et al.*, 2021). For interpretation of the formative process of this structure, see Fig. 7.

Some intervals in the Sm facies succession can be differentiated, mainly by the pattern of concretions (Fig. 3). Occasionally, granule- to pebble-size mud clasts occur in aggregates with dense packing (Figs. 5, 6E). In the upper part of the lowest occurrence of FS1 (14.5–16.5 m in Fig. 3), a “rotated clump” of aggregated clasts can be observed (Fig. 6E).

Interpretation.--- FS1 is interpreted to have been deposited mostly by very poorly-confined to unconfined shallow flows (Fisher *et al.*, 2008; North & Davidson, 2012), which eventually approached Froude-supercritical conditions, evidenced by the incipient undulations (Kennedy, 1960). Mud deposits generated in ephemeral ponds between floods were eroded to form lags of mudstone intraclasts (Abdullatif, 1989; Fielding & Alexander, 1996; Alexander *et al.*, 1999). Grain size uniformity, rapid deposition, and high sediment load are interpreted as factors which prevented the formation of sedimentary structures (Lowe & LoPiccolo, 1974; Baas *et al.*, 2011). These flows are interpreted to have swept across a wide alluvial plain with a relatively low recurrence interval, which allowed the obliteration of sedimentary structures through pedogenesis, but not the formation of developed paleosol horizons, adding to the overall structureless aspect of the deposits (Retallack, 2001). Levels with blocky structure represented greater halts in deposition and more developed pedogenesis (Retallack, 2001), and subsequent flows were of higher energy, with greater erosive power, generating conglomerates (Gh facies; Figs. 4–6B). Overall, discharge frequency was low. Formation of carbonate concretions in alluvial arid or semiarid settings may be the result of evaporation of infiltrated water (from rain or floods, the *per descensum* model), or evaporation from groundwater due to a water table close to the surface (the *per ascensum* model; Alonso-Zarza & Wright, 2010). As an example, the carbonate concretions of the Santa Maria Formation, a Middle- to Upper-Triassic unit overlying the SCF (Fig. 1) are interpreted by Horn *et al.* (2013) as the result of both processes. The alignment of concretions on horizons in the SCF is interpreted here as resulting from precipitation from the water-table surface, added to preferential precipitation on bedding surfaces (which are often imperceptible due to the reasons stated above).

The seemingly “rotated” aggregates are interpreted as *en masse* deposition resulting from hydraulic jumps (Fig. 7), in an interpretation similar to that of

Zellman *et al.* (2021, their Figure 3B). Experimental studies have commonly observed hydraulic jumps which generated structureless deposits (Alexander *et al.*, 2001). At the point where the flow turns from supercritical to subcritical, an abrupt loss of capacity would cause *en masse* deposition, causing the suspended particles to “freeze” (Alexander *et al.*, 2001; Ono *et al.*, 2021; Zellman *et al.*, 2021). The apparent “rotating” aspect of the mud intraclasts is interpreted to reflect the turbulent eddies of the hydraulic jump at the moment of *en masse* deposition (Fig. 7). This feature, in turn, indicates eventual deeper flows.

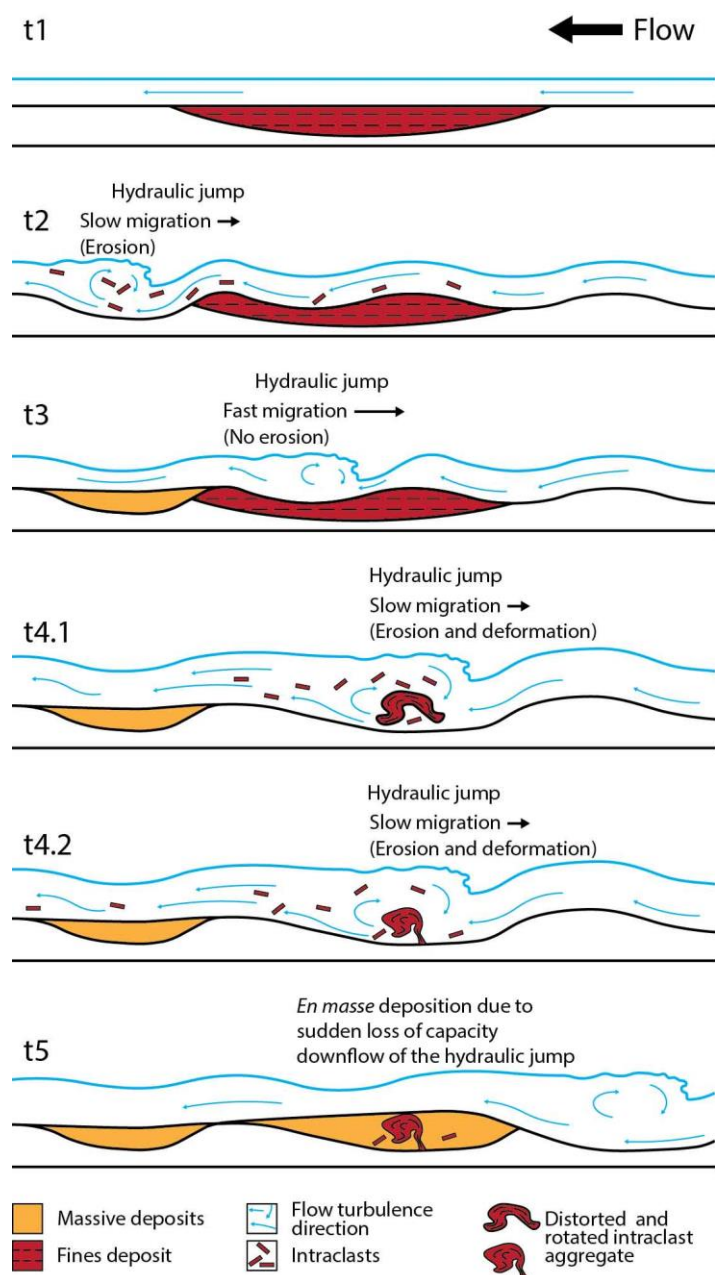


Fig. 7.--- Interpretation of formative process of the “rotated intraclast clump” of Figure 6E. **T1:** idealized initial conditions. Flow to the left passes over a mudstone deposit. **T2:** Froude-supercritical flow establishes erosive conditions, and a hydraulic jump is formed. The mudstone deposit is partially eroded. **T3:** Hydraulic jump migrates fast upflow and does not erode completely the mudstone deposit. **T4.1:** the hydraulic jump returns to slow migration and erodes the mudstone deposit. A relatively big block is detached from the substrate by the powerful supercritical underflow. As it is rotated, folded, and deformed by the hydraulic jump countercurrent turbulence, the mudstone breaks into millimeter-size clasts. **T4.2:** The now mudstone-intraclast aggregate is deformed to the observed form in up to a few seconds. **T5:** When this dense aggregate of sediment passes to the front of the hydraulic jump, where the flow is Froude-subcritical ($Fr \leq 1$), the flow abruptly loses erosive and transport capacity, causing *en masse* deposition (the sediment cloud “freezes” with the mud-clast aggregate within).

4.2 Fluvial Style 2

Description.--- This fluvial style is characterized by dominance of erosionally based structures and presents as tabular lithosomes up to approx. 4 m thick and up to approx. 82 m wide, with an upwards-fining overall trend (Figs. 3, 5, 8, 9), from pebbly intraclastic conglomerates to very fine-grained sand. It can be further subdivided in three intervals with more closely associated facies, which have internally a fining-upwards trend. The intermediate and upper intervals are commonly eroded, such that the lower part occurs more frequently.

The lower interval is approx. 0.5 to 1 m thick, and the basalmost layer is composed of the Gcs or Scs facies (Figs. 5, 8–10). It is characteristic of this fluvial style that the upper laminae which onlap the steep face of the asymmetric depressions (Gcs, Scs), when leaving the excavation, start to undulate and transition to the Gut, Su, or Sut facies (Figs. 5, 8–10A, C), which may present imbrication of the clasts (Fig. 10B). Contacts may also be sharp erosional (Fig. 11A). In some places, the steep face of the scour truncates the gentle face from the next upflow scour, causing lateral amalgamation (Fig. 11B). Gs facies is present laterally to the Gut facies, as scour fill (Figs. 8B, 11C). Locally, a succession of “wedges” bounded by inclined erosional surfaces and filled with low-angle backsets can be observed (Fig. 12). It rests erosionally upflow from a “mound-shaped” layer of sandstone with blocky structure, and the last wedge extends upflow into a long scour (Fig. 12).

The intermediate interval is dominantly sandy and presents a complex and diverse arrange of truncated and amalgamated erosionally based lithofacies, generated mainly by Froude-supercritical flows (Figs. 5, 8, 9, 13). At some places, small-scale Sut facies may occur laterally continuous, with subordinate small Scp facies (scours up to approx. 30 cm deep and 1 m long; Fig. 9). In other places, larger Scp facies (scours 0.1–1 m deep and 1–3 m long) occur amalgamated, and laterally associated with Sh, Sut, Su, and Sm facies, all with erosional contacts (Figs. 8, 14). Non-transported carbonate-cemented sandstone concretions occur along the scour planes (Figs. 8, 14). Sh facies may transition to very low-amplitude and long-wavelength Su facies (Fig. 8C), and locally Su facies transitions to Sr facies (Fig. 8C). Sandstone with blocky structure (Sb facies) may occur superimposed on other facies (Fig. 5). Mainly at the top of this

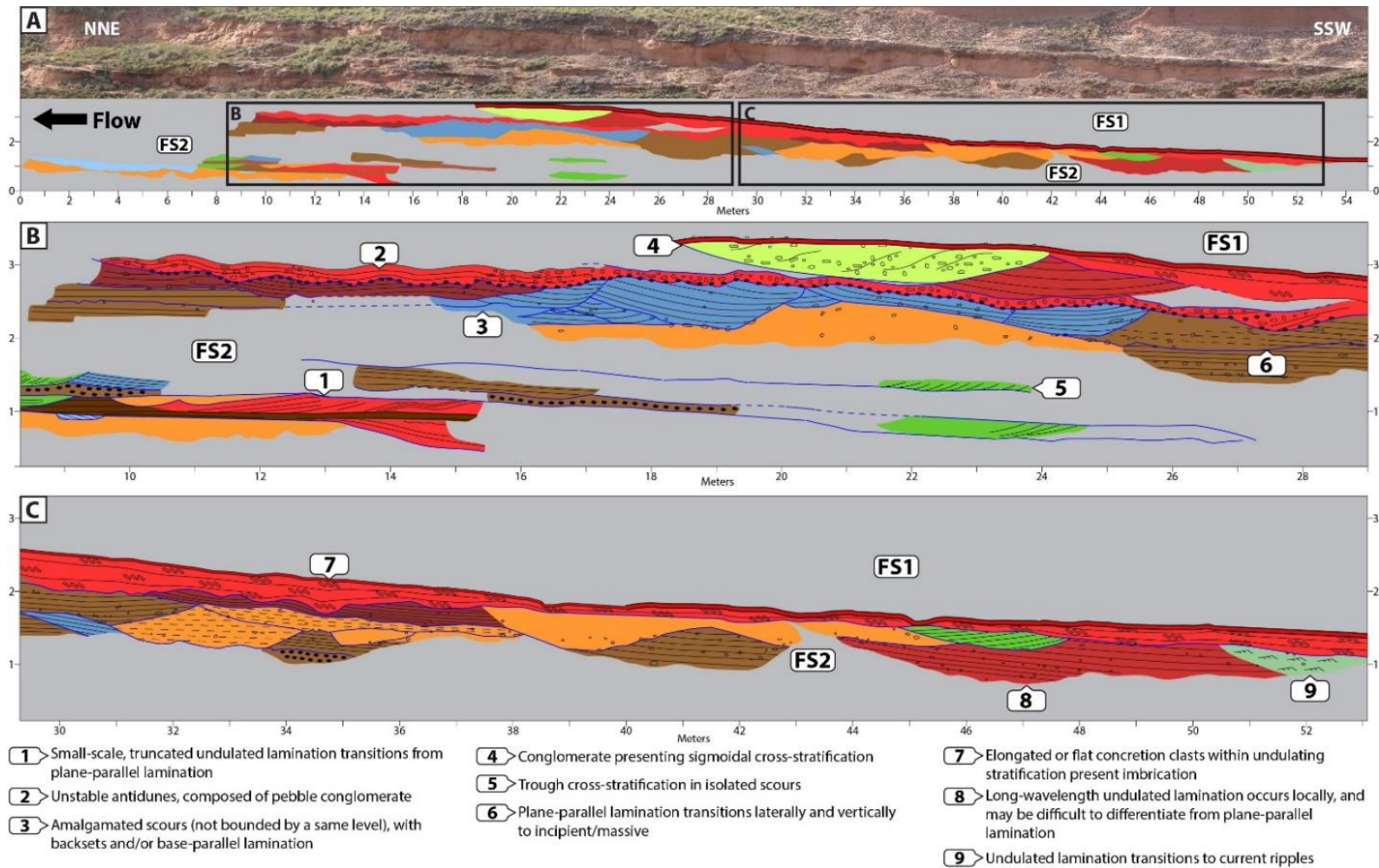


Fig. 8.--- Panel displaying facies distribution of Fluvial Style 2 on the northern east exposition of the studied outcrop. **A)** General view. **B)** Close-up of the northern part, shown in Part A. **C)** Close-up of the southern part, shown in Part A. Numbered balloons indicate features of special interest. See text for further explanation.

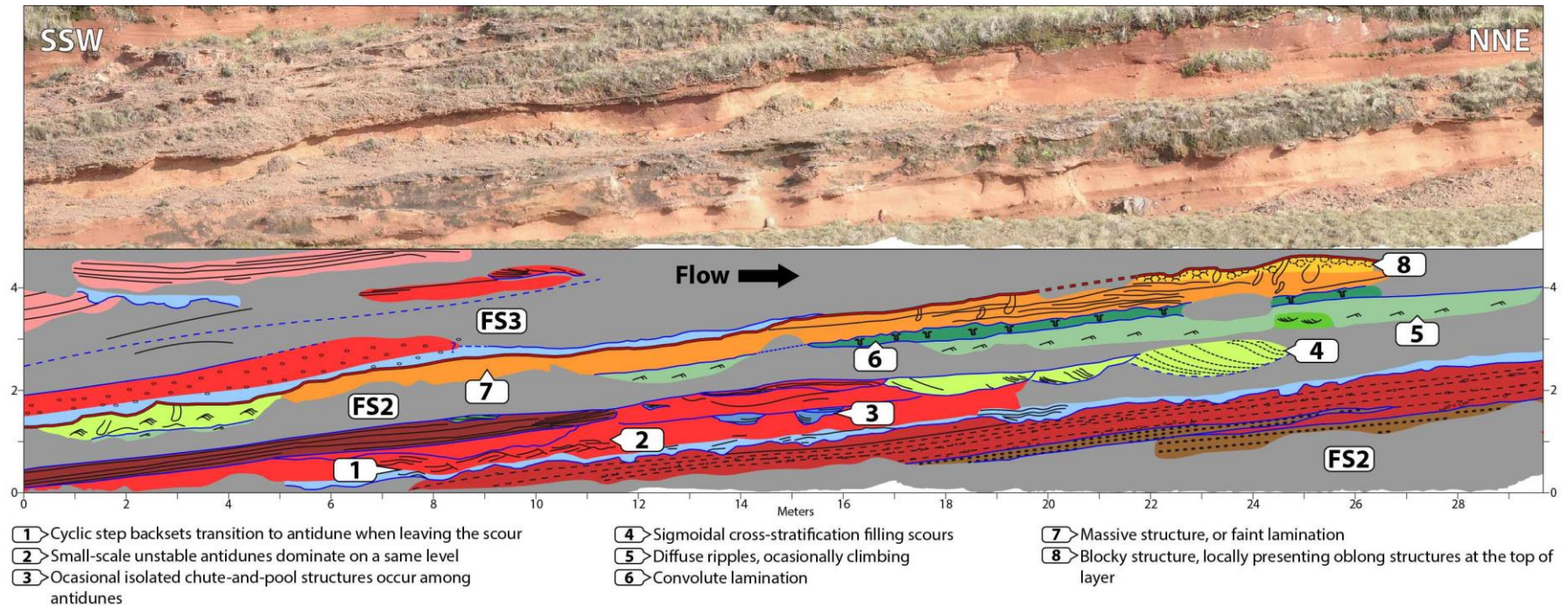


Fig. 9.--- Panel displaying facies distribution of Fluvial Style 2 on the west exposition of the studied outcrop. Numbered balloons indicate features of special interest. See text for further explanation.

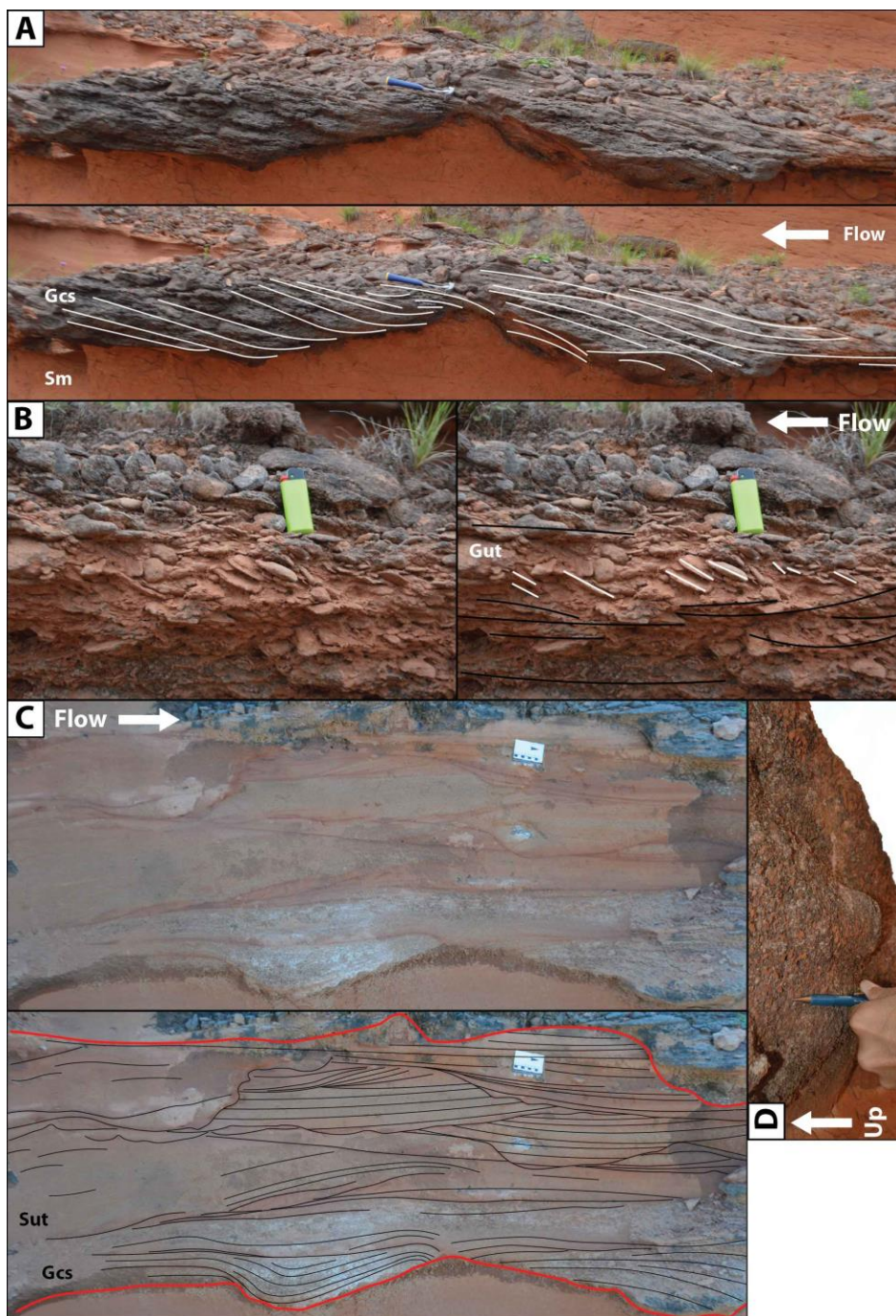


Fig. 10.--- Basal facies of Fluvial Style 2. **A)** Gcs facies, interpreted as deposited by conglomeratic cyclic steps. Figure displays two successive scours showing well-developed backsets. Left-side backsets show upwards inflection near the upflow face of the scour. Right-side backsets show transition to undulatory laminae (Gut facies). Hammer is 28 cm long. **B)** Close-up of Gut facies, interpreted as deposited by conglomeratic unstable antidunes. Stratification is largely noticeable through alignment of clasts, which are mostly composed of carbonate-cemented sandstone concretions. Note imbrication of clasts in center. Lighter is 8 cm long. **C)** Successive asymmetric scours filled by mud-clast conglomerate backsets, transitioning to undulatory truncated lamination in amalgamated lenses (Gcs to Sut facies). Scour in center shows pinching of the laminae at the extremities of the scour. Note that for the Sut facies, concave-up laminae are more common and well preserved than convex-up (mainly on the top-right of picture), and massive structure is also common (left side of picture). Scale is in centimeters. **D)** Picture rotated counterclockwise. Basal view of a scour, showing cone-shaped structure interpreted as a flute cast. Visible part of mechanical pencil is approx. 7 cm.

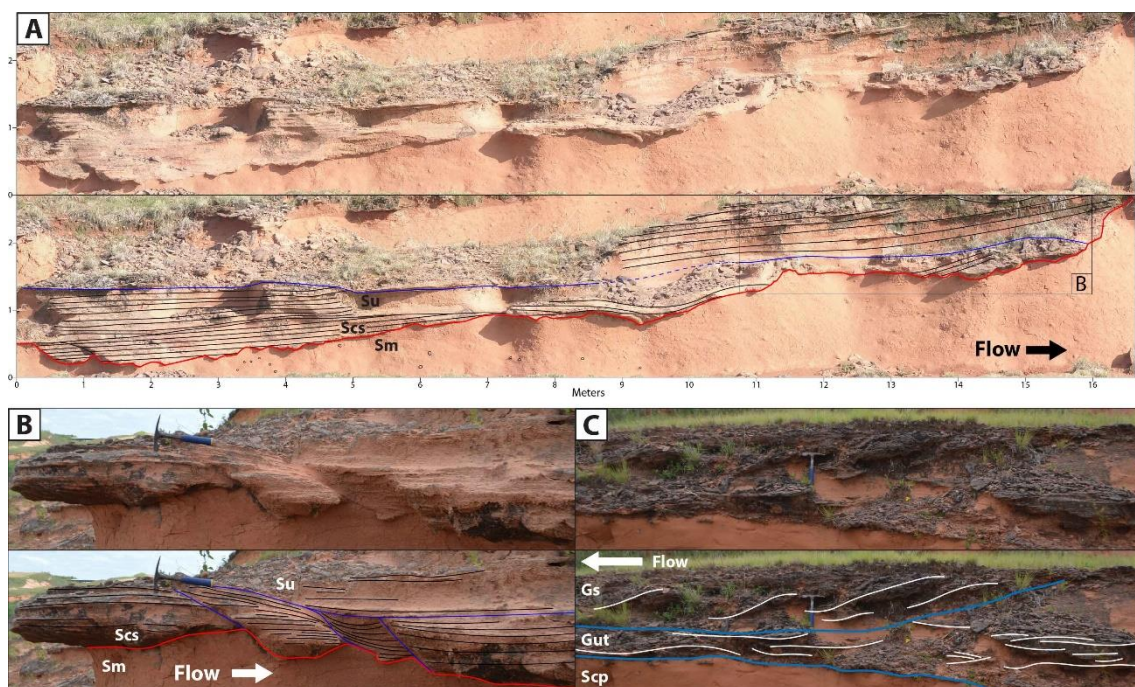


Fig. 11.--- Basal facies of Fluvial Style 2. **A)** Series of asymmetric scours with very low-angle backsets, interpreted as sandy cyclic-step deposits. These present low depth-to-width ratio in comparison to the conglomeratic Gcs facies. Note lateral amalgamation of scours on the lower left corner of the image and pinching of the second scour to the left. Low-amplitude continuous undulatory laminae rest erosionally over the backsets. **B)** Laterally amalgamated asymmetric scours. The upflow step face truncates the downflow long face of the scour behind. Backsets of third scour from the left show upwards inflection and pinching of laminae. Hammer is 28 cm long. **A)** Conglomerate with sigmoidal cross-stratification (Gs). Upper blue line delineates the scour which the conglomerate fills. Gut facies occurs below and lateral to the sigmoidal set. Hammer is 28 cm long.

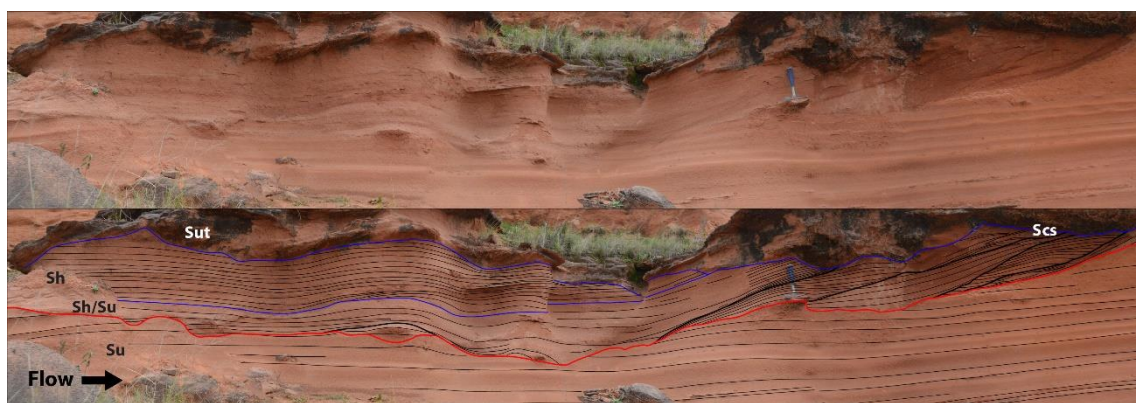


Fig. 12.--- Photomosaic showing, from bottom to top: large-scale continuous undulatory laminae (stable-antidune deposit); wedges with backsets (right) which transition laterally to planar lamination and/or very low-amplitude undulatory continuous laminae (left); planar lamination. Red line shows erosional surface dividing Fluvial Style 3 from Fluvial Style 2. Thicker black lines mark limits of wedges. Blue lines mark erosional limits between different facies. See Figure 16 for interpretation of generation of the wedges. Hammer is 28 cm long.

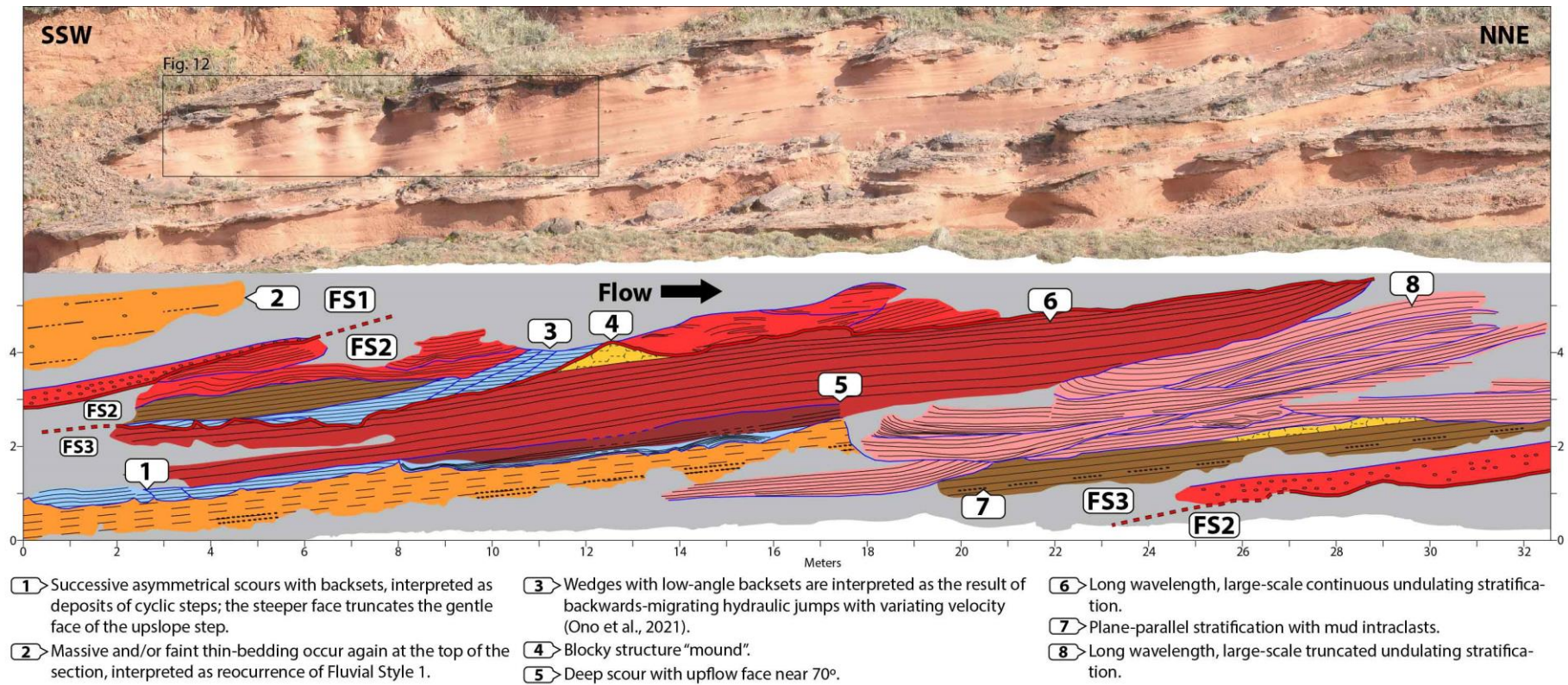


Fig. 13.--- Panel displaying distribution of facies of Fluvial Styles 1, 2 and 3 on the west exposition of the studied outcrop. Numbered balloons indicate features of special interest. See text for further explanation.

intermediate interval, scours (approx. 0.3–0.5 m deep and 1–2.5 m long) filled by medium-grained and moderately sorted St or Ss (larger-type occurrence) facies can be observed (Figs. 5, 8, 9, 14).

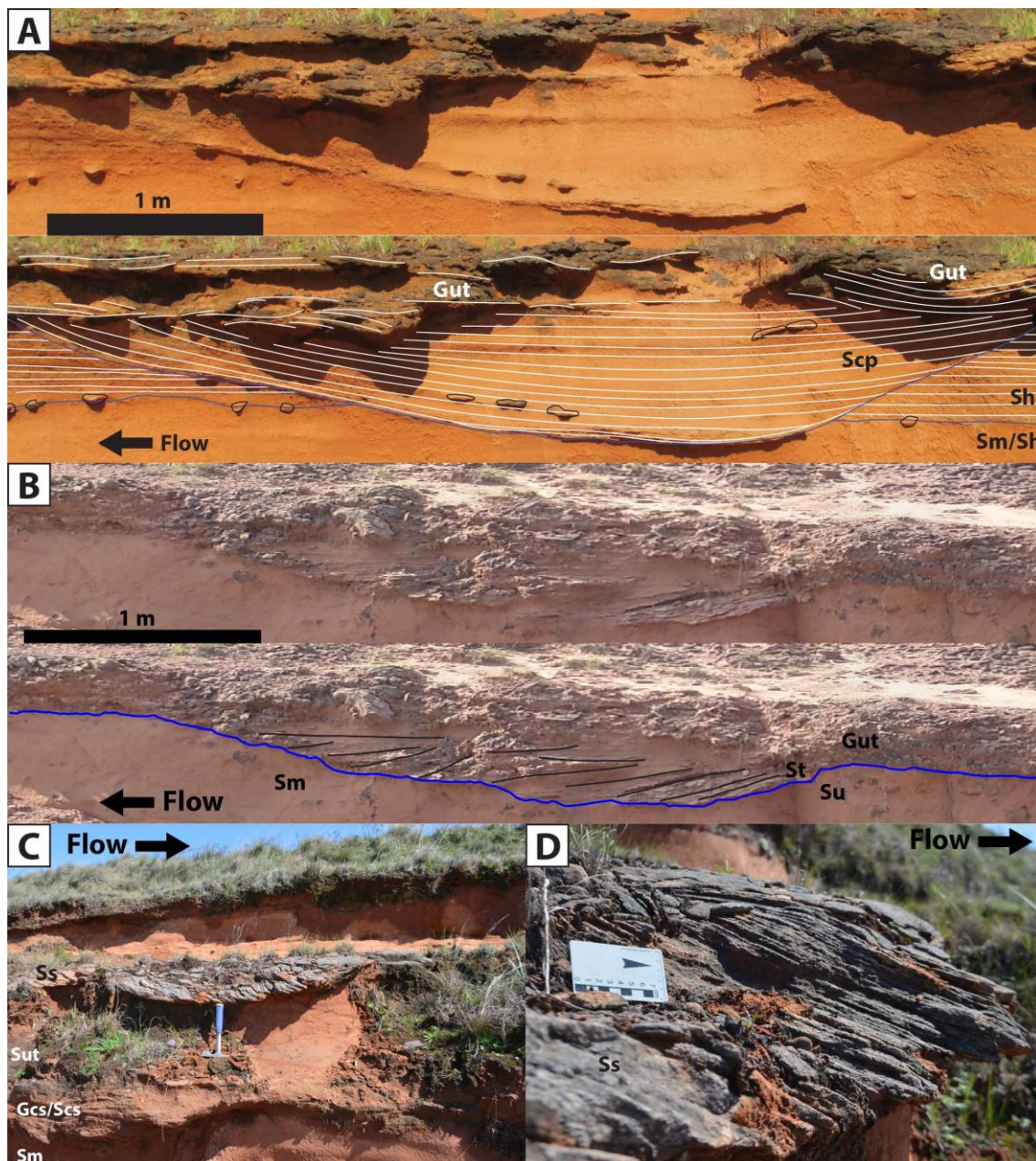


Fig. 14.--- Intermediate facies of Fluvial Style 2. **A)** Scp facies, interpreted as sandy chute-and-pool deposits. Isolated asymmetric scour with an upflow steep face and a downflow gentle face. Laminae are concordant to the gentle face, causing them to dip upflow at a low angle. Laminae inflect upwards near and then onlap the steep upflow face, up until the scour starts to fill up, at which point the laminae start to flatten. Note preferential formation of carbonate-cemented sandstone concretions along scour surfaces and parallel to lamination. **B)** Trough cross-stratification (St facies) filling a scour at the top of an intermediate section of a FS2 succession. Stratification angle becomes gentler as the scour fills. **C)** Scour depression filled by sandstone with larger-scale sigmoidal cross-stratification. Hammer is 28 cm long. **D)** Close-up of sigmoidal cross-stratification in Part C. Scale is in centimeters.

The upper interval of the lithosomes is marked by predominance of fine-grained sandstone with diffuse lamination, and structures are not internally erosional (Figs. 5, 9, 15), although erosional surfaces still occur. Facies succession typically starts with layers containing small-type occurrence of facies Ss (Fig. 15A), which may preserve humpback-dune external form (Fig. 14B), and transitioning laterally and/or vertically to Sr facies, also with diffuse lamination, which may present climbing angles (Figs. 9, 15C, D). Overlying the Sr facies, a lens of disturbed Sr(c) facies occur, and is followed above by Sm facies, with Sb facies at the top (Figs. 14C). In some places, the blocky structure is superimposed over other sedimentary structures, such as lamination, which is usually faint, and may appear laterally, and abruptly, within a single layer (Figs. 5, 15B).

Locally, at the top of this succession, a series of vertical irregular oblong structures, approx. 20 cm high and 10 cm wide, formed by discoloration aureoles, can be observed among massive (Sm) or blocky (Sb) structure (Figs. 5, 9, 15C, E).

Interpretation.--- The overall fining-upwards trend is interpreted to represent an inconstant yet gradual reduction of the energy of the flows. Presence of mudstone intraclasts in various levels (Figs. 5, 8–10) indicates flow intermittence, to allow the settling of fines (Alexander *et al.*, 1999). Thus, the energy reduction was a phenomenon developing through various flows.

Onset of FS2 marked an abrupt increase in discharge in relation to FS1, as attested by the Gcs and Scs facies (Figs. 5, 8–11). The frequency of discharge, however, was similar, as an abundance of nontransported carbonate concretions (i.e., at the position they were precipitated) can be found amidst the lithosomes, especially in the intermediate part (Figs. 5, 8, 9, 14). These levels were then eroded by subsequent flows, supplying the carbonate intraclasts of the lower part. Sediment supply was high, so that partially depositional cyclic steps formed (Slotman & Cartigny, 2020), however, conditions of these initial flows were not enough to sustain the high Froude number, and the cyclic steps transitioned to antidunes (Figs. 5, 8–11).

The flows which generated the lower strata were competent, capable of transporting carbonate-cemented sandstone concretions within cyclic steps and

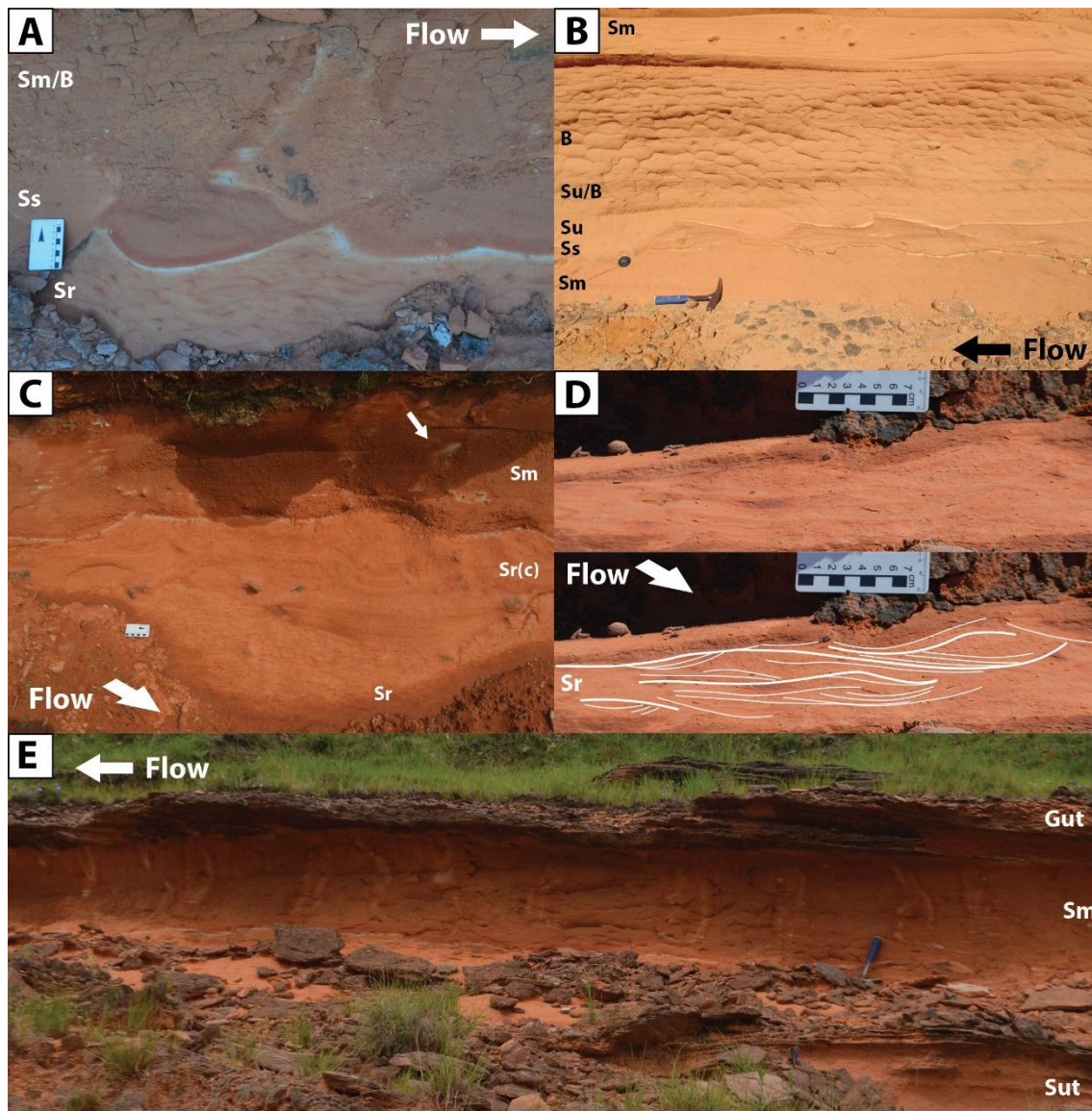


Fig. 15.--- Upper facies of Fluvial Style 2. **A)** Small-scale sigmoidal cross-stratification, with diffuse laminae. Presents partial preservation of external form (humpback dune), and a climbing angle, which indicates high deposition rate. Scale is in centimeters. **B)** Succession of facies, starting with massive sandstone (Sm) at the bottom, followed by small-scale sigmoidal cross-stratification (Ss), with good preservation of external form of the humpback dunes. Stratification is diffuse. Ss facies is overlain by undulated lamination (Su). Blocky structure develops upwards, superimposed on the top laminae of the Su facies. Sm facies occurs again at the top. Hammer is 28 cm long. **C)** Succession of facies, showing diffuse ripple lamination (Sr facies) at the base, followed by convolute laminae (Sr(c) facies) and massive sandstone (Sm facies) at the top. Arrow indicates an oblong vertical discoloration structure. Scale indicates 7 centimeters. **D)** Ripple lamination, with a climbing component. **E)** Oblong vertical discoloration structures interpreted as generated by infiltration of water in a paleosol, creating a redox gradient. Hammer is 28 cm long.

antidunes (Figs. 5, 8–11) when such coarse clasts should theoretically make difficult the formation of such structures, as a much higher flow speed or competency would be needed to suspend these dense clasts and organize them in the framework of a sedimentary structure (Southard & Boguchwal, 1990;

Cartigny *et al.*, 2014). The lateral and vertical transition of the cyclic step backsets to antidunes (Figs. 10C) is interpreted to be the result of the variation of Froude Number caused by the hydraulic jump, such that Fr is greater upflow of the jump, lowers to $Fr < 1$ at the trough (causing deposition), and starts to increase again when leaving the trough (Alexander *et al.*, 2001; Cartigny *et al.*, 2014). Such lateral coexistence has been experimentally produced (Ono *et al.*, 2021) and was interpreted in other settings (Zhong *et al.*, 2015). The low degree of lateral amalgamation and absence of vertical amalgamation at this lower interval (Figs. 5, 8–10A, C, 11A) are interpreted to be the result of relatively rapid decrease in flow energy (or competence), allied to high sediment supply and deposition, generating partly to fully depositional cyclic steps (Slootman & Cartigny, 2020; Figs. 10A, C, 11A). In contrast, the successive wedges (Fig. 12) are interpreted as the result of the migration, with varying velocity, of relatively stable hydraulic jumps, as observed in the flume experiment of Ono *et al.* (2021). When the erosive jump migrates upflow, it bypasses a region of the sediment bed, and resumes eroding when migration slows, creating the “mound configuration” on the previous bed, and deposition overlapping the upflow side of the “mound”. Repetition of this process generates the “wedge-shaped” deposits (Fig. 16).

Flows forming the intermediate part of the lithosomes had less energy, and thus reduced erosive power and competency, as conglomerates no longer form, and intraclasts are restricted to mud clasts. Flows were still highly erosive, as Sut, Scp, Sh, and Sm facies are amalgamated and present many erosional cuts (Figs. 5, 8, 9, 14). However, they could not erode layers which had already undergone precipitation of carbonate cement and formed concretions, and thus there are no conglomerates. The structureless or incipiently laminated deposits (Sm facies; Figs. 5, 8) in this intermediate interval are interpreted as the result mainly of rapid deposition from suspension (Alexander *et al.*, 2001; Ono *et al.*, 2021) and high sediment load inhibiting the formation of structures (Baas *et al.*, 2011). Reduction of energy progressed, as flow causing erosional scours lost the capacity to deposit backsets, filling the troughs with facies St and Ss at the top of this intermediate interval (Figs. 5, 8, 9, 14).

A drop in energy of formative flow can be inferred in the superior part of Fluvial Style 2 from the reduction of grain size, and non-erosional nature and size of structures (Figs. 5, 9, 15). Conditions decrease rapidly from Froude transcritical

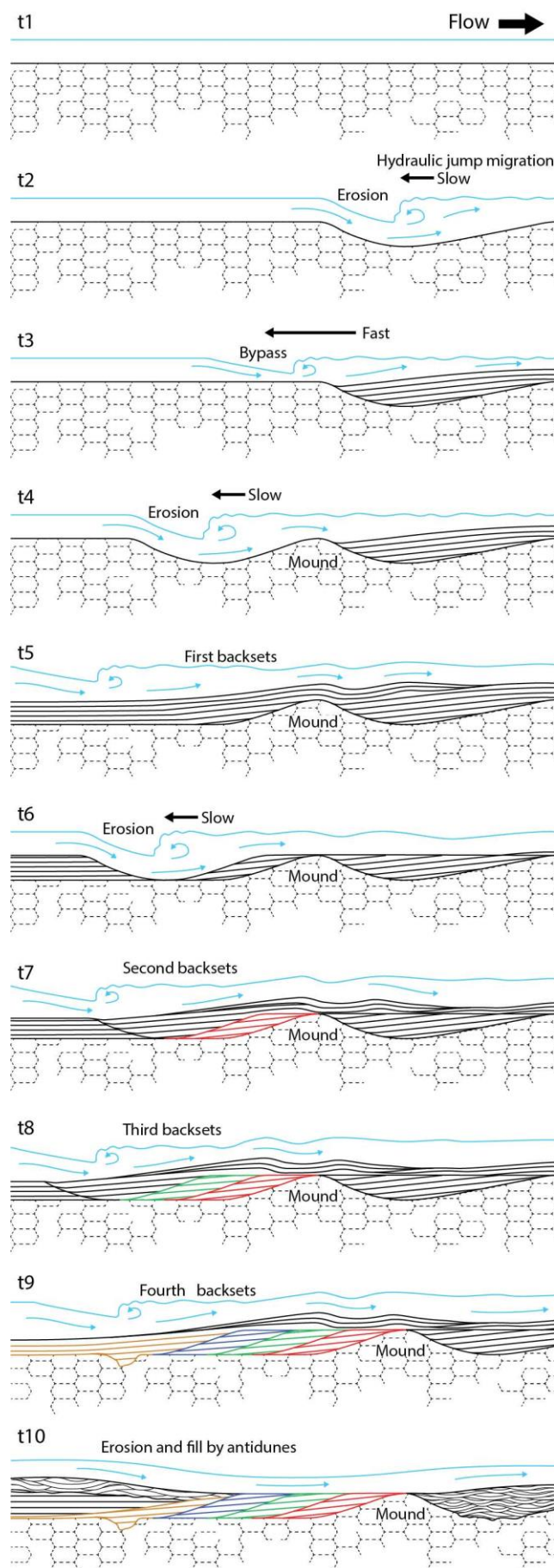


Fig. 16.--- Interpreted generation of the successive wedges with backsets, based on the observations of Ono *et al.* (2021). **T1:** initial idealized conditions. Flow to the right, over sandstone with blocky structure. **T2:** A first hydraulic jump is established. The jump migrates slowly upflow, and so it erodes the substrate. **T3:** the jump deposits backsets in the trough, and afterwards starts to migrate fast upflow, so that it does not erode the substrate. **T4:** The jump migrates slowly again, and so it erodes the substrate. The region between the two scours becomes mound-shaped, as seen in the outcrop (see Fig. 13). **T5:** The first jump migrates upflow and deposits low-angle backsets which extend laterally and transition to planar and/or low-amplitude undulatory lamination, and also transitions vertically to undulatory lamination. **T6:** another hydraulic jump is established. It erodes the upper undulatory lamination and starts to migrate slowly upflow from where the first backsets onlap the mound, and thus creates a scour at that position. **T7:** this second jump deposits a second set of backsets upflow from the mound in the new scour, causing the first backsets to become enclosed in a wedge between two scour surfaces (red). **T8:** The process repeats, generating a second wedge (green) and a third set of backsets. **T9:** The third wedge (blue) and the fourth set of backsets (yellow) are generated. The last set will not be enclosed between erosional surfaces, and therefore the lamination will continue upflow. **T10:** subsequent flows and bedforms cause erosion and fill by planar or undulatory truncated lamination, generating the configuration seen in outcrop (Figs. 12 and 13).

($Fr \approx 1$, represented by Ss facies) to low-energy Froude subcritical ($Fr < 1$, ripples), as trough cross-stratification (St facies) is very rare outside of scours (Fig. 9). It is a feature of this and other supercritical-flow-dominated environments that the conditions of the flows either do not stay at the stability field of subcritical dunes, or inhibit their preservation (Fielding & Alexander, 1996; Fielding *et al.*, 2009, 2018; Plink-Björklund, 2015; Lang *et al.*, 2021).

Lamination in the superior part of FS2 is diffuse (Fig. 15) and this may be in part because of pedogenesis. However, the presence of soft-sediment-deformed laminae (Figs. 15C) suggests water escape due to high deposition rates (McKee *et al.*, 1967; Singh & Bhardwaj, 1991), and suppression of formation of structures from the high sediment load (Baas *et al.*, 2011). Deposition then ceases, and the aforementioned pedogenesis ensues. The oblong vertical discoloration structures (Figs. 5, 9, 15C, E) are difficult to interpret. They were initially thought to be lungfish burrows (Francischini *et al.*, 2018) or the result of alterations caused by plant roots, but no physical fossils were found within the dozens of structures. In addition, there are no perceivable physical discontinuities between the structures and the surrounding rock, or within them (Fig. 15). The limits are solely gradients of color. Thus, they are here interpreted as the result of localized water infiltration on the paleosol and the creation of a local redox gradient.

Lateral relations between the Fluvial Styles were not observed. However, the erosional base of FS2 with abundant intraclasts (facies Gcs, Gut, Scs and Sut; Figs. 5, 8–13) indicate a channel base. Depositional surfaces present only slight relief, with gentle overall erosion (Figs. 5, 8, 9), indicating wide channels. The abundance of Froude-supercritical structures indicates shallow flows, as Froude number is dependent on flow depth (Cartigny *et al.*, 2014).

4.3 Fluvial Style 3

Description.--- The third observed fluvial style crops out as tabular lithosomes up to approx. 5.5 m thick and are continuous laterally for up to approx. 70 m in the studied section (Fig. 13). It is characterized by wide lenticular layers of fine- to medium-grained sandstone with large-scale continuous undular stratification (Su facies; Figs. 12, 13, 17A) and truncated undulatory stratification (Sut facies; Figs. 13, 17B). Layers of the Su facies are 0.5 to 2 m thick and can extend laterally for more than 60 m, being formed by fine- to medium-grained

sandstone. Undulations are 4.5–7.80 m in wavelength and very low in amplitude, up to 32 cm, sometimes approaching planar stratification. Sut facies occurs in amalgamated lenses, usually around 7 m long, but lenses 4 m long and up to 14.5 m long are also observed (Fig. 13). The base of the lenses is erosional, generally with mud intraclasts and medium sand, rarely coarse, while parting lineation can be observed on bedding planes (Fig. 17C). Erosional cuts can be steep, up to nearly 70° (Fig. 13). Facies Scs (transitioning to Su), Sm (with incipient planar lamination) and Sb facies occur vertically to the layers of large-scale undulatory facies, with erosional contacts (Fig. 13), and the larger structures tend to have more conspicuous stratification.

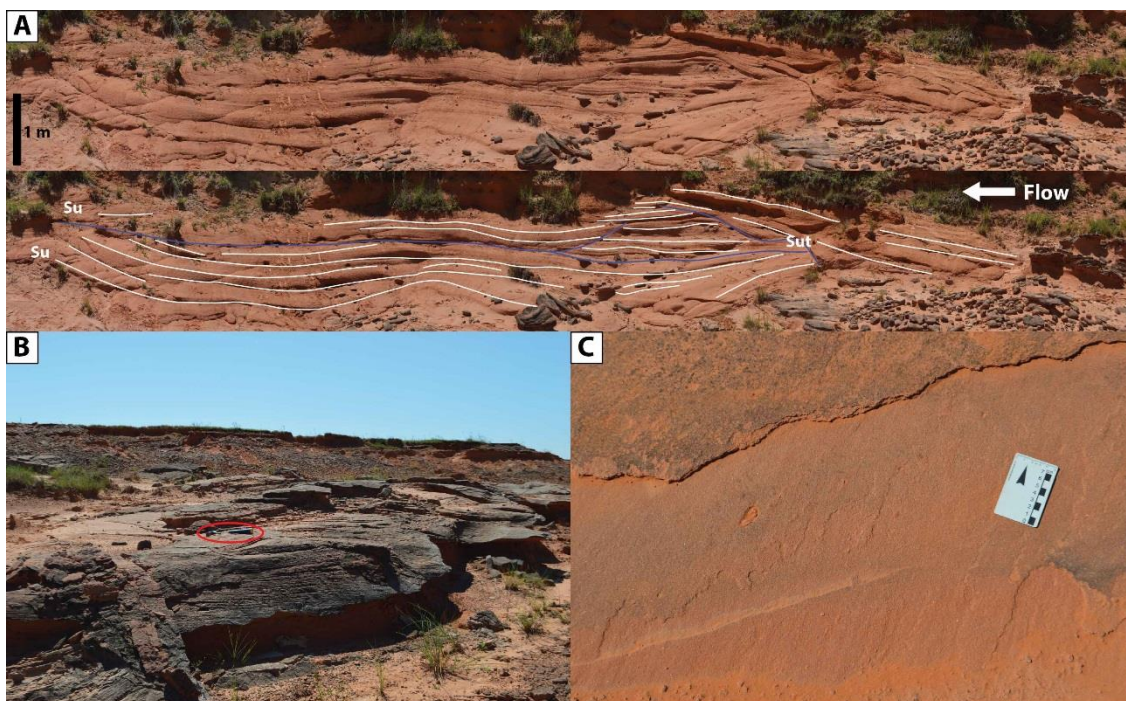


Fig. 17.--- Some antidunes of Fluvial Style 3. **A)** Lamination transitioning laterally from continuous undulatory stratification (Su facies; left) to truncated undulatory stratification (Sut facies; right). Note how stratification on the left can be traced generally for more than the distance of one or two times its wavelength; while on the right, lamination is truncated in sets less than the width of the wavelength. **B)** Undulatory truncated lamination, as generally observed in the outcrop. Circled hammer for scale is 28 cm long. **C)** Surface of lamination where the hammer in Part B was. Parting lineation can be observed. Scale is in centimeters.

Concretions tend not to be as nodular as in the other fluvial styles, usually accompanying set boundaries, erosional surfaces, or stratification more continually, forming carbonate-cemented surfaces which make stratification more conspicuous (Fig. 13).

Interpretation.--- FS3 marks yet another increase in discharge volume, attested by the large-scale undulatory laminae (Fig. 13). Flow conditions must have stayed relatively stable when the large-scale Su facies was deposited, such that the stability field of stable antidunes did not transition to that of unstable antidunes (Cartigny *et al.*, 2014), despite high energy of the flow.

The high-angle scours filled by lenses of the Sut facies are of considerable size (up to 1.5 m deep) and angle may be above repose (approx. 70°; Fig. 13). The structures recognized in the present study show prevalence of Froude-supercritical structures (Alexander *et al.*, 2001; Fielding, 2006), and scours generated by hydraulic jumps are typically asymmetrical with a high-angle upflow face (Cartigny *et al.*, 2014; Ono *et al.*, 2021). In addition, Cartigny *et al.* (2014) observed experimentally that in some conditions, the steep upflow face of the hydraulic jump scour could go beyond the angle of repose, but the authors also noted that preservation potential is very low. However, it is here hypothesized that the eroded layers had increased cohesion from pedogenesis, initial cementation, or a combination of both, and thus have preserved the steep upflow face of the hydraulic jump scour.

Sediment supply must have been high and constant to allow the accretion of well-spaced and conspicuous stratification (Yokokawa *et al.*, 2010; Cartigny *et al.*, 2014). Conspicuousness of the stratification is aided by carbonate precipitation along the stratification (Fig. 13).

The high discharge generating these flows were, however, commonly succeeded by long periods without deposition, as incipient stratification, massive structure (Sm), blocky structure (Sb) and carbonate concretions are interpreted as the result of pedogenesis (Retallack, 1988; Kraus, 1999; Alonso-Zarza & Wright, 2010), similarly to FS1 and FS2. The differential pattern of within-sediment carbonate precipitation is attributed to the easier percolation of water in the erosional surfaces and stratification, which is generally more well developed in this fluvial style.

Similar to FS2, FS3 also has an erosional base with abundant intraclasts, and gentle overall relief (Fig. 13), being interpreted as deposited in wide channels. Although flows were deeper in relation to FS1 and FS2, they still needed to be shallow, in order to generate Froude-supercritical structures (Cartigny *et al.*, 2014).

4.4 Paleohydraulics

Antidunes, and particularly stable antidunes, develop in-phase with water-surface waves. This means that bedform dimensions are directly related to the formative surface waves (Alexander *et al.*, 2001; Cartigny *et al.*, 2014). Because of this direct relationship, antidunes have been used as reliable paleoflow indicators for decades (Kennedy, 1960, 1963; Froude *et al.*, 2017). However, and especially for breaking antidunes, if deposition rate is not very high, the antidune crests are commonly eroded, and only lenses formed by trough fills are preserved. Alexander *et al.* (2001) found that the mean length of the laminaset is approximately 0.5 times that of mean antidune length. With these measurements, it is possible to infer the flow velocity using the equation of Kennedy (1963):

$$\lambda = 2\pi U^2 / g \quad (1)$$

So that

$$U = \sqrt[2]{\lambda g / 2\pi} \quad (2)$$

With U being the flow velocity, λ the antidune wavelength (in meters), and g the acceleration due to gravity (9.8 ms^{-2}). The same author also defined the relation between λ and mean flow depth d_m :

$$\lambda = Fr^2 \cdot 2\pi d_m \quad (3)$$

So that

$$d_m = \frac{\lambda}{(Fr^2)2\pi} \quad (4)$$

with the condition that the crest-parallel length is long compared to the wavelength.

As expressed in Equation 4, estimation of mean flow depth is dependent on the Froude Number. The range of existence of antidunes is known to be between $0.84 \leq Fr \leq 1.77$ (Allen, 1982). Considering that (1) surface waves start to break at higher Froude numbers, (2) chute-and-pool bedforms start to occur at the

higher end of antidune existence (Cartigny *et al.*, 2014), and (3) unstable antidunes in FS2 coexist with chute-and-pool bedforms, it is here considered reasonable to assume $Fr = 1.7$ is in good accordance with the described antidune deposits. In the same line of thought, the aggrading, stable antidune deposits of FS3 are considered as coherent with a value of $Fr = 1.0$.

Results of the measures and estimates of the bedforms, and paleoflow parameters are displayed in Table 2.

Froude *et al.* (2017) compared direct measurements and deposits from antidunes of a flash flood in the Beham River in Montserrat, West Indies. Antidune wavelengths ranged from 0.32 m to 8.33 m, with a highest mean length of 3.96 m. Highest flow velocity reported was 3.6 ms^{-1} , while highest mean flow velocity was 2.42 ms^{-1} . Highest average depth was, in turn, 1.3 m. Alexander *et al.* (2020) report antidune wavelengths for the Burdekin River 16.4 to 28.8 m, flow velocities of 5.1 to 6.7 ms^{-1} , and flow depths of 2.6 to 4.6 m. Both of these works considered $Fr = 1$ for the antidunes when estimating flow depth. In the Bijou Creek historical flood of 1965, McKee *et al.* (1967) report flow velocities on the main channel ranging from 5.15 to 6.85 ms^{-1} , and mean flow depths from 1.34 to 2.40 m. These authors did not report the presence of antidunes, the deposits being dominated by planar stratification.

Walker and Holbrook (2022) estimated paleoflow parameters from the Tecovas and Trujillo formations of an Upper Triassic succession in the state of Texas, USA. Antidune wavelength in the Tecovas Formation varied from 1.4 to 5.62 m, with a mean of 3.31 m, resulting in paleoflow velocities from 1.5 to 2.96 ms^{-1} , with a mean of 2.21 ms^{-1} , and paleoflow depth ranging from 0.23 to 0.89 m and mean 0.53 m. For the Trujillo Sandstone, antidune wavelengths were 1.64 to 4.49 m with a mean of 2.81 m; paleoflow velocity was estimated at 1.60 – 2.65 ms^{-1} with a mean of 2.07 ms^{-1} ; and paleoflow depth yielded values from 0.26 to 0.71 m and a mean 0.45 m. The authors highlight that these values, as other antidune-based calculations, are estimates of formative flow. Peak flow may have as high as five to ten times the discharge of formative flow.

In a different setting, Duller *et al.* (2008) describe the deposits of a jökulhlaup (glacial outburst flow) resulting from the eruption of the subglacial Katla volcano, in southern Iceland. These authors report antidunes resulting from this extreme event with wavelengths ranging from 24 m to impressive 96 m, which would have

been formed by flows with velocities of 6.1 to 12.2 ms⁻¹. Average depth was calculated within a range of possible Froude Numbers, and ranged from 2.3–3.2 m to 12.6–18.9 m.

Considering the results from different works, FS2 antidunes are relatively small, with maximum wavelengths of 4.2 m and mean flow velocity of 1.91 ms⁻¹. The competency of the flow to reach supercritical conditions is here interpreted as being the result of the poor confinement (Zerfass *et al.*, 2003, 2004), generating thin flows (average $d_m = 0.13$ m), which facilitates reaching Froude Numbers above unity (Cartigny *et al.*, 2014). A similar interpretation can be extended to the sheet floods of FS1, though weaker.

The parameters of FS3, on the other hand, are comparable to the Bijou Creek, Beham, and Burdekin Rivers' floods. With mean wavelengths of 15.4 m and reaching a maximum of 28.92 m, and mean formative flow of 4.9 ms⁻¹ reaching up to 6.72 ms⁻¹, the unstable antidunes of FS3 attest a high-velocity and high-magnitude flow.

The stable antidunes of FS3, with an average wavelength of 6.72 m, are estimated to have been formed by a flow 1.07 m deep with a velocity of 3.24 ms⁻¹. This is not a particularly strong flow; however, the vertical aggradation of the antidunes is striking. The formation of these structures required a very high deposition rate and a remarkable stability of the flow. This feature is again attributed to the poorly confined nature of these flows, as well as the low gradient and uniformity of the cratonic interior basin of southwestern Gondwana in the Early Triassic (Zerfass *et al.*, 2003, 2004). Conditions would be similar to the terminus of the Río Colorado, Bolivia (Donselaar *et al.*, 2013), where the extremely low-gradient of the endorheic Altiplano Basin causes poorly-confined flows and numerous avulsions, but discharge in the Sanga do Cabral river system would be much higher, and flows much faster, allowing the formation of cyclic steps, chutes and pools, and large antidunes.

5. DISCUSSION

5.1 Climate Control of Discharge Cycles

Each fluvial style is the record of varied conditions of hydraulic power, frequency of discharge, sediment yield, and erosive power. These parameters

1 Table 2. Measured parameters of antidunes, and the resulting calculated estimates for paleoflow parameters.

	Lens length (m)		Antidune wavelength - λ (m)			Flow velocity - U (m/s)		Flow average depth - dn^2 (m)	
	Measured		Estimated			Estimated		Estimated (Fr = 1.7)	
FS2 unstable antidunes	min	0.5	min	1.0	min	1.25	min	0.05	3
	max	2.1	max	4.2	max	2.56	max	0.23	4
	mean	1.16	mean	2.32	mean	1.9	mean	0.13	5
FS3 unstable antidunes	min	4.0	min	8.0	min	3.53	min	0.44	6
	max	14.46	max	28.92	max	6.72	max	1.59	
	mean	7.7	mean	15.4	mean	4.9	mean	0.85	
FS3 stable antidunes			Measured			Estimated		Estimated (Fr = 1.0)	
	min	-	min	4.54	min	2.66	min	0.72	
	max	-	max	7.85	max	3.5	max	1.24	
	mean	-	mean	6.72	mean	3.24	mean	1.07	

are the result of the interplay between water discharge and discharge variability. This relation is, in turn, controlled by the climate.

The tabular external form of the lithosomes and the lack of marked increase in grain size of the extraclasts suggest that tectonic conditions remained relatively stable, with no clear indication of uplift in the source area (Allen *et al.*, 2014). Therefore, it is here interpreted that the variations of paleohydraulic conditions were the result of climatic cycles (Walker & Holbrook, 2022).

All three fluvial styles here interpreted are considered as deposits of high variable-discharge rivers, for they exhibit many of the key characteristics associated with these systems (Fielding & Alexander, 1996; Fielding *et al.*, 2009, 2018; Plink-Björklund, 2015): (1) abundance and predominance of Froude-supercritical and high-deposition rate sedimentary structures; (2) erosionally based channel-fill lithosomes with complex lateral facies change; (3) complex internal architecture with few to no macroform elements; (4) presence of mud in the river channel and abundance of mud-clast conglomerates; (5) soft-sediment deformation; and (6) in-channel pedogenic modifications.

In the classification of Fielding *et al.* (2018), the deposits of the SCF are more similar to the “very high peak discharge variance” type, as Froude-subcritical structures are almost absent, and there is no evidence of lateral migration of the river channel, indicating a high degree of avulsion (Bryant *et al.*, 1995). The main example of this type of river has been the Burdekin River of northeastern Australia (Fielding & Alexander, 1996; Fielding *et al.*, 2009), and it is compared in the deposits of the Pennsylvanian Sydney Mines Formation of Atlantic Canada. These share many of the sedimentary characteristics found in the SCF, but some important differences are present. Firstly, great emphasis is given to the presence of vegetation and preserved *in situ* tree trunks, which are absent in the SCF, as are mud partings, which indicates greater erosive potential of this river system. The Burdekin model also mentions pedogenesis on the mud partings. However, in the SCF, pedogenesis occurs in the channel sandstones and conglomerates. This indicates that flows in the SCF river system are less frequent, remaining without deposition for many years, maybe decades (Alonso-Zarza & Wright, 2010), and inhibiting the growth of riparian vegetation. This, in turn, indicates a drier climate. The Burdekin River drains areas with a subhumid to semiarid climate, with strongly seasonal precipitation, and mean annual rainfall of 500-700 mm (Fielding *et al.*, 2009). Thus, from this comparison the SCF

could be interpreted to have been deposited in an arid to semiarid climate, with less frequent precipitation. Lithosomes formed by unconfined flows (FS1) are not present in these comparative models. The Burdekin River model is thus considered as more similar to FS2 and FS3.

Plink-Björklund (2015) proposed a classification specifically for rivers in the monsoonal and subtropical domains. Although there is no direct match from the rock record facies to modern example analogs, this classification presents plausible and interesting models for comparisons, insights, and considerations, and are tentatively employed here. The SCF deposits are similar to their “amalgamated lithosomes with thick flood units”, for the tabularity of the lithosomes, the overwhelming majority of Froude-supercritical deposits, and lack of mud drapes or layers. Comparisons are made to the Kobo Basin, the Sinai Peninsula, and the Karoo, where mean annual precipitation is around 750 mm, but it falls in a few downpours which last from hours to a few days. An ancient example is made of the flood units of the Uinta Basin, where the sandstones are vertically and laterally amalgamated, lacking mudstone drapes or finer-grained sandstones, the visual homogeneity being broken only by the mudclast conglomerates at the bases of deposits. However, the presence of lower-energy “top of flood deposits” containing ripples, convoluted laminae, and pedogenically altered massive fine-grained sandstones in FS2 approximates this fluvial style to the “lithosomes with variable flood units”, where floods would last longer, maybe through a whole monsoon season. It is of note that the same fluvial style in the present study which has the lowest-Froude-number bedform structures (ripples and dunes, facies Sr and St) also has the highest ones as well (cyclic steps, facies Scs and Gcs). Modern examples of this classification range from monsoonal rivers with mean annual precipitation of 1100–1600 mm, or even greater in some cases, or rivers in the arid subtropics with mean annual precipitation of only a few hundred millimeters. Both of these classifications imply that the SCF would have very little, if any, perennial runoff, and most of the greater part of the deposition would be the result of high-magnitude floods, which is in good agreement with the interpretations above. However, the various classifications here applied to the FSC imply that FS3 would be deposited by a “flashier” flood, in which the rain events were more intense and of shorter duration and flow strength also declined extremely fast. The alternation of stable and unstable antidunes may be indicative that erratic storms were the source of water discharge, instead of a monsoonal season (Zellman *et al.*, 2021). FS2 would be deposited by

floods occurring during a longer time interval, though maybe not a whole monsoon season, as they still have very few Froude-subcritical structures. FS1 deposits are, again, not represented by these authors.

A classical model of reference for highly-variable-discharge rivers that may present similarities to FS1 is the “Bijou Creek type braided fluvial style” of Miall (1977), based on the study of McKee *et al.* (1967). The Bijou Creek lies in subhumid climate and has mean annual precipitation around 330–355 mm. Deposits of the flash flood of 1965 had very high proportion of planar bedding, which bears some similarity to FS1 of the present study. However, presence of cross-strata and climbing ripples record waning-flow conditions, not observed in FS1. Also, the condition of occurrence of mud and eroded mudclasts are different. While in the Bijou Creek there is a “mudball zone” of rounded clasts eroded from pre-flood strata, in FS1 mud occurs as granule- and pebble-size intraclasts in many levels, attesting multiple small flood events. In addition, the Bijou Creek 1965 flood deposited layers of up to 4 m in thickness. A more similar modern analogue to FS1 may be the Colorado River in the endorheic Altiplano Basin in Bolivia (Donselaar *et al.*, 2013) or the Gash River in Kassala, Sudan (Abdullatif, 1989). Both show unconfined-flow deposits with predominance of planar lamination. Still, in contrast to FS1, ripple cross-lamination is still common, as well as mud layers. A much more similar deposit can be found in the Candelária sequence of the Santa Maria Supersequence, which is the unit overlying the FSC. Horn *et al.* (2018) describe a succession consisting of a series of thin-bedded massive sandstones. These authors interpret these deposits as distal “sheetfloods”, the massive structure resulting from deconfinement or avulsion of hyperconcentrated flows. As the flow quickly becomes unconfined, the rapid deceleration and grain fallout inhibit the formation of tractional structures.

These comparisons allow paleoenvironmental interpretations of the fluvial styles of the SCF, depicted in Fig. 18. FS1 would represent a dry period, in which rainfall would reach the area only as thin, distal, hyperconcentrated unconfined flows, with eventual and rare thicker flows (Fig. 18A). The interval between flows, and avulsions, allowed pedogenesis and the precipitation of carbonate concretions. Thin mud drapes dried and desiccated, being eroded and transported by subsequent floods. In turn, FS2 would represent perhaps the least dry period of the SCF, as rainwater would be discharged in floods in wide shallow channels throughout a longer period, but still in very strongly concentrated floods (Fig. 18B). This would also explain the higher degree

of erosion, as there are more flood events. Nevertheless, time between flood events and avulsion allowed pedogenesis and formation of carbonate concretions, which were then eroded and incorporated into the sediment load. FS3 represents extremely concentrated water discharges in catastrophic flash floods (Fig. 18C), in similarly wide and shallow channels. Mean annual precipitation might have been less than FS2, but the concentration allowed deeper and stronger flows (around 5 ms^{-1}), which had a rapid waning phase, not allowing the formation of any Froude-subcritical sedimentary structures.

In the Estrada de Ferro Inacabada Outcrop, all three fluvial styles occur more than once, revealing a cyclicity of the aforementioned precipitation and discharge variability conditions (Fig. 3). The exact duration of these cycles is difficult to infer without other proxies. Transitions from one fluvial style to the other are cycles of change in the interplay of water volume discharge, interannual variability, and *pattern* (i.e., more distributed or concentrated). Walker and Holbrook (2022) describe Froude-supercritical structures in the Tecovas and Trujillo formations of the Upper Triassic Dockum Group in the Palo Duro Canyon, in the state of Texas, USA. The lower Tecovas Formation presents a variety of depositional environments: floodplain mudflat, paleosol, and notably lacustrine, where large deltas could form, existing beside lower- and upper-flow-regime-generated channel fills. This formation is interpreted as generated mostly by infrequent storm events, but the system also sustained low flow after floods. In turn, the Trujillo Sandstone has a dominance of amalgamated channel fills, with higher frequency of incised valleys. This unit is interpreted as formed by more frequent flood events in relation to aggradation rates, and thus floodplain deposits are scarce. These authors stress the low declivity and absence of tectonic tilting during the Dockum Group deposition, similarly to the SCF. Such variations in these already variable-discharge river systems are therefore inferred to be the result of climate-induced variations in discharge, such as resulting from stronger, more concentrated, or more dispersed megamonsoonal storms. One possible allogenic control of these variations may be Milankovitch cycles, as these have been interpreted as conditioning climatic changes during the Triassic (Olsen & Kent, 1996; Wu *et al.*, 2012), and could plausibly cause variations in magnitude and concentration of megamonsoonal precipitation. The Early Triassic, on the other hand, presented some unique conditions which could have exerted allogenic control of climate, such as the fluctuations of

atmospheric $\delta^{13}\text{C}$, which occurred throughout the Early Triassic (Benton & Newell, 2014; Fielding *et al.*, 2019), and other characteristic factors.

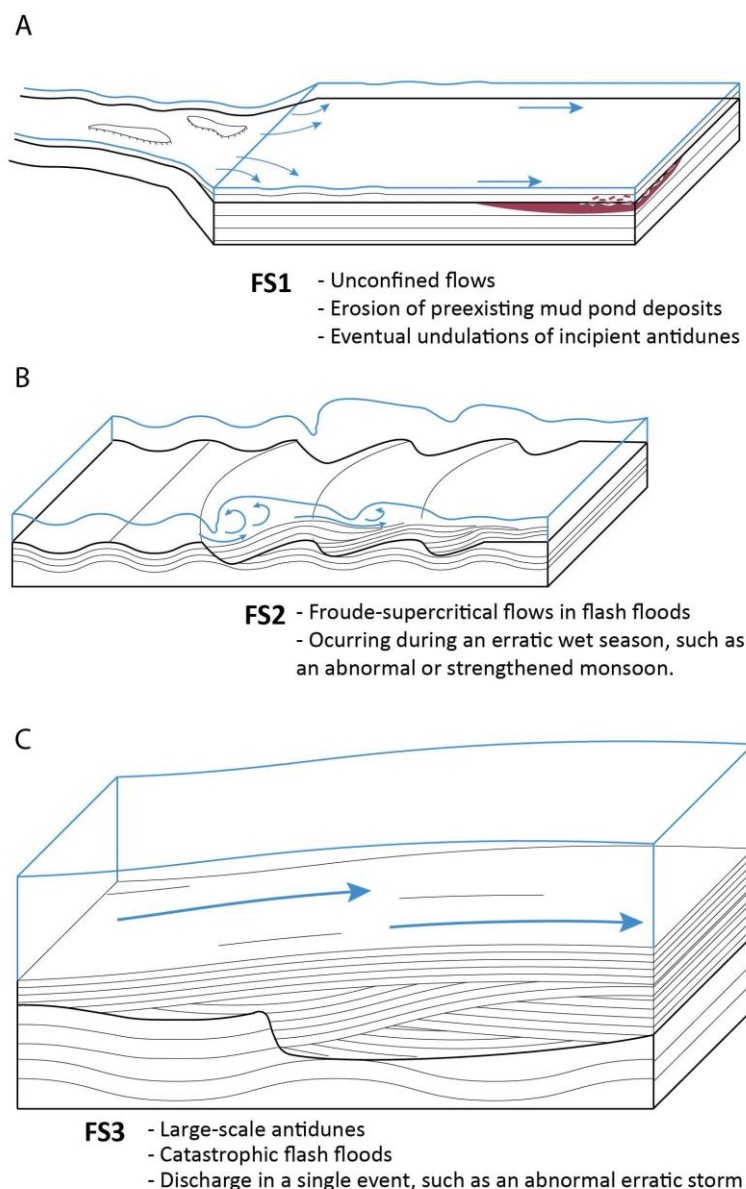


Fig. 18.--- Diagram idealization of interpreted Fluvial Styles. **A)** Fluvial Style 1 (FS1) is interpreted as a distal part of a fluvial system. Water discharge reaches the study area as unconfined flows, which deposit mainly massive thin beds, or planar lamination. Some regions may reach near-supercritical conditions, aided by the shallow depth, and create incipient undulations and therefore incipient antidune bedforms. Mud deposits from dried-out ponds of previous floods are eroded to form mud-clast lags. **B)** Fluvial Style 2 (FS2) is interpreted as formed by Froude-supercritical shallow flash floods. Flows achieve supercriticality and therefore great erosive power and competence. Previous deposits are eroded and mud clasts and concretions are mobilized by the powerful hydraulic jumps of cyclic-step bedforms. Energy decreases and cyclic steps give way to antidunes. Floods of FS2 are here hypothesized to occur due to erratic wet seasons, such as abnormal or strengthened monsoons (Plink-Björklund, 2015). **C)** Fluvial Style 3 (FS3) is interpreted as generated by catastrophic flash floods of high energy. Powerful flows generate long-wavelength antidunes and have high erosive power, but high sediment discharge allows preservation of structures. Due to the vertical alternation of (relatively) lower- and higher-energy structures (i.e., stable and unstable antidunes), floods of FS3 are here hypothesized to be caused by forces which would deliver its discharge in a single event, such as abnormal or erratic storms.

5.2 Climate in the Early Triassic

Global climate in the Early Triassic was unique for many reasons, some of the major being the continental disposition, as Pangea was united and stretched symmetrically from the Equator up to high latitudes; high sea level, absence of polar ice caps; and high levels and variation of CO₂, which stabilized only in the Anisian (Chen & Benton, 2012; Mancuso *et al.*, 2021). These factors caused intense seasonality at lower latitudes, which drove increasing aridity in the continental interior's mid to low latitudes (Parrish, 1993; Winguth *et al.*, 2015; Mancuso *et al.*, 2021).

The Triassic global climate models (GCMs) suggest a strong monsoonal circulation developed as a result of the symmetrical positioning of Pangea across the Equator (Kutzbach & Gallimore, 1989; Parrish, 1993; Wilson *et al.*, 1994; Sellwood & Valdes, 2006; Holz, 2015; Harris *et al.*, 2017). This configuration led to the development of an arid continental hinterland, restricting the areas of greatest precipitation to latitudes greater than 45° S where westerly winds brought moisture from the Panthalassa Ocean (Parrish, 1993; Wilson *et al.*, 1994; Sellwood & Valdes, 2006; Preto *et al.*, 2010; Holz, 2015; Harris *et al.*, 2017; Dunne *et al.*, 2021). The SCF was located at a paleolatitude of around 45°, positioned on the boundary between the arid and humid belts. This perhaps explains the high variability discharge regime of the river system, where short and intense periods of high precipitation would occur in this transition zone between the more arid and wetter regions, due to stronger-than-average storms or monsoonal events.

The SCF has been interpreted as deposited by an association of braided rivers (the intraformational conglomerates) and eolian sand sheets (the low-angle and planar stratification, and thin-bedded sandstones; Faccini, 2000). Or as “shallow braided streams, in an approximate 1:100 thickness/width scale, whereas the orange fine sandstones are interpreted as massive, or presenting planar stratification, and denote a broad semiarid plain.” (Dias-da-Silva *et al.*, 2017). Reinterpretation of the SCF under the light of new knowledge regarding supercritical structures and high-discharge-variability rivers allowed new, finer interpretations of its paleoclimate. Climate is here interpreted as semiarid to arid, with strong variation in the intensity and pattern of water discharge throughout the deposition of the formation. Other Early Triassic geologic units present similar suites of structures and interpretations.

The Talampaya Formation of the Ischigualasto–Villa Uinón Basin in Argentina spans the Late Permian and the earliest Triassic. It is interpreted as recording a

transition from low- to medium-sinuosity rivers to fluvio-eolian, sheetflood, and ephemeral rivers and lake deposits (Gulbranson *et al.*, 2015). The Tarjados Formation, which overlies the Talampaya, presents mudclast intraformational conglomerates, and fine- to medium-grained sandstones with cross-stratification, planar lamination, and occasional massive sandstones. It is interpreted as deposited by ephemeral rivers which form repetitions of an upwards-fining succession that starts with the intraformational conglomerates, going upwards to planar-stratified and trough cross-stratified sandstones, to planar-laminated sandstones, and occasionally massive sandstones (Krapovickas *et al.*, 2013). Also in Argentina, the Vera Formation of Los Menucos Basin shows evidence of braided rivers and ephemeral lakes, with alternating wet and dry conditions (Gallego, 2010). In the Karoo Basin, the Katberg Formation is reported as presenting evidence of ephemeral channels and flashy discharge, such as mudclast conglomerates and carbonate concretions, as well as amalgamated sandstone bodies with massive and trough cross-bedded structures. All these geologic units present conditions similar to the SCF. Identification of supercritical structures in these deposits may allow finer interpretations of variability of discharge in these past environments in the Early Triassic.

Zellman *et al.* (2021) studied the difference of prevalence of Froude-supercritical structures in channel facies associations from the Late Paleocene and Early Eocene of the Uinta Basin, USA, as well as overbank deposits. These authors conclude that channel facies are proxies for frequency and magnitude of high-intensity precipitation events, while floodplain deposits are better indicators of climate. The present study seems to corroborate this hypothesis, as the different fluvial styles vary in the sedimentary structures, and estimated paleohydraulics show a clear difference in flow velocity and depth, while there is no evidence for significant change in climate. Although the Estrada de Ferro Inacabada Outcrop shows no floodplain deposits, the ephemeral characteristic of the FSC causes the channels to undergo pedogenesis, which then record the semiarid to arid climate with oxidizing coloring and carbonate concretions.

6. CONCLUSIONS

New knowledge of supercritical structures applied to the SCF allowed reinterpretation of its sedimentary structures and a finer interpretation of the role of climate and the variability of water discharge in an Early Triassic arid to semiarid river system. Three fluvial styles were interpreted to have existed during the time recorded

by these rocks. Constant to all three were the long interval between flows (many years), which allowed pedogenesis and precipitation of carbonate concretions; weak to near-absent channelization; and the formation of ephemeral ponds or lakes which deposited mud, and were and eroded by subsequent flows, generating mudclast conglomerates. FS1 facies are interpreted as deposited by hyperconcentrated, unconfined flows in a distal part of the fluvial system, which resulted in thin beds with massive structure or planar lamination, and incipient antidunes. FS2 was deposited by flash floods that occurred repeatedly during a short period of time of a wet season, generating a succession of Froude-supercritical bedforms, and rapidly waned, generating ripples and only a few dunes. FS3 was deposited by catastrophic flash floods of high discharge and flow velocity, possibly generated by erratic storms, which poured in single events. These catastrophic flows generated long-wavelength antidunes and other Froude-supercritical structures, the floods waning extremely rapidly, not enabling the generation of Froude-subcritical structures.

The present work sheds light on cycles of variations in water discharge in an already highly variable-discharge river system and corroborates the role of Froude-supercritical structures to interpret these systems in finer detail. This approach may be usable to better understand the many arid, semiarid, or strongly seasonal environments of the Early Triassic of Gondwana, or even other regions and geological times.

ACKNOWLEDGMENTS

The authors acknowledge Francyne do Amarante, Rossano Michel, and Bruno Angonese for the help in the fieldwork. We thank the Scherer family for the kindness of heartwarming reception and for providing lodgment, even ceding their house during Covid-19 times. A special salute is given in memoriam to Lúcio Scherer, who has, sadly, recently left us. We send our hearts and condolences to his family members. We also thank Cesar Schultz and Bruno Horn for studies in the early stages of the project, even though it took a very different path from when they were involved. Further acknowledgement is given to the editors Kathleen Marsaglia, Melissa Lester, Janok Bhattacharya, and John Southard, as well as to reviewer Chris Fielding and the anonymous reviewer, whose comments greatly improved the manuscript. Finally, we thank Larissa Tononi for the companionship and encouraging support.

REFERENCES

- Abdullatif, O.M.** (1989) Channel-fill and sheet-flood facies sequences in the ephemeral terminal River Gash, Kassala, Sudan. *Sediment. Geol.*, **63**, 171–184.
- Alexander, J., Bridge, J.S., Cheel, R.J. and Leclair, S.F.** (2001) Bedforms and associated sedimentary structures formed under supercritical water flows over aggrading sand beds. *Sedimentology*, **48**, 133–152.
- Alexander, J. and Fielding, C.R.** (1997) Gravel antidunes in the tropical Burdekin River, Queensland, Australia. *Sedimentology*, **44**, 327–337.
- Alexander, J., Fielding, C.R. and Pocock, G.D.** (1999) Flood behaviour of the Burdekin River, tropical north Queensland, Australia. *Floodplains Interdiscip. Approaches*, 27–40.
- Alexander, J., Herbert, C.M., Fielding, C.R. and Amos, K.J.** (2020) Controls on channel deposits of highly variable rivers: Comparing hydrology and event deposits in the Burdekin River, Australia. *Sedimentology*, **67**, 2721–2746.
- Allen, J.P., Fielding, C.R., Gibling, M.R. and Rygel, M.C.** (2014) Recognizing products of palaeoclimate fluctuation in the fluvial stratigraphic record: An example from the Pennsylvanian to Lower Permian of Cape Breton Island, Nova Scotia. *Sedimentology*, **61**, 1332–1381.
- Allen, J.R.L.** (1982) Bedforms in Supercritical and Related Flows: Transverse Ribs, Rhomboid Features, and Antidunes. In: *Sedimentary Structures Their Character and Physical Basis* (Ed. J.R.L. Allen), Elsevier, Amsterdam, 383–417.
- Allen, J.R.L.** (1969) Erosional Current Marks of Weakly Cohesive Mud Beds. *SEPM J. Sediment. Res.*, Vol. **39**, 607–623.
- Allen, J.R.L.** (1968) Current Ripples, Their Relation to Patterns of Water and Sediment Motion. *North-Holland Publishing Company*, Amsterdam, 433 pp.
- Alonso-Zarza, A.M.** (2003) Palaeoenvironmental significance of palustrine carbonates and calcretes in the geological record. *Earth-Science Rev.*, **60**, 261–298.
- Alonso-Zarza, A.M. and Wright, V.P.** (2010) Calcretes. In: *Carbonates in Continental Settings: Facies, Environments, and Processes* (Ed. A.M. Alonso-Zarza and L.H. Tanner), Elsevier, Oxford, 61, 225–267.
- Andreis, R.R., Bossi, G.E. and Montardo, D.K.** (1980) O Grupo Rosário do Sul (Triássico) no Rio Grande do Sul - Brasil. In: *XXXI Congresso Brasileiro de Geologia, Sociedade Brasileira de Geologia*, Balneário Camboriú, SC, 2, 659–673.
- Arakel, A. V. and McConchie, D.** (1982) Classification and Genesis of Calcrete and Gypsite Lithofacies in Paleodrainage Systems of Inland Australia and their Relationship to Carnotite Mineralization. *SEPM J. Sediment. Res.*, **52**, 1149–1170.
- Arnott, R.W.C. and Hand, B.M.** (1989) Bedforms, Primary Structures and Grain Fabric in the Presence of Suspended Sediment Rain. *J. Sediment. Res.*, **59**, 1062–1069.
- Azevedo, S.A., Lavina, E.L., Barberena, M.C., Ferrando, L. and Andreis, R.R.** (1985) Evidências de correlação entre a Formação Yaguari (Uruguai) e as Formações Rio do Rasto e Sanga do Cabral (Rio Grande do Sul - Brasil). *Pesqui. em Geociências*, **17**, 112–121.
- Baas, J.H., Best, J.L. and Peakall, J.** (2011) Depositional processes, bedform development and hybrid bed formation in rapidly decelerated cohesive (mud-sand) sediment flows. *Sedimentology*, **58**, 1953–1987.
- Barberena, M.C., Araújo, D.C.F., Lavina, E.L. and Azevedo, S.A.K.** (1985) O estado atual do conhecimento sobre os tetrapodes permianos e triássicos do Brasil meridional. In: *Coletânea de trabalhos paleontológicos, Trabalhos apresentados no VIII Congresso Brasileiro de Paleontologia* (Ed. D. de A. Campos and R.C.G. Armesto), Departamento Nacional de Produção Mineral - DNPM, Brasília, 21–28.
- Baud, A., Magaritz, M. and Holser, W.T.** (1989) Permian-Triassic of the Tethys: Carbon isotope studies. *Geol. Rundschau*, **78**, 649–677.
- Benton, M.J.** (2008) When Life Nearly Died - The greatest mass extinction of all time, 2nd edn. *Thames & Hudson*, London, 336 pp.
- Benton, M.J.** (2018) Hyperthermal-driven mass extinctions: Killing models during the Permian-Triassic mass extinction. *Philos Trans R Soc A Math Phys Eng Sci.* doi: 10.1098/rsta.2017.0076
- Benton, M.J. and Newell, A.J.** (2014) Impacts of global warming on Permo-Triassic terrestrial ecosystems. *Gondwana Res.*, **25**, 1308–1337.
- Blakey, R.C., Peterson, F. and Kocurek, G.** (1988) Synthesis of late Paleozoic and Mesozoic eolian deposits of the Western Interior of the United States. *Sediment. Geol.*, **56**, 3–125.
- Botha, J. and Smith, R.M.H.** (2006) Rapid vertebrate recuperation in the Karoo Basin of South Africa following the End-Permian extinction. *J. African Earth Sci.*, **45**, 502–514.
- Botha, J. and Smith, R.M.H.** (2020) Biostratigraphy of the Lystrosaurus declivis Assemblage Zone

- (Beaufort Group, Karoo Supergroup), South Africa. *South African J. Geol.*, **123**, 207–216.
- Boucot, A.J., Xu, C., Scotese, C.R. and Morley, R.J.** (2013) Phanerozoic Paleoclimate. *Society for Sedimentary Geology (SEPM)*, Tulsa, Oklahoma, U.S.A., 360 pp.
- Brierley, G.J. and Hickin, E.J.** (1991) Channel planform as a non-controlling factor in fluvial sedimentology: the case of the squamish river floodplain, British Columbia. *Sediment. Geol.*, **75**, 67–83.
- Bryant, M., Falk, P. and Paola, C.** (1995) Experimental study of avulsion frequency and rate of deposition. *Geology*, **23**, 365–368.
- Bullock, P. and Murphy, C.P.** (1979) Evolution of a paleo-argillic brown earth (paleudalf) from oxfordshire, England. *Geoderma*, **22**, 225–252.
- Burroughs, W.A.** (1985) The hydraulic equivalence of mica; discussion. *J. Sediment. Res.*, **55**, 291–292.
- Cao, C., Love, G.D., Hays, L.E., Wang, W., Shen, S. and Summons, R.E.** (2009) Biogeochemical evidence for euxinic oceans and ecological disturbance presaging the end-Permian mass extinction event. *Earth Planet. Sci. Lett.*, **281**, 188–201.
- Cartigny, M.J.B., Postma, G., van den Berg, J.H. and Mastbergen, D.R.** (2011) A comparative study of sediment waves and cyclic steps based on geometries, internal structures and numerical modeling. *Mar. Geol.*, **280**, 40–56.
- Cartigny, M.J.B., Ventra, D., Postma, G. and van Den Berg, J.H.** (2014) Morphodynamics and sedimentary structures of bedforms under supercritical-flow conditions: New insights from flume experiments. *Sedimentology*, **61**, 712–748.
- Chan, M.A.** (1999) Triassic loessite of north-central Utah; stratigraphy, petrophysical character, and paleoclimate implications. *J. Sediment. Res.*, **69**, 477–485.
- Chen, Z.Q. and Benton, M.J.** (2012) The timing and pattern of biotic recovery following the end-Permian mass extinction. *Nat. Geosci.*, **5**, 375–383.
- Chester, R., Elderfield, H., Griffin, J.J., Johnson, L.R. and Padgham, R.C.** (1972) Eolian dust along the eastern margins of the Atlantic Ocean. *Mar. Geol.*, **13**, 91–105.
- Choquette, P.W. and Pray, L.C.** (1970) Geologic Nomenclature and Classification of Porosity in Sedimentary Carbonates. *Am. Assoc. Pet. Geol. Bull.*, **54**, 207–250.
- Chow, V. Te** (1959) Open-channel Hydraulics, 1st edn. *McGraw-Hill Books*, New York, 697 pp.
- Cisneros, J.C.** (2008) Taxonomic status of the reptile genus Procolophon from the Gondwanan Triassic. *Palaeontol. Africana*, **43**, 7–18.
- Cisneros, J.C. and Schultz, C.L.** (2002) Procolophon brasiliensis n. sp., a new procolophonid reptile from the Lower Triassic of southern Brazil. *Neues Jahrb. für Geol. und Paläontologie - Monatshefte*, **2002**, 641–648.
- Cohen, K.M., Finney, S.C., Gibbard, P.L. and Fan, J.-X.** (2013) The ICS International Chronostratigraphic Chart. *Episodes*, **36**, 199–204.
- Cornish, V.** (1899) On Kumatology. (The Study of the Waves and Wave-Structures of the Atmosphere, Hydrosphere, and Lithosphere). *Geogr. J.*, **13**, 624.
- Covault, J.A., Kostic, S., Paull, C.K., Sylvester, Z. and Fildani, A.** (2017) Cyclic steps and related supercritical bedforms: Building blocks of deep-water depositional systems, western North America. *Mar. Geol.*, **393**, 4–20.
- CPRM** (2006) Mapa Geológico do Rio Grande do Sul.
- Dal Corso, J., Song, H., Callegaro, S., Chu, D., Sun, Y., Hilton, J., Grasby, S.E., Joachimski, M.M. and Wignall, P.B.** (2022) Environmental crises at the Permian–Triassic mass extinction. *Nat. Rev. Earth Environ.*, **3**, 197–214.
- Dalrymple, R.W.** (2010) Interpreting Sedimentary Successions: Facies, Facies Analysis and Facies Models. In: *Facies Models 4*, 4th edn. (Ed. N.P. James and R.W. Dalrymple), *Geological Association of Canada*, St. John's, 3–18.
- Dario, E.M.** (2017) Arquitetura de fácies e modelo deposicional dos depósitos fluviais efêmeros da Formação Sanga do Cabral, Triássico Inferior da Bacia Do Paraná, na região central do Rio Grande Do Sul. Universidade Federal do Rio Grande do Sul - UFRGS, Porto Alegre
- de Santa Ana, H., Goso, C. and Daners, G.** (2006) Cuenca Norte: estratigrafía del Carbonífero–Pérmico. In: *Cuenas Sedimentarias de Uruguay – Paleozoico* (Ed. G. Verolavsky, M. Ubilla, and S. Martínez), *DIRAC*, Montevideo, 147–208.
- Dias-Da-Silva, S. and Marsicano, C.** (2011) Phylogenetic reappraisal of Rhytidosteidae (Stereospondyli: Trematosauria), temnospondyl amphibians from the Permian and Triassic. *J. Syst. Palaeontol.*, **9**, 305–325.
- Dias-Da-Silva, S., Marsicano, C. and Schultz, C.L.** (2006) Rhytidosteid temnospondyls in Gondwana: A new taxon from the Lower Triassic of Brazil. *Palaeontology*, **49**, 381–390.
- Dias-da-Silva, S., Pinheiro, F.L., Stock Da-Rosa, Á.A., Martinelli, A.G., Schultz, C.L., Silva-Neves, E. and Modesto, S.P.** (2017) Biostratigraphic reappraisal of the Lower Triassic Sanga do Cabral

- Supersequence from South America, with a description of new material attributable to the parareptile genus *Procolophon*. *J. South Am. Earth Sci.*, **79**, 281–296.
- Dickinson, W.R.** (1985) Interpreting Provenance Relations from Detrital Modes of Sandstones. In: *Provenance of Arenites*, Springer Netherlands, Dordrecht, 333–361.
- Donselaar, M.E., Cuevas Gozalo, M.C. and Moyano, S.** (2013) Avulsion processes at the terminus of low-gradient semi-arid fluvial systems: Lessons from the Río Colorado, Altiplano endorheic basin, Bolivia. *Sediment. Geol.*, **283**, 1–14.
- Doyle, L.J., Carder, K.L. and Steward, R.** (1985) The hydraulic equivalence of mica; reply. *J. Sediment. Res.*, **55**, 293–294.
- Doyle, L.J., Carder, K.L. and Steward, R.G.** (1983) The hydraulic equivalence of mica. *J. Sediment. Petrol.*, **53**, 643–648.
- Du, Y., Song, H., Grasby, S.E., Xing, T., Song, H., Tian, L., Chu, D., Wu, Y., Dal Corso, J., Algeo, T.J. and Tong, J.** (2023) Recovery from persistent nutrient-N limitation following the Permian–Triassic mass extinction. *Earth Planet. Sci. Lett.*, **602**, 117944.
- Duller, R.A., Mountney, N.P., Russel, A.J. and Cassidy, N.C.** (2008) Architectural analysis of a volcanoclastic jökulhlaup deposit, southern Iceland: sedimentary evidence for supercritical flow. *Sedimentology*, **55**, 939–964.
- Dunne, E.M., Farnsworth, A., Greene, S.E., Lunt, D.J. and Butler, R.J.** (2021) Climatic drivers of latitudinal variation in Late Triassic tetrapod diversity. *Palaeontology*, **64**, 101–117.
- Eltink, E., Da-Rosa, Á.A.S. and Dias-da-Silva, S.** (2017) A capitosauroid from the Lower Triassic of South America (Sanga do Cabral Supersequence: Paraná Basin), its phylogenetic relationships and biostratigraphic implications. *Hist. Biol.*, **29**, 863–874.
- Ernesto, M., Demarco, P.N., Xavier, P., Sanchez, L., Schultz, C. and Piñeiro, G.** (2020) Age constraints on the Paleozoic Yaguarí-Buena Vista succession from Uruguay: paleomagnetic and paleontologic information. *J. South Am. Earth Sci.*, **98**, 102489.
- Erwin, D.H.** (2006) Extinction: How Life on Earth Nearly Ended 250 Million Years Ago. *Princeton University Press*, Princeton, 296 pp.
- Erwin, D.H.** (1994) The Permo–Triassic extinction. *Nature*, **367**, 231–236.
- Erwin, D.H.** (2001) Lessons from the past: Biotic recoveries from mass extinctions. *Proc. Natl. Acad. Sci. U. S. A.*, **98**, 5399–5403.
- Ethridge, F.G.** (2011) Interpretation of Ancient Fluvial Channel Deposits: Review and Recommendations. In: *From River to Rock Record: The preservation of fluvial sediments and their subsequent interpretation — SEPM Special Publication 97* (Ed. S.K. Davidson, S. Leleu, and C.P. North), *SEPM Society for Sedimentary Geology*, Tulsa, Oklahoma, U.S.A., 9–36.
- Faccini, U.F.** (2000) Estratigrafia do Permo-Triássico do Rio Grande do Sul: estilos deposicionais versus espaço de acomodação. Universidade Federal do Rio Grande do Sul - UFRGS
- Faccini, U.F.** (1989) O Permo-Triássico do Rio Grande do Sul: uma análise sob o ponto de vista das seqüências deposicionais. Universidade Federal do Rio Grande do Sul - UFRGS
- Fielding, C.R.** (2006) Upper flow regime sheets, lenses and scour fills: Extending the range of architectural elements for fluvial sediment bodies. *Sediment. Geol.*, **190**, 227–240.
- Fielding, C.R.** (1993) A review of recent research in fluvial sedimentology. *Sediment. Geol.*, **85**, 3–14.
- Fielding, C.R. and Alexander, J.** (1996) Sedimentology of the Upper Burdekin River of North Queensland, Australia—an example of a tropical, variable discharge river. *Terra Nov.*, **8**, 447–457.
- Fielding, C.R., Alexander, J. and Allen, J.P.** (2018) The role of discharge variability in the formation and preservation of alluvial sediment bodies. *Sediment. Geol.*, **365**, 1–20.
- Fielding, C.R., Allen, J.P., Alexander, J. and Gibling, M.R.** (2009) Facies model for fluvial systems in the seasonal tropics and subtropics. *Geology*, **37**, 623–626.
- Fielding, C.R., Frank, T.D., McLoughlin, S., Vajda, V., Mays, C., Tevyaw, A.P., Winguth, A., Winguth, C., Nicoll, R.S., Bocking, M. and Crowley, J.L.** (2019) Age and pattern of the southern high-latitude continental end-Permian extinction constrained by multiproxy analysis. *Nat Commun.* doi: 10.1038/s41467-018-07934-z
- Fielding, C.R., Frank, T.D., Tevyaw, A.P., Savatic, K., Vajda, V., McLoughlin, S., Mays, C., Nicoll, R.S., Bocking, M. and Crowley, J.L.** (2021) Sedimentology of the continental end-Permian extinction event in the Sydney Basin, eastern Australia. *Sedimentology*, **68**, 30–62.
- Fildani, A., Normark, W.R., Kostic, S. and Parker, G.** (2006) Channel formation by flow stripping: Large-scale scour features along the Monterey East Channel and their relation to sediment waves. *Sedimentology*, **53**, 1265–1287.
- Fisher, J.A., Krapf, C.B.E., Langs, S.C., Nichols, G.J. and Payenberg, T.H.D.** (2008) Sedimentology and architecture of the Douglas Creek terminal splay, Lake Eyre, central Australia. *Sedimentology*, **55**, 1915–1930.
- Folk, R.L.** (1981) Petrology of Sedimentary Rocks, 2nd edn. *Hemphill*, Austin, Texas, 184 pp.
- Francischini, H., Dentzien-Dias, P., Guerra-Sommer, M., Menegat, R., Santos, J.O.S., Manfroi, J.**

- and **Schultz, C.L.** (2018) A middle Permian (Roadian) lungfish aestivation burrow from the Rio do Rasto Formation (Paraná Basin, Brazil) and associated U-Pb dating. *Palaios*, **33**, 69–84.
- Froude, M.J., Alexander, J., Barclay, J. and Cole, P.** (2017) Interpreting flash flood palaeoflow parameters from antidunes and gravel lenses: An example from Montserrat, West Indies. *Sedimentology*, **64**, 1817–1845.
- Gallego, O.F.** (2010) A new crustacean clam shrimp (Spinicaudata: Eosestheriidae) from the Upper Triassic of Argentina and its importance for 'conchostracan' taxonomy. *Alcheringa An Australas. J. Palaeontol.*, **34**, 179–195.
- Gastaldo, R.A. and Neveling, J.** (2016) Comment on: "Anatomy of a mass extinction: Sedimentological and taphonomic evidence for drought-induced die-offs at the Permo-Triassic boundary in the main Karoo Basin, South Africa" by R.M.H. Smith and J. Botha-Brink, *Palaeogeography, Palaeoclimatology, Palaeogeogr. Palaeoclimatol. Palaeoecol.*, **447**, 88–91.
- Ghienne, J.F., Normandeau, A., Dietrich, P., Bouyssou, M., Lajeunesse, P. and Schuster, M.** (2021) The depositional signature of cyclic steps: A late Quaternary analogue compared to modern active delta slopes. *Sedimentology*, **68**, 1502–1538.
- Gilbert, G.K. and Murphy, E.C.** (1914) The transport of debris by running water. Sacramento, 265 pp.
- Goldberg, K.** (2001) The Paleoclimatic evolution of the Permian in the Paraná Basin in southern Brazil. University of Chicago
- Golden, D.C., Dixon, J.B. and Chen, C.C.** (1986) Ion Exchange, Thermal Transformations, and Oxidizing Properties of Birnessite. *Clays Clay Miner.*, **34**, 511–520.
- Goso, C., Piñeiro, G., de Santa Ana, H., Rojas, A., Verde, M. and Alves, C.** (2001) Caracterización estratigráfica de los depósitos continentales cuspidales neopérmicos (Formaciones Yaguari y Buena Vista) en el borde oriental de la Cuenca Norte Uruguay. In: *Actas del XI Congreso Latinoamericano de Geología*, Montevideo, 18 (CD-ROM).
- Goudie, A.** (1973) Duricrusts in tropical and subtropical landscapes. *Clarendon Press*, Oxford, Uited Kingdom, 174 pp.
- Goudie, A.S.** (1983) Calcrete. In: *Chemical Sediments and Geomorphology* (Ed. A.S. Goudie and K. Pye), *Academic Press*, London, UK, 93–131.
- Gould, S.J.** (1991) Seta do Tempo, Ciclo do Tempo. *Cia. das Letras*, São Paulo, 221 pp.
- Gulbranson, E.L., Ciccioli, P.L., Montañez, I.P., Marensi, S.A., Limarino, C.O., Schmitz, M.D. and Davydov, V.** (2015) Paleoenvironments and age of the Talampaya Formation: The Permo-Triassic boundary in northwestern Argentina. *J. South Am. Earth Sci.*, **63**, 310–322.
- Guy, H.P., Simons, D.B. and Richardson, E.V.** (1966) Summary of Alluvial Channel Data From Flume Experiments, 1956-61. *U. S. Geol. Surv. Prof. Pap.*, **462-I**, 1–104.
- Hallam, A. and Wignall, P.B.** (1997) Mass Extinctions and their Aftermath. *Oxford University Press*, Oxford, Uited Kingdom, 328 pp.
- Hansford, M.R., Plink-Björklund, P. and Jones, E.R.** (2020) Global quantitative analyses of river discharge variability and hydrograph shape with respect to climate types. *Earth-Science Rev.* doi: 10.1016/j.earscirev.2019.102977
- Harris, R., McCall, R., Randall, O., Bin Tawang, M.H., Williams, R., Fairman, J.G. and Schultz, D.M.** (2017) Climate change during the Triassic and Jurassic. *Geol. Today*, **33**, 210–215.
- Holz, M.** (2015) Mesozoic paleogeography and paleoclimates – A discussion of the diverse greenhouse and hothouse conditions of an alien world. *J. South Am. Earth Sci.*, **61**, 91–107.
- Horn, B.L.D., Goldberg, K. and Schultz, C.L.** (2018a) Interpretation of massive sandstones in ephemeral fluvial settings: A case study from the Upper Candelária Sequence (Upper Triassic, Paraná Basin, Brazil). *J. South Am. Earth Sci.*, **81**, 108–121.
- Horn, B.L.D., Goldberg, K. and Schultz, C.L.** (2018b) A loess deposit in the Late Triassic of southern Gondwana, and its significance to global paleoclimate. *J. South Am. Earth Sci.*, **81**, 189–203.
- Horn, B.L.D., Melo, T.P., Schultz, C.L., Philipp, R.P., Kloss, H.P. and Goldberg, K.** (2014) A new third-order sequence stratigraphic framework applied to the Triassic of the Paraná Basin, Rio Grande do Sul, Brazil, based on structural, stratigraphic and paleontological data. *J. South Am. Earth Sci.*, **55**, 123–132.
- Horn, B.L.D., Pereira, V.P. and Schultz, C.L.** (2013) Calcretes of the Santa Maria Supersequence, Middle Triassic, Rio Grande do Sul, Brazil: Classification, genesis and paleoclimatic implications. *Palaeogeogr. Palaeoclimatol. Palaeoecol.*, **376**, 39–47.
- Irmis, R.B. and Whiteside, J.H.** (2012) Delayed recovery of non-marine tetrapods after the end-permian mass extinction tracks global carbon cycle. *Proc. R. Soc. B Biol. Sci.*, **279**, 1310–1318.
- James, M.R. and Robson, S.** (2012) Straightforward reconstruction of 3D surfaces and topography with a camera: Accuracy and geoscience application. *J. Geophys. Res. Earth Surf.*, **117**, 1–17.
- Jefferson, I., Rosenbaum, M. and Smalley, I.** (2002) Mercia Mudstone as a Triassic aeolian desert sediment. *Mercian Geol.*, **15**, 157–162.

- Jeong, G.Y.** (2008) Bulk and single-particle mineralogy of Asian dust and a comparison with its source soils. *J Geophys Res Atmos.* doi: 10.1029/2007JD008606
- Jeong, G.Y., Hillier, S. and Kemp, R.A.** (2011) Changes in mineralogy of loess-paleosol sections across the Chinese Loess Plateau. *Quat. Res.*, **75**, 245–255.
- Johnson, S.Y.** (1989) Significance of Loessite in the Maroon Formation (Middle Pennsylvanian to Lower Permian), Eagle Basin, Northwest Colorado. *J. Sediment. Res.*, **Vol. 59**, 782–791.
- Kabata-Pendias, A.** (2010) Trace Elements in Soils and Plants, 4th edn. *CRC Press*, Boca Raton, USA, 548 pp.
- Kemp, R.A.** (1987) Genesis and environmental significance of a buried middle pleistocene soil in Eastern England. *Geoderma*, **41**, 49–77.
- Kennedy, J.F.** (1963) The mechanics of dunes and antidunes in erodible-bed channels. *J. Fluid Mech.*, **16**, 521–544.
- Kennedy, J.F.** (1960) Stationary waves and antidunes in alluvial channels. California Institute of Technology
- Kessler, J.L.P., Soreghan, G.S. and Wacker, H.J.** (2001) Equatorial Aridity in Western Pangea: Lower Permian Loessite and Dolomitic Paleosols in Northeastern New Mexico, U.S.A. *J. Sediment. Res.*, **71**, 817–832.
- Kiessling, W., Flügel, E. and Golonka, J.** (eds) (2002) Phanerozoic Reef Patterns. *SEPM (Society for Sedimentary Geology)*, 775 pp.
- Kirchner, J.W. and Weil, A.** (2000) Delayed biological recovery from extinctions throughout the fossil record. *Nature*, **404**, 177–180.
- Knapp, J.** (2020) Alluvial Fans, Loess Plains, Lakes, and Distributive Fluvial Systems: Depositional Systems of the Permian-Triassic Red Beds and Evaporites of Wyoming (USA). West Virginia University
- Krapovickas, V., Mancuso, A.C., Marsicano, C.A., Domnanovic, N.S. and Schultz, C.L.** (2013) Large tetrapod burrows from the Middle Triassic of Argentina: a behavioural adaptation to seasonal semi-arid climate? *Lethaia*, **46**, 154–169.
- Kraus, M.J.** (1999) Paleosols in clastic sedimentary rocks: their geologic applications. *Earth-Science Rev.*, **47**, 41–70.
- Kutzbach, J.E. and Gallimore, R.G.** (1989) Pangaeen climates: Megamonsoons of the megacontinent. *J. Geophys. Res.*, **94**, 3341–3357.
- Labandeira, C. and Sepkoski, J.** (1993) Insect diversity in the fossil record. *Science (80-)*, **261**, 310–315.
- Lamb, M.P., Parsons, J.D., Mullenbach, B.L., Finlayson, D.P., Orange, D.L. and Nittrouer, C.A.** (2008) Evidence for superlevation, channel incision, and formation of cyclic steps by turbidity currents in Eel Canyon, California. *Bull. Geol. Soc. Am.*, **120**, 463–475.
- Lang, J., Le Heron, D.P., Van den Berg, J.H. and Winsemann, J.** (2021) Bedforms and sedimentary structures related to supercritical flows in glacial settings. *Sedimentology*, **68**, 1539–1579.
- Lang, J., Sievers, J., Loewer, M., Igel, J. and Winsemann, J.** (2017) 3D architecture of cyclic-step and antidune deposits in glacial subaqueous fan and delta settings: Integrating outcrop and ground-penetrating radar data. *Sediment. Geol.*, **362**, 83–100.
- Lang, J. and Winsemann, J.** (2013) Lateral and vertical facies relationships of bedforms deposited by aggrading supercritical flows: From cyclic steps to humpback dunes. *Sediment. Geol.*, **296**, 36–54.
- Lavina, E.L.C.** (1983) *Procolophon pricei* sp.n., um novo réptil procolofonídeo do Triássico do Rio Grande do Sul. *Iheringia, Série Geológica*, **9**, 51–78.
- Lavina, E.L.C.** (1991) Geologia sedimentar e paleogeografia do Neopermiano e Eotriássico (intervalo Kazanian-Scythiano) da Bacia do Paraná. Universidade Federal do Rio Grande do Sul - UFRGS
- Li, J., Gastaldo, R.A., Neveling, J. and Geissman, J.W.** (2017) Siltstones across the Daptocephalus (Dicynodon) and Lystrosaurus assemblage zones, Karoo Basin, South Africa, show no evidence for aridification. *J. Sediment. Res.*, **87**, 653–671.
- Li, Y., Shi, W., Aydin, A., Beroya-Eitner, M.A. and Gao, G.** (2020) Loess genesis and worldwide distribution. *Earth-Science Rev.*, **201**, 22.
- Lighthill, J.** (1978) Waves in Fluids. *Cambridge University Press*, Cambridge, 504 pp.
- Looy, C. V., Brugman, W.A., Dilcher, D.L. and Visscher, H.** (1999) The delayed resurgence of equatorial forests after the Permian–Triassic ecologic crisis. *Proc. Natl. Acad. Sci.*, **96**, 13857–13862.
- Lowe, D.R. and LoPiccolo, R.D.** (1974) The Characteristics and Origins of Dish and Pillar Structures. *J. Sediment. Res.*, **44**, 484–501.
- Luppo, T., López de Luchi, M.G., Rapalini, A.E., Martínez Dopico, C.I. and Fanning, C.M.** (2018) Geochronologic evidence of a large magmatic province in northern Patagonia encompassing the Permian-Triassic boundary. *J. South Am. Earth Sci.*, **82**, 346–355.

- MacDougall, M.J., Brocklehurst, N. and Fröbisch, J.** (2019) Species richness and disparity of parareptiles across the end-Permian mass extinction. *Proc. R. Soc. B Biol. Sci.*, **286**, 20182572.
- Mancuso, A.C., Horn, B.L.D., Benavente, C.A., Schultz, C.L. and Irmis, R.B.** (2021) The paleoclimatic context for South American Triassic vertebrate evolution. *J. South Am. Earth Sci.*, **110**, 103321.
- Manna, M.O., Scherer, C.M. dos S., Bállico, M.B., Reis, A.D. dos, Moraes, L.V., Ferrari, L.A.B., Roisenberg, H.B. and Oliveira, V.G. de** (2021) Changes in fluvial architecture induced by discharge variability, Jaicós Formation (Silurian-Devonian), Parnaíba Basin, Brazil. *Sediment. Geol.*, **420**, 105924.
- Mao, X., Liu, X. and Zhou, X.** (2021) Permo-Triassic aeolian red clay of southwestern England and its palaeoenvironmental implications. *Aeolian Res.*, **52**, 100726.
- Mays, C., McLoughlin, S., Frank, T.D., Fielding, C.R., Slater, S.M. and Vajda, V.** (2021) Lethal microbial blooms delayed freshwater ecosystem recovery following the end-Permian extinction. *Nat. Commun.*, **12**, 5511.
- Mays, C., Vajda, V., Frank, T.D., Fielding, C.R., Nicoll, R.S., Tevyaw, A.P. and McLoughlin, S.** (2020) Refined Permian–Triassic floristic timeline reveals early collapse and delayed recovery of south polar terrestrial ecosystems. *GSA Bull.*, **132**, 1489–1513.
- McKee, E.D., Crosby, E.J. and Berryhill, H.L.** (1967) Flood deposits, Bijou Creek, Colorado, June 1965. *J. Sediment. Res.*, **37**, 829–851.
- McKenzie, R.M.** (1989) Manganese Oxides and Hydroxides. In: *Minerals in Soil environments*, 2nd edn. (Ed. J.B. Dixon and S.B. Weed), *Soil Science Society of America*, Madison, USA, 439–465.
- Meijer, N., Dupont-Nivet, G., Licht, A., Trabucho-Alexandre, J., Bourquin, S. and Abels, H.A.** (2020) Identifying eolian dust in the geological record. *Earth-Science Rev.* doi: 10.1016/j.earscirev.2020.103410
- Miall, A.D.** (1985) Architectural-element analysis: A new method of facies analysis applied to fluvial deposits. *Earth Sci. Rev.*, **22**, 261–308.
- Miall, A.D.** (2016) *Stratigraphy: A Modern Synthesis*. Springer International Publishing, Cham, Switzerland, 454 pp.
- Miall, A.D.** (1988) Facies architecture in clastic sedimentary basins. In: *New perspectives in basin analysis* (Ed. K. Kleinspehn and C. Paola), Springer-Verlag, New York, 67–81.
- Miall, A.D.** (1977) A review of the braided-river depositional environment. *Earth-Science Rev.*, **13**, 1–62.
- Michell, J.H.** (1893) XLIV. The highest waves in water. *London, Edinburgh, Dublin Philos. Mag. J. Sci.*, **36**, 430–437.
- Milani, E.J.** (2004) Comentários sobre a origem e a evolução tectônica da Bacia do Paraná. In: *Geologia do Continente Sul-Americano: evolução da obra de Fernando Flávio Marques de Almeida* (Ed. V. Mantesso-Neto, A. Bartorelli, C.D.R. Carneiro, and B.B. de Brito-Neves), Beca, São Paulo, 265–280.
- Milani, E.J.** (1997) Evolução tectono-estratigráfica da Bacia do Paraná e seu relacionamento com a geodinâmica fanerozóica do Gondwana sul-ocidental. Universidade Federal do Rio Grande do Sul
- Milani, E.J., Melo, J.H.G., Souza, P.A., Fernandes, L.A. and França, A.B.** (2007) Bacia do Paraná. *Bol. Geociências da Petrobras*, **15**, 265–287.
- Milani, E.J. and Thomaz Filho, A.** (2000) Sedimentary Basins of South America. In: *Tectonic Evolution of South America* (Ed. U.G. Cordani, E.J. Milani, A. Thomaz Filho, and D. de A. Campos), 31st International Geological Congress, Rio de Janeiro, 389–449.
- Neveling, J., Rubidge, B.S. and Hancox, P.J.** (1999) A lower Cynognathus Assemblage Zone fossil from the Katberg Formation (Beaufort Group, South Africa). *S. Afr. J. Sci.*, **95**, 555–556.
- Nicholas, A.P., Sambrook Smith, G.H., Amsler, M.L., Ashworth, P.J., Best, J.L., Hardy, R.J., Lane, S.N., Orfeo, O., Parsons, D.R., Reesink, A.J.H., Sandbach, S.D., Simpson, C.J. and Szupiany, R.N.** (2016) The role of discharge variability in determining alluvial stratigraphy. *Geology*, **44**, 3–6.
- Nicolas, M. and Rubidge, B.S.** (2010) Changes in Permo-Triassic terrestrial tetrapod ecological representation in the Beaufort Group (Karoo Supergroup) of South Africa. *Lethaia*, **43**, 45–59.
- North, C.P. and Davidson, S.K.** (2012) Unconfined alluvial flow processes: Recognition and interpretation of their deposits, and the significance for palaeogeographic reconstruction. *Earth-Science Rev.*, **111**, 199–223.
- North, C.P. and Taylor, K.S.** (1996) Ephemeral-fluvial deposits: Integrated outcrop and simulation studies reveal complexity. *Am. Assoc. Pet. Geol. Bull.*, **80**, 811–830.
- Olsen, P.E. and Kent, D. V.** (1996) Milankovitch climate forcing in the tropics of Pangaea during the Late Triassic. *Palaeogeogr. Palaeoclimatol. Palaeoecol.*, **122**, 1–26.
- Ono, K., Plink-Björklund, P., Eggenhuisen, J.T. and Cartigny, M.J.B.** (2021) Froude supercritical flow processes and sedimentary structures: New insights from experiments with a wide range of grain sizes. *Sedimentology*, **68**, 1328–1357.

- Ore, H.T.** (1964) Some criteria for recognition of braided stream deposits. *Rocky Mt. Geol.*, **3**, 1–14.
- Owens, J.S.** (1908) Experiments on the Transporting Power of Sea Currents. *Geogr. J.*, **31**, 415.
- Parker, G.** (1996) Some Speculations on the Relation Between Channel Morphology and Channel-scale Flow Structures. In: *Coherent Flow Structures in Open Channels* (Ed. P.J. Ashworth, S.J. Bennett, J.L. Best, and S.J. McLelland), *John Wiley & Sons*, Chichester, 423–458.
- Parker, G.** and **Izumi, N.** (2000) Purely erosional cyclic and solitary steps created by flow over a cohesive bed. *J. Fluid Mech.*, **419**, 203–238.
- Parrish, J.T.** (1993) Climate of the Supercontinent Pangea. *J. Geol.*, **101**, 215–233.
- Payton, R.W.** (1993) Fragipan formation in argillic brown earths (Fragiudalfs) of the Milfield Plain, north-east England. II. Post Devonian developmental processes and the origin of fragipan consistence. *J. Soil Sci.*, **44**, 703–723.
- Penn, J.L., Deutsch, C., Payne, J.L.** and **Sperling, E.A.** (2018) Temperature-dependent hypoxia explains biogeography and severity of end-Permian marine mass extinction. *Science* (80-). doi: 10.1126/science.aat1327
- Phillips, J.** (1860) *Life on the earth : its origin and succession.* *Macmillan and co.*, Cambridge, London, 276 pp.
- Piñeiro, G., Ferigolo, J., Ribeiro, A.M.** and **Velozo, P.** (2015) Reassessing the affinities of vertebral remains from Permo-Triassic beds of Gondwana. *Comptes Rendus - Palevol*, **14**, 387–401.
- Piñeiro, G., Marsicano, C., Goso, C.** and **Morosi, E.** (2007) Temnospondyl diversity of the Permian-Triassic Colonia Orozco Local Fauna (Buena Vista Formation) of Uruguay. *Rev. Bras. Paleontol.*, **10**, 169–180.
- Piñeiro, G., Ramos, A.** and **Marsicano, C.** (2012) A rhinesuchid-like temnospondyl from the Permo-Triassic of Uruguay. *Comptes Rendus - Palevol*, **11**, 65–78.
- Piñeiro, G., Rojas, A.** and **Ubilla, M.** (2004) A new procolophonoid (Reptilia, Parareptilia) from the Upper Permian of Uruguay. *J. Vertebr. Paleontol.*, **24**, 814–821.
- Piñeiro, G., Verde, M., Ubilla, M.** and **Ferigolo, J.** (2003) First basal synapsids (“pelycosaurs”) from the Upper Permian–Lower Triassic of Uruguay, South America. *J. Paleontol.*, **77**, 389–392.
- Pinheiro, F.L., França, M.A.G., Lacerda, M.B., Butler, R.J.** and **Schultz, C.L.** (2016) An exceptional fossil skull from South America and the origins of the archosauriform radiation. *Sci. Rep.*, **6**, 1–7.
- Plink-Björklund, P.** (2015) Morphodynamics of rivers strongly affected by monsoon precipitation: Review of depositional style and forcing factors. *Sediment. Geol.* **323**:110–147.
- Potter, R.M.** and **Rossmann, G.R.** (1979) Mineralogy of manganese dendrites and coatings. *Am. Mineral.*, **64**, 1219–1226.
- Preto, N., Kustatscher, E.** and **Wignall, P.B.** (2010) Triassic climates — State of the art and perspectives. *Palaeogeogr. Palaeoclimatol. Palaeoecol.*, **290**, 1–10.
- Pye, K.** (1987) *Aeolian Dust and Dust Deposits.* *Academic Press*, London, UK, 334 pp.
- Racki, G.** (1999) Silica-secreting biota and mass extinctions: survival patterns and processes. *Palaeogeogr. Palaeoclimatol. Palaeoecol.*, **154**, 107–132.
- Raup, D.M.** (1979) Size of the Permo-Triassic Bottleneck and Its Evolutionary Implications. *Science* (80-), **206**, 217–218.
- Reis, A.D. dos, Scherer, C.M. dos S., Amarante, F.B. do, Rossetti, M. de M.M., Kifumbi, C., Souza, E.G. de, Ferronato, J.P.F.** and **Owen, A.** (2019) Sedimentology of the proximal portion of a large-scale, Upper Jurassic fluvial-aeolian system in Paraná Basin, southwestern Gondwana. *J. South Am. Earth Sci.*, **95**, 102248.
- Reis, A.D. Dos, Scherer, C.M.D.S., Owen, A., Amarante, F.B. Do, Ferronato, J.P.F., Pantopoulos, G., de Souza, E.G., Bállico, M.B.** and **Aguilar, C.A.G.** (2022) a Quantitative Depositional Model of a Large Distributive Fluvial System (Megafan) With Terminal Aeolian Interaction: the Upper Jurassic Guará Dfs in Southwestern Gondwana. *J. Sediment. Res.*, **92**, 460–485.
- Retallack, G.J.** (1988) Field recognition of paleosols. In: *Paleosols and Weathering Through Geologic Time: Principles and Applications* (Ed. J. Reinhardt and W.R. Sigleo), *Geological Society of America*, 1–20.
- Retallack, G.J.** (2001) *Soils of the Past: An Introduction to Paleopedology*, 2nd edn. *Wiley*, 404 pp.
- Retallack, G.J., Veevers, J.J.** and **Morante, R.** (1996) Global coal gap between Permian–Triassic extinction and Middle Triassic recovery of peat-forming plants. *Geol. Soc. Am. Bull.*, **108**, 195–207.
- Robertson, J.M.** and **Rouse, H.** (1941) On the Four Regimes of Open Channel Flow. *Civ. Eng. (New York)*, **11**, 169–171.
- Rubidge, B.S.** (2005) Re-uniting lost continents - Fossil reptiles from the ancient Karoo and their wanderlust. *South African J. Geol.*, **108**, 135–172.
- Ruta, M.** and **Benton, M.J.** (2008) Calibrated diversity, tree topology and the mother of mass extinctions: The lesson of temnospondyls. *Palaeontology*, **51**, 1261–1288.
- Sahney, S.** and **Benton, M.J.** (2008) Recovery from the most profound mass extinction of all time. *Proc.*

- R. Soc. B Biol. Sci.*, **275**, 759–765.
- Saunderson, H.C. and Lockett, F.P.J.** (1983) Flume Experiments on Bedforms and Structures at the Dune-Bed Transition. In: *Modern and Ancient Fluvial Systems* (Ed. J.D. Collinson and J. Lewin), Blackwell Publishing Ltd., Oxford, UK, 49–58.
- Scherer, C.M. dos S., Lavina, E.L.C., Reis, A.D. dos and Horn, B.L.D.** (2021) Estratigrafia da sucessão sedimentar mesozoica da Bacia do Paraná no Rio Grande do Sul. In: *Contribuições a Geologia do Rio Grande do Sul e de Santa Catarina* (Ed. A.R. Jelinek and C.A. Sommer), Sociedade Brasileira de Geologia Núcleo RS/SC, Compasso Lugar-Cultura, Porto Alegre, 289–304.
- Scherer, C.M.S., Reis, A.D., Horn, B.L.D., Bertolini, G., Lavina, E.L.C., Kifumbi, C. and Goso Aguiar, C.** (2023) The stratigraphic puzzle of the permo-mesozoic southwestern Gondwana: The Paraná Basin record in geotectonic and palaeoclimatic context. *Earth-Science Rev.*, **240**, 104397.
- Schmidt, V. and McDonald, D.A.** (1979) The Role of Secondary Porosity in the Course of Sandstone Diagenesis. In: *Aspects of Diagenesis*, Special Pu (Ed. P.A. Scholle and P.R. Schluger), SEPM (Society for Sedimentary Geology), Tulsa, Oklahoma, U.S.A., 175–207.
- Schneider, R.L., Mühlmann, H., Tommasi, E., Medeiros, R.A., Daemon, R.F. and Nogueira, A.A.** (1974) Revisão estratigráfica da Bacia do Paraná. In: *Anais do Congresso Brasileiro de Geologia, Sociedade Brasileira de Geologia*, Porto Alegre, 1, 41–65.
- Schultz, C.L., Martinelli, A.G., Soares, M.B., Pinheiro, F.L., Kerber, L., Horn, B.L.D., Pretto, F.A., Müller, R.T. and Melo, T.P.** (2020) Triassic faunal successions of the Paraná Basin, southern Brazil. *J. South Am. Earth Sci.*, **104**, 102846.
- Sellwood, B.W. and Valdes, P.J.** (2006) Mesozoic climates: General circulation models and the rock record. *Sediment. Geol.*, **190**, 269–287.
- Sepkoski, J.J.** (1984) A kinetic model of Phanerozoic taxonomic diversity. III. Post-Paleozoic families and mass extinctions. *Paleobiology*, **10**, 246–267.
- Simons, D.B. and Richardson, E.V.** (1961) Forms of Bed Roughness in Alluvial Channels. *J. Hydraul. Div.*, **87**, 87–105.
- Singer, A.** (1988) Illite in aridic soils, desert dusts and desert loess. *Sediment. Geol.*, **59**, 251–259.
- Singh, A. and Bhardwaj, B.D.** (1991) Fluvial facies model of the Ganga River sediments, India. *Sediment. Geol.*, **72**, 135–146.
- Slotman, A. and Cartigny, M.J.B.** (2020) Cyclic steps: Review and aggradation-based classification. *Earth-Science Rev.* doi: 10.1016/j.earscirev.2019.102949
- Slotman, A., Vellinga, A.J., Moscariello, A. and Cartigny, M.J.B.** (2021) The depositional signature of high-aggradation chute-and-pool bedforms: The build-and-fill structure. *Sedimentology*, **68**, 1640–1673.
- Smith, R.M.H. and Botha-Brink, J.** (2014) Anatomy of a mass extinction: Sedimentological and taphonomic evidence for drought-induced die-offs at the Permo-Triassic boundary in the main Karoo Basin, South Africa. *Palaeogeogr. Palaeoclimatol. Palaeoecol.*, **396**, 99–118.
- Sneh, A.** (1983) Desert Stream Sequences in the Sinai Peninsula. *J. Sediment. Res.*, **53**, 1271–1279.
- Soreghan, G.S.L., Elmore, R.D. and Lewchuck, M.T.** (2002) Sedimentologic-magnetic record of western Pangean climate in upper Paleozoic loessite (lower Cutler beds, Utah). *Bull. Geol. Soc. Am.*, **114**, 1019–1035.
- Southard, J.B. and Boguchwal, L.A.** (1990) Bed configuration in steady unidirectional water flows; Part 2, Synthesis of flume data. *J. Sediment. Res.*, **60**, 658–679.
- Spinewine, B., Sequeiros, O.E., Garcia, M.H., Beaubouef, R.T., Sun, T., Savoye, B. and Parker, G.** (2009) Experiments on wedge-shaped deep sea sedimentary deposits in minibasins and/or on channel levees emplaced by turbidity currents. Part II. Morphodynamic evolution of the wedge and of the associated bedforms. *J. Sediment. Res.*, **79**, 608–628.
- Stanley, S.M.** (2016) Estimates of the magnitudes of major marine mass extinctions in earth history. *Proc. Natl. Acad. Sci.*, **113**, E6325–E6334.
- Tan, C. and Plink-Björklund, P.** (2021) Morphodynamics of supercritical flow in a linked river and delta system, Daihai Lake, Northern China. *Sedimentology*, **68**, 1606–1639.
- Trendell, A.M., Nordt, L.C., Atchley, S.C., Leblanc, S.L. and Dworkin, S.I.** (2013) Determining floodplain plant distributions and populations using paleopedology and fossil root traces: Upper Triassic Sonsela Member of the Chinle Formation at Petrified Forest National Park, Arizona. *Palaios*, **28**, 471–490.
- Tunbridge, I.P.** (1981) Sandy high-energy flood sedimentation — Some criteria for recognition, with an example from the Devonian of S.W. England. *Sediment. Geol.*, **28**, 79–95.
- Vail, P.R., Mitchum, R.M. and Thompson, S.** (1977) Seismic stratigraphy and global changes of sea level, part 3: relative changes of sea level from coastal onlap. In: *Seismic stratigraphy - applications to hydrocarbon exploration*, Memoir 26 (Ed. C.E. Payton), American Association of Petroleum Geologists, Tulsa, 63–81.

- Vaisblat, N., Harris, N.B., Ayranci, K., Power, M., DeBhur, C., Bish, D.L., Chalaturnyk, R., Krause, F., Crombez, V., Euzen, T. and Rohais, S. (2021) Compositional and diagenetic evolution of a siltstone, with implications for reservoir quality; an example from the Lower Triassic Montney Formation in western Canada. *Mar. Pet. Geol.*, **129**, 29.
- Van Valen, L.M. (1984) A resetting of Phanerozoic community evolution. *Nature*, **307**, 50–52.
- Viglietti, P.A., Rojas, A., Rosvall, M., Klimes, B. and Angielczyk, K.D. (2022) Network-based biostratigraphy for the late Permian to mid-Triassic Beaufort Group (Karoo Supergroup) in South Africa enhances biozone applicability and stratigraphic correlation. *Palaeontology*. doi: 10.1111/pala.12622
- Walker, S. and Holbrook, J. (2022) Structures, architecture, vertical profiles, palaeohydrology and taphonomy of an upper-flow-regime-dominated fluvial system, the Triassic Dockum Group of the Palo Duro Canyon, Texas. *Sedimentology*, **70**, 645–684.
- Walker, T.R., Waugh, B. and Grone, A.J. (1978) Diagenesis in first-cycle desert alluvium of Cenozoic age, southwestern United States and northwestern Mexico. *Geol. Soc. Am. Bull.*, **89**, 19.
- Wilkins, A.D., Hurst, A., Wilson, M.J. and Archer, S. (2018) Palaeo-environment in an ancient low-latitude, arid lacustrine basin with loessite: The Smith Bank Formation (Early Triassic) in the Central North Sea, UK Continental Shelf. *Sedimentology*, **65**, 335–359.
- Wilson, K.M., Pollard, D., Hay, W.W., Thompson, S.L. and Wold, C.N. (1994) General circulation model simulations of Triassic climates: Preliminary results. *Pangea Paleoclimate, Tectonics, Sediment. Dur. Accretion, Zenith, Break. a Supercontinent*, **288**, 91–116.
- Wilson, M.J., Hurst, A., Wilkins, A.D., Wilson, L. and Bowen, L. (2020) Mineralogical evidence for multiple dust sources in an early Triassic loessite. *Sedimentology*, **67**, 239–260.
- Winguth, A.M.E., Shields, C.A. and Winguth, C. (2015) Transition into a Hothouse World at the Permian–Triassic boundary—A model study. *Palaeogeogr. Palaeoclimatol. Palaeoecol.*, **440**, 316–327.
- Wright, V.P. (2007) Calcrete. In: *Geochemical Sediments and Landscapes* (Ed. D.J. Nash and S.J. McLaren), *Blackwell Publishing Ltd.*, 10–45.
- Wright, V.P. (1990) A micromorphological classification of fossil and recent calcic and petrocalcic microstructures. In: *Soil Micromorphology: A Basic and Applied Science* (Ed. L.A. Douglas), *Elsevier*, Amsterdam, 401–407.
- Wright, V.P., Marriott, S.B. and Vanstone, S.D. (1991) A “reg” palaeosol from the Lower Triassic of south Devon: stratigraphic and palaeoclimatic implications. *Geol. Mag.*, **128**, 517–523.
- Wright, V.P. and Tucker, M.E. (1991) Calcretes: an introduction. In: *Calcretes* (Ed. V.P. Wright and M.E. Tucker), *Blackwell Scientific Publications*, Oxford, United Kingdom, 1–22.
- Wu, H., Zhang, S., Feng, Q., Jiang, G., Li, H. and Yang, T. (2012) Milankovitch and sub-Milankovitch cycles of the early Triassic Daye Formation, South China and their geochronological and palaeoclimatic implications. *Gondwana Res.*, **22**, 748–759.
- Xavier, P.L.A., Scherer, C.M. dos S., Reis, A.D. dos, Souza, E.G. de, Guadagnin, F. and Piñeiro, G. (2023) Supercritical fluvial styles and the shifting aridity in the Early Triassic: the example of the Sanga do Cabral Formation, Paraná Basin, Brazil. *J Sediment Res.* doi: 10.2110/jsr.2022.063
- Yokokawa, M., Hasegawa, K., Kanbayashi, S. and Endo, N. (2010) Formative conditions and sedimentary structures of sandy 3D antidunes: An application of the gravel step-pool model to fine-grained sand in an experimental flume. *Earth Surf. Process. Landforms*, **35**, 1720–1729.
- Zálan, P.V., Wolff, S., Conceição, J.C.J., Astolfi, M.A.M., Vieira, I.S., Appi, V.T., Zanotto, O.A. and Marques, A. (1991) Tectonics and sedimentation of the Paraná Basin. In: *Proceedings of the 7th International Gondwana Symposium* (Ed. H.H.G.J. Ulbrich and A.C. Rocha-Campos), *Instituto de Geociências, USP*, São Paulo, 83–117.
- Zellman, K.L., Plink-Björklund, P. and Fricke, H.C. (2021) Testing hypotheses on signatures of precipitation variability in the river and floodplain deposits of the Paleogene San Juan Basin, New Mexico, U.S.A. *J. Sediment. Res.*, **90**, 1770–1801.
- Zerfass, H. (1998) Estratigrafia da Sedimentação Meso e Neotriássica no Município de São Pedro do Sul, RS: Faciologia, Análise de Proveniência e História Diagenética. Universidade do Vale do Rio dos Sinos - UNISINOS
- Zerfass, H., Chemale, F., Schultz, C.L. and Lavina, E. (2004) Tectonics and sedimentation in Southern South America during Triassic. *Sediment. Geol.*, **166**, 265–292.
- Zerfass, H., Garcia, A.J.V., Suszczunski, A.M. and Lavina, E.L.C. (2000) Análise de proveniência dos arenitos Neopermianos e Triássicos da Bacia do Paraná na região de São Pedro do Sul (RS): uma contribuição para o conhecimento da arquitetura estratigráfica e da evolução tectono-sedimentar. *Acta Geol. Leopoldensia*, **XXIII**, 61–84.
- Zerfass, H., Lavina, E.L., Schultz, C.L., Garcia, A.J.V., Faccini, U.F. and Chemale Jr, F. (2003) Sequence stratigraphy of continental Triassic strata of Southernmost Brazil: a contribution to Southwestern Gondwana palaeogeography and palaeoclimate. *Sediment. Geol.*, **161**, 85–105.

- Zhao, C., Fang, H., Liu, Y., Dey, S. and He, G.** (2020) Impact of Particle Shape on Saltating Mode of Bedload Transport Sheared by Turbulent Flow. *J. Hydraul. Eng.*, **146**, 1–13.
- Zhong, G., Cartigny, M.J.B., Kuang, Z. and Wang, L.** (2015) Cyclic steps along the South Taiwan Shoal and West Penghu submarine canyons on the northeastern continental slope of the South China Sea. *Bull. Geol. Soc. Am.*, **127**, 804–824.

SEGUNDO ARTIGO

O segundo artigo, intitulado “*The role of calcretes in multi-cycle intraformational conglomerates from a supercritical-dominated fluvial system with eolian dust contribution (Early Triassic, Paraná Basin, Brazil)*” de Xavier, P.L.A.; Scherer, C.M.S.; Rodrigues, A.G.; Reis, A.D.; Souza, E.G.; Guadagnin, F.; Piñeiro, G., foi submetido ao periódico *Sedimentary Geology* em 27 de novembro de 2023.



Pedro Luis Xavier <xavier.pedroluis@gmail.com>

Acknowledgement of receipt of your submitted article - SEDGEO9756

Sedimentary Geology <em@editorialmanager.com>
Responder a: Sedimentary Geology <support@elsevier.com>
Para: Pedro Luis Xavier <xavier.pedroluis@gmail.com>

27 de novembro de 2023 às 13:08

Dear Mr. Xavier,

Your submission entitled "The role of calcretes in multi-cycle intraformational conglomerates from a supercritical-dominated fluvial system with eolian dust contribution (Early Triassic, Paraná Basin, Brazil)" has been received by Sedimentary Geology.

Your paper will be considered as belonging to the category Review Article. Please contact us if this is not correct.

The submission has been assigned the following manuscript number: SEDGEO9756.

Please note that submission of an article is understood to imply that the article is original and is not being considered for publication elsewhere. Submission also implies that all authors have approved the paper for release and are in agreement with its content.

You will be able to check on the progress of your paper by logging on to <https://www.editorialmanager.com/sedgeo/> as Author.

Thank you for submitting your work to this journal.

Kind regards,

Editorial Manager
Sedimentary Geology

This journal uses the Elsevier Article Transfer Service. This means that if an editor feels your manuscript is more suitable for an alternative journal, then you might be asked to consider transferring the manuscript to such a journal. The recommendation might be provided by a Journal Editor, a dedicated Scientific Managing Editor, a tool assisted recommendation, or a combination. For more details see the journal guide for authors.

#AU_SEDGEO#

To ensure this email reaches the intended recipient, please do not delete the above code

In compliance with data protection regulations, you may request that we remove your personal registration details at any time. (Remove my information/details). Please contact the publication office if you have any questions.

The role of calcretes in multi-cycle intraformational conglomerates from a supercritical-dominated fluvial system with eolian dust contribution (Early Triassic, Paraná Basin, Brazil)

Xavier, Pedro L. A.^{a*}

Scherer, Claiton M. dos S.^a

Rodrigues, Amanda Goulart^a

Reis, Adriano Domingos dos^b

Souza, Ezequiel Galvão de^c

Guadagnin, Felipe^c

Piñeiro, Graciela^d

^a Programa de Pós-Graduação em Geociências, Universidade Federal do Rio Grande do Sul; Av. Bento Gonçalves, 9500, CEP 91501-970 Porto Alegre, Rio Grande do Sul, Brazil.

^b Instituto de Geociências, Universidade de Brasília; Campus Universitário Darcy Ribeiro ICC - Ala Central, CEP 70910-900, Brasília, Distrito Federal, Brazil.

^c Universidade Federal do Pampa; Av. Pedro Anunciação, 111, CEP 96570-000, Caçapava do Sul, Rio Grande do Sul, Brazil.

^d Departamento de Paleontología, Facultad de Ciencias, Universidad de la República; Iguá, 4225, 11400 Montevideo, Uruguay.

* Corresponding author. E-mail: pedro.xavier@ufrgs.br

Claiton Scherer: claiton.scherer@ufrgs.br

Amanda Rodrigues: goulart.rodriques@ufrgs.br

Adriano dos Reis: adriano.reis@unb.br

Ezequiel de Souza: ezequielsouza@unipampa.edu.br

Felipe Guadagnin: felipeguadagnin@unipampa.edu.br

Graciela Piñeiro: fossil@fcien.edu.uy

ABSTRACT

Fluvial systems with high variability of discharge have been increasingly recognized in the modern and sedimentary record, owing to recent advances in the comprehension of supercritical sedimentary structures. These structures are considered as proxies for pluviometric regimes with high variability of discharge. However, they do not provide paleoclimatic information. The Lower Triassic Sanga do Cabral Formation of the Paraná Basin (southern Brazil) presents a high-variability fluvial system, and bears abundant carbonate nodules and carbonate-cemented intraclasts, as well as incipient paleosols, which can be used to identify paleoclimatic conditions. An integrated facies-petrographic analysis identified that the genesis of the carbonate in the nodules and intraclasts has undergone incipient pedogenesis and early diagenesis under arid climate, that the carbonates are groundwater calcretes, and that sedimentation has an important contribution of aeolian dust. A formation model for the nodules and for the carbonate-cemented intraclasts is also presented. These findings allowed to estimate the rainfall as a minimum of approx. 100, and a maximum of approx. 400–600 mm/year, corroborating the previous semi-arid to arid, and paleogeographic interpretations for the formation.

Keywords: Sanga do Cabral Formation; Early Triassic; calcrete; eolian dust; intraformational conglomerate

1. INTRODUCTION

Sedimentary structures are products of the physical conditions in which the sediments were transported and ultimately deposited, and can thus be used to infer these conditions in the geologic past. In the past decade, supercritical structures (sedimentary structures formed by bedforms generated under flows where the Froude number $Fr \geq 1$; Cartigny *et al.*, 2014) have received an increase in studies (Slootman & Cartigny, 2020), especially after the description of a new structure, cyclic steps, by Parker (1996), and its identification in turbidite systems as the explanation for “sediment waves” (Cartigny *et al.*, 2011).

In the continental realm, these structures are being associated to rivers with high variability in discharge (Fielding *et al.*, 2009; Fielding & Alexander, 1996; Plink-Björklund, 2015), and point towards interpretations of pluviometric regimes, which have great potential for interpretation of the past (Plink-Björklund, 2015; Fielding *et al.*, 2018;

Hansford *et al.*, 2020). However, these pluviometric regimes do not specify climate, necessitating other proxies to reach such interpretation (Plink-Björklund, 2015; Zellman *et al.*, 2021). Calcretes and carbonate nodules in continental environments, on the other hand, are typical of warm and/or arid climates (Alonso-Zarza & Wright, 2010; Goudie, 1973), and may be used to identify paleoclimatic conditions.

The Sanga do Cabral Formation (SCF) is a sedimentary unit in southern Brazil (Fig. 1) which has recently been reinterpreted as generated by a high-variability fluvial system (Dario, 2017; Xavier *et al.*, 2023). This unit, of Olenekian Age (Fig. 2), was deposited during a critical moment, not long after the greatest extinction of Earth's history, the End-Permian Mass Extinction (Raup, 1979; Sepkoski, 1984; Erwin, 2006; Benton, 2008). This critical period for the recuperation of Earth's biomes is termed the "Recovery Phase" (Chen & Benton, 2012; Erwin, 2001; Kirchner & Weil, 2000), lasting until the end of the Early Triassic, and is considered the period of highest temperatures in the Phanerozoic eon (Benton, 2018; Parrish, 1993; Preto *et al.*, 2010; Sellwood & Valdes, 2006).

The SCF presents an impressive number of carbonate nodules, which are identified amidst siltstones and fine-grained sandstones, as well as carbonate-cemented siltstone and sandstone intraclasts in intraformational conglomerates. A study of the genesis of these carbonate nodules and previously-cemented intraclasts has the potential to contribute to the comprehension of paleoclimatic conditions after the "Great Dying", at the beginning of the Triassic, and of the dynamics of "auto-erosion" and reworking in high-variability fluvial systems.

2. GEOLOGICAL CONTEXT

The Paraná Basin is an intracratonic basin occurring in an area of approximately 1.5 million km² in the center-east region of South America (Fig. 1; Milani *et al.*, 2007). It contains a volcano-sedimentary succession of up to over 7 km that spans the Ordovician to the Cretaceous (Milani *et al.*, 2007).

The Sanga do Cabral Formation (SCF), focus of this study, was considered by Zerfass *et al.* (2003) as a distinct second-order supersequence, as it was identified to be bound by regional unconformities (Fig. 2). This unit has received varied interpretations of its depositional environment (see Dias-da-Silva *et al.*, 2017; Scherer

et al., 2023; Xavier *et al.*, 2023) , from meandering rivers to a braidplain system (Andreis *et al.*, 1980; Faccini, 1989, 2000).

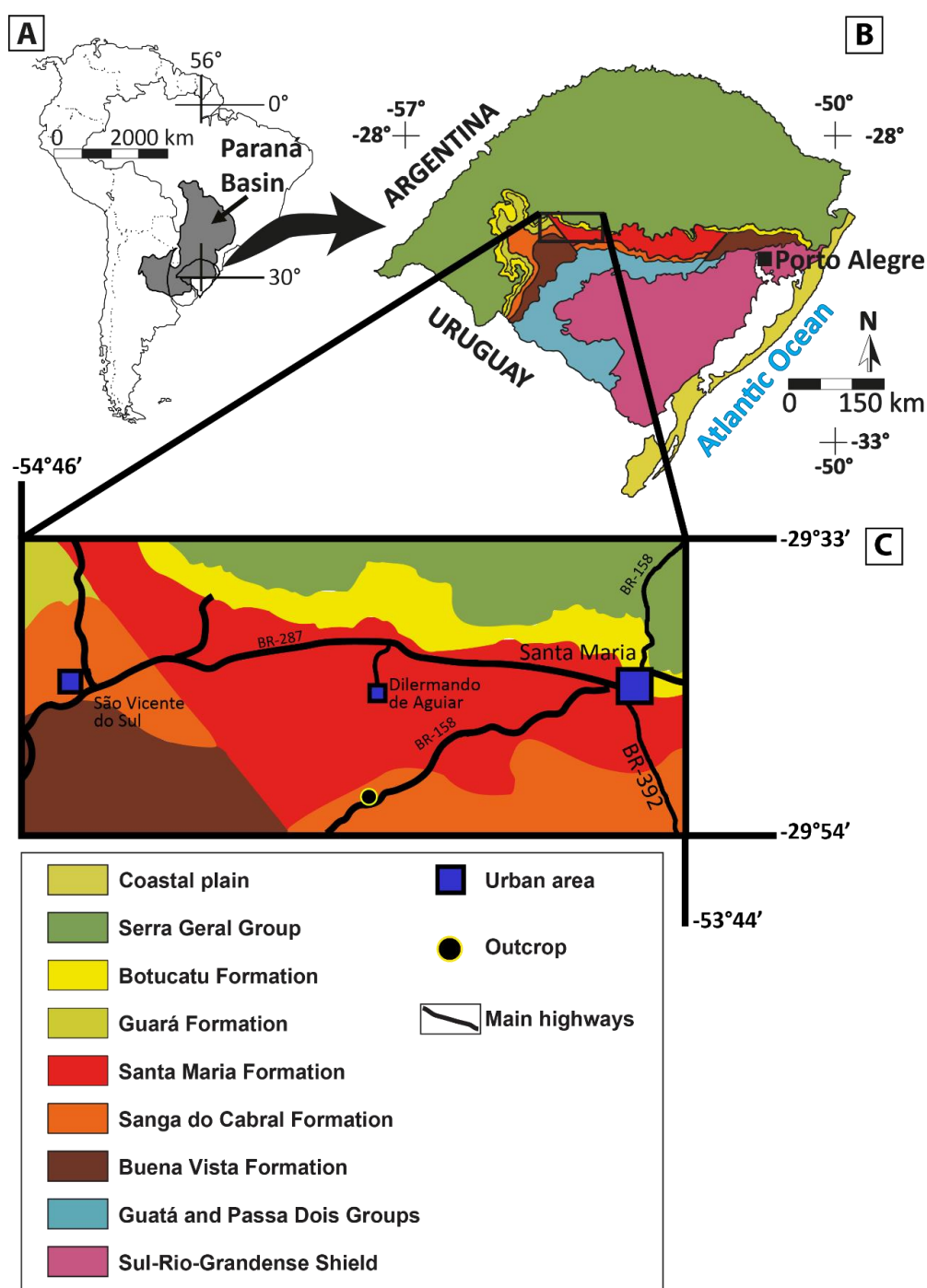


Fig. 1. Location of the study area. A) Location of the Paraná Basin and of the Rio Grande do Sul state in South America. B) Simplified Geological map of the state of Rio Grande do Sul, southernmost Brazil, and location of study area. C) Simplified geological map of the outcrop region, showing main urban areas, and main highways. Modified from CPRM (2006) and Goldberg (2001).

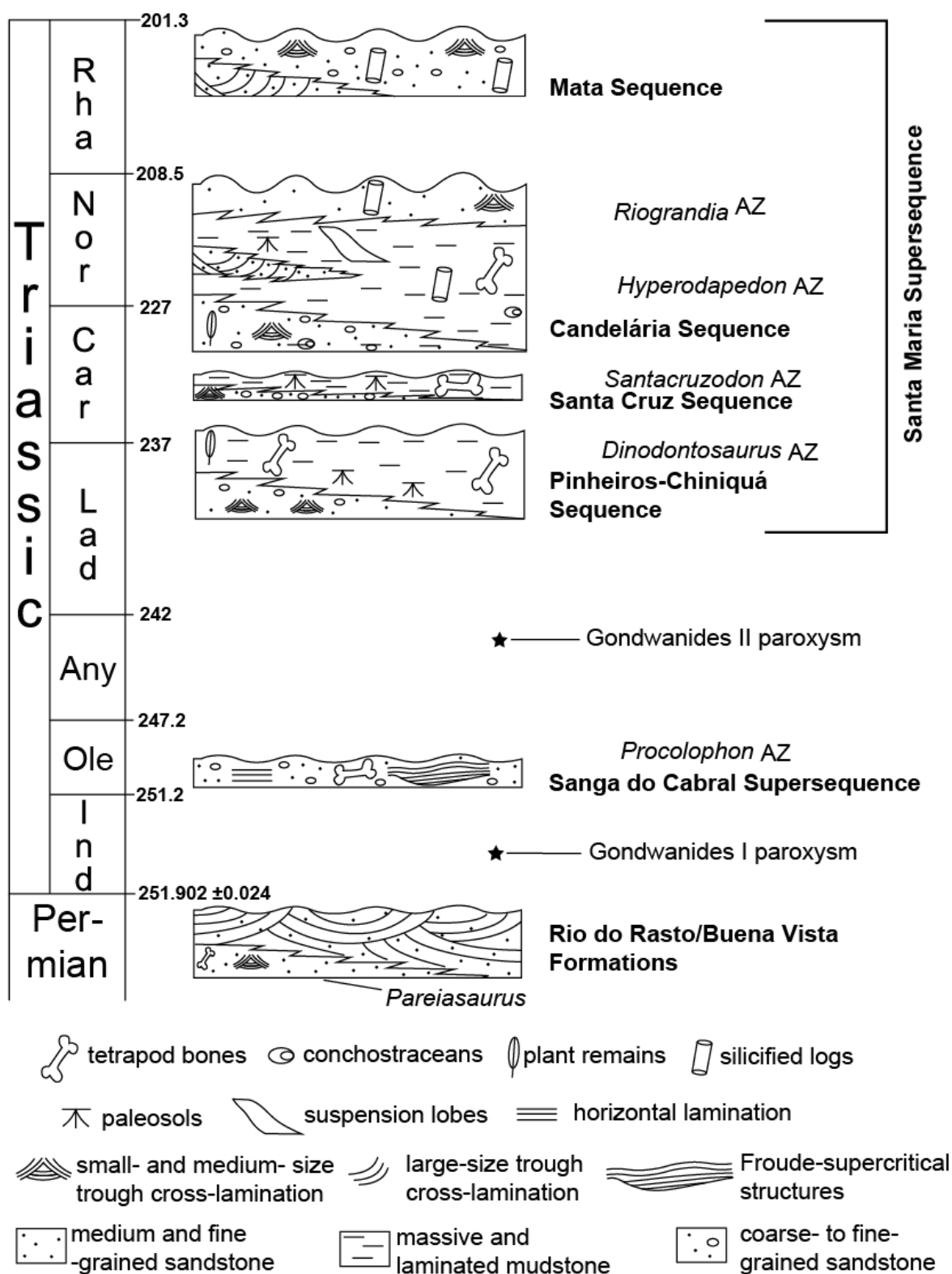


Fig. 2. Chronostratigraphic column depicting positioning, simplified main sedimentary features, and biostratigraphic zones of Upper Paleozoic and Triassic stratigraphic units. Modified from Horn *et al.* (2014), after Zeffass *et al.* (2003). Other modifications: of the Buena Vista Formation after Scherer *et al.* (2023); of the Santa Maria Supersequence after Schultz *et al.* (2020); range of the Sanga do Cabral Formation and Supersequence correlated to the Upper Katberg 1 & 2 stratigraphical bin intervals of Viglietti *et al.* (2022), in the Karoo Basin of South Africa, where *Procolophon trigoniceps* is the dominant taxon.

The present work follows the interpretations of Zeffass *et al.* (2004, 2003) and Scherer *et al.* (2023), which consider its depositional environment to be an alluvial plain with low gradient and low accommodation, under a strongly seasonal semiarid or arid climate, generating flash floods. These interpretations are added by the works of Dario (2017) and Xavier *et al.* (2023), which identify Froude-supercritical sedimentary structures and interpret this fluvial system as high to very high in discharge variance (Fielding *et al.*, 2018, 2009; Fielding & Alexander, 1996; Hansford *et al.*, 2020; Plink-Björklund, 2015).

Xavier *et al.* (2023) recognizes three different fluvial styles in the formation (Fig. 3). Fluvial Style 1 (FS1) is characterized by tabular lithosomes consisting of successions of thin-bedded, fine-grained, and massive to faintly-laminated sandstones, with interruptions of decimetric layers of intraclastic conglomerates with parallel stratification. Trains of granule- to pebble-size mud clasts occasionally occur in some bedding surfaces. It is interpreted as the distal part of a fluvial system, where flash floods would generate unconfined and hyperconcentrated flows. Mud deposited as drapes or in ponds at the final stages of previous floods would be eroded by the next, and in between floods the plain would be subjected to pedogenesis and formation of calcretes. Fluvial Style 2 (FS2) is composed by upwards-fining successions: sandstones or intraclastic conglomerates in successive scours filled by backsets, transitioning to truncated undulatory stratification (cyclic steps bedforms to unstable antidunes; Cartigny *et al.*, 2014; Parker, 1996); these are overlapped by sandstones in isolated scours with backsets (chute-and-pool bedforms; Cartigny *et al.*, 2014; Simons and Richardson, 1961) and truncated undulatory lamination, followed by sigmoidal and tangential cross-stratification or massive sandstone within scours; and at the top, very-fine-grained sandstones with faint sigmoidal cross-lamination, ripples, convoluted lamination, blocky structure, and structureless sandstones. FS2 is interpreted to have been deposited by flash floods occurring repeatedly during a wet season (Plink-Björklund, 2015), with diminishing magnitude. Fluvial Style 3 (FS3) is identified by the occurrence of large-scale undulatory and truncated undulatory stratification (wavelengths up to 28 m), interpreted as deposited by large stable and unstable antidunes. These would have been generated by catastrophic flash floods, in turn caused by erratic storms which poured in single events (Plink-Björklund, 2015).

The presence of the fossil *Procolophon trigniceps* allowed correlation to the Katberg Formation in South Africa, positioning the SCF in the Lower Triassic (Cisneros,

2008; Lavina, 1983). The formation and supersequence was historically considered as continuous to the Uruguayan Buena Vista Formation (Azevedo *et al.*, 1985), because of similarities of lithology and broad stratigraphic position. However, more recent paleontological (Piñeiro, 2006; Piñeiro *et al.*, 2012, 2007, 2004; Piñeiro & Ubilla, 2004), magnetic (Ernesto *et al.*, 2020), and stratigraphic (Scherer *et al.*, 2023) evidences have challenged this historical notion, and so the two units are now considered as separate, with the Uruguayan Buena Vista Formation considered as Late Permian.

3. SAMPLING AND METHODS

Twenty samples from varied stratigraphic positions (Fig. 3) in the Estrada de Ferro Abandonada outcrop (Fig. 1) were prepared for confection of thin sections, and impregnated with blue-colored epoxy resin. The focus was to describe in detail the massive to faintly-laminated siltstones to fine-grained silty sandstones, which typically present carbonate nodules on a same level (Fig. 4A, B), and the intraclastic conglomerates (Fig. 4C–F), which contain carbonate-cemented siltstone and sandstone intraclasts. Two of these carbonate-cemented intraclasts were studied separately for comparison to the carbonate nodules of the fine-grained silty sandstones. Microscopic description was undertaken with the aid of a Zeiss AXIO microscope, and photomicrography was made with an attached AxioCam MRc.

For mineral characterization, five samples were analyzed by scanning electron microscopy (SEM), using secondary electron image (SEI) and backscattered electrons (BSE), in order to better comprehend the paragenetic relationships of primary and diagenetic constituents. Analysis was held in the Laboratório de Geologia Isotópica (LGI) of Federal University of Rio Grande do Sul (UFRGS), with a Jeol 6610-LV electron microscope, and a Bruker XFLASH 5030 energy-dispersive spectrometer (EDS) was used for identification of the qualitative elemental composition of the constituents.

Five samples were subjected to X-ray diffractometry (XRD) with the purpose of identification of clay minerals. Process was held in the Laboratório de Difractometria de Raios-X of UFRGS using a Siemens Diffractometer (BRUKER AXS) model D-5000, equipped with a fixed Cu K α anode ($\lambda = 1.5406 \text{ \AA}$) operating at 40 kV and 30 mA in the primary beam and curved graphite monochromator in the secondary beam. Samples

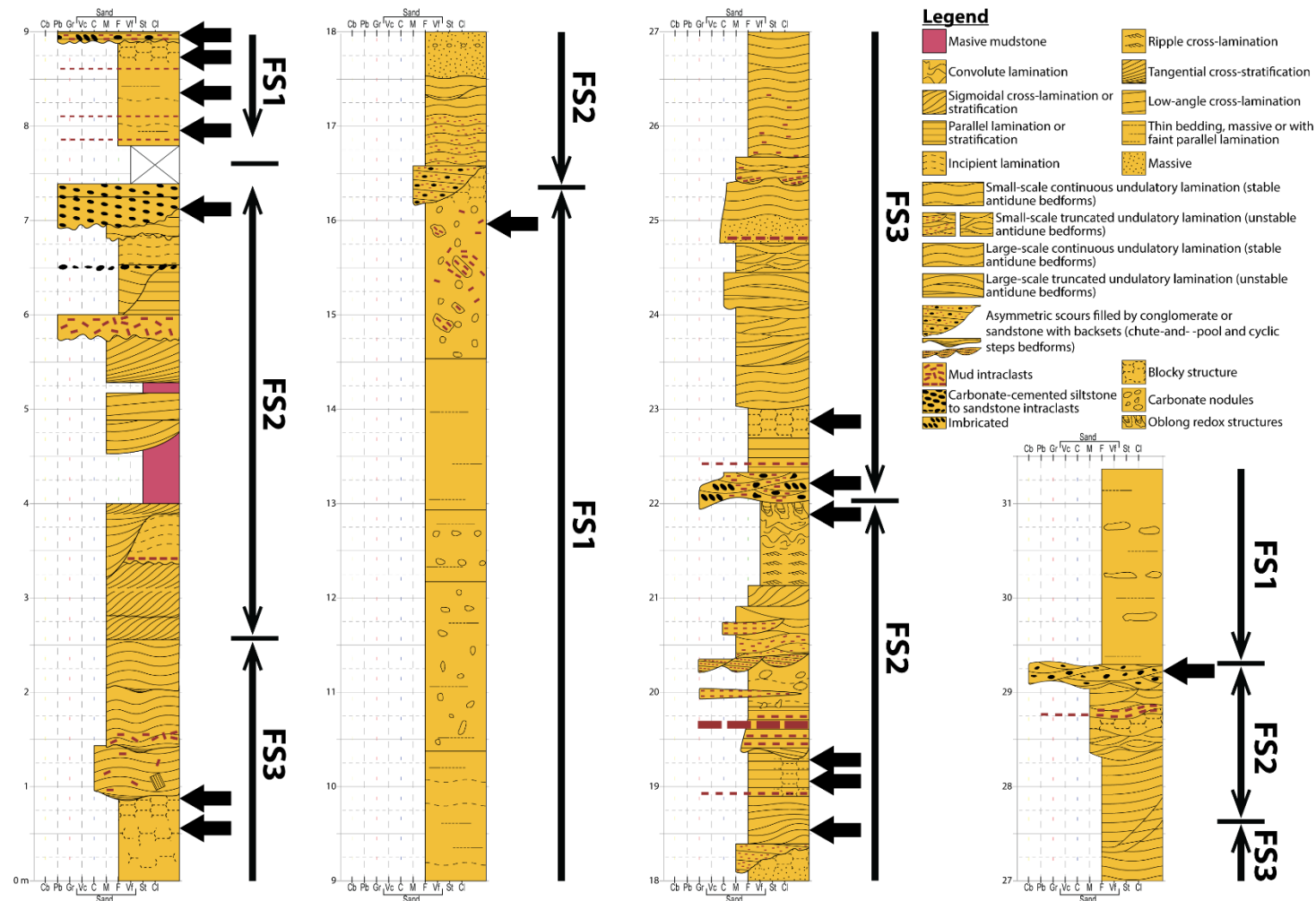


Fig. 3. Stratigraphic positioning of samples retrieved for the present study (arrows) in the composite columnar profile of the Estrada de Ferro Inacabada Outcrop of the Sanga do Cabral Formation in central Rio Grande do Sul state. Interpreted fluvial styles (FS) by Xavier *et al.* (2023).



Fig. 4. Display of examples in outcrop of rocks from which samples were retrieved, and relevant sedimentary structures. A) Thin-bedded siltstones to fine-grained sandstones, with massive structure or displaying faint parallel lamination. Samples were taken from varied stratigraphic positions. Note the carbonate nodules formed on a same level, and how the ones in the center of the picture coalesce. Hammer is 40 cm long. B) Fine-grained sandstones with less well-pronounced differentiation of thin bedding. Picture displays samples “J” and “I” taken side by side. The former is a nodule, while the latter presents little calcite cementation. Person is approx. 1,7 m tall. C) Siltstone to fine-grained sandstone with blocky structure (base; interpreted as incipient paleosol), erosively overlapped by intraclastic conglomerate with parallel stratification (dominated by mud clasts). Hammer is 28 cm long. D) Position where samples of intraclastic conglomerate and a large cemented clast (15 cm longest axis) were retrieved. Conglomerate fills an asymmetric scour, with imbrication of clasts. Lens cap is 52 mm in diameter. E) Picture and interpretation of successive asymmetric scours filled with conglomerate with backsets, which transition to truncated undulatory stratification. This configuration is interpreted as deposited by migration and aggradation of cyclic steps bedforms, transitioning to unstable antidunes (Cartigny *et al.*, 2014). Hammer is 28 cm long. F) Picture and interpretation of a scour filled by conglomerate with sigmoidal cross-stratification. It is interpreted as a humpback dune filling an erosional scour generated by an hydraulic jump (Cartigny *et al.*, 2014; Xavier *et al.*, 2023). Hammer is 28 cm long.

were disaggregated first with porcelain mortar and pestle, then in an orbital shaker for 14 hours, and after that by an ultrasonic probe for five minutes, with the samples in solution. Temperature was then stabilized for viscosity control, and a regular settling process was used in order to separate the fraction $< 4 \mu\text{m}$. Stipulated settling time was calculated using Stokes Law as 1 h 12 min 51 s. Separated fraction was oriented in thin sections by pipetting (natural oriented samples). In this process, the (001) faces are privileged. Part of the natural oriented samples were saturated with glycol (glycolated samples), and part was heated to 550°C for two hours (calcinated samples). Natural oriented and calcinated samples were analyzed in an angular interval from 3° to $32^{\circ} 2\theta$ with a $0.02^{\circ}/2 \text{ s}$ step, using divergence and anti-spread gaps of 2 mm and 0.2 mm in the detector. Glycolated samples were analyzed with a $0.02^{\circ}/3 \text{ s}$ step, while other parameters were the same.

4. RESULTS

4.1. Texture, structure, and framework components

Studied rocks are siltstones to fine-grained silty sandstones, massive or presenting faint lamination (Fig. 5), and intraclastic conglomerates (Figs. 6, 7). Common to all samples, including conglomerates, is the presence of medium to coarse-grained silt, with red-colored coatings (Figs. 5–8; further commented in sections 4.2.2 and 5.3).

Siltstones to fine-grained sandstones (Fig. 4A, B) are red-colored. They occur in laterally-extensive tabular lithosomes up to 7 m in thickness, organized in series of thin beds with massive structure, or presenting faint parallel lamination. Presence of rounded, horizontally-elongated carbonate-cemented sandstone concretions are common. These concretions are dispersed in some intervals, but are in most places concentrated on a same level (Figs. 3; 4A, B). Blocky structure can be observed on the siltstones and sandstones at places (Fig. 4C).

Siltstones are well-sorted (Fig. 5A), while the fine-grained sandstones are moderately- to poorly-sorted (Fig. 5B–E). Granule- to pebble-size intraclasts, composed of mudstone or carbonate-cemented siltstone, are common (Fig. 5A–E),

and may locally form trains of clasts. There is no clear observable normal or inverse grading, or coarsening or fining trend along the studied section (Fig. 3). Packing

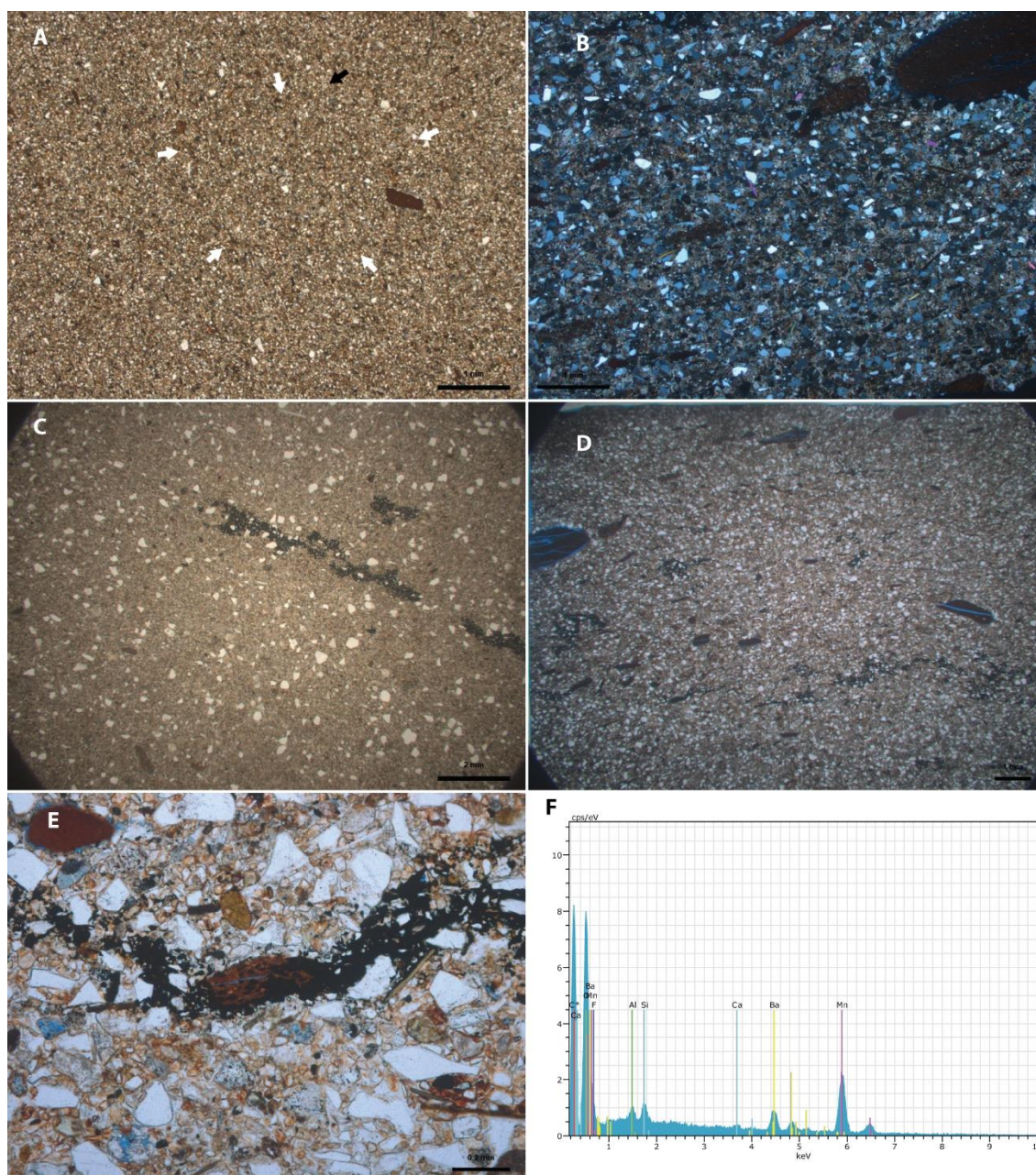


Fig. 5. Massive siltstone. White arrows highlight a circular accumulation of iron oxy-hydroxides, interpreted as a rhizohalo. Black arrow points towards a muscovite grain, oriented nearly 90° from the mudstone intraclast. Uncrossed polarizers. B) Fine-grained silty sandstone presenting oriented mudstone intraclasts, and filling of interstitial pores by calcite cementation. Crossed polarizers. C) Fine-grained silty sandstone. The irregular linear accumulation of opaque minerals is composed mainly of Fe-Mn oxides with relatively high concentration of Ba, and is interpreted as a rhizohalo. Uncrossed polarizers. D) Fine-grained silty sandstone presenting a more discontinuous accumulation of opaque minerals, also interpreted as rhizohalo. Uncrossed polarizers. E) close-up of rhizohalo, showing filling of intergranular pores, and substitution of framework grains, especially a mud intraclast. Uncrossed polarizers. F) Specter from energy-dispersive spectrometer (EDS) taken from the opaque minerals. Compositional table is on Supplementary Material 1.

is normal, even in silty sandstones with partial to complete calcite cementation (Fig. 5B). Rhizohalos are marked by circular accumulations of iron-manganese oxihydroxides, approx. 2–4 mm in diameter (Fig. 5A), and at places occur as irregular, linear and discontinuous concentrations of opaque minerals, around 0.5 mm wide and several mm in length (Fig. 5C–E), presenting considerable amounts of barium (Figs. 5F; SF1; Table S1).

The intraclastic conglomerates (Figs. 4C–F; 6) are clast-supported, and disposed in laterally extensive tabular layers up to approx. 1 m thick, presenting transitional, upper-flow, and Froude-supercritical sedimentary structures. Most common structures are successive asymmetrical scours along a same bounding surface, filled by backsets, which transition vertically to undulating truncated stratification (Fig. 4D, E). Parallel stratification is also common (Fig. 4C), and locally conglomerates occur with sigmoidal cross-stratification, in scours (Fig. 4F).

The fabric of the conglomerates is characterized by mud clasts (Fig. 6A, B), and clasts composed of carbonate-cemented siltstone or sandstone up to 40 cm in length (here termed “cemented clasts”; Fig. 6C–F; Fig. 7). Mud clasts and cemented clasts are elongated and oriented sub-horizontally (Fig. 6A), and some are imbricated (Fig. 4D). Mud clasts may dominate (Fig. 6A), or occur in equal proportion to cemented clasts (Fig. 6G). Sorting is very poor, as grain sizes up to silt are also present. Silt grains are dispersed, with local concentrations (Fig. 6A, B, G). Packing is normal to loose, due to the presence of pre-compactional calcite cement (Fig. 6G, H).

Carbonate-cemented siltstone to sandstone clasts (cemented clasts) in the conglomerates have a variety of shapes, but are mostly oblate, flattened prolate (Fig. 7A), or rounded. They are usually around 10–15 cm in the longest axis, but may reach around 40 cm. The larger cemented clasts (pebble to cobble size) usually contain smaller cemented clasts (coarse-sand to granule in size) (Figs. 7B–D). The smaller cemented clasts are usually composed of silt grains cemented by finer-textured calcite cement (Fig. 7C–E).

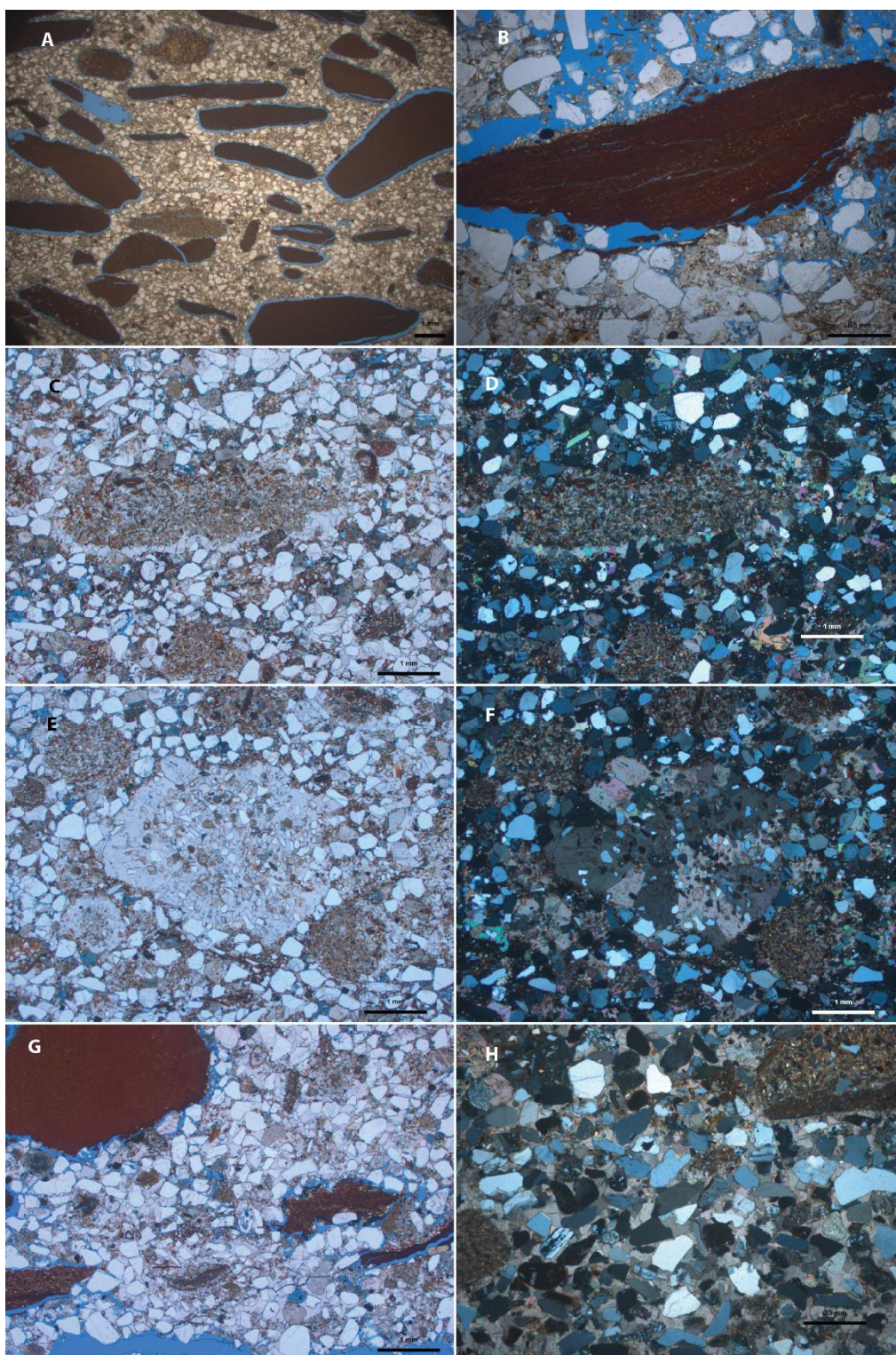


Fig. 6. Intraclastic conglomerates. Rock disaggregated easily, especially around mud clasts, and therefore intergranular space was increased or created by abrasion during preparation of thin sections. A) mud-clast-dominated. Disposition of clasts is sub-parallel. Uncrossed polarizers. B) Detail of mud clast. Mainly argillite but with silt-rich levels. Uncrossed polarizers. C) Detail of calcite-cemented siltstone intraclast. Note calcite fringe. Uncrossed polarizers. D) Crossed-polarizers view of C. E) Calcite-cemented sandstone intraclast. Calcite shows poikilotopic character on the center, which passes to a displacive character near the margin. Uncrossed polarizers. F) Crossed-polarizers view of E. G) Display of silt and cement distribution in conglomerates. Silt occurs preferably in clusters. Uncrossed polarizers. H) Display of calcite cement distribution in conglomerates, under crossed-polarizers view.

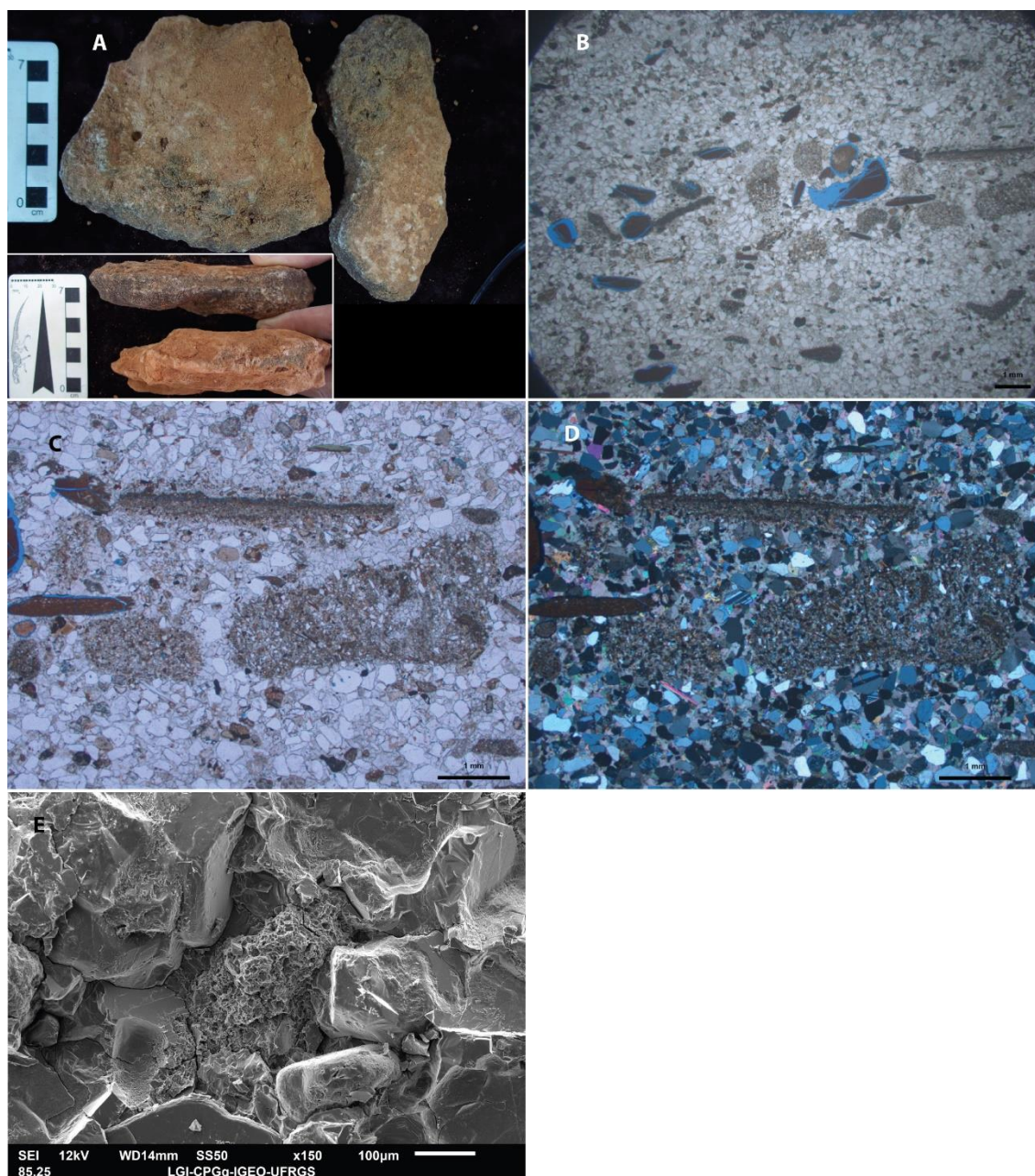


Fig. 7. A) External form of two large carbonate-cemented siltstone to sandstone intraclasts: oblate and flattened prolate. B) Thin section of cemented intraclast. Smaller mudstone and siltstone intraclasts accumulate on a certain level and oriented subparallel. Uncrossed polarizers. C) Detail of siltstone cemented intraclasts within a sandstone cemented intraclast. Uncrossed polarizers. D) Crossed-polarizers view of C. E) Secondary-electron image of scanning electron microscope showing cemented siltstone clast (center) surrounded by sand-size grains and coarse-crystalline calcite.

Quartz is the dominant detrital constituent and occurs dominantly as monocrystalline grains (Fig. 8A, B). Among the feldspars, orthoclase dominates over plagioclase and microcline. Feldspars may be fresh or altered, the main alteration being dissolution — from partial (vacuolized) to complete (Fig. 8C, D). Other common constituents are muscovite and biotite, which are usually one to two grain-size

categories larger than other framework constituents (Fig. 9). Extrabasinal lithic fragments are volcanic, plutonic, and low-grade metamorphic rock fragments, and also chert, occurring as sand-sized grains. There is no clear predominance of one kind of extrabasinal lithic fragment, although volcanic fragments are more common in some samples, and are partly substituted by opaque minerals, mainly iron oxi-hydroxides and titanium oxides minerals. Intrabasinal lithic fragments are mostly coarse-sand-size to pebble-size mud clasts, ranging from siltstone to argillite, and the aforementioned cemented clasts, which are composed usually by silt-size grains, by may be composed by sand-size grains (Figs. 6, 7). Heavy minerals include zircon, tourmaline, and opaque minerals.

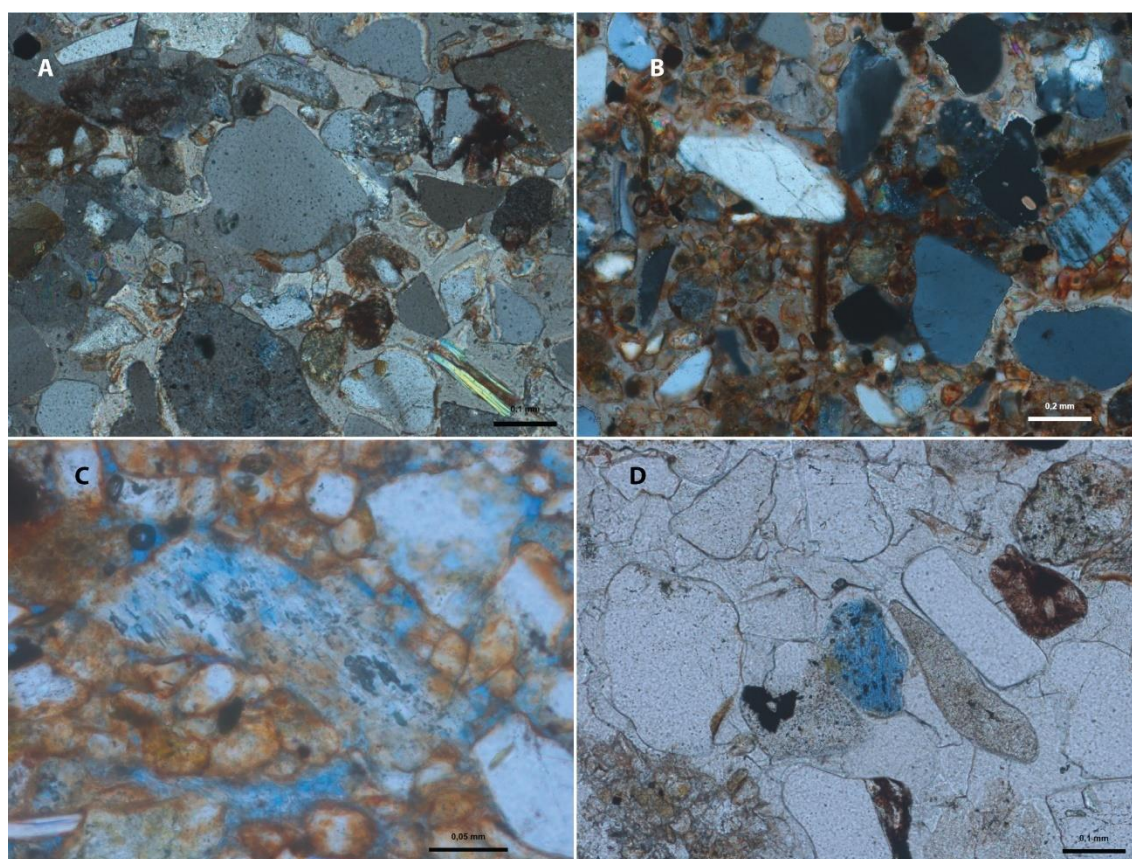


Fig. 8. A) Quartz grain showing quartz overgrowth which grows over and is engulfed by discontinuous iron-rich clay cuticle (mostly smectite). Crossed polarizers. B) Quartz grain on up and left of center presenting quartz overgrowth overlain by iron-rich clay cuticle (mostly smectite). Crossed polarizers. C) Partially dissolved (vacuolized) orthoclase presenting discontinuous clay cuticle. Black spots on the feldspar are thin section defects. Uncrossed polarizers. D) Almost-completely dissolved feldspar. Black spots are thin section defects. Uncrossed polarizers.

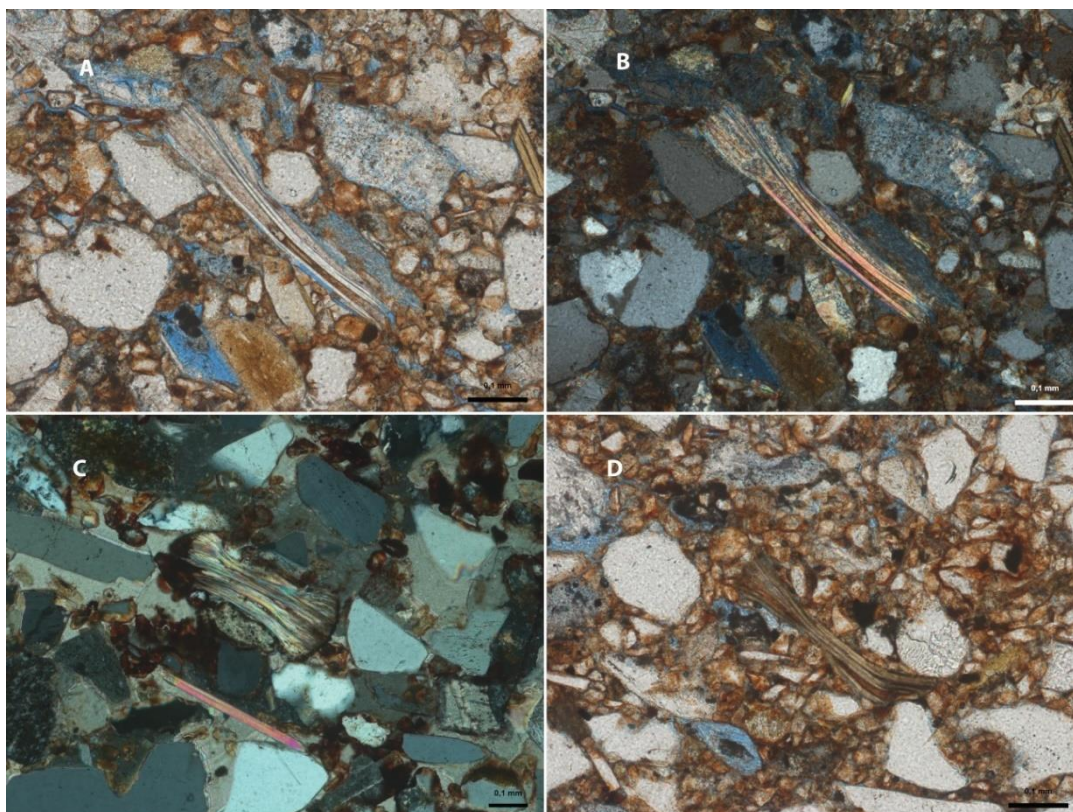


Fig. 9. A) Expanded muscovite grain with interlayer space filled by illite and infiltrated clay. Uncrossed polarizers. B) Crossed-polarizers view of A. C) Muscovite expanded and substituted by kaolinite and partially substituted by iron oxy-hydroxide. Crossed polarizers. D) Expanded biotite with interlayer space filled by infiltrated clay.

Present composition of studied rocks is arkose *sensu* (Folk, 1981; Fig. 10A) which corresponds to uplifted-basement and transitional-continental provenance detrital modes of the Dickinson (1985) diagram (Fig. 10B). Similar results were previously obtained by Zeffass (1998) and Zeffass *et al.* (2000). Coexistence of rounded and angular grains of quartz and feldspars, however, indicates that sediments were subjected to reworking. The difference in grain size category of the micas in relation to the other framework grains is likely due to hydraulic equivalence (Doyle *et al.*, 1983, 1985; Burroughs, 1985).

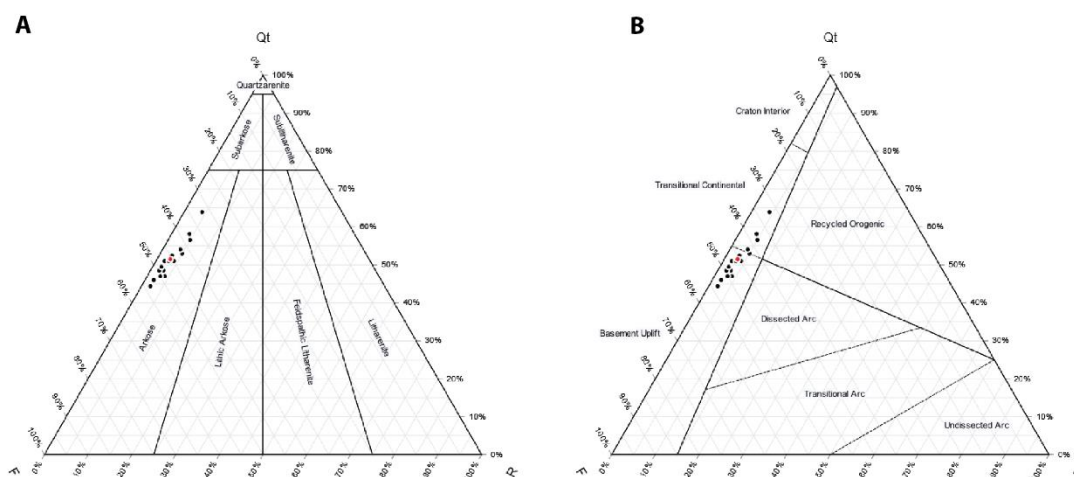


Fig. 10. A) Compositional classification diagram of Folk (1981) with plotted samples as black dots. Red dot is the mean composition. B) Provenance diagram of Dickinson (1985). Representations are the same as in A.

4.2. Diagenetic constituents

4.2.1. Calcite

Precompactional calcite has poikilotopic (Fig. 6E, F) and coarse mosaic habits (crystal size 0,05–0,2 mm; Fig. 11A), but varies locally to microcrystalline when cementing silt-size grains (Fig. 11B), and may also occur with displacive habit (Fig. 11C, D). It fills intergranular pores, engulfing and partially replacing and/or corroding other framework grains and diagenetic constituents (Fig. 12A–C). It also forms fringes around mud intraclasts (Fig. 6C, D; 7C, D). It composes almost the entirety of the interstitial material in the nodules and cemented clasts (Figs. 7B–D). Postcompactional microcrystalline calcite precipitated mainly in dissolution secondary pores (Fig. 12D). Calcite varies between 1–30 vol.% of the studied rocks, in which composition is nearly 100% CaCO₃ (Fig. 12E, F).

4.2.2. Clay Minerals

As mentioned in section 4.1, common to all samples, including conglomerates, is the presence of medium to coarse-grained silt, enveloped by a cuticle of infiltrated clay mixed with iron oxides (Figs. 5–9, 11–13). These are more developed around silt-sized grains of quartz and feldspar (Figs. 8B, C; 11A;

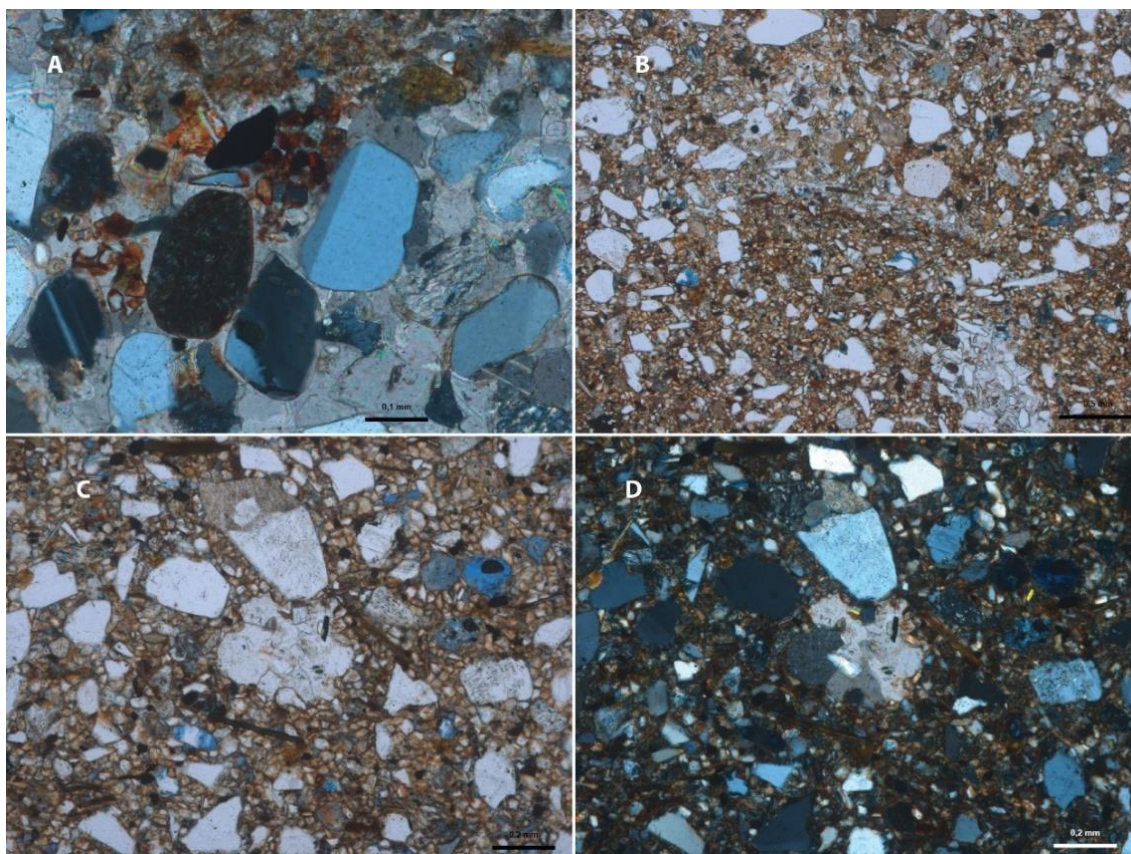


Fig. 11. A) Calcite in coarse crystalline mosaic, cementing fine-grained sandstone. Crossed polarizers. B) Fine-grained silty sandstone, partially cemented. Calcite habit shifts from coarse-crystalline mosaic when cementing sand grains without silt (lower right), to fine-crystalline mosaic when cementing sediments with abundant silt grains (top half of photomicrography). Calcite is absent in the middle of photomicrography and to the sides of the coarse-crystalline area. Uncrossed polarizers. C) Calcite showing displacive habit. Uncrossed polarizers. D) Crossed-polarizers view of C.

12D; 13A). This development around silt-size grains is better observed in secondary electron microscopy (SEM), where imaging reveals the typical honeycomb aggregates of smectites (Fig. 13B–D). The cuticles are engulfed by calcite (Fig. 12C; 13B), and the clay fills intergranular pores, especially in samples not thoroughly cemented by carbonate (Figs. 5A, C, D; 6A; 8C; 9A, B, D; 10D–F; 13A), as well as interlayer space of micas (Fig. 9D). Sand-sized grains of quartz and feldspar contain discontinuous and thin cuticles, which may overlay and/or be engulfed by quartz overgrowths (Fig. 8A, B). Interstitial clay and clay cuticles may account for up to 15 vol.% of the studied rocks.

XRD has identified that mixed-layers of smectite-mica-illite or mica-illite are common (Fig. 14A), and these are corroborated by EDS analysis focused on the cuticles, which identify Mg, K, Ca and, in greater proportion, Fe (Fig. 14B; S2;

Table S2). The mentioned composition is closely similar to that of the mudstone intraclasts (Fig. 14C; S3; Table S3).

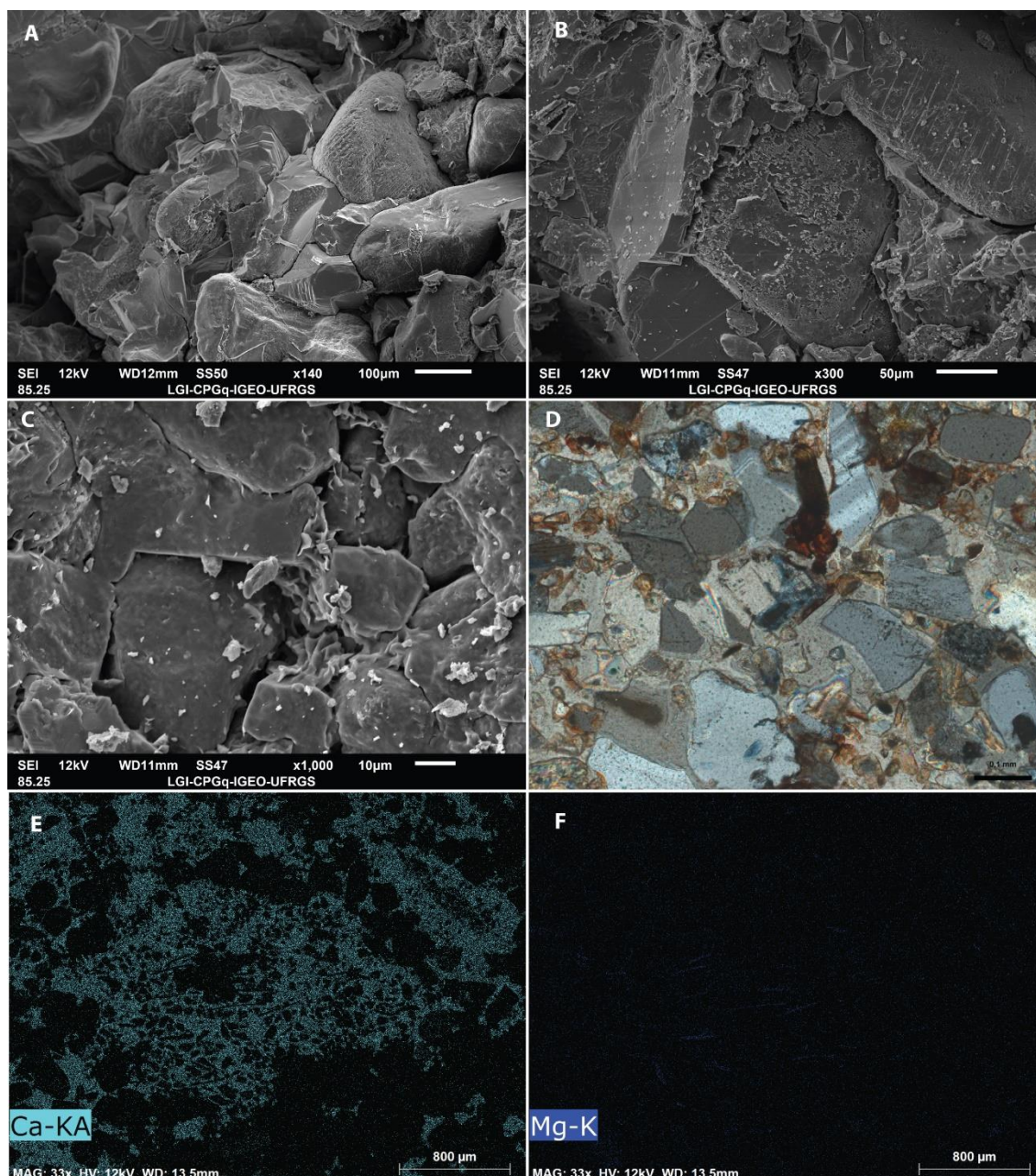


Fig. 12. A) Secondary-electron image of scanning electron microscope (SEM-SEI) showing calcite cement with coarse crystalline habit cementing sand-size grains. B) Closer view of calcite cement engulfing sand-size grain. C) SEM-SEI calcite cement engulfing clay lamellae. D) Calcite and iron-titanium oxide partially filling solution pore. Iron oxide-clay cuticle was not dissolved and preserved outline of dissolved grain. E) Compositional map generated by energy-dispersive-spectrometer (EDS) detecting calcium (Ca). All calcite is highlighted. F) EDS compositional map of the same view of E, but detecting magnesium (Mg). The muscovites are more highlighted than the calcite, revealing the magnesium content in the latter is very low, if present at all.

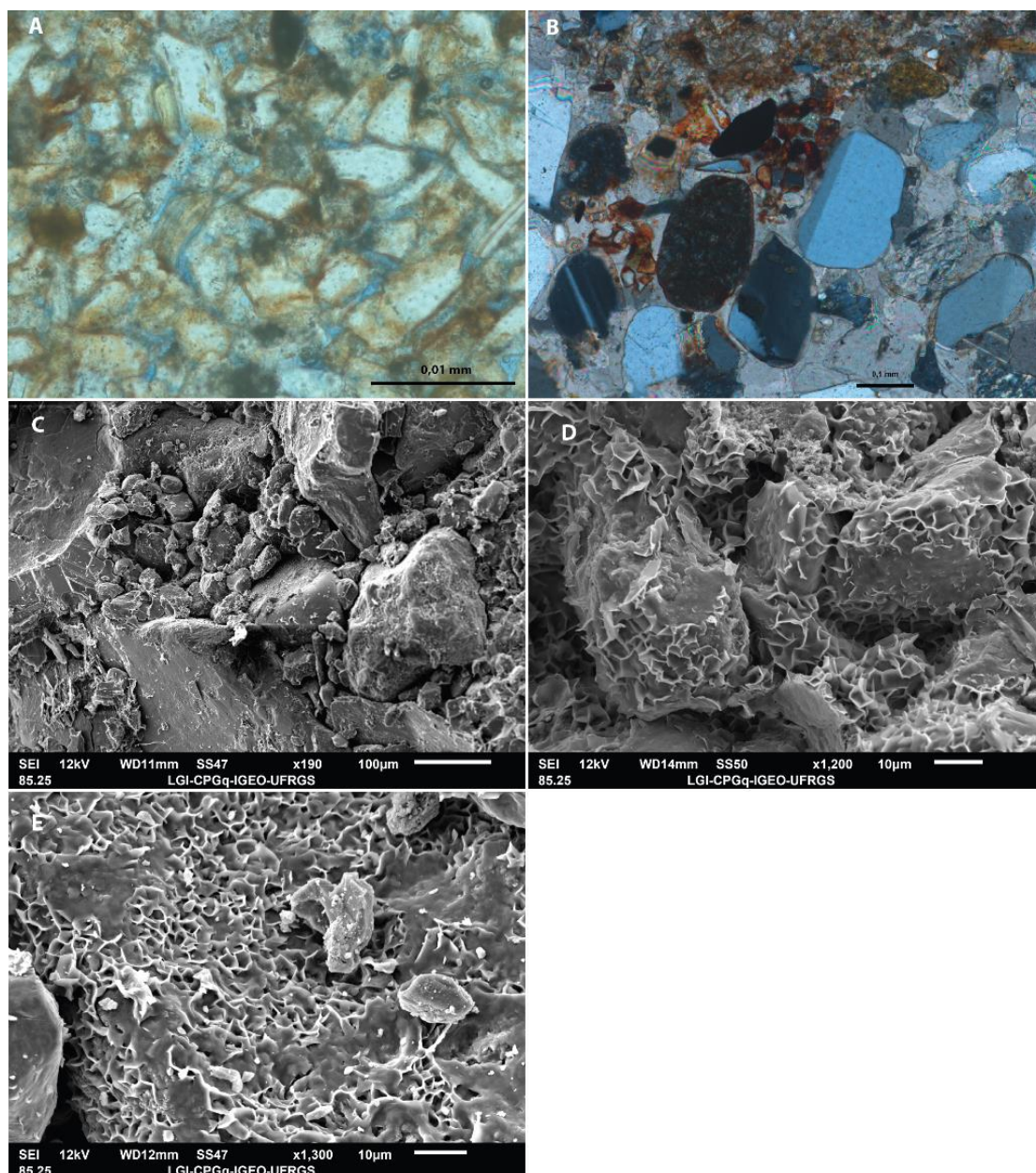


Fig. 13. A) Siltstone presenting mostly continuous cuticles of infiltrated clay mixed with iron oxihydroxides. Uncrossed polarizers. B) Secondary-electron image of scanning electron microscope (SEM-SEI) showing silt-size grains with clay lamellae on their surface, in contrast to the sand-size grains. B) SEM-SEI Close-up view of silt-size grains, displaying the honeycomb structure of clay lamellae. C) SEM-SEI close up view of clay aggregate, showing in greater detail the honeycomb structure of clay lamellae.

4.2.3. Iron oxihydroxides

Microcrystalline iron oxihydroxides occur mainly mixed with clay (detailed in section 4.2.2). Microcrystalline hematite and titanium diagenetic minerals replace calcite and clay mineral cuticles (Fig. 15A). These oxides also commonly occur partially filling feldspar dissolution pores (Fig. 15B), and account for up to 8 vol.% of rocks.

Some reddish redoximorphic circular features occur. They are 1–5 mm in diameter (Fig. 5A), in which iron oxides delimit the structure.

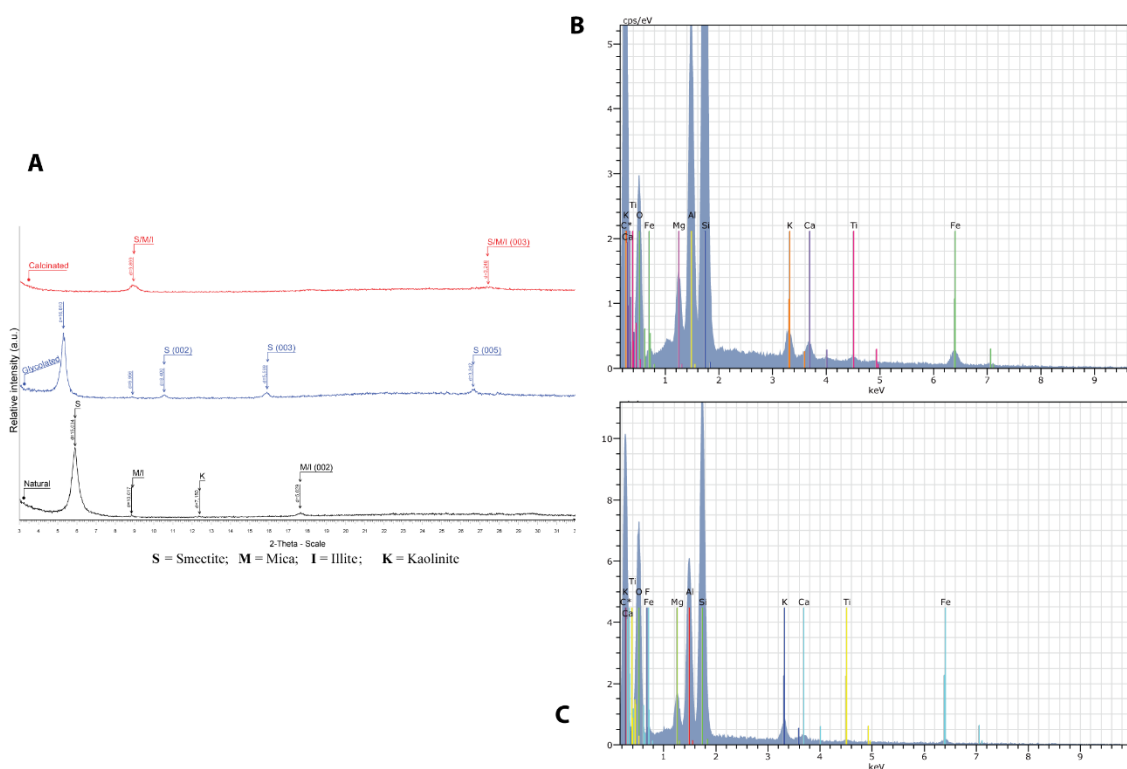


Fig. 14. X-ray diffraction (XRD) graph of clay-size particles, in natural oriented (black, bottom), glycolated (blue, middle), and calcinated (top, red) samples. It shows the occurrence of smectite, kaolinite, and mixed-layers mica/illite (M/I) and smectite/mica/illite (S/M/I). B) Specter from energy-dispersive spectrometer (EDS) taken from clay mineral cuticle. Compositional table is on Supplementary Material 1. C) Specter from energy-dispersive spectrometer (EDS) taken from a mudstone intraclast. Composition is very similar to that of the clay cuticle shown in B. Compositional table is on Supplementary Material 1.

4.2.4. Minor diagenetic minerals

Discontinuous syntaxial quartz overgrowths occur in low volumes (< 1 vol.%), but are constant throughout the studied thin sections (Fig. 8A, B).

Albitization and sericitization are common in feldspars, although in low volumes (< 1 vol.%). Kaolinite is a minor component (< 1 vol.%) and occurs expanding micas, displaying the typical fan-like shape (Fig. 9C), or filling dissolution pores (Fig. 15C–E). In the secondary electron image (SEI) of the scanning electron microscope (SEM), kaolinite is shown to be in also-typical booklet aggregates (Fig. 15F).

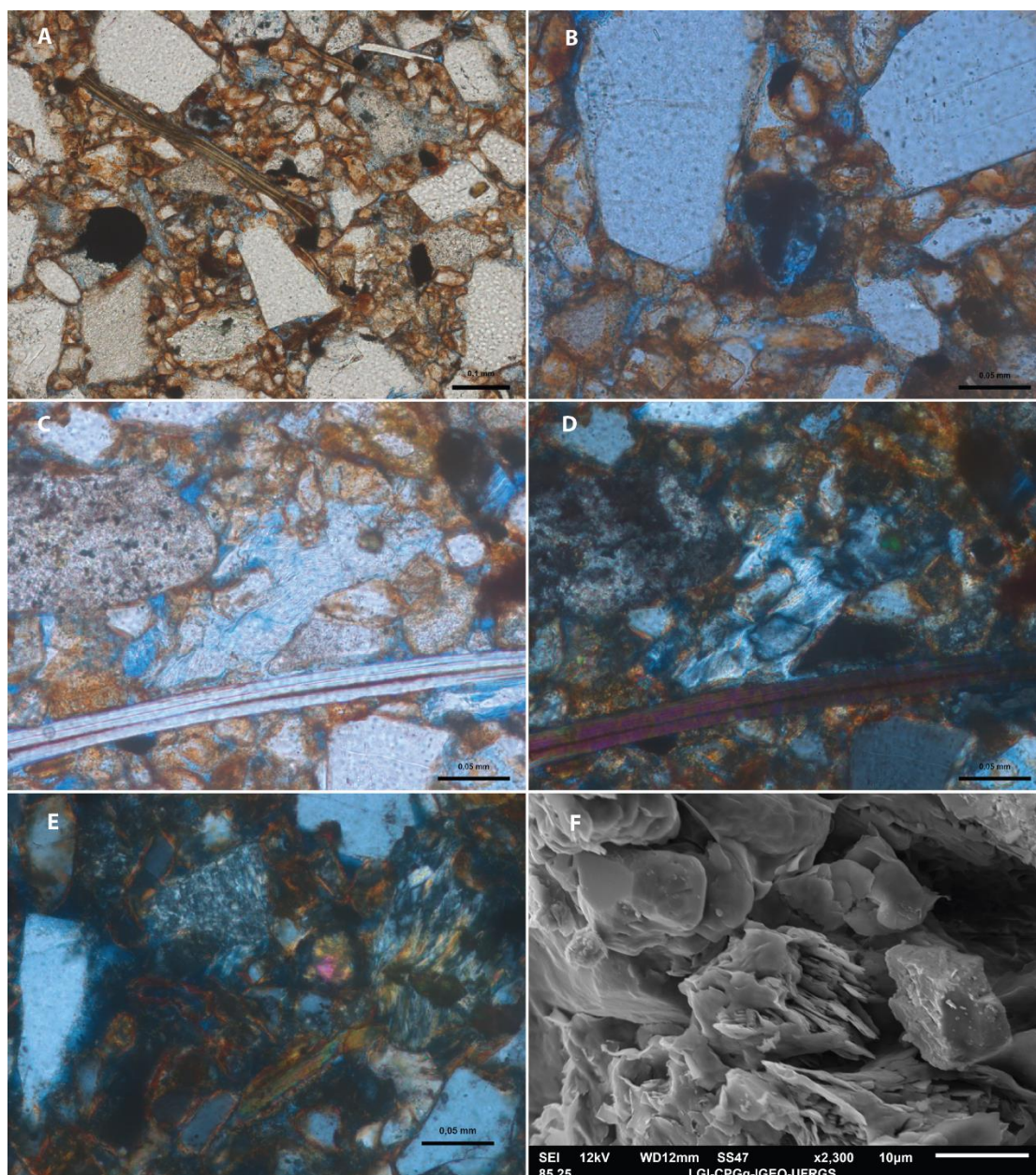


Fig. 15. A) Opaque minerals of iron-titanium oxi-hydroxides overgrow cement and primary constituents. Uncrossed polarizers. B) Dissolution pore partially filled by iron-titanium oxi-hydroxides. Uncrossed polarizers. C) dissolution pore and intergranular space filled by kaolinite. Uncrossed polarizers. D) Crossed polarizers view of C. E) Non-vermicular kaolinite filling dissolution pore (left). Crossed polarizers. F) Secondary-electron image of scanning electron microscope (SEM-SEI) displaying typical booklet-shape aggregate of kaolinite.

4.2.5. Pore types

Porosity is dominantly secondary, resulting from dissolution of the feldspars (intragranular and moldic porosity; Figs. 5E; 7C; 8C, D; 9A, D; 11D; 12D; 15A–E). Some fracture pores are present, but can be artifacts of thin section preparation.

Intergranular porosity is scarce (< 1 vol.%), having been greatly reduced by calcite cementation (Figs. 5B–E; 6H; 7B–D; 8A, B, D; 9C; 11A; 12D) and by infiltrated clay minerals (Figs. 5A, C, D; 6A; 8C; 9A, B, D; 10D–F; 13A).

5. DISCUSSION

5.1. Diagenesis and genesis of the carbonate-cemented intraclasts and nodules

Petrographic evidence suggests that the evolution of the studied rocks took place almost entirely during eodiagenesis (*sensu* Choquette & Pray, 1970; Schmidt & McDonald, 1979), with contribution from incipient pedogenesis (Retallack, 2001). Clay mineral cuticles are well-developed and continuous around silt-sized grains, while cuticles developed over sand-size grains are discontinuous and may engulf and/or be engulfed by other diagenetic components (such as quartz overgrowths; Fig. 8A, B). The well-developed cuticles on silt-size grains may be due to the increased contact surface of the finer-grained sediments. Alternatively, these sediments might have been transported and deposited already with the developed clay cuticles, by wind processes (Pye, 1987). The latter hypothesis will be further developed in section 5.3.

Infiltration of clay minerals is commonly associated with arid climates, especially in soils and exposed sediments (Walker *et al.*, 1978; Bullock & Murphy, 1979; Kemp, 1987; Jeong *et al.*, 2011). Substitution of smectite by illite forming I/S mixed layers, as observed in the XRD analysis, is also a process occurring in arid soils (Singer, 1988). Precipitation of Mn and Fe oxi-hydroxides is common in soils subjected to wetting and drying cycles (McKenzie, 1989), which were enhanced by the chemical alterations caused by presence or decaying of roots or waterlogging conditions in root voids (Payton, 1993; Trendell *et al.*, 2013), creating rhizohalos (Figs. 5A, C–E).

Dissolution of feldspars was constant almost throughout the pedogenesis and diagenesis processes, as different precipitates fill dissolution pores (Fig. 8C, D). Expansion of micas must have occurred early, as other diagenetic minerals occupy interlayer space (Fig. 9), including infiltrated clay (Fig. 9D). Furthermore, the micas are

replaced by illite (Fig. 9A, B), kaolinite, or iron oxi-hydroxides (Fig. 9C). Precipitation of Fe and Ti oxi-hydroxides is inferred to be eodiagenetic (Walker *et al.*, 1978).

Precipitation of precompactonal calcite was not widespread, as there are rocks where it is absent or nearly absent (Figs. 5A, C, D; 6A; 8C; 9A, B, D; 10D–F; 13A), although it was concentrated, probably at the superior part of the groundwater table, where evaporation is most effective (Alonso-Zarza & Wright, 2010). Calcite also fills feldspar dissolution pores (Fig. 12D), but many pores are unfilled (Figs. 7C; 8D; 9A, D; 11A–C), which means that some dissolution occurred after calcite precipitation. A small volume of Fe and Ti oxi-hydroxides grows over and thus postdates calcite cement.

Studied samples present no evidence of organic contribution in the precipitation of calcite, and thus can be classified as an alpha-type fabric calcrete (*sensu* Wright, 1990; Wright and Tucker, 1991). These carbonates also lack horizontal zonation, indicating they possibly have a groundwater origin. Groundwater calcretes are mostly distinguished by the lack of features which would point towards a pedogenic or paludal origin (Alonso-Zarza, 2003). The observation that the nodules occur along bedding, stratification and erosional surfaces (Figs. 4A–C; 7B–D; Xavier *et al.*, 2023) is also indicative of groundwater origin (Alonso-Zarza & Wright, 2010); and the coarse crystalline texture, here present, is more common in this type of calcrete (Wright, 2007).

However, the occurrence of rhizohalos (Fig. 5) evidences the development of plants, and thus, soil (Retallack, 1988). In addition, presence of small quantities of illite in mixed layers I/S is indicative of initial stages of pedogenesis in arid soils (Singer, 1988). This, together with the occurrences in the outcrop of blocky structures, interpreted as peds (Fig. 4D; Xavier *et al.*, 2023), indicates that carbonate deposition may have a minor pedogenic contribution.

Groundwater calcretes are indicative of arid environments (Alonso-Zarza & Wright, 2010; Goudie, 1973; Wright & Tucker, 1991), and presence of illite in S/I mixed layers are indicative of aridisols (Singer, 1988). Abundance of smectite and iron oxi-hydroxides indicates eodiagenesis under arid climate (Walker *et al.*, 1978). In addition, the root molds filled by Mn oxi-hydroxides have high concentration of Ba (Fig. 5F, Supl. 1). Precipitation of Fe and/or Mn oxi-hydroxides indicates variation of redox conditions, and thus, alternation of waterlogged and dry conditions (McKenzie, 1989). Presence

of voids which allow accumulation of stagnant water promote localized reducing conditions, especially when coupled with decomposing organic matter, such as root voids (Payton, 1993; Trendell *et al.*, 2013). Concerning the high concentration of Ba, Mn oxi-hydroxides have a natural affinity with Ba (Golden *et al.*, 1986), and trees and bushes in arid climates concentrate greater quantities of Ba (Kabata-Pendias, 2010). In deserts, Potter and Rossman (1979) found that the vast majority of Mn-dendrites are composed by romanèchite [“psilomelane” (Ba, H₂O)₂Mn₅O₁₀] or hollandite (BaMn₈O₁₆). These interpretations corroborate previous works regarding the deposition of the SCF in a semiarid to arid environment, with variations of water discharge (Zerfass *et al.*, 2003, 2004; Dario, 2017; Scherer *et al.*, 2023; Xavier *et al.*, 2023).

One characteristic feature of exposed materials are desiccation features (Alonso-Zarza & Wright, 2010; Horn *et al.*, 2013), but in the SCF these are absent. This absence would imply a constant water table, which is not consistent with other interpretations in the present study, nor other studies of the SCF (Zerfass *et al.*, 2003, 2004; Scherer *et al.*, 2023; Xavier *et al.*, 2023). It is here interpreted that the lack of desiccation features is due to the absence of mud deposits in the original sediments, causing the host sediments not to expand and shrink. Deposition of mud was mostly restricted to drapings and ephemeral ponds, which would then be eroded by subsequent flows and incorporated to the deposits almost solely as mud intraclasts (Abdullatif, 1989; Xavier *et al.*, 2023).

The supply model for the carbonate in the SCF is interpreted as the *per ascensum* model of Goudie (1983), where carbonate enters the profile in solution from groundwater, and is transported up through evaporation processes. The source of Ca in an arid environment, as interpreted for the SCF, must be dust and rainfall (Alonso-Zarza & Wright, 2010), as there is no local rock which could have been a source of Ca (Zerfass, 1998; Zerfass *et al.*, 2000, 2003, 2004; CPRM, 2006).

Alonso-Zarza and Wright (2010) state that most known ‘warm’ calcretes form where rainfall ranges from around 100 and 500 mm/year and attribute this information to Goudie (1983). However, Goudie (1983) does not present this information, but states that the humid limit to the formation of calcrete is generally between 400–600 mm/year, although making the caveat that it may be much greater. Goudie (1973) lists

a number of localities in which calcretes develop, and at most locations the 400–600 mm/year rainfall isohyet matches the distribution of calcrete; while at the lower limit of around 100 mm/year rainfall, carbonate cement starts to be replaced by gypsum. These limits are coherent with the estimations in Xavier *et al.* (2023) for the mean annual precipitation of the SCF as less than the Burdekin River of Australia (500–700 mm/year; Fielding *et al.*, 2009), and closer to the Bijou Creek's (USA) 330–355 mm/year (McKee *et al.*, 1967).

5.2. Sediment reworking

Smaller-sized carbonate-cemented intraclasts within larger cemented intraclasts (Fig. 7) evidence the multi-cyclical nature of these deposits. The process of formation of multi-cycle intraclast deposits is illustrated in Fig. 16. The carbonate-cemented siltstone intraclasts, mostly around granule in size, were formed in siltstones during arid times (t1), as the high evaporation rate causes increase in carbonate concentration and promotes precipitation in the rock hosting the groundwater (Goudie, 1973). Growth of bushes and pedogenesis also took place, and roots caused preferential precipitation of Fe and Mn-Ba oxi-hydroxides, forming rhizohalos. A wet phase followed (t2) and the siltstones were eroded by unconfined flows. Mudstone intraclasts were generated when each flood eroded mud deposits from the final stages of previous floods (Xavier *et al.*, 2023). The unconfined flows deposited thin beds of massive to faintly laminated sandstones. Lags of mudstone and cemented-siltstone intraclasts (colored red) accumulate in some of these beds. Return of arid conditions (t3) caused the concentration and precipitation of carbonate, resulting in the formation of nodules (colored green). Many of the nodules engulfed mudstone intraclasts and carbonate-cemented siltstone intraclasts, and eventually, rhizohalos. Nodules are generally rounded, slightly longer horizontally, but it is common for two or more adjacent nodules to coalesce, generating elongated forms. In a subsequent wet period (t4), Froude-subcritical to supercritical flows eroded the sandstones, transporting these younger nodules as carbonate-cemented sandstone intraclasts, as well as other carbonate-cemented siltstone intraclasts, and also mudstone intraclasts. The intraclastic conglomerates in successive asymmetrical scours along a same bounding surface, filled by backsets, which transition vertically to undulating truncated,

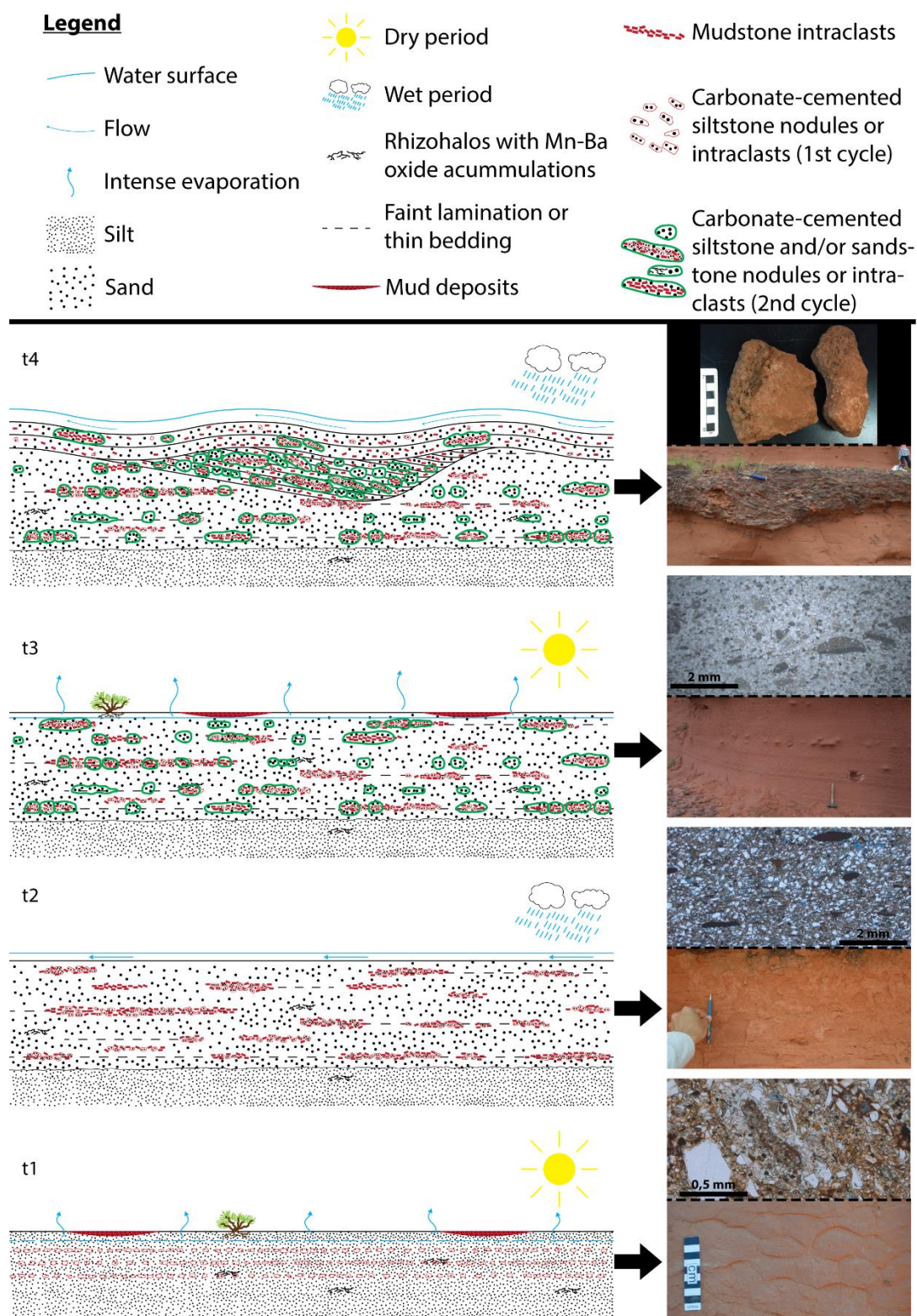


Fig.16. Generational model for the multi-cycle, calcite cemented siltstone and sandstone intraclasts, and multi-cycle intraclastic conglomerates. t1 — Silt-rich deposit, with significant contribution from wind-blown dust is subjected to a dry period in arid to semi-arid climate. Low deposition rate allows growth of bushes, which concentrate barium, and incipient pedogenesis, generating blocky structure. Root biochemistry facilitates precipitation of iron oxi-hydroxides, generating circular rhizohalos. Death and decay of bushes and their roots generate voids, which will be filled by precipitation of iron-manganese minerals, generating the linear rhizohalos. The high evaporation rate causes carbonate near the groundwater surface to concentrate, precipitating low-Mg calcite. The first nucleation points,

which can be around previous intraclasts, facilitate further precipitation, generating regions with more intense cementation, and eventually, nodules (red). The last flood left lenses of deposited mud. t2 — A wet period causes flash floods and erosion of the siltstone. Unconfined flows deposit massive or faintly-laminated thin-beds of fine-grained sandstone. Nodules are remobilized into cemented siltstone clasts, which are incorporated to the framework, together with mudstone clasts, with subparallel orientation, and commonly in lags or accumulations. t3 — Return of dry conditions causes evaporation rate to increase again and new precipitation of calcite. New cementation engulfs sand grains and previous intraclasts, as well as rhizohalos, forming new nodules (green). Nodule formation tends to accompany thin bedding and/or lamination/stratification, and some nodules coalesce. t4 — Subsequent wet period with more intense, episodic rainfall causes flash floods which generate Froude-supercritical flows, and supercritical bedforms. Cyclic steps and unstable antidune bedforms erode the sandstone and remobilize the new nodules (delineated green) into carbonate-cemented sandstone clasts. These are incorporated and accumulated, together with new mudstone clasts, in scour-filling backsets, and undulatory stratification.

are interpreted as deposited by the migration and aggradation of cyclic steps (Parker, 1996; Cartigny *et al.*, 2014), transitioning to unstable antidunes (Cartigny *et al.*, 2014; Xavier *et al.*, 2023). The conglomerates with sigmoidal cross-stratification (Fig. 4F) are interpreted as the formation of humpback dunes, filling erosional cuts downflow from hydraulic jumps, in the transition of upper- and lower-flow regime (Cartigny *et al.*, 2014; Xavier *et al.*, 2023). Elongated cemented intraclasts are proportionally more common in the conglomerates than elongated nodules in sandstones. This is interpreted as preferential transport of elongated (especially flattened) intraclasts by the flow due to proportionally larger surface area, which increases clast buoyancy and facilitates transport (Zhao *et al.*, 2020).

This interpreted process requires a minimum of two events of cementation and erosion. It is certain, however, that the process occurred several times, as multiple levels of nodules can be observed (Figs. 3; 4A, B). In addition, the concentration of intraclasts in the conglomerates is much greater than the frequency of nodules in the sandstones (Compare figures 4A and 4D). This requires the conglomerates to erode multiple levels of sandstones, and it is extremely likely that presently-seen conglomerates reworked previous conglomerates, in order to achieve the observed level of intraclast concentration.

Occurrence of these large (up to cobble size) cemented intraclasts oriented in structures and presenting signs of transport, such as imbrication (Fig. 4D), as well as supercritical structures (Fig. 4D–F; Xavier *et al.*, 2023), attest the high energy of the system. However, extrabasinal sediments of greater size than coarse-grained sand are completely absent. This is evidence that the high energy is not due to proximity to the source area or uplift, but rather solely due to high discharge.

5.3. Eolian dust contribution

The ubiquitousness of silt-size grains with clay cuticles is notable. These can be found composing all studied rocks in the SCF: as massive siltstones, or dispersed amidst coarser sediments, from fine-grained silty sandstones to the intraclastic conglomerates, as well as composing intraclasts (Figs. 5–9, 11–13, 15). Clay mineral cuticles observed in coarser grains are discontinuous (fig. 8A, B). This grain size bias may be the result of the greater contact area of silt grains in comparison to sand grains, facilitating chemical reactions. Another possibility here proposed, is that the silt-size grains were transported in suspension by wind, already with the developed clay cuticles (Pye, 1987). Formation of iron-rich clay coatings in arid soils, and more specifically in loessic deposits is extremely common (Walker *et al.*, 1978; Pye, 1987; Jeong, 2008), and the transport of coated silt is characteristic feat of wind-blown dust (Pye, 1987; Singer, 1988; Jeong, 2008). This phenomenon is in fact one of the main methods of transport of clay by wind, as well as silt-size clay aggregates (Pye, 1987).

The paleogeographic position of the SCF is also consistent with the interpretation of a significant eolian dust contribution (Fig. 17; Scherer *et al.*, 2023; Zeffass *et al.*, 2004, 2003). A wide arid belt in the central region of Gondwana is believed to have existed during Triassic times (Blakey *et al.*, 1988; Boucot *et al.*, 2013; Sellwood & Valdes, 2006), and the SCF was near the margin of this arid area (Fig. 17). Although not the only one, peri-desertic areas are typical regions for the accumulation of wind-blown dust sediments (Li *et al.*, 2020). However, Early Triassic loessite (i.e., paleoloess or lithified loess) is known from the Midwestern USA (Johnson, 1989; Kessler *et al.*, 2001), and has been found in the North Sea (Wilkins *et al.*, 2018; Wilson *et al.*, 2020), both of which are well within the arid belt in Early Triassic times (Fig. 17), which indicates that arid areas are also prone to wind-blown dust accumulation.

In the northern part of Midwestern USA and in British Columbia, Canada, Knapp (2020) and Vaisblat *et al.* (2021) interpret continental and marine deposits with abundant silt to have a significant contribution from wind-blown dust. The same interpretation is held by Wright *et al.* (1991) for the Budleigh Salterton Pebble Beds in Devon, UK. (Smith & Botha-Brink, 2014) report loessites in the Early Permian Katberg

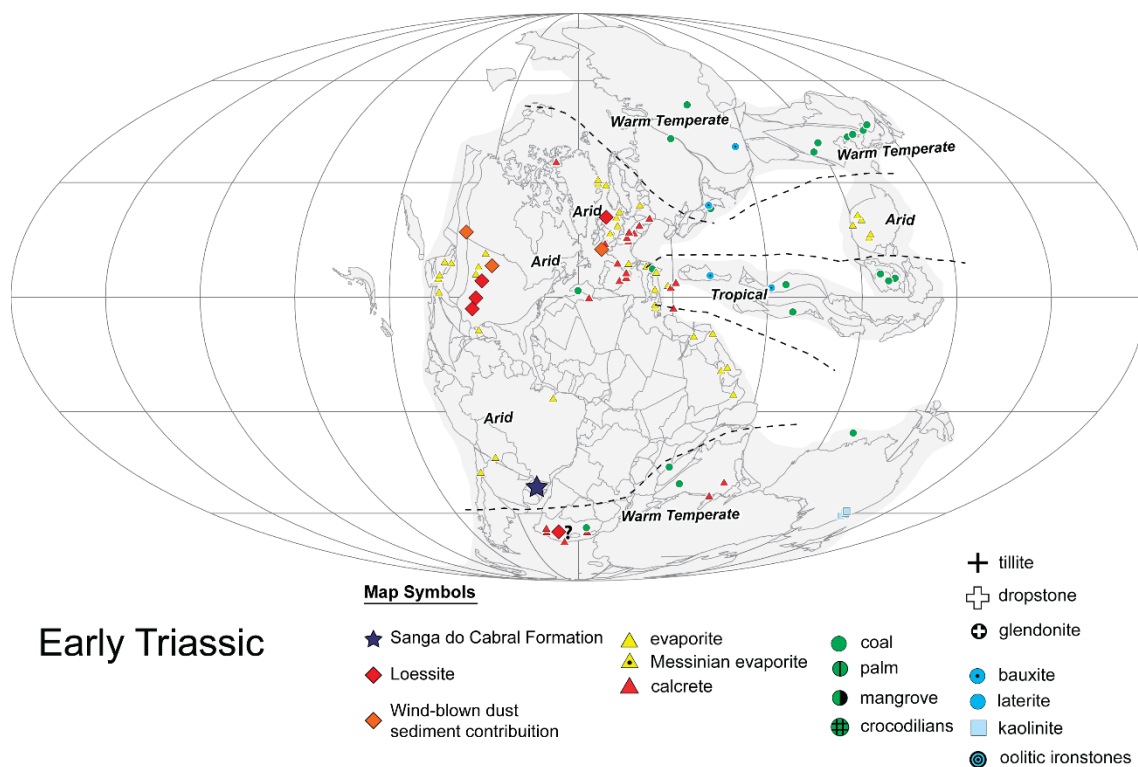


Fig. 17. Paleogeographic and paleoclimatic map of Pangea during the early Triassic by Boucot *et al.* (2013). Location of study area, as well as the mentioned Early Triassic loessite and deposits with aeolian dust contribution are highlighted. The Sanga do Cabral Formation was near the southern limit of the inferred arid belt.

Formation in South Africa, and relate it to the harsh arid conditions after the End-Permian Mass Extinction (although this interpretation has been disputed — Gastaldo and Neveling, 2016; Li *et al.*, 2017). In particular, (Knapp, 2020) interprets the Red Peak Formation in central-north Wyoming (USA) as a thick sequence of fine-grained beds, deposited in a weakly confined distributive fluvial system, with unconfined overland flow, eolian processes, and ephemeral saline lakes and mudflats. It presents laterally extensive tabular lithosomes with abundant silt, and intraformational rip-up mud clasts, as well as erosional bases, upper-flow regime parallel lamination, ripples, and convolute lamination. The author interprets that “widespread wind-driven deposition of silt and smaller sized sediment contributed large volumes of fine sediment, [and] subsequent reworking by wind and unconfined flow would result in [the observed] sedimentary features”. The Red Peak Formation thus presents a similar condition to the SCF. Differences would lie in the lack of Froude-supercritical sedimentary structures and carbonate nodules, and presence of evaporites. This in

turn indicates a more consistently arid environment, with less seasonality (Fielding *et al.*, 2018; Fielding & Alexander, 1996; Hansford *et al.*, 2020; Plink-Björklund, 2015).

Lower Triassic deposits interpreted as loessites or with significant eolian dust contribution found in the literature by the present work are restricted to the USA and UK. This is most likely because eolian dust deposits are still hardly recognized in the rock record (Meijer *et al.*, 2020). The SCF may thus be the first recognized in the southern hemisphere for the Lower Triassic.

On the other hand, eolian dust deposits are also known in the Midwestern USA in the Upper Pennsylvanian–Lower Permian (Maroon Formation; Johnson, 1989; Lower Cutler Beds; Soreghan *et al.*, 2002), Upper Permian (Goose Egg Formation; Knapp, 2020), as well as for the Middle Triassic (Ankareh Formation; Chan, 1999). This shows that the region was prone for the accumulation of eolian dust for a long geologic time. Similarly, eolian dust deposits are recognized in the Late Permian and the Middle–Late Triassic of the UK, in the Aylesbeare and Mercia Mudstone Groups, respectively (Jefferson *et al.*, 2002; Mao *et al.*, 2021). In the Paraná Basin, a continuity of the contribution of aeolian dust to sedimentation is present in the interpreted paleoloess of the Pinheiros-Chiniquá and Santa Cruz Sequences of the Santa Maria Supersequence (Fig. 2), which also present poorly- to unconfined and ephemeral fluvial systems, as well as calcretes in the form of carbonate nodules (Horn *et al.*, 2013, 2014, 2018a; b).

6. CONCLUSIONS

The present work and past studies on the Sanga do Cabral Formation show consistent evidence for the interpretation of this unit as deposited in a semi-arid to arid, strongly seasonal environment, by poorly- to unconfined flows in a distal low-relief alluvial plain (Andreis *et al.*, 1980; Faccini, 1989, 2000; Lavina, 1991; Zeffass *et al.*, 2000, 2003, 2004; Dario, 2017; Scherer *et al.*, 2023; Xavier *et al.*, 2023). The present study adds to the existing knowledge by:

- (1) Recognizing petrographic evidence of incipient pedogenesis (root marks, Mn-Ba oxides, I/S mixed layers — aridisol) emphasizing the occurrence of relatively long periods of non-deposition.

(2) Identification of precipitation of iron oxi-hydroxides and interpretation of calcretes as groundwater in origin, indicating alternance of wet and dry periods and low relief ; also allowing estimates of precipitation around a minimum of 100 mm/year (for the lack of evaporites such as gypsum; Goudie, 1973), and a maximum of around 400–600 mm/year (general maximum rainfall for calcretes; (Goudie, 1973, 1983).

(3) Describing and interpreting the multi-cyclic and autophagic nature of the deposits, indicating that despite their high energy, the system was distal, and thus these high energy deposits can be attributed to concentrated high discharge.

(4) Recognizing significant contribution of eolian dust to the deposit, which corroborates the paleoclimatic interpretation of the region being in at the margin of an arid belt.

Global Climate Models (GCMs) for the Triassic indicate that the symmetrical positioning of the Pangea Supercontinent over the equator, associated to the long distances from the ocean to the continent's interior would generate widespread aridity in the hinterland, and a 'megamonsoonal' circulation regime (Kutzbach & Gallimore, 1989; Parrish, 1993; Wilson *et al.*, 1994; Sellwood & Valdes, 2006; Preto *et al.*, 2010; Holz, 2015; Harris *et al.*, 2017; Dunne *et al.*, 2021). Considering the paleogeographic positioning of the SCF, the present work corroborates these models and interpretations.

ACKNOWLEDGEMENTS

We thank Francyne do Amarante, Rossano Michel, and Bruno Angonese for helping in the fieldwork. Special thanks go to the Scherer family, who kindly received us in their home, and even let us use the house during Covid-19 times, while they stayed in another place. We also acknowledge Cesar Schultz and Bruno Horn for studies in the early stages of the project, even though the research deviated greatly from when they were involved. The National Council of Scientific and Technological Development (CNPq) of Brazil provided grant 141101/2018-0 for the corresponding author; there was no involvement of CNPq in the conduction of this research.

REFERENCES

- Abdullatif, O.M.** (1989) Channel-fill and sheet-flood facies sequences in the ephemeral terminal River Gash, Kassala, Sudan. *Sediment. Geol.*, **63**, 171–184.
- Alexander, J., Bridge, J.S., Cheel, R.J. and Leclair, S.F.** (2001) Bedforms and associated sedimentary structures formed under supercritical water flows over aggrading sand beds. *Sedimentology*, **48**, 133–152.
- Alexander, J. and Fielding, C.R.** (1997) Gravel antidunes in the tropical Burdekin River, Queensland, Australia. *Sedimentology*, **44**, 327–337.
- Alexander, J., Fielding, C.R. and Pocock, G.D.** (1999) Flood behaviour of the Burdekin River, tropical north Queensland, Australia. *Floodplains Interdiscip. Approaches*, 27–40.
- Alexander, J., Herbert, C.M., Fielding, C.R. and Amos, K.J.** (2020) Controls on channel deposits of highly variable rivers: Comparing hydrology and event deposits in the Burdekin River, Australia. *Sedimentology*, **67**, 2721–2746.
- Allen, J.P., Fielding, C.R., Gibling, M.R. and Rygel, M.C.** (2014) Recognizing products of palaeoclimate fluctuation in the fluvial stratigraphic record: An example from the Pennsylvanian to Lower Permian of Cape Breton Island, Nova Scotia. *Sedimentology*, **61**, 1332–1381.
- Allen, J.R.L.** (1982) Bedforms in Supercritical and Related Flows: Transverse Ribs, Rhomboid Features, and Antidunes. In: *Sedimentary Structures Their Character and Physical Basis* (Ed. J.R.L. Allen), Elsevier, Amsterdam, 383–417.
- Allen, J.R.L.** (1969) Erosional Current Marks of Weakly Cohesive Mud Beds. *SEPM J. Sediment. Res.*, Vol. **39**, 607–623.
- Allen, J.R.L.** (1968) Current Ripples, Their Relation to Patterns of Water and Sediment Motion. *North-Holland Publishing Company*, Amsterdam, 433 pp.
- Alonso-Zarza, A.M.** (2003) Palaeoenvironmental significance of palustrine carbonates and calcretes in the geological record. *Earth-Science Rev.*, **60**, 261–298.
- Alonso-Zarza, A.M. and Wright, V.P.** (2010) Calcretes. In: *Carbonates in Continental Settings: Facies, Environments, and Processes* (Ed. A.M. Alonso-Zarza and L.H. Tanner), Elsevier, Oxford, 61, 225–267.
- Andreis, R.R., Bossi, G.E. and Montardo, D.K.** (1980) O Grupo Rosário do Sul (Triássico) no Rio Grande do Sul - Brasil. In: *XXXI Congresso Brasileiro de Geologia, Sociedade Brasileira de Geologia*, Balneário Camboriú, SC, 2, 659–673.
- Arakel, A. V. and McConchie, D.** (1982) Classification and Genesis of Calcrete and Gypsite Lithofacies in Paleodrainage Systems of Inland Australia and their Relationship to Carnotite Mineralization. *SEPM J. Sediment. Res.*, **52**, 1149–1170.

- Arnott, R.W.C. and Hand, B.M.** (1989) Bedforms, Primary Structures and Grain Fabric in the Presence of Suspended Sediment Rain. *J. Sediment. Res.*, **59**, 1062–1069.
- Azevedo, S.A., Lavina, E.L., Barberena, M.C., Ferrando, L. and Andreis, R.R.** (1985) Evidências de correlação entre a Formação Yaguari (Uruguai) e as Formações Rio do Rasto e Sanga do Cabral (Rio Grande do Sul - Brasil). *Pesqui. em Geociências*, **17**, 112–121.
- Baas, J.H., Best, J.L. and Peakall, J.** (2011) Depositional processes, bedform development and hybrid bed formation in rapidly decelerated cohesive (mud-sand) sediment flows. *Sedimentology*, **58**, 1953–1987.
- Barberena, M.C., Araújo, D.C.F., Lavina, E.L. and Azevedo, S.A.K.** (1985) O estado atual do conhecimento sobre os tetrapodes permianos e triássicos do Brasil meridional. In: *Coletânea de trabalhos paleontológicos, Trabalhos apresentados no VIII Congresso Brasileiro de Paleontologia* (Ed. D. de A. Campos and R.C.G. Armesto), *Departamento Nacional de Produção Mineral - DNPM*, Brasília, 21–28.
- Baud, A., Magaritz, M. and Holser, W.T.** (1989) Permian-Triassic of the Tethys: Carbon isotope studies. *Geol. Rundschau*, **78**, 649–677.
- Benton, M.J.** (2008) *When Life Nearly Died - The greatest mass extinction of all time*, 2nd edn. *Thames & Hudson*, London, 336 pp.
- Benton, M.J.** (2018) Hyperthermal-driven mass extinctions: Killing models during the Permian-Triassic mass extinction. *Philos Trans R Soc A Math Phys Eng Sci*. doi: 10.1098/rsta.2017.0076
- Benton, M.J. and Newell, A.J.** (2014) Impacts of global warming on Permo-Triassic terrestrial ecosystems. *Gondwana Res.*, **25**, 1308–1337.
- Blakey, R.C., Peterson, F. and Kocurek, G.** (1988) Synthesis of late Paleozoic and Mesozoic eolian deposits of the Western Interior of the United States. *Sediment. Geol.*, **56**, 3–125.
- Botha, J. and Smith, R.M.H.** (2006) Rapid vertebrate recuperation in the Karoo Basin of South Africa following the End-Permian extinction. *J. African Earth Sci.*, **45**, 502–514.
- Botha, J. and Smith, R.M.H.** (2020) Biostratigraphy of the *Lystrosaurus declivis* Assemblage Zone (Beaufort Group, Karoo Supergroup), South Africa. *South African J. Geol.*, **123**, 207–216.
- Boucot, A.J., Xu, C., Scotese, C.R. and Morley, R.J.** (2013) *Phanerozoic Paleoclimate*. *Society for Sedimentary Geology (SEPM)*, Tulsa, Oklahoma, U.S.A., 360 pp.
- Brierley, G.J. and Hickin, E.J.** (1991) Channel planform as a non-controlling factor in fluvial sedimentology: the case of the squamish river floodplain, British Columbia. *Sediment. Geol.*, **75**, 67–83.
- Bryant, M., Falk, P. and Paola, C.** (1995) Experimental study of avulsion frequency and rate of deposition. *Geology*, **23**, 365–368.
- Bullock, P. and Murphy, C.P.** (1979) Evolution of a paleo-argillic brown earth (paleudalf) from

- oxfordshire, England. *Geoderma*, **22**, 225–252.
- Burroughs, W.A.** (1985) The hydraulic equivalence of mica; discussion. *J. Sediment. Res.*, **55**, 291–292.
- Cao, C., Love, G.D., Hays, L.E., Wang, W., Shen, S. and Summons, R.E.** (2009) Biogeochemical evidence for euxinic oceans and ecological disturbance presaging the end-Permian mass extinction event. *Earth Planet. Sci. Lett.*, **281**, 188–201.
- Cartigny, M.J.B., Postma, G., van den Berg, J.H. and Mastbergen, D.R.** (2011) A comparative study of sediment waves and cyclic steps based on geometries, internal structures and numerical modeling. *Mar. Geol.*, **280**, 40–56.
- Cartigny, M.J.B., Ventra, D., Postma, G. and van Den Berg, J.H.** (2014) Morphodynamics and sedimentary structures of bedforms under supercritical-flow conditions: New insights from flume experiments. *Sedimentology*, **61**, 712–748.
- Chan, M.A.** (1999) Triassic loessite of north-central Utah; stratigraphy, petrophysical character, and paleoclimate implications. *J. Sediment. Res.*, **69**, 477–485.
- Chen, Z.Q. and Benton, M.J.** (2012) The timing and pattern of biotic recovery following the end-Permian mass extinction. *Nat. Geosci.*, **5**, 375–383.
- Chester, R., Elderfield, H., Griffin, J.J., Johnson, L.R. and Padgham, R.C.** (1972) Eolian dust along the eastern margins of the Atlantic Ocean. *Mar. Geol.*, **13**, 91–105.
- Choquette, P.W. and Pray, L.C.** (1970) Geologic Nomenclature and Classification of Porosity in Sedimentary Carbonates. *Am. Assoc. Pet. Geol. Bull.*, **54**, 207–250.
- Chow, V. Te** (1959) Open-channel Hydraulics, 1st edn. *McGraw-Hill Books*, New York, 697 pp.
- Cisneros, J.C.** (2008) Taxonomic status of the reptile genus Procolophon from the Gondwanan Triassic. *Palaeontol. Africana*, **43**, 7–18.
- Cisneros, J.C. and Schultz, C.L.** (2002) Procolophon brasiliensis n. sp., a new procolophonid reptile from the Lower Triassic of southern Brazil. *Neues Jahrb. fur Geol. und Palaontologie - Monatshefte*, **2002**, 641–648.
- Cohen, K.M., Finney, S.C., Gibbard, P.L. and Fan, J.-X.** (2013) The ICS International Chronostratigraphic Chart. *Episodes*, **36**, 199–204.
- Cornish, V.** (1899) On Kumatology. (The Study of the Waves and Wave-Structures of the Atmosphere, Hydrosphere, and Lithosphere). *Geogr. J.*, **13**, 624.
- Covault, J.A., Kostic, S., Paull, C.K., Sylvester, Z. and Fildani, A.** (2017) Cyclic steps and related supercritical bedforms: Building blocks of deep-water depositional systems, western North America. *Mar. Geol.*, **393**, 4–20.
- CPRM** (2006) Mapa Geológico do Rio Grande do Sul.

- Dal Corso, J., Song, H., Callegaro, S., Chu, D., Sun, Y., Hilton, J., Grasby, S.E., Joachimski, M.M. and Wignall, P.B.** (2022) Environmental crises at the Permian–Triassic mass extinction. *Nat. Rev. Earth Environ.*, **3**, 197–214.
- Dalrymple, R.W.** (2010) Interpreting Sedimentary Successions: Facies, Facies Analysis and Facies Models. In: *Facies Models 4*, 4th edn. (Ed. N.P. James and R.W. Dalrymple), *Geological Association of Canada*, St. John's, 3–18.
- Dario, E.M.** (2017) Arquitetura de fácies e modelo deposicional dos depósitos fluviais efêmeros da Formação Sanga do Cabral, Triássico Inferior da Bacia Do Paraná, na região central do Rio Grande Do Sul. Universidade Federal do Rio Grande do Sul - UFRGS, Porto Alegre
- de Santa Ana, H., Goso, C. and Daners, G.** (2006) Cuenca Norte: estratigrafía del Carbonífero–Pérmico. In: *Cuencas Sedimentarias de Uruguay – Paleozoico* (Ed. G. Verolavsky, M. Ubilla, and S. Martínez), *DIRAC*, Montevideo, 147–208.
- Dias-Da-Silva, S. and Marsicano, C.** (2011) Phylogenetic reappraisal of Rhytidosteidae (Stereospondyli: Trematosauria), temnospondyl amphibians from the Permian and Triassic. *J. Syst. Palaeontol.*, **9**, 305–325.
- Dias-Da-Silva, S., Marsicano, C. and Schultz, C.L.** (2006) Rhytidosteid temnospondyls in Gondwana: A new taxon from the Lower Triassic of Brazil. *Palaeontology*, **49**, 381–390.
- Dias-da-Silva, S., Pinheiro, F.L., Stock Da-Rosa, Á.A., Martinelli, A.G., Schultz, C.L., Silva-Neves, E. and Modesto, S.P.** (2017) Biostratigraphic reappraisal of the Lower Triassic Sanga do Cabral Supersequence from South America, with a description of new material attributable to the parareptile genus Procolophon. *J. South Am. Earth Sci.*, **79**, 281–296.
- Dickinson, W.R.** (1985) Interpreting Provenance Relations from Detrital Modes of Sandstones. In: *Provenance of Arenites*, *Springer Netherlands*, Dordrecht, 333–361.
- Donselaar, M.E., Cuevas Gozalo, M.C. and Moyano, S.** (2013) Avulsion processes at the terminus of low-gradient semi-arid fluvial systems: Lessons from the Río Colorado, Altiplano endorheic basin, Bolivia. *Sediment. Geol.*, **283**, 1–14.
- Doyle, L.J., Carder, K.L. and Steward, R.** (1985) The hydraulic equivalence of mica; reply. *J. Sediment. Res.*, **55**, 293–294.
- Doyle, L.J., Carder, K.L. and Steward, R.G.** (1983) The hydraulic equivalence of mica. *J. Sediment. Petrol.*, **53**, 643–648.
- Du, Y., Song, H., Grasby, S.E., Xing, T., Song, H., Tian, L., Chu, D., Wu, Y., Dal Corso, J., Algeo, T.J. and Tong, J.** (2023) Recovery from persistent nutrient-N limitation following the Permian–Triassic mass extinction. *Earth Planet. Sci. Lett.*, **602**, 117944.
- Duller, R.A., Mountney, N.P., Russel, A.J. and Cassidy, N.C.** (2008) Architectural analysis of a volcanoclastic jökulhlaup deposit, southern Iceland: sedimentary evidence for supercritical flow. *Sedimentology*, **55**, 939–964.

- Dunne, E.M., Farnsworth, A., Greene, S.E., Lunt, D.J. and Butler, R.J.** (2021) Climatic drivers of latitudinal variation in Late Triassic tetrapod diversity. *Palaeontology*, **64**, 101–117.
- Eltink, E., Da-Rosa, Á.A.S. and Dias-da-Silva, S.** (2017) A capitosauroid from the Lower Triassic of South America (Sanga do Cabral Supersequence: Paraná Basin), its phylogenetic relationships and biostratigraphic implications. *Hist. Biol.*, **29**, 863–874.
- Ernesto, M., Demarco, P.N., Xavier, P., Sanchez, L., Schultz, C. and Piñeiro, G.** (2020) Age constraints on the Paleozoic Yaguari-Buena Vista succession from Uruguay: paleomagnetic and paleontologic information. *J. South Am. Earth Sci.*, **98**, 102489.
- Erwin, D.H.** (2006) Extinction: How Life on Earth Nearly Ended 250 Million Years Ago. *Princeton University Press*, Princeton, 296 pp.
- Erwin, D.H.** (1994) The Permo–Triassic extinction. *Nature*, **367**, 231–236.
- Erwin, D.H.** (2001) Lessons from the past: Biotic recoveries from mass extinctions. *Proc. Natl. Acad. Sci. U. S. A.*, **98**, 5399–5403.
- Ethridge, F.G.** (2011) Interpretation of Ancient Fluvial Channel Deposits: Review and Recommendations. In: *From River to Rock Record: The preservation of fluvial sediments and their subsequent interpretation — SEPM Special Publication 97* (Ed. S.K. Davidson, S. Leleu, and C.P. North), *SEPM Society for Sedimentary Geology*, Tulsa, Oklahoma, U.S.A., 9–36.
- Faccini, U.F.** (2000) Estratigrafia do Permo-Triássico do Rio Grande do Sul: estilos deposicionais versus espaço de acomodação. Universidade Federal do Rio Grande do Sul - UFRGS
- Faccini, U.F.** (1989) O Permo-Triássico do Rio Grande do Sul : uma análise sob o ponto de vista das seqüências deposicionais. Universidade Federal do Rio Grande do Sul - UFRGS
- Fielding, C.R.** (2006) Upper flow regime sheets, lenses and scour fills: Extending the range of architectural elements for fluvial sediment bodies. *Sediment. Geol.*, **190**, 227–240.
- Fielding, C.R.** (1993) A review of recent research in fluvial sedimentology. *Sediment. Geol.*, **85**, 3–14.
- Fielding, C.R. and Alexander, J.** (1996) Sedimentology of the Upper Burdekin River of North Queensland, Australia—an example of a tropical, variable discharge river. *Terra Nov.*, **8**, 447–457.
- Fielding, C.R., Alexander, J. and Allen, J.P.** (2018) The role of discharge variability in the formation and preservation of alluvial sediment bodies. *Sediment. Geol.*, **365**, 1–20.
- Fielding, C.R., Allen, J.P., Alexander, J. and Gibling, M.R.** (2009) Facies model for fluvial systems in the seasonal tropics and subtropics. *Geology*, **37**, 623–626.
- Fielding, C.R., Frank, T.D., McLoughlin, S., Vajda, V., Mays, C., Tevyaw, A.P., Winguth, A., Winguth, C., Nicoll, R.S., Bocking, M. and Crowley, J.L.** (2019) Age and pattern of the southern high-latitude continental end-Permian extinction constrained by multiproxy analysis. *Nat Commun.* doi: 10.1038/s41467-018-07934-z
- Fielding, C.R., Frank, T.D., Tevyaw, A.P., Savatic, K., Vajda, V., McLoughlin, S., Mays, C., Nicoll,**

- R.S., Bocking, M. and Crowley, J.L.** (2021) Sedimentology of the continental end-Permian extinction event in the Sydney Basin, eastern Australia. *Sedimentology*, **68**, 30–62.
- Fildani, A., Normark, W.R., Kostic, S. and Parker, G.** (2006) Channel formation by flow stripping: Large-scale scour features along the Monterey East Channel and their relation to sediment waves. *Sedimentology*, **53**, 1265–1287.
- Fisher, J.A., Krapf, C.B.E., Langs, S.C., Nichols, G.J. and Payenberg, T.H.D.** (2008) Sedimentology and architecture of the Douglas Creek terminal splay, Lake Eyre, central Australia. *Sedimentology*, **55**, 1915–1930.
- Folk, R.L.** (1981) Petrology of Sedimentary Rocks, 2nd edn. *Hemphill*, Austin, Texas, 184 pp.
- Francischini, H., Dentzien-Dias, P., Guerra-Sommer, M., Menegat, R., Santos, J.O.S., Manfroi, J. and Schultz, C.L.** (2018) A middle Permian (Roadian) lungfish aestivation burrow from the Rio do Rasto Formation (Paraná Basin, Brazil) and associated U-Pb dating. *Palaios*, **33**, 69–84.
- Froude, M.J., Alexander, J., Barclay, J. and Cole, P.** (2017) Interpreting flash flood palaeoflow parameters from antidunes and gravel lenses: An example from Montserrat, West Indies. *Sedimentology*, **64**, 1817–1845.
- Gallego, O.F.** (2010) A new crustacean clam shrimp (Spinicaudata: Eosestheriidae) from the Upper Triassic of Argentina and its importance for ‘conchostracan’ taxonomy. *Alcheringa An Australas. J. Palaeontol.*, **34**, 179–195.
- Gastaldo, R.A. and Neveling, J.** (2016) Comment on: “Anatomy of a mass extinction: Sedimentological and taphonomic evidence for drought-induced die-offs at the Permo-Triassic boundary in the main Karoo Basin, South Africa” by R.M.H. Smith and J. Botha-Brink, *Palaeogeography, Palaeoclimatology, Palaeoecol.*, **447**, 88–91.
- Ghienne, J.F., Normandeau, A., Dietrich, P., Bouysson, M., Lajeunesse, P. and Schuster, M.** (2021) The depositional signature of cyclic steps: A late Quaternary analogue compared to modern active delta slopes. *Sedimentology*, **68**, 1502–1538.
- Gilbert, G.K. and Murphy, E.C.** (1914) The transport of debris by running water. Sacramento, 265 pp.
- Goldberg, K.** (2001) The Paleoclimatic evolution of the Permian in the Paraná Basin in southern Brazil. University of Chicago
- Golden, D.C., Dixon, J.B. and Chen, C.C.** (1986) Ion Exchange, Thermal Transformations, and Oxidizing Properties of Birnessite. *Clays Clay Miner.*, **34**, 511–520.
- Goso, C., Piñero, G., de Santa Ana, H., Rojas, A., Verde, M. and Alves, C.** (2001) Caracterización estratigráfica de los depósitos continentales cuspidales neopérmicos (Formaciones Yaguari y Buena Vista) en el borde oriental de la Cuenca Norte Uruguay. In: *Actas del XI Congreso Latinoamericano de Geología*, Montevideo, 18 (CD-ROM).

- Goudie, A.** (1973) Duricrusts in tropical and subtropical landscapes. *Clarendon Press*, Oxford, Uited Kingdom, 174 pp.
- Goudie, A.S.** (1983) Calcrete. In: *Chemical Sediments and Geomorphology* (Ed. A.S. Goudie and K. Pye), *Academic Press*, London, UK, 93–131.
- Gould, S.J.** (1991) Seta do Tempo, Ciclo do Tempo. *Cia. das Letras*, São Paulo, 221 pp.
- Gulbranson, E.L., Ciccioli, P.L., Montañez, I.P., Marensi, S.A., Limarino, C.O., Schmitz, M.D. and Davydov, V.** (2015) Paleoenvironments and age of the Talampaya Formation: The Permo-Triassic boundary in northwestern Argentina. *J. South Am. Earth Sci.*, **63**, 310–322.
- Guy, H.P., Simons, D.B. and Richardson, E.V.** (1966) Summary of Alluvial Channel Data From Flume Experiments , 1956-61. *U. S. Geol. Surv. Prof. Pap.*, **462-I**, 1–104.
- Hallam, A. and Wignall, P.B.** (1997) Mass Extinctions and their Aftermath. *Oxford University Press*, Oxford, Uited Kingdom, 328 pp.
- Hansford, M.R., Plink-Björklund, P. and Jones, E.R.** (2020) Global quantitative analyses of river discharge variability and hydrograph shape with respect to climate types. *Earth-Science Rev.* doi: 10.1016/j.earscirev.2019.102977
- Harris, R., McCall, R., Randall, O., Bin Tawang, M.H., Williams, R., Fairman, J.G. and Schultz, D.M.** (2017) Climate change during the Triassic and Jurassic. *Geol. Today*, **33**, 210–215.
- Holz, M.** (2015) Mesozoic paleogeography and paleoclimates – A discussion of the diverse greenhouse and hothouse conditions of an alien world. *J. South Am. Earth Sci.*, **61**, 91–107.
- Horn, B.L.D., Goldberg, K. and Schultz, C.L.** (2018a) Interpretation of massive sandstones in ephemeral fluvial settings: A case study from the Upper Candelária Sequence (Upper Triassic, Paraná Basin, Brazil). *J. South Am. Earth Sci.*, **81**, 108–121.
- Horn, B.L.D., Goldberg, K. and Schultz, C.L.** (2018b) A loess deposit in the Late Triassic of southern Gondwana, and its significance to global paleoclimate. *J. South Am. Earth Sci.*, **81**, 189–203.
- Horn, B.L.D., Melo, T.P., Schultz, C.L., Philipp, R.P., Kloss, H.P. and Goldberg, K.** (2014) A new third-order sequence stratigraphic framework applied to the Triassic of the Paraná Basin, Rio Grande do Sul, Brazil, based on structural, stratigraphic and paleontological data. *J. South Am. Earth Sci.*, **55**, 123–132.
- Horn, B.L.D., Pereira, V.P. and Schultz, C.L.** (2013) Calcretes of the Santa Maria Supersequence, Middle Triassic, Rio Grande do Sul, Brazil: Classification, genesis and paleoclimatic implications. *Palaeogeogr. Palaeoclimatol. Palaeoecol.*, **376**, 39–47.
- Irmis, R.B. and Whiteside, J.H.** (2012) Delayed recovery of non-marine tetrapods after the end-permian mass extinction tracks global carbon cycle. *Proc. R. Soc. B Biol. Sci.*, **279**, 1310–1318.
- James, M.R. and Robson, S.** (2012) Straightforward reconstruction of 3D surfaces and topography with a camera: Accuracy and geoscience application. *J. Geophys. Res. Earth Surf.*, **117**, 1–17.

- Jefferson, I., Rosenbaum, M. and Smalley, I.** (2002) Mercia Mudstone as a Triassic aeolian desert sediment. *Mercian Geol.*, **15**, 157–162.
- Jeong, G.Y.** (2008) Bulk and single-particle mineralogy of Asian dust and a comparison with its source soils. *J Geophys Res Atmos.* doi: 10.1029/2007JD008606
- Jeong, G.Y., Hillier, S. and Kemp, R.A.** (2011) Changes in mineralogy of loess-paleosol sections across the Chinese Loess Plateau. *Quat. Res.*, **75**, 245–255.
- Johnson, S.Y.** (1989) Significance of Loessite in the Maroon Formation (Middle Pennsylvanian to Lower Permian), Eagle Basin, Northwest Colorado. *J. Sediment. Res.*, **Vol. 59**, 782–791.
- Kabata-Pendias, A.** (2010) Trace Elements in Soils and Plants, 4th edn. *CRC Press*, Boca Raton, USA, 548 pp.
- Kemp, R.A.** (1987) Genesis and environmental significance of a buried middle pleistocene soil in Eastern England. *Geoderma*, **41**, 49–77.
- Kennedy, J.F.** (1963) The mechanics of dunes and antidunes in erodible-bed channels. *J. Fluid Mech.*, **16**, 521–544.
- Kennedy, J.F.** (1960) Stationary waves and antidunes in alluvial channels. California Institute of Technology
- Kessler, J.L.P., Soreghan, G.S. and Wacker, H.J.** (2001) Equatorial Aridity in Western Pangea: Lower Permian Loessite and Dolomitic Paleosols in Northeastern New Mexico, U.S.A. *J. Sediment. Res.*, **71**, 817–832.
- Kiessling, W., Flügel, E. and Golonka, J.** (eds) (2002) Phanerozoic Reef Patterns. *SEPM (Society for Sedimentary Geology)*, 775 pp.
- Kirchner, J.W. and Weil, A.** (2000) Delayed biological recovery from extinctions throughout the fossil record. *Nature*, **404**, 177–180.
- Knapp, J.** (2020) Alluvial Fans, Loess Plains, Lakes, and Distributive Fluvial Systems: Depositional Systems of the Permian-Triassic Red Beds and Evaporites of Wyoming (USA). West Virginia University
- Krapovickas, V., Mancuso, A.C., Marsicano, C.A., Domnanovic, N.S. and Schultz, C.L.** (2013) Large tetrapod burrows from the Middle Triassic of Argentina: a behavioural adaptation to seasonal semi-arid climate? *Lethaia*, **46**, 154–169.
- Kraus, M.J.** (1999) Paleosols in clastic sedimentary rocks: their geologic applications. *Earth-Science Rev.*, **47**, 41–70.
- Kutzbach, J.E. and Gallimore, R.G.** (1989) Pangaeian climates: Megamonsoons of the megacontinent. *J. Geophys. Res.*, **94**, 3341–3357.
- Labandeira, C. and Sepkoski, J.** (1993) Insect diversity in the fossil record. *Science (80-.)*, **261**, 310–315.

- Lamb, M.P., Parsons, J.D., Mullenbach, B.L., Finlayson, D.P., Orange, D.L. and Nittrouer, C.A.** (2008) Evidence for superelevation, channel incision, and formation of cyclic steps by turbidity currents in Eel Canyon, California. *Bull. Geol. Soc. Am.*, **120**, 463–475.
- Lang, J., Le Heron, D.P., Van den Berg, J.H. and Winsemann, J.** (2021) Bedforms and sedimentary structures related to supercritical flows in glacial settings. *Sedimentology*, **68**, 1539–1579.
- Lang, J., Sievers, J., Loewer, M., Igel, J. and Winsemann, J.** (2017) 3D architecture of cyclic-step and antidune deposits in glacial subaqueous fan and delta settings: Integrating outcrop and ground-penetrating radar data. *Sediment. Geol.*, **362**, 83–100.
- Lang, J. and Winsemann, J.** (2013) Lateral and vertical facies relationships of bedforms deposited by aggrading supercritical flows: From cyclic steps to humpback dunes. *Sediment. Geol.*, **296**, 36–54.
- Lavina, E.L.C.** (1983) *Procolophon pricei* sp.n., um novo réptil procolofonídeo do Triássico do Rio Grande do Sul. *Iheringia, Série Geológica*, **9**, 51–78.
- Lavina, E.L.C.** (1991) Geologia sedimentar e paleogeografia do Neopermiano e Eotriássico (intervalo Kazaniano-Scythiano) da Bacia do Paraná. Universidade Federal do Rio Grande do Sul - UFRGS
- Li, J., Gastaldo, R.A., Neveling, J. and Geissman, J.W.** (2017) Siltstones across the *Daptocephalus* (*Dicynodon*) and *Lystrosaurus* assemblage zones, Karoo Basin, South Africa, show no evidence for aridification. *J. Sediment. Res.*, **87**, 653–671.
- Li, Y., Shi, W., Aydin, A., Beroya-Eitner, M.A. and Gao, G.** (2020) Loess genesis and worldwide distribution. *Earth-Science Rev.*, **201**, 22.
- Lighthill, J.** (1978) *Waves in Fluids*. Cambridge University Press, Cambridge, 504 pp.
- Looy, C. V., Brugman, W.A., Dilcher, D.L. and Visscher, H.** (1999) The delayed resurgence of equatorial forests after the Permian–Triassic ecologic crisis. *Proc. Natl. Acad. Sci.*, **96**, 13857–13862.
- Lowe, D.R. and LoPiccolo, R.D.** (1974) The Characteristics and Origins of Dish and Pillar Structures. *J. Sediment. Res.*, **44**, 484–501.
- Luppo, T., López de Luchi, M.G., Rapalini, A.E., Martínez Dopico, C.I. and Fanning, C.M.** (2018) Geochronologic evidence of a large magmatic province in northern Patagonia encompassing the Permian-Triassic boundary. *J. South Am. Earth Sci.*, **82**, 346–355.
- MacDougall, M.J., Brocklehurst, N. and Fröbisch, J.** (2019) Species richness and disparity of parareptiles across the end-Permian mass extinction. *Proc. R. Soc. B Biol. Sci.*, **286**, 20182572.
- Mancuso, A.C., Horn, B.L.D., Benavente, C.A., Schultz, C.L. and Irmis, R.B.** (2021) The paleoclimatic context for South American Triassic vertebrate evolution. *J. South Am. Earth Sci.*, **110**, 103321.
- Manna, M.O., Scherer, C.M. dos S., Bállico, M.B., Reis, A.D. dos, Moraes, L.V., Ferrari, L.A.B.,**

- Roisenberg, H.B. and Oliveira, V.G. de** (2021) Changes in fluvial architecture induced by discharge variability, Jaicós Formation (Silurian-Devonian), Parnaíba Basin, Brazil. *Sediment. Geol.*, **420**, 105924.
- Mao, X., Liu, X. and Zhou, X.** (2021) Permo-Triassic aeolian red clay of southwestern England and its palaeoenvironmental implications. *Aeolian Res.*, **52**, 100726.
- Mays, C., McLoughlin, S., Frank, T.D., Fielding, C.R., Slater, S.M. and Vajda, V.** (2021) Lethal microbial blooms delayed freshwater ecosystem recovery following the end-Permian extinction. *Nat. Commun.*, **12**, 5511.
- Mays, C., Vajda, V., Frank, T.D., Fielding, C.R., Nicoll, R.S., Tevyaw, A.P. and McLoughlin, S.** (2020) Refined Permian–Triassic floristic timeline reveals early collapse and delayed recovery of south polar terrestrial ecosystems. *GSA Bull.*, **132**, 1489–1513.
- McKee, E.D., Crosby, E.J. and Berryhill, H.L.** (1967) Flood deposits, Bijou Creek, Colorado, June 1965. *J. Sediment. Res.*, **37**, 829–851.
- McKenzie, R.M.** (1989) Manganese Oxides and Hydroxides. In: *Minerals in Soil environments*, 2nd edn. (Ed. J.B. Dixon and S.B. Weed), *Soil Science Society of America*, Madison, USA, 439–465.
- Meijer, N., Dupont-Nivet, G., Licht, A., Trabucho-Alexandre, J., Bourquin, S. and Abels, H.A.** (2020) Identifying eolian dust in the geological record. *Earth-Science Rev.* doi: 10.1016/j.earscirev.2020.103410
- Miall, A.D.** (1985) Architectural-element analysis: A new method of facies analysis applied to fluvial deposits. *Earth Sci. Rev.*, **22**, 261–308.
- Miall, A.D.** (2016) *Stratigraphy: A Modern Synthesis*. Springer International Publishing, Cham, Switzerland, 454 pp.
- Miall, A.D.** (1988) Facies architecture in clastic sedimentary basins. In: *New perspectives in basin analysis* (Ed. K. Kleinspehn and C. Paola), Springer-Verlag, New York, 67–81.
- Miall, A.D.** (1977) A review of the braided-river depositional environment. *Earth-Science Rev.*, **13**, 1–62.
- Michell, J.H.** (1893) XLIV. The highest waves in water. *London, Edinburgh, Dublin Philos. Mag. J. Sci.*, **36**, 430–437.
- Milani, E.J.** (2004) Comentários sobre a origem e a evolução tectônica da Bacia do Paraná. In: *Geologia do Continente Sul-Americano: evolução da obra de Fernando Flávio Marques de Almeida* (Ed. V. Mantesso-Neto, A. Bartorelli, C.D.R. Carneiro, and B.B. de Brito-Neves), *Beca*, São Paulo, 265–280.
- Milani, E.J.** (1997) Evolução tectono-estratigráfica da Bacia do Paraná e seu relacionamento com a geodinâmica fanerozóica do Gondwana sul-ocidental. Universidade Federal do Rio Grande do Sul
- Milani, E.J., Melo, J.H.G., Souza, P.A., Fernandes, L.A. and França, A.B.** (2007) Bacia do Paraná.

Bol. Geociências da Petrobras, **15**, 265–287.

- Milani, E.J. and Thomaz Filho, A.** (2000) Sedimentary Basins of South America. In: *Tectonic Evolution of South America* (Ed. U.G. Cordani, E.J. Milani, A. Thomaz Filho, and D. de A. Campos), *31st International Geological Congress*, Rio de Janeiro, 389–449.
- Neveling, J., Rubidge, B.S. and Hancox, P.J.** (1999) A lower Cynognathus Assemblage Zone fossil from the Katberg Formation (Beaufort Group, South Africa). *S. Afr. J. Sci.*, **95**, 555–556.
- Nicholas, A.P., Sambrook Smith, G.H., Amsler, M.L., Ashworth, P.J., Best, J.L., Hardy, R.J., Lane, S.N., Orfeo, O., Parsons, D.R., Reesink, A.J.H., Sandbach, S.D., Simpson, C.J. and Szupiany, R.N.** (2016) The role of discharge variability in determining alluvial stratigraphy. *Geology*, **44**, 3–6.
- Nicolas, M. and Rubidge, B.S.** (2010) Changes in Permo-Triassic terrestrial tetrapod ecological representation in the Beaufort Group (Karoo Supergroup) of South Africa. *Lethaia*, **43**, 45–59.
- North, C.P. and Davidson, S.K.** (2012) Unconfined alluvial flow processes: Recognition and interpretation of their deposits, and the significance for palaeogeographic reconstruction. *Earth-Science Rev.*, **111**, 199–223.
- North, C.P. and Taylor, K.S.** (1996) Ephemeral-fluvial deposits: Integrated outcrop and simulation studies reveal complexity. *Am. Assoc. Pet. Geol. Bull.*, **80**, 811–830.
- Olsen, P.E. and Kent, D. V.** (1996) Milankovitch climate forcing in the tropics of Pangaea during the Late Triassic. *Palaeogeogr. Palaeoclimatol. Palaeoecol.*, **122**, 1–26.
- Ono, K., Plink-Björklund, P., Eggenhuisen, J.T. and Cartigny, M.J.B.** (2021) Froude supercritical flow processes and sedimentary structures: New insights from experiments with a wide range of grain sizes. *Sedimentology*, **68**, 1328–1357.
- Ore, H.T.** (1964) Some criteria for recognition of braided stream deposits. *Rocky Mt. Geol.*, **3**, 1–14.
- Owens, J.S.** (1908) Experiments on the Transporting Power of Sea Currents. *Geogr. J.*, **31**, 415.
- Parker, G.** (1996) Some Speculations on the Relation Between Channel Morphology and Channel-scale Flow Structures. In: *Coherent Flow Structures in Open Channels* (Ed. P.J. Ashworth, S.J. Bennett, J.L. Best, and S.J. McLelland), *John Wiley & Sons*, Chichester, 423–458.
- Parker, G. and Izumi, N.** (2000) Purely erosional cyclic and solitary steps created by flow over a cohesive bed. *J. Fluid Mech.*, **419**, 203–238.
- Parrish, J.T.** (1993) Climate of the Supercontinent Pangea. *J. Geol.*, **101**, 215–233.
- Payton, R.W.** (1993) Fragipan formation in argillic brown earths (Fragiudalfs) of the Milfield Plain, north-east England. II. Post Devensian developmental processes and the origin of fragipan consistence. *J. Soil Sci.*, **44**, 703–723.
- Penn, J.L., Deutsch, C., Payne, J.L. and Sperling, E.A.** (2018) Temperature-dependent hypoxia explains biogeography and severity of end-Permian marine mass extinction. *Science* (80-). doi: 10.1126/science.aat1327

- Phillips, J.** (1860) Life on the earth : its origin and succession. *Macmillan and co.*, Cambridge, London, 276 pp.
- Piñeiro, G., Ferigolo, J., Ribeiro, A.M. and Velozo, P.** (2015) Reassessing the affinities of vertebral remains from Permo-Triassic beds of Gondwana. *Comptes Rendus - Palevol*, **14**, 387–401.
- Piñeiro, G., Marsicano, C., Goso, C. and Morosi, E.** (2007) Temnospondyl diversity of the Permian-Triassic Colonia Orozco Local Fauna (Buena Vista Formation) of Uruguay. *Rev. Bras. Paleontol.*, **10**, 169–180.
- Piñeiro, G., Ramos, A. and Marsicano, C.** (2012) A rhinesuchid-like temnospondyl from the Permo-Triassic of Uruguay. *Comptes Rendus - Palevol*, **11**, 65–78.
- Piñeiro, G., Rojas, A. and Ubilla, M.** (2004) A new procolophonoid (Reptilia, Parareptilia) from the Upper Permian of Uruguay. *J. Vertebr. Paleontol.*, **24**, 814–821.
- Piñeiro, G., Verde, M., Ubilla, M. and Ferigolo, J.** (2003) First basal synapsids (“pelycosaurs”) from the Upper Permian-Lower Triassic of Uruguay, South America. *J. Paleontol.*, **77**, 389–392.
- Pinheiro, F.L., França, M.A.G., Lacerda, M.B., Butler, R.J. and Schultz, C.L.** (2016) An exceptional fossil skull from South America and the origins of the archosauriform radiation. *Sci. Rep.*, **6**, 1–7.
- Plink-Björklund, P.** (2015) Morphodynamics of rivers strongly affected by monsoon precipitation: Review of depositional style and forcing factors. *Sediment. Geol.* **323**:110–147.
- Potter, R.M. and Rossman, G.R.** (1979) Mineralogy of manganese dendrites and coatings. *Am. Mineral.*, **64**, 1219–1226.
- Preto, N., Kustatscher, E. and Wignall, P.B.** (2010) Triassic climates — State of the art and perspectives. *Palaeogeogr. Palaeoclimatol. Palaeoecol.*, **290**, 1–10.
- Pye, K.** (1987) Aeolian Dust and Dust Deposits. *Academic Press*, London, UK, 334 pp.
- Racki, G.** (1999) Silica-secreting biota and mass extinctions: survival patterns and processes. *Palaeogeogr. Palaeoclimatol. Palaeoecol.*, **154**, 107–132.
- Raup, D.M.** (1979) Size of the Permo-Triassic Bottleneck and Its Evolutionary Implications. *Science* (80-), **206**, 217–218.
- Reis, A.D. dos, Scherer, C.M. dos S., Amarante, F.B. do, Rossetti, M. de M.M., Kifumbi, C., Souza, E.G. de, Ferronato, J.P.F. and Owen, A.** (2019) Sedimentology of the proximal portion of a large-scale, Upper Jurassic fluvial-aeolian system in Paraná Basin, southwestern Gondwana. *J. South Am. Earth Sci.*, **95**, 102248.
- Reis, A.D. Dos, Scherer, C.M.D.S., Owen, A., Amarante, F.B. Do, Ferronato, J.P.F., Pantopoulos, G., de Souza, E.G., Bállico, M.B. and Aguilar, C.A.G.** (2022) a Quantitative Depositional Model of a Large Distributive Fluvial System (Megafan) With Terminal Aeolian Interaction: the Upper Jurassic Guar4 Dfs in Southwestern Gondwana. *J. Sediment. Res.*, **92**, 460–485.
- Retallack, G.J.** (1988) Field recognition of paleosols. In: *Paleosols and Weathering Through Geologic*

Time: Principles and Applications (Ed. J. Reinhardt and W.R. Sigleo), *Geological Society of America*, 1–20.

- Retallack, G.J.** (2001) *Soils of the Past: An Introduction to Paleopedology*, 2nd edn. *Wiley*, 404 pp.
- Retallack, G.J., Veevers, J.J. and Morante, R.** (1996) Global coal gap between Permian–Triassic extinction and Middle Triassic recovery of peat-forming plants. *Geol. Soc. Am. Bull.*, **108**, 195–207.
- Robertson, J.M. and Rouse, H.** (1941) On the Four Regimes of Open Channel Flow. *Civ. Eng. (New York)*, **11**, 169–171.
- Rubidge, B.S.** (2005) Re-uniting lost continents - Fossil reptiles from the ancient Karoo and their wanderlust. *South African J. Geol.*, **108**, 135–172.
- Ruta, M. and Benton, M.J.** (2008) Calibrated diversity, tree topology and the mother of mass extinctions: The lesson of temnospondyls. *Palaeontology*, **51**, 1261–1288.
- Sahney, S. and Benton, M.J.** (2008) Recovery from the most profound mass extinction of all time. *Proc. R. Soc. B Biol. Sci.*, **275**, 759–765.
- Saunderson, H.C. and Lockett, F.P.J.** (1983) Flume Experiments on Bedforms and Structures at the Dune-Bed Transition. In: *Modern and Ancient Fluvial Systems* (Ed. J.D. Collinson and J. Lewin), *Blackwell Publishing Ltd.*, Oxford, UK, 49–58.
- Scherer, C.M. dos S., Lavina, E.L.C., Reis, A.D. dos and Horn, B.L.D.** (2021) Estratigrafia da sucessão sedimentar mesozoica da Bacia do Paraná no Rio Grande do Sul. In: *Contribuições a Geologia do Rio Grande do Sul e de Santa Catarina* (Ed. A.R. Jelinek and C.A. Sommer), *Sociedade Brasileira de Geologia Núcleo RS/SC, Compasso Lugar-Cultura*, Porto Alegre, 289–304.
- Scherer, C.M.S., Reis, A.D., Horn, B.L.D., Bertolini, G., Lavina, E.L.C., Kifumbi, C. and Goso Aguiar, C.** (2023) The stratigraphic puzzle of the permo-mesozoic southwestern Gondwana: The Paraná Basin record in geotectonic and palaeoclimatic context. *Earth-Science Rev.*, **240**, 104397.
- Schmidt, V. and McDonald, D.A.** (1979) The Role of Secondary Porosity in the Course of Sandstone Diagenesis. In: *Aspects of Diagenesis*, Special Pu (Ed. P.A. Scholle and P.R. Schluger), *SEPM (Society for Sedimentary Geology)*, Tulsa, Oklahoma, U.S.A., 175–207.
- Schneider, R.L., Mühlmann, H., Tommasi, E., Medeiros, R.A., Daemon, R.F. and Nogueira, A.A.** (1974) Revisão estratigráfica da Bacia do Paraná. In: *Anais do Congresso Brasileiro de Geologia, Sociedade Brasileira de Geologia*, Porto Alegre, 1, 41–65.
- Schultz, C.L., Martinelli, A.G., Soares, M.B., Pinheiro, F.L., Kerber, L., Horn, B.L.D., Pretto, F.A., Müller, R.T. and Melo, T.P.** (2020) Triassic faunal successions of the Paraná Basin, southern Brazil. *J. South Am. Earth Sci.*, **104**, 102846.
- Sellwood, B.W. and Valdes, P.J.** (2006) Mesozoic climates: General circulation models and the rock

- record. *Sediment. Geol.*, **190**, 269–287.
- Sepkoski, J.J.** (1984) A kinetic model of Phanerozoic taxonomic diversity. III. Post-Paleozoic families and mass extinctions. *Paleobiology*, **10**, 246–267.
- Simons, D.B.** and **Richardson, E.V.** (1961) Forms of Bed Roughness in Alluvial Channels. *J. Hydraul. Div.*, **87**, 87–105.
- Singer, A.** (1988) Illite in aridic soils, desert dusts and desert loess. *Sediment. Geol.*, **59**, 251–259.
- Singh, A.** and **Bhardwaj, B.D.** (1991) Fluvial facies model of the Ganga River sediments, India. *Sediment. Geol.*, **72**, 135–146.
- Slotman, A.** and **Cartigny, M.J.B.** (2020) Cyclic steps: Review and aggradation-based classification. *Earth-Science Rev.* doi: 10.1016/j.earscirev.2019.102949
- Slotman, A., Vellinga, A.J., Moscariello, A.** and **Cartigny, M.J.B.** (2021) The depositional signature of high-aggradation chute-and-pool bedforms: The build-and-fill structure. *Sedimentology*, **68**, 1640–1673.
- Smith, R.M.H.** and **Botha-Brink, J.** (2014) Anatomy of a mass extinction: Sedimentological and taphonomic evidence for drought-induced die-offs at the Permo-Triassic boundary in the main Karoo Basin, South Africa. *Palaeogeogr. Palaeoclimatol. Palaeoecol.*, **396**, 99–118.
- Sneh, A.** (1983) Desert Stream Sequences in the Sinai Peninsula. *J. Sediment. Res.*, **53**, 1271–1279.
- Soreghan, G.S.L., Elmore, R.D.** and **Lewchuck, M.T.** (2002) Sedimentologic-magnetic record of western Pangean climate in upper Paleozoic loessite (lower Cutler beds, Utah). *Bull. Geol. Soc. Am.*, **114**, 1019–1035.
- Southard, J.B.** and **Boguchwal, L.A.** (1990) Bed configuration in steady unidirectional water flows; Part 2, Synthesis of flume data. *J. Sediment. Res.*, **60**, 658–679.
- Spinewine, B., Sequeiros, O.E., Garcia, M.H., Beaubouef, R.T., Sun, T., Savoye, B.** and **Parker, G.** (2009) Experiments on wedge-shaped deep sea sedimentary deposits in minibasins and/or on channel levees emplaced by turbidity currents. Part II. Morphodynamic evolution of the wedge and of the associated bedforms. *J. Sediment. Res.*, **79**, 608–628.
- Stanley, S.M.** (2016) Estimates of the magnitudes of major marine mass extinctions in earth history. *Proc. Natl. Acad. Sci.*, **113**, E6325–E6334.
- Tan, C.** and **Plink-Björklund, P.** (2021) Morphodynamics of supercritical flow in a linked river and delta system, Daihai Lake, Northern China. *Sedimentology*, **68**, 1606–1639.
- Trendell, A.M., Nordt, L.C., Atchley, S.C., Leblanc, S.L.** and **Dworkin, S.I.** (2013) Determining floodplain plant distributions and populations using paleopedology and fossil root traces: Upper Triassic Sonsela Member of the Chinle Formation at Petrified Forest National Park, Arizona. *Palaios*, **28**, 471–490.
- Tunbridge, I.P.** (1981) Sandy high-energy flood sedimentation — Some criteria for recognition, with an

example from the Devonian of S.W. England. *Sediment. Geol.*, **28**, 79–95.

- Vail, P.R., Mitchum, R.M. and Thompson, S.** (1977) Seismic stratigraphy and global changes of sea level, part 3: relative changes of sea level from coastal onlap. In: *Seismic stratigraphy - applications to hydrocarbon exploration*, Memoir 26 (Ed. C.E. Payton), *American Association of Petroleum Geologists*, Tulsa, 63–81.
- Vaisblat, N., Harris, N.B., Ayranci, K., Power, M., DeBhur, C., Bish, D.L., Chalaturnyk, R., Krause, F., Crombez, V., Euzen, T. and Rohais, S.** (2021) Compositional and diagenetic evolution of a siltstone, with implications for reservoir quality; an example from the Lower Triassic Montney Formation in western Canada. *Mar. Pet. Geol.*, **129**, 29.
- Van Valen, L.M.** (1984) A resetting of Phanerozoic community evolution. *Nature*, **307**, 50–52.
- Viglietti, P.A., Rojas, A., Rosvall, M., Klimes, B. and Angielczyk, K.D.** (2022) Network-based biostratigraphy for the late Permian to mid-Triassic Beaufort Group (Karoo Supergroup) in South Africa enhances biozone applicability and stratigraphic correlation. *Palaeontology*. doi: 10.1111/pala.12622
- Walker, S. and Holbrook, J.** (2022) Structures, architecture, vertical profiles, palaeohydrology and taphonomy of an upper-flow-regime-dominated fluvial system, the Triassic Dockum Group of the Palo Duro Canyon, Texas. *Sedimentology*, **70**, 645–684.
- Walker, T.R., Waugh, B. and Grone, A.J.** (1978) Diagenesis in first-cycle desert alluvium of Cenozoic age, southwestern United States and northwestern Mexico. *Geol. Soc. Am. Bull.*, **89**, 19.
- Wilkins, A.D., Hurst, A., Wilson, M.J. and Archer, S.** (2018) Palaeo-environment in an ancient low-latitude, arid lacustrine basin with loessite: The Smith Bank Formation (Early Triassic) in the Central North Sea, UK Continental Shelf. *Sedimentology*, **65**, 335–359.
- Wilson, K.M., Pollard, D., Hay, W.W., Thompson, S.L. and Wold, C.N.** (1994) General circulation model simulations of Triassic climates: Preliminary results. *Pangea Paleoclimate, Tectonics, Sediment. Dur. Accretion, Zenith, Break. a Supercontinent*, **288**, 91–116.
- Wilson, M.J., Hurst, A., Wilkins, A.D., Wilson, L. and Bowen, L.** (2020) Mineralogical evidence for multiple dust sources in an early Triassic loessite. *Sedimentology*, **67**, 239–260.
- Winguth, A.M.E., Shields, C.A. and Winguth, C.** (2015) Transition into a Hothouse World at the Permian–Triassic boundary—A model study. *Palaeogeogr. Palaeoclimatol. Palaeoecol.*, **440**, 316–327.
- Wright, V.P.** (2007) Calcrete. In: *Geochemical Sediments and Landscapes* (Ed. D.J. Nash and S.J. McLaren), *Blackwell Publishing Ltd.*, 10–45.
- Wright, V.P.** (1990) A micromorphological classification of fossil and recent calcic and petrocalcic microstructures. In: *Soil Micromorphology: A Basic and Applied Science* (Ed. L.A. Douglas), *Elsevier*, Amsterdam, 401–407.

- Wright, V.P., Marriott, S.B. and Vanstone, S.D.** (1991) A “reg” palaeosol from the Lower Triassic of south Devon: stratigraphic and palaeoclimatic implications. *Geol. Mag.*, **128**, 517–523.
- Wright, V.P. and Tucker, M.E.** (1991) Calcretes: an introduction. In: *Calcretes* (Ed. V.P. Wright and M.E. Tucker), *Blackwell Scientific Publications*, Oxford, Uited Kingdom, 1–22.
- Wu, H., Zhang, S., Feng, Q., Jiang, G., Li, H. and Yang, T.** (2012) Milankovitch and sub-Milankovitch cycles of the early Triassic Daye Formation, South China and their geochronological and paleoclimatic implications. *Gondwana Res.*, **22**, 748–759.
- Xavier, P.L.A., Scherer, C.M. dos S., Reis, A.D. dos, Souza, E.G. de, Guadagnin, F. and Piñeiro, G.** (2023) Supercritical fluvial styles and the shifting aridity in the Early Triassic: the example of the Sanga do Cabral Formation, Paraná Basin, Brazil. *J Sediment Res.* doi: 10.2110/jsr.2022.063
- Yokokawa, M., Hasegawa, K., Kanbayashi, S. and Endo, N.** (2010) Formative conditions and sedimentary structures of sandy 3D antidunes: An application of the gravel step-pool model to fine-grained sand in an experimental flume. *Earth Surf. Process. Landforms*, **35**, 1720–1729.
- Zálan, P.V., Wolff, S., Conceição, J.C.J., Astolfi, M.A.M., Vieira, I.S., Appi, V.T., Zanotto, O.A. and Marques, A.** (1991) Tectonics and sedimentation of the Paraná Basin. In: *Proceedings of the 7th International Gondwana Symposium* (Ed. H.H.G.J. Ulbrich and A.C. Rocha-Campos), *Instituto de Geociências, USP*, São Paulo, 83–117.
- Zellman, K.L., Plink-Björklund, P. and Fricke, H.C.** (2021) Testing hypotheses on signatures of precipitation variability in the river and floodplain deposits of the Paleogene San Juan Basin, New Mexico, U.S.A. *J. Sediment. Res.*, **90**, 1770–1801.
- Zerfass, H.** (1998) Estratigrafia da Sedimentação Meso e Neotriássica no Município de São Pedro do Sul, RS: Faciologia, Análise de Proveniência e História Diagenética. Universidade do Vale do Rio dos Sinos - UNISINOS
- Zerfass, H., Chemale, F., Schultz, C.L. and Lavina, E.** (2004) Tectonics and sedimentation in Southern South America during Triassic. *Sediment. Geol.*, **166**, 265–292.
- Zerfass, H., Garcia, A.J.V., Susczunski, A.M. and Lavina, E.L.C.** (2000) Análise de proveniência dos arenitos Neopermianos e Triássicos da Bacia do Paraná na região de São Pedro do Sul (RS): uma contribuição para o conhecimento da arquitetura estratigráfica e da evolução tectono-sedimentar. *Acta Geol. Leopoldensia*, **XXIII**, 61–84.
- Zerfass, H., Lavina, E.L., Schultz, C.L., Garcia, A.J.V., Faccini, U.F. and Chemale Jr, F.** (2003) Sequence stratigraphy of continental Triassic strata of Southernmost Brazil: a contribution to Southwestern Gondwana palaeogeography and palaeoclimate. *Sediment. Geol.*, **161**, 85–105.
- Zhao, C., Fang, H., Liu, Y., Dey, S. and He, G.** (2020) Impact of Particle Shape on Saltating Mode of Bedload Transport Sheared by Turbulent Flow. *J. Hydraul. Eng.*, **146**, 1–13.
- Zhong, G., Cartigny, M.J.B., Kuang, Z. and Wang, L.** (2015) Cyclic steps along the South Taiwan Shoal and West Penghu submarine canyons on the northeastern continental slope of the South

China Sea. *Bull. Geol. Soc. Am.*, **127**, 804–824.

ANEXOS

Anexo I — Material suplementar do segundo artigo.

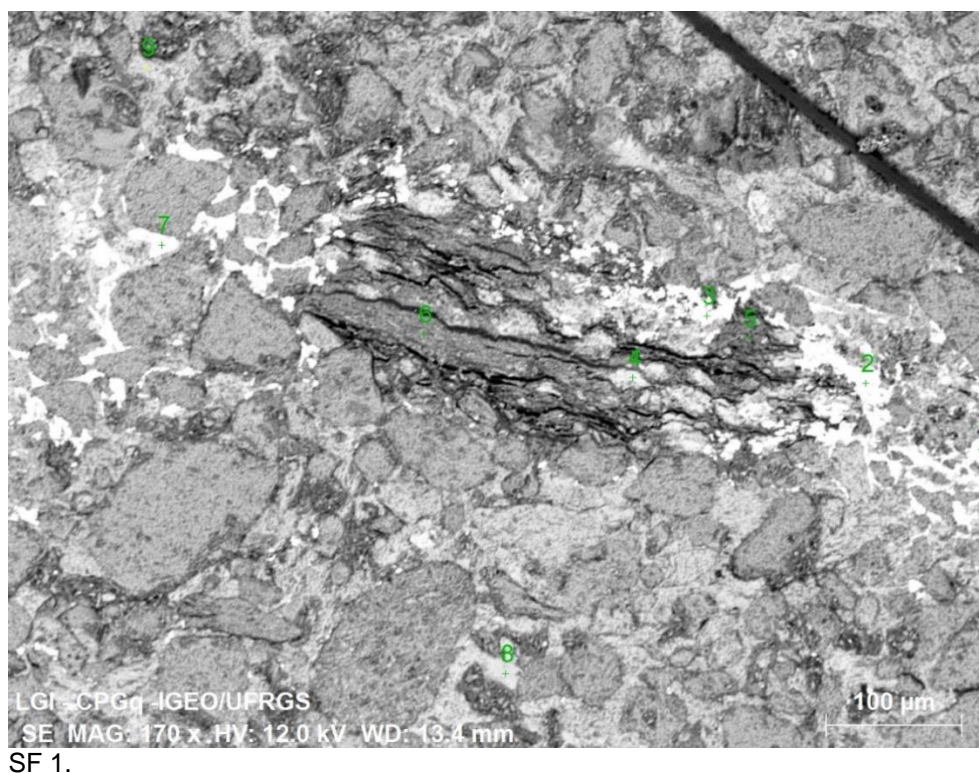


Table S1.

Spectrum: 1

El	AN	Series	unn. C norm.	C norm.	C Atom.	C Compound	Comp.	C norm.	Comp.	C Error (1 Sigma)
			[wt.%]	[wt.%]	[at.%]		[wt.%]	[wt.%]		[wt.%]
C	6	K-series	0.00	0.00	0.00		0.00	0.00		0.00
O	8	K-series	14.99	20.71	45.53		0.00	0.00		1.94
F	9	K-series	4.88	6.75	12.49		6.75	4.88		0.92
Al	13	K-series	1.07	1.47	1.92	Al ₂ O ₃	2.79	2.02		0.09
Si	14	K-series	1.50	2.08	2.60	SiO ₂	4.44	3.22		0.10
Ca	20	K-series	0.55	0.75	0.66	CaO	1.06	0.76		0.06
Mn	25	K-series	36.40	50.29	32.19	MnO	64.93	47.00		1.30
Ba	56	L-series	12.99	17.94	4.60	BaO	20.04	14.50		0.48

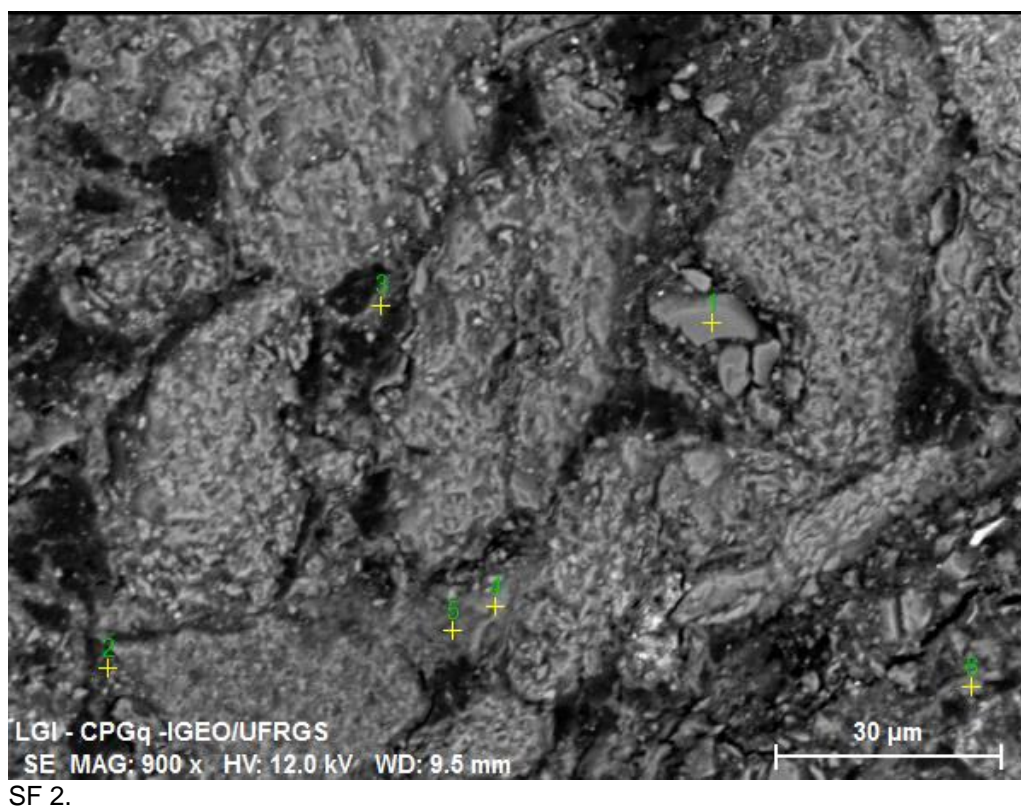
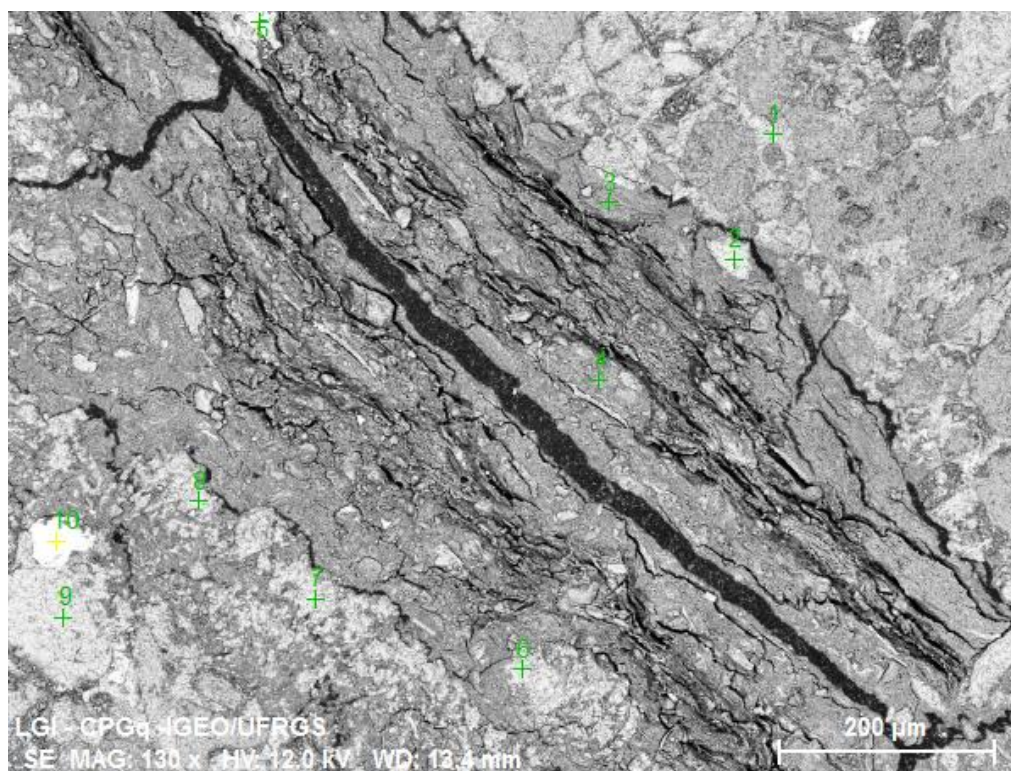


Table S2.

Spectrum: 3

El	AN	Series	unn. C	norm. C	Atom. C	Compound	Comp. C	norm. Comp. C	Error (1 Sigma)
			[wt.%]	[wt.%]	[at.%]		[wt.%]	[wt.%]	[wt.%]
C	6	K-series	0.00	0.00	0.00		0.00	0.00	0.00
O	8	K-series	33.10	47.22	63.06		0.00	0.00	4.42
Mg	12	K-series	1.34	1.92	1.68	MgO	3.18	2.23	0.10
Al	13	K-series	7.10	10.13	8.03	Al ₂ O ₃	19.15	13.42	0.35
Si	14	K-series	20.72	29.56	22.49	SiO ₂	63.23	44.33	0.88
K	19	K-series	1.24	1.76	0.96	K ₂ O	2.12	1.49	0.07
Ca	20	K-series	0.75	1.08	0.57	CaO	1.50	1.05	0.06
Ti	22	K-series	0.16	0.23	0.10	TiO ₂	0.38	0.27	0.04



SF 3.

Table S3.

Spectrum: 3

El	AN	Series	unn. [wt.%]	C norm. [wt.%]	C Atom. [at.%]	C Compound	Comp. [wt.%]	C norm. [wt.%]	Comp. [wt.%]	C Error (1 Sigma) [wt.%]
C	6	K-series	0.00	0.00	0.00		0.00	0.00		0.00
O	8	K-series	33.19	47.29	62.50		0.00	0.00		4.29
F	9	K-series	0.39	0.55	0.61		0.55	0.39		0.16
Mg	12	K-series	1.41	2.01	1.75	MgO	3.33	2.34		0.11
Al	13	K-series	7.51	10.70	8.39	Al ₂ O ₃	20.22	14.19		0.38
Si	14	K-series	20.60	29.35	22.10	SiO ₂	62.78	44.06		0.88
K	19	K-series	2.48	3.53	1.91	K ₂ O	4.25	2.98		0.12
Ca	20	K-series	1.03	1.47	0.78	CaO	2.06	1.44		0.08
Ti	22	K-series	0.44	0.62	0.28	TiO ₂	1.04	0.73		0.06

Anexo II

Age constraints on the Paleozoic Yaguarí-Buena Vista succession from Uruguay: paleomagnetic and paleontologic information

Marcia Ernesto¹, Pablo Núñez Demarco², Pedro Xavier³, Leda Sanchez², Cesar Schultz³, Graciela Piñeiro⁴

¹Instituto de Astronomia, Geofísica e Ciências Atmosféricas, Universidade de São Paulo, São Paulo, Brazil

²Instituto de Ciencias Geológicas, Facultad de Ciencias, Iguá 4225, CP. 11400, Montevideo, Uruguay

³Departamento de Estratigrafia e Paleontologia, Universidade Federal do Rio Grande do Sul, Porto Alegre, Brazil

⁴Departamento de Paleontología, Facultad de Ciencias, Iguá 4225, CP. 11400, Montevideo, Uruguay

Abstract

The Yaguarí and the Buena Vista formations from Uruguay are historically correlated to the Brazilian Rio do Rasto and Sanga do Cabral formations, respectively, as they have some lithostratigraphic similarities, indicating a Permo-Triassic or even Triassic age of the Yaguarí-Buena Vista succession. However, they differ in the fossil indexes that characterize the faunistic communities present in both countries. A paleomagnetic work was carried out on some sections of the Buena Vista and the Yaguarí formations, as well as on some layers of bentonites, underlying the Buena Vista sediments. The alternating field and thermal demagnetization procedures revealed both normal and reversed magnetization components, but the samples showed evidence of secondary magnetic minerals and possibly remagnetizations. The calculated paleomagnetic pole for the Yaguarí-Buena Vista Formation plots near to the poles for the Choiyoi magmatism that is believed to be responsible for the bentonite accumulation, it is also in agreement with other Permian paleomagnetic poles for South America. Based on

the paleomagnetic results, the available radiometric data for the bentonites, and the fossiliferous content, a Late Permian (Lopingian) age is assigned to the Yaguarí-Buena Vista rocks.

DOI: <https://doi.org/10.1016/j.jsames.2019.102489>

Anexo III

Enigmatic wood and first evidence of tetrapods in the Yaguarí Formation (Middle-Late Permian), Uruguay

Graciela Helena Piñeiro¹, Lorenzo Marchetti², Sebastián Marmol³, Antonella Celio³, Pedro Luis Xavier⁴, Martin Francia³, Cesar Leandro Schultz⁵

¹Universidad de la República, Facultad de Ciencias, Departamento de Paleontología, Montevideo, Uruguay

²Museum für Naturkunde Berlin, Leibniz-Institut für Evolutions- und Biodiversitätsforschung, Berlin, Germany

³Universidad de la República, Facultad de Agronomía, Departamento de suelos y aguas, Montevideo, Uruguay

⁴Universidade Federal do Rio Grande do Sul, Programa de Pós-Graduação em Geociências, Porto Alegre, Brasil

⁵Universidade Federal do Rio Grande do Sul, Departamento de Estratigrafia e Paleontologia, Porto Alegre, Brasil

Abstract

This article describes an intriguing fossil material recently found in the fine-grained sandstone levels from the upper section of the Yaguarí Formation of Uruguay. The nature of this specimen and its relationships were, initially, not easy to determine with confidence although it was subjected to several analyses, such as morphological and comparative examination complemented with preparation of thin sections and microanatomical and chemical studies under SEM. However, the anatomical structure shown in the performed transversal thin sections allowed solving the issue on the different animal or plant interpretations of the fossil specimen, which was finally discerned in favor of the latter. Therefore, after a detailed comparative study of the thin

sections, we concluded that the specimen is a wood fragment related to the Dadoxylon-Araucarioxylon complex. Moreover, in order to provide a better biostratigraphic calibration for these deposits until now devoid of fossils, we include a preliminary description of recently found fossil footprints, which represent the first evidence of the presence of tetrapods in levels of the Yaguarí Formation (sensu Elizalde et al., 1970), below the conglomerates that have yielded the Colonia Orozco Fauna. The footprints were preliminary assigned to the ichnotaxa cf. Karooipes isp, cf. Capitosauroides isp., and cf. Pachypes isp., suggesting the presence of gorgonopsids and therocephalian therapsids and pareiasauromorphs, respectively. The Middle-Late Permian age recently suggested for the Yaguarí Formation based on paleomagnetic and radioisotopic studies is here supported by the described fossils, which thus constitute preliminary but nonetheless relevant discoveries for deposits whose fossiliferous potential has yet to be explored.

DOI: <https://doi.org/10.31285/AGRO.26.504>

ANEXO I

Título da Tese:

“SISTEMAS FLUVIAIS DOMINADOS POR ESTRUTURAS SUPERCRÍTICAS EM CLIMA SEMIÁRIDO NO EOTRIÁSSICO: REINTERPRETAÇÃO SEDIMENTAR DA FORMAÇÃO SANGA DO CABRAL”

Área de Concentração: Estratigrafia

Autor: **Pedro Luis Ammon Xavier**

Orientador: Prof. Dr. Claiton Marlon dos Santos Scherer
Coorientadora: Profa. Dra. Graciela Piñeiro

Examinador: Dr. Bruno Ludovico Dihl Horn

Data: 09/01/2024

Conceito: A

PARECER:

O aluno realizou um trabalho muito necessário, com um excelente tema, abordando conceitos litoestratigráficos e sedimentológicos essenciais para a compreensão da Bacia do Paraná. É um trabalho de alta complexidade, difícil interpretação de fácies pela natureza do sistema deposicional de difícil preservação.

As rochas estão bem descritas e a interpretação de fácies bem feita. Descrições petrográficas boas, possível visualizar bem as rochas trabalhadas. O aluno domina o assunto estudado, e aplicou bem os conceitos na tese.

Esta tese destaca a importância de utilizar a hidrodinâmica e os artigos experimentais para entender a dinâmica de rios no registro geológico.

Juntar a análise petrográfica com a análise de fácies é uma ideia excelente, que às vezes é ignorada.

Finalmente os rios enigmáticos do passado estão começando a serem entendidos, principalmente pelo abandono dos modelos de rios perenes de alta latitude.

Esta tese contribui para a descoberta um cinturão semi-árido Triássico em volta de um mega deserto gondwanico que a o registro ainda é esparso.

Algumas críticas e sugestões:

No artigo 1 não está claro no artigo se a foi trabalhado a unidade ou o afloramento. Entendo que o sistema deposicional é o mais importante, mas faltou um pouco de descrição do afloramento, principalmente a questão estrutural, que é muito importante neste afloramento. Também faltaram as paleocorrentes.

No artigo 2 como sugestões:

Revisar a introdução, pois está parece muito similar ao primeiro artigo, dá a impressão que o tema são as estruturas sedimentares, não a petrografia.

Figura 02 usar a de Schultz et al. 2020

Cuidar com Arid X dry. O clima é árido e as condições são secas. E.g. "Return of arid dry conditions (t3) caused the concentration and precipitation of carbonate"

Tá praticamente um resumo do artigo 1 na parte de interpretação da formação dos depósitos de carbonato. Acho que não precisa, acaba deixando meio cansativo.

Assinatura: Bruno Ludovico Dihl Horn

Data: 10/01/2024

Ciente do Orientador:

Ciente do Aluno:

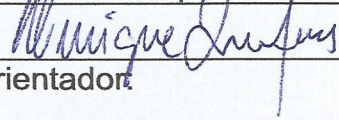
ANEXO I	
Título da Tese:	
“SISTEMAS FLUVIAIS DOMINADOS POR ESTRUTURAS SUPERCRÍTICAS EM CLIMA SEMIÁRIDO NO EOTRIÁSSICO: REINTERPRETAÇÃO SEDIMENTAR DA FORMAÇÃO SANGA DO CABRAL”	
Área de Concentração: Estratigrafia	
Autor: Pedro Luis Ammon Xavier	
Orientador: Prof. Dr. Claiton Marlon dos Santos Scherer Coorientadora: Profa. Dra. Graciela Piñeiro	
Examinador: Prof. Dr. Ernesto Luiz Correa Lavina	
Data: 09\01\2024	
Conceito: A (Excelente)	
PARECER:	
<p>A tese do Pedro está muito bem elaborada. Não tem erros ou omissões. O tema foi muito bem delimitado, os objetivos foram definidos de modo claro e os resultados alcançados são muito importantes. Os resultados possibilitam, mais do que uma reinterpretação sedimentar, como está no título, uma nova visão sedimentar e climática do início da era mesozoica no Sudoeste do Gondwana. O fato de o artigo principal já estar publicado em periódico altamente qualificado no Qualis Capes é um indicativo do aqui afirmado. Os processos sedimentares foram muito bem identificados e interpretados, bem como sua organização na evolução sedimentar da Formação Sanga do Cabral.</p> <p>Deste modo, o conceito apresentado (Excelente) está plenamente justificado. Recomendo ao Pedro, caso siga a carreira universitária, continuar neste tema, incluindo também o Neopermiano. Apesar do muito que já se publicou sobre o limite Permo-Triássico na Bacia do Paraná, este ainda não está equacionado, e o Pedro tem todo o potencial para explorá-lo, talvez como uma atividade de pós-doutorado.</p> <p>Finalizando, parabéns ao Pedro pela mais impactante tese de que participei nos últimos anos, e ao Dr. Claiton Scherer pela contínua qualificação de sua pesquisa, sempre garimpando e abrindo espaço para jovens de excepcional talento.</p>	
Assinatura: Lavina	Data: 12\01\2024
Ciente do Orientador:	
Ciente do Aluno:	

ANEXO I
Título da Tese:
“SISTEMAS FLUVIAIS DOMINADOS POR ESTRUTURAS SUPERCRÍTICAS EM CLIMA SEMIÁRIDO NO EOTRIÁSSICO: REINTERPRETAÇÃO SEDIMENTAR DA FORMAÇÃO SANGA DO CABRAL”
Área de Concentração: Estratigrafia
Autor: Pedro Luis Ammon Xavier
Orientador: Prof. Dr. Claiton Marlon dos Santos Scherer Coorientadora: Profa. Dra. Graciela Piñeiro
Examinador: Dr. Henrique Zerfass
Data: 09/01/2024
Conceito: A (Excelente)
PARECER:
<p>A presente tese apresenta pesquisa sedimentológica de alto nível técnico. Em um contexto de mudança de paradigma, em que antidunas – juntamente com outras famílias de estruturas produzidas por fluxos supercríticos – passaram a ter sua preservação demonstrada por meio de modelagem física e começaram a ser reconhecidas no registro geológico, o candidato propôs o estudo da Fm. Sanga do Cabral sob a óptica desse novo paradigma, unidade estratigráfica que se mostra muito apropriada para objeto dessa investigação dado o seu contexto deposicional. Dito isso, a única ressalva seria a de ter sido feita a escolha de um único afloramento que, apesar de extenso, apresenta uma única direção de corte, o que será mais bem exposto na sequência. A metodologia aplicada é adequada, fazendo uso das modernas técnicas de imageamento de afloramentos e tendo análises microscópicas e de DRX como ferramentas complementares. Os resultados são robustos, oriundos de uma base de dados muito rica e as interpretações são bem alicerçadas nos dados, levando a um avanço no conhecimento dos paleoambientes triássicos. Também chama a atenção a vasta bibliografia referenciada. O artigo 1, que aborda o tema principal, é de excelente qualidade. O artigo 2, que trata de temas complementares, é também de boa qualidade. Entretanto, no conjunto da tese há alguns aspectos que merecem aperfeiçoamentos. O texto integrador não cumpre seu papel de situar o leitor no contexto da tese e de prepará-lo para a leitura dos artigos. Não se trata exatamente de apresentar o estado da arte: embora isto tenha sido feito de alguma forma para os tópicos “formas de leito supercríticas e seus produtos sedimentares” e “rios de alta variabilidade”, os demais tópicos – “calcretes freáticos”, “paleossolos” e “poeira eólica” estão longe disso, tendo apresentado uma revisão bibliográfica pobre. No item de “materiais e métodos”, onde seria oportuno apresentar de forma mais livre como a tese foi desenvolvida, o texto é conciso como nos artigos, não trazendo informação adicional. Além disso, no contexto geológico poderiam ter sido acrescentadas mais informações sobre o contexto paleogeográfico e paleoclimático em que se deu a deposição da Fm.</p>

Sanga do Cabral. Ainda sobre o conjunto da tese, embora os dois artigos sejam complementares, realizados sobre o mesmo afloramento e o conhecimento levantado no primeiro artigo foi o ponto de partida, os dois artigos nem sempre dialogam entre si, em especial em termos de fácies e interpretações, como será discutido mais adiante. O artigo 1 apresenta uma base de dados faciologicos muito robusta. As interpretações são coerentes com os dados, à luz do crescente número de publicações identificando e descrevendo estruturas de regime de fluxo supercrítico, tanto no ambiente fluvial - atual e pretérito - como de modelagem física. Dentro desta faciologia cuidadosamente detalhada, destaca-se a presença de feições erosivas assimétricas preenchidas por estratificações de baixo ângulo e sigmoidais, dando a ideia de que a Fm. Sanga do Cabral teve sua deposição, em grande parte, regida por processos físicos onde erosão e deposição ocorreram em um contínuo e de forma sincrônica, o que é muito bem explicado no contexto dos fluxos supercríticos. Ressalva deve ser feita, o afloramento estudado apresenta uma única direção, de forma que algumas estruturas poderiam não ter sido caracterizadas por completo, ou seja, nas três dimensões. Um exemplo é o das laminações onduladas truncadas que poderiam se tratar de vistas frontais de formas de leito 3D de pequena altura, em uma situação de transição entre os regimes de fluxo inferior e superior, mas ainda no campo subcrítico. A incerteza quanto a isso é muito pequena, dada a preservação de algumas convexidades, mas o reconhecimento dessas estruturas em outras direções de corte seria a sua demonstração definitiva. Estudos em afloramentos na mesma região e com outra orientação seriam uma boa forma de confirmar as interpretações. Dados de paleocorrentes e de direção de mergulho de superfícies de acreção deveriam ser dois campos adicionais na tabela de fácies, sente-se falta deste tipo de dado. O desdobramento quantitativo do tópico de paleohidráulica é um complemento importante em uma época em que a Geologia recebe uma crescente demanda por informação quantitativa. Além disso, é uma contribuição relevante ao conhecimento dos regimes hídricos e paleoclimas do Gondwana. A utilização do termo "fluvial style" para designar o agrupamento tripartite das associações de fácies tem algumas implicações estratigráficas. Se as alternâncias de estilos fluviais se deram na escala interanual, decadal ou mesmo secular, cada associação de fácies representa determinadas condições meteorológicas em um mesmo regime climático. Em adição, o tempo representado seria muito curto para que os rios assumissem estilos diferentes, os rios teriam um único estilo, caracterizado justamente pela alta variabilidade. Neste caso, a escolha do termo não seria apropriada. Em contrapartida, se as associações de fácies representam variações em escala de tempo geológico (milhares a centenas de milhares de anos), o controle seria astronômico, levando a ciclos climáticos. Neste caso, as variações nos regimes climáticos - não mais variações meteorológicas em um mesmo regime climático - levariam a variações no estilo fluvial no tempo geológico, sendo o uso de "fluvial style" perfeitamente justificado. Parece ser este o caso conforme discutido na arguição, mas nos textos o autor apenas tangencia o problema da amplitude temporal do afloramento estudado. Esta questão poderia ter sido mais bem trabalhada, o que só valorizaria ainda mais o trabalho, em uma época que mudanças climáticas estão em foco. O artigo 2 apresenta um bom aporte de dados e interpretações que contribuem para o conhecimento do paleoclima do Gondwana. A organização do artigo torna difícil sua leitura e a correlação dado-interpretação, pois os resultados são apresentados por feição diagenética e não por nível ou fácies. No momento da discussão é difícil saber a

que fácies determinada interpretação corresponde. Sugere-se ainda acrescentar como figura um croqui do afloramento com a posição das amostras e uma tabela indicando o tipo de material e outros dados relevantes que possibilitem uma rápida associação entre a escala do afloramento e os dados na escala microscópica. A interpretação de que na Fm. Sanga do Cabral há depósitos de *loess* (p. 150) é questionável, uma vez que no primeiro artigo não há descrição de fácies produzida por decantação de poeira eólica. Assim como no artigo 1, falta assertividade sobre o afloramento estudado representar um momento fossilizado do tempo geológico regido por um determinado paleoclima ou se a sucessão de associações de fácies – os “fluvial styles” - registram a evolução de sistemas fluviais em um intervalo de tempo (geológico) em que mudanças climáticas se processaram. As observações aqui feitas são o resultado da avaliação do conjunto da tese, em nada desmerecendo a sua qualidade, de alto nível técnico e propiciando a publicação de dois artigos relevantes, que se tornarão em breve referência no assunto.

Assinatura:



Data: 09/01/2024

Ciente do Orientador:

Ciente do Aluno: